Synthesis of new organic and organometallic Porphyrin Assemblies for Optics

Areej Merhi

Thèse

THESE INSA Rennes
sous le sceau de l'Université européenne de Bretagne
pour obtenir le titre de
DOCTEUR DE L'INSA DE RENNES
Spécialité : Chimie

présentée par
Areej MERHI
ECOLE DOCTORALE : *SDLM*
LABORATOIRE : *UMR 6226-ISCR, OMC*

Synthèse de Nouveaux Assemblages à base de Porphyrines Organiques et Organométalliques Pour l'Optique

Thèse soutenue le 20.09.2013
devant le jury composé de :

Isabelle LEDOUX
Professeur de l'ENS Cachan / présidente du jury
Raphaël TRIPIER
Professeur à l'Université de Brest/ rapporteur
Didier DUBREUIL
Professeur à l'Université de Nantes/ rapporteur
Fréderic PAUL
Directeur de Recherche CNRS à l'Université de Rennes1 / examinateur
Olivier MONGIN
Maître de Conférences (HDR) à l'Université de Rennes1 / examinateur
Christine PAUL-ROTH
Maître de Conférences (HDR) à l'INSA de Rennes / Directrice de thèse

Synthèse de Nouveaux Assemblages à base de Porphyrines Organiques et Organométalliques Pour l'Optique

Areej MERHI

En partenariat avec

To you, my driving force to go forward

My only motivation to run the last few meters of the marathon

Infinity thanks my undefined you

Thank you for being always here!

My pathway was lit by your warm love

To you mom!

Acknowledgements

I would like to thank the French Government and the INSA de RENNES for the funding of my project throughout the three years. Specifically, I'm grateful to Region Bretagne for my ARED grant "Lumiclip".

I would like to thank M. Raphael TRIPIER, Professeur à l'Université de Brest and Didier DUBREUIL, Professeur à l'Université de Nantes to accept to be reporters for this manuscript.

I would also thank Mme Isabelle LEDOUX; Professeur de l'ENS Cachan, Mr. Marek SAMOC; Professeur à l'Université de Wroclaw (Pologne), Mr. Olivier MONGIN; Maître de Conférences à l'Université de Rennes and Mr. Fréderic PAUL ; Directeur de Recherche à l'Université de Rennes to accept to be the examinators of this work.

I am deeply indebted to Christine PAUL-ROTH, my supervisor, for it was a great pleasure to work together over the last three years. I would like to thank her for the mixture of her kindness, objectivity, serious work, disponibility, advice, care, and guide. Many special thanks are dedicated to her as well for the great professional fruitful opportunities that were offered to me that enriched my scientific career.

I would thank Frédéric PAUL for having me in his group and for all the scientific advice and international collaborations.

I would like to thank Mark HUMPHREY and his group as well for having me in his laboratory (Australia) for three months.

Special dedications to the "Service de la Recherche de l'INSA" for their gentle help, specially for Aurore GOUIN, and Marie-Claire TEIGNE : simply your presence made life in France magnificent! Thank you for all the nice moments we shared.

My lab friends! I owe you a big thank you : Alison, Amédé, Nicolas, and Victoria for making my stay in the lab a great pleasure and fun, Guillaume for all the helpful nice and fruitful scientific advice specially during the period in Australia!

Gwénael : Monsieur le Maître qui m'a bien formé, merci!

My step family in RENNES, my lovely friends : Elise, Fidaa, Doha, Salwa, Ayman thanks for having you always there as the source of happiness and smile, and specially tolerating and supporting me during my writing period.

My secondary academic supervisor: thank you Mr. Moufid KHALIL for your support since 2001. I wouldn't have been here without your support since that.

My family who supported me with all the possible means : simply this work is because of you, motivated by you and dedicated to you! I love you.

Abbreviation list

TPP : Tetraphenylporphyrin

TFP : Tetrafluorenylporphyrin

CV : Cyclic voltammetry

TFA : Trifluoroacetic acid

DDQ : 2,3-dichloro-5,6-dicyano-1,4-benzoquinone

NMR : Nuclear Magnetic resonance

HOMO : Highest Occupied Molecular Orbital

LUMO : Lowest Unoccupied Molecular Orbital

TPA : Two photon absorption

TPEF : Two photon excited fluorescence

DFDPP : Difluorenyl-diphenylporphyrin

DFDHP : Difluorenyl-dihydrogenporphyrin

TOFP : Tetra-oxyfluorenylphenylporphyrin

OOFP : Octa-oxyfluorenylphenylporphyrin

SOFP : Sixteen-oxyfluorenylphenylporphyrin

DFWM : Degenerate four-wave mixing

EFISH : Electric field-induced second harmonic generation

NLO : Nonlinear optics

SA : Saturable absorption

RSA : Reverse saturable absorption

THG : Third-harmonic generation

DFWM : Degenerate four-wave mixing

TTP : tetra-*p*-tolylporphyrin

SCE : Saturated calomel electrode

OPA : One photon absorption

MLCT : Metal to ligand charge transfer

Table of contents

Chapter 1 : porphyrins and fluorenes interesting building blocks for Optics

Chapter 2 : Synthesis of Porphyrin Dendrimers

Chapter 3 : Multiporphyrin arrays

Chapter 4 : Porphyrin Organometallic Assemblies for Nonlinear Optics of Third Order

Chapter 5 : New Porphyrin complexes for OLEDs……

Chapter 1

Porphyrins and Fluorenes

Interesting building blocks for optics

I. Porphyrins

As a word, porphyrin is of greek origin : *porphura* that means violet. This meaning might have a direct reflection to that porphyrins are colored molecules. Porphyrins can be synthesized but it is important to mention that they already exist in nature.

Porphyrins are called the pigments of life due to their extreme importance among natural compounds. Without porphyrins, the life cycle is interrupted. That is because the vitality of all living things is of porphyrin nature.

To live, it is indispensible to respire : to take in oxygen and to release carbon dioxide. The main agent to do this is the **heme** in **hemoglobin**. In fact, heme is a porphyrin metallated with iron as seen in **Figure 1**.

On the other hand, plants constitute an essential part in the life cycle. Green plants are homophytes, that is, they do their own food by a process called photosynthesis. To do so, a green pigment – **chlorophyll** – is needed. Again, the chlorophyll is a porphyrin metallated by magnesium as presented in **Figure 1**.

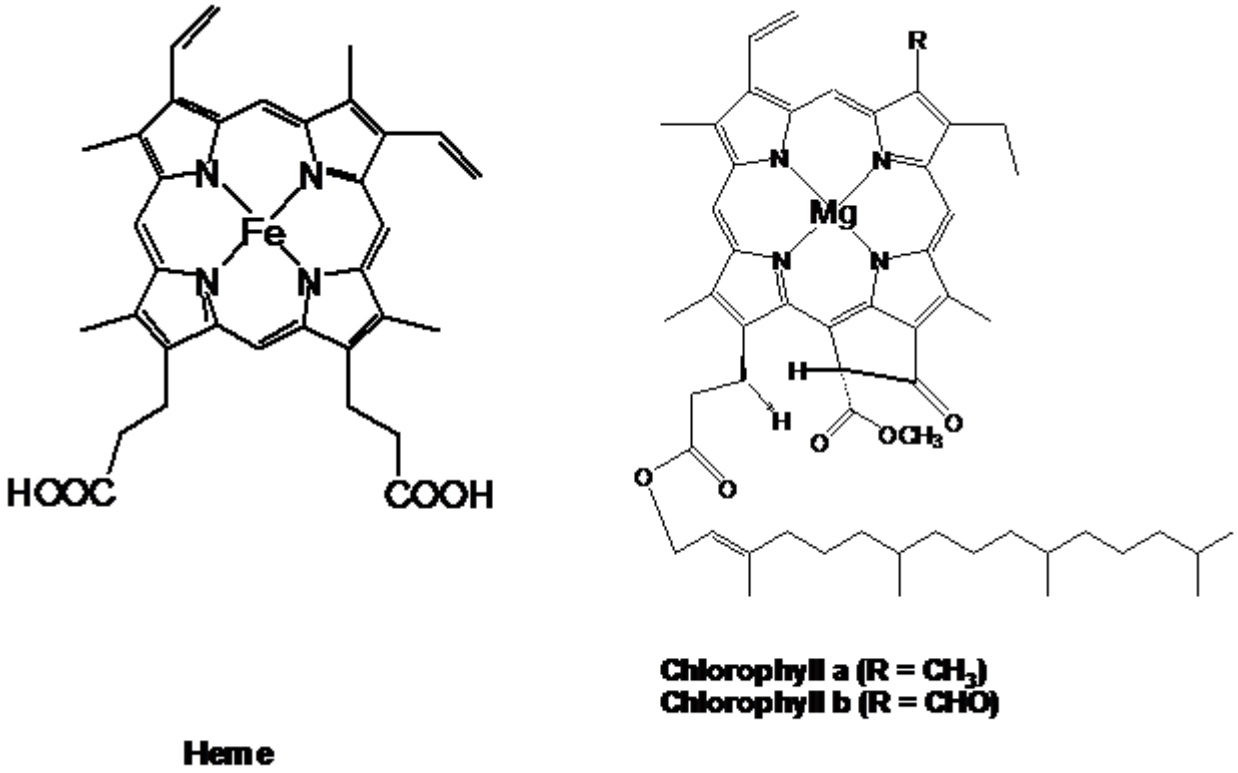

Figure 1 : Natural occurring porphyrins

1. Structure

Before detailing the structure of the porphyrins, it is important to mention the discovery of this macrocycle through time. The first proposal of the porphyrin structure was given in 1884 : Nencki suggested that the chemical structure of porphyrins is based on pyrroles.[1] Many years later, Kuster[2] was able to specify that this macrocycle is made up of only four units of pyrroles. In addition the name porphine was given to this macrocycle in 1912. Finally, this structure was confirmed in 1926, that was when Fischer synthesized the etioporphyrin.[3]

Chemically, as seen in **Figure 2**, the porphyrin macrocycle is made up of four pyrroles connected by methine bridges. These compounds are aromatic following Huckel's rule (4n + 2), in our case n = 4 since there are 18 π conjugated electrons. Maybe it is worth to tell that there are 22 π electrons but only 18 are delocalized.[4] This strong conjugation gives porphyrins stability and unique photophysical properties.

For example, porphyrins absorb in the visible region. These characteristics gave these compounds great attention to be candidates for a variety of applications. The simplest form of porphyrins is referred as porphine, as seen in **Figure 2**.

The porphyrin macrocycle can form complexes with a variety of metal ions, so we can find both free base and metallated porphyrins. That depends on the interest for expected properties or applications.

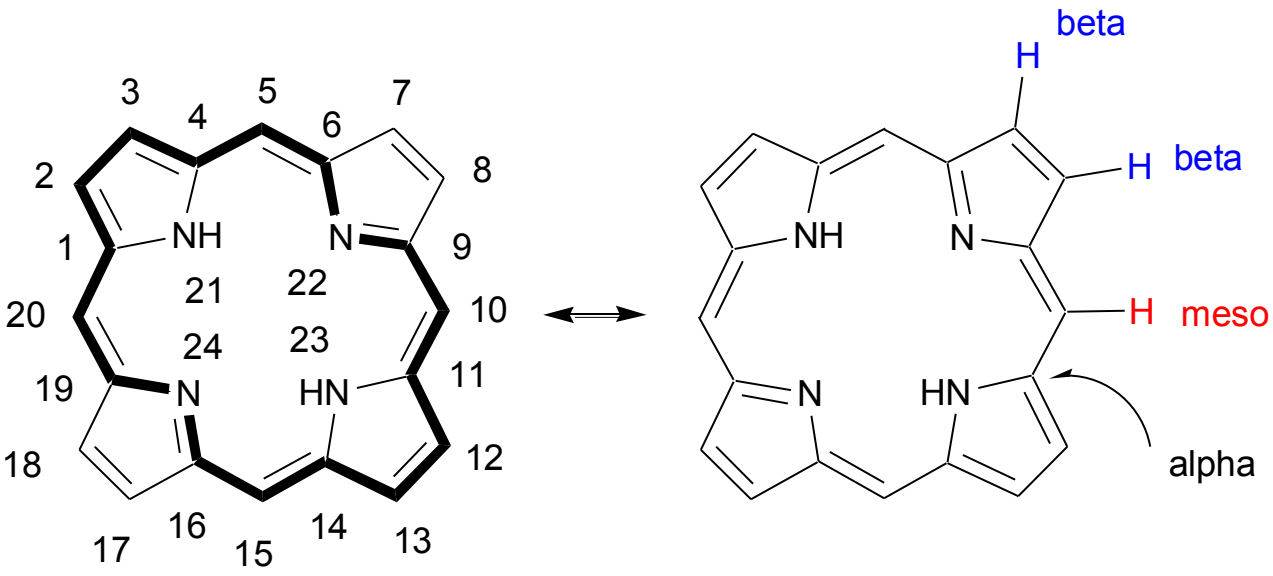

Figure 2 : The structure of **porphine**

A porphyrin macrocycle can be substituted at three different positions : *alpha*, *beta* and *meso* as seen in **Figure 2**. For a free base porphyrin, the 2, 3, 7, 8, 12, 13, 17 and 18 positions have referred to be as *beta* positions. In a similar way, the positions at 1, 4, 6, 9, 11, 14, 16 and 19 are identified as *alpha* positions, the positions 5, 10, 15 and 20 are referred commonly as "*meso*-positions". Respectively, a proton bonded to a *meso* carbon is cited as H_{meso} and that to a *beta* carbon as H_{β}.

Normally, porphyrin macrocycles are planar compounds,[4] but distortion of the macrocycle can also be observed in many cases and due to many factors. That can be due to the metallation of the porphyrin macrocycle for example. Another reason could be related to the substitution of the macrocycle at *beta* or *meso* positions by bulky groups.

As a last point to mention about the structure, it is interesting to present the porphyrin derivatives that are found in nature (**Figure 3**).

As one can notice, the difference between the structures in **Figure 3** is due to that one or more double bonds are reduced. Double bonds are related to conjugation, and the latter has to deal with photophysical properties. As a consequence, these porphyrins will not possess same characteristics.

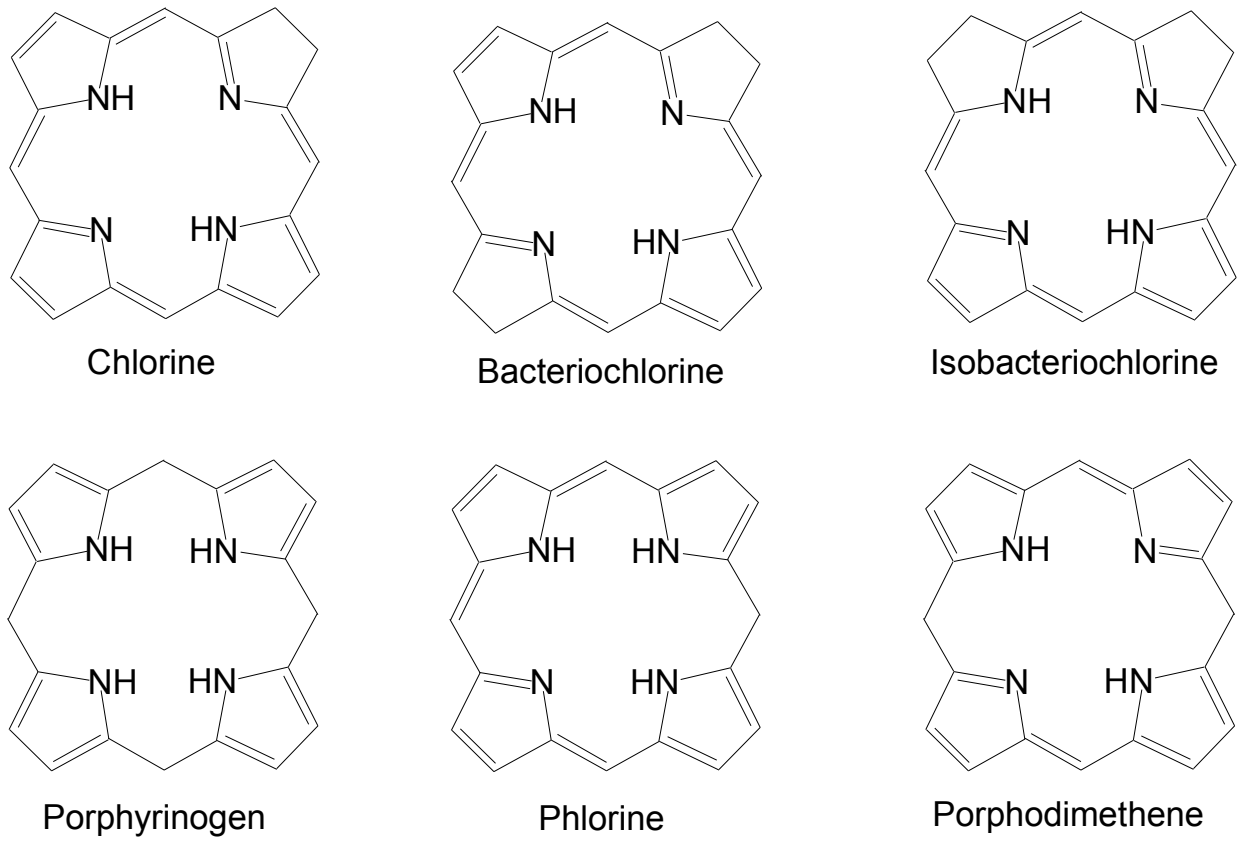

Figure 3 : Porphine derivative structures

2. Synthesis of porphyrins

Many methods have been reported for porphyrin synthesis. These methods gave porphyrins substituted at *beta* and or *meso* positions with different yields. Every method has its advantages and disadvantages.

Historically, the synthesis of a symmetrical substituted porphyrin was reported for the first time in 1935 by Rothemund.[5] The synthesis of this porphyrin was carried out in methanol at different temperatures. It was the condensation between pyrroles and ethanol as aldehyde. It was also tried using different aldehydes as well.

The negative point of this synthesis is that the yield was very low. Six years later, Rothemund succeeded in improving the yield of his reaction (till 10%) by changing the conditions.[6] It was by condensing the pyrrole and the benzaldehyde in sealed tubes at 220°C using pyridine solution. The reaction took 48 hours to give **TPP** as lustrous blue needle- crystals. These conditions gave **TPP** as a major compound rather to be equally mixed with its isomer.

Later, Calvin *et al.*[7] have proved that two porphyrins obtained from the condensation of pyrrole and benzaldehyde are not isomers; they are two different compounds. This group developed a direct synthesis to zinc metallated **TPP**, in high yields.

Many years later, **Adler** and **Longo**[8] developed the synthesis of substituted porphyrins by simple condensation of pyrrole and aldehyde in propanoic acid at reflux. This method was very useful but with some limitations. Then, these limitations were overcome by another method developed by **Lindsey** in 1986.[9]

It is worth to mention that the last two methods : **Adler-Longo** and **Lindsey** are the most used. They are efficient for synthesizing porphyrins substituted at the *meso* position. That is why they will be discussed in details as seen below.

2.1. Adler Longo's method

This method is based on refluxing the aldehyde and pyrrole in propanoic acid for 30 minutes as seen in **Scheme 1**. It is not under argon since oxygen is needed.[8] The oxygen in air is used for the oxidation of the porphyrinogen intermediate.

After slight cooling, filtration of the dark reaction mixture yields to get the glittering purple crystals of the **TPP**.

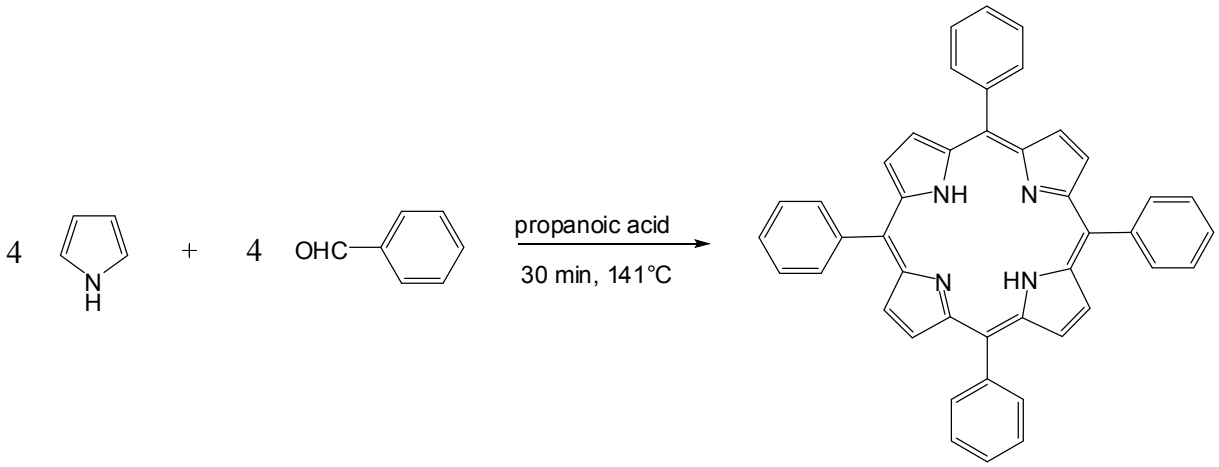

Scheme 1 : Synthesis of **TPP** using **Adler's** method

Such a method is very efficient for the synthesis of symmetrical porphyrins. But, still even for symmetrical porphyrins there exists an important limitation. It is that this method can't be used in case of aldehydes with sensitive groups. That is due to the harsh reaction conditions concerning the reflux at 141°C. Another limitation is the lack of any access to porphyrins bearing two or more distinct *meso* substituents.

2.2. Lindsey's method

In the early 1980s, the first limitation of Adler-Longo's method was overcome by Lindsey's method.[9] The synthesis of porphyrins was achieved under mild conditions. The condensation of pyrrole and aldehyde was carried under argon, using a chlorinated solvent such as dichloromethane or chloroform. It was catalyzed by a Lewis acid, where the tetrapyrrolmethane is formed. At this stage, there is a competition between the formation of porphyrinogen in case of cyclization, and the polymerization to give polypyrromethane as shown in **Figure 4**. Lewis acids that could be used are : $BF_3.OEt_2$ or trifluoroacetic acid (TFA).

The porphyrinogen is not stable; it needs to be oxidized to form the stable porphyrin macrocycle. Given that, oxygen in air is not sufficient to oxidize it, so in this synthesis, an oxidant is added. Oxidant such as tetrachloro-1,4-benzoquinone (*p*-chloranil) or 2,3-dichloro-5,6-dicyano-1,4-benzoquinone (DDQ) could be used to carry out the $6e^-/6H^+$ oxidative dehydrogenation of the porphyrinogen to form the porphyrin macrocycle. After addition of the oxidant at room temperature, reflux for one hour is needed. Then, the porphyrins and the possible polymers are formed. Optimal concentration of pyrrole and aldehyde is around 10^{-2} M; that is to favor the cyclization over the polymerization. In the ideal case, yields in the range of 40 to 50% are reported.

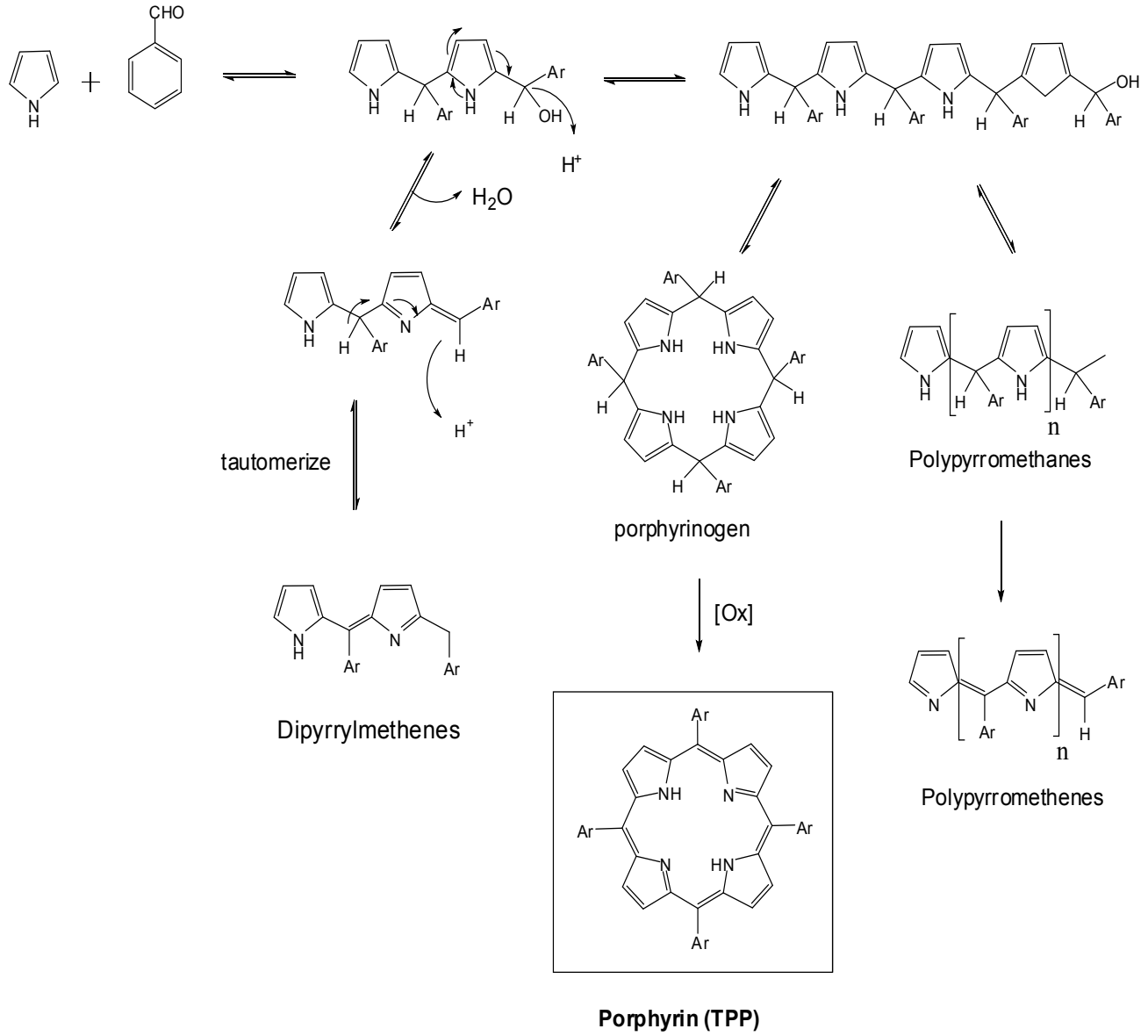

Figure 4 : Mechanism of the porphyrin formation using **Lindsey's** method

In the late 1980's, Lindsey's method was not limited for symmetric porphyrins. On the contrary, developing this method covered the second limitation of Adler-Longo. It was by condensing two different aldehydes with pyrrole as presented in **Scheme 2**.

But, in this case, a statistical mixture of porphyrins is the result in addition to the polymer.[10] So, here comes the hard step of this method which is the purification. It is not impossible, but it is difficult and requires large quantities of fine silica. If separation is successful, one will have the access to different substituted porphyrins (like $\mathbf{A_2B_2}$ or $\mathbf{A_3B}$) from one reaction. These *meso*-substituted porphyrins are important building blocks for further synthesis (see **chapter 3**).

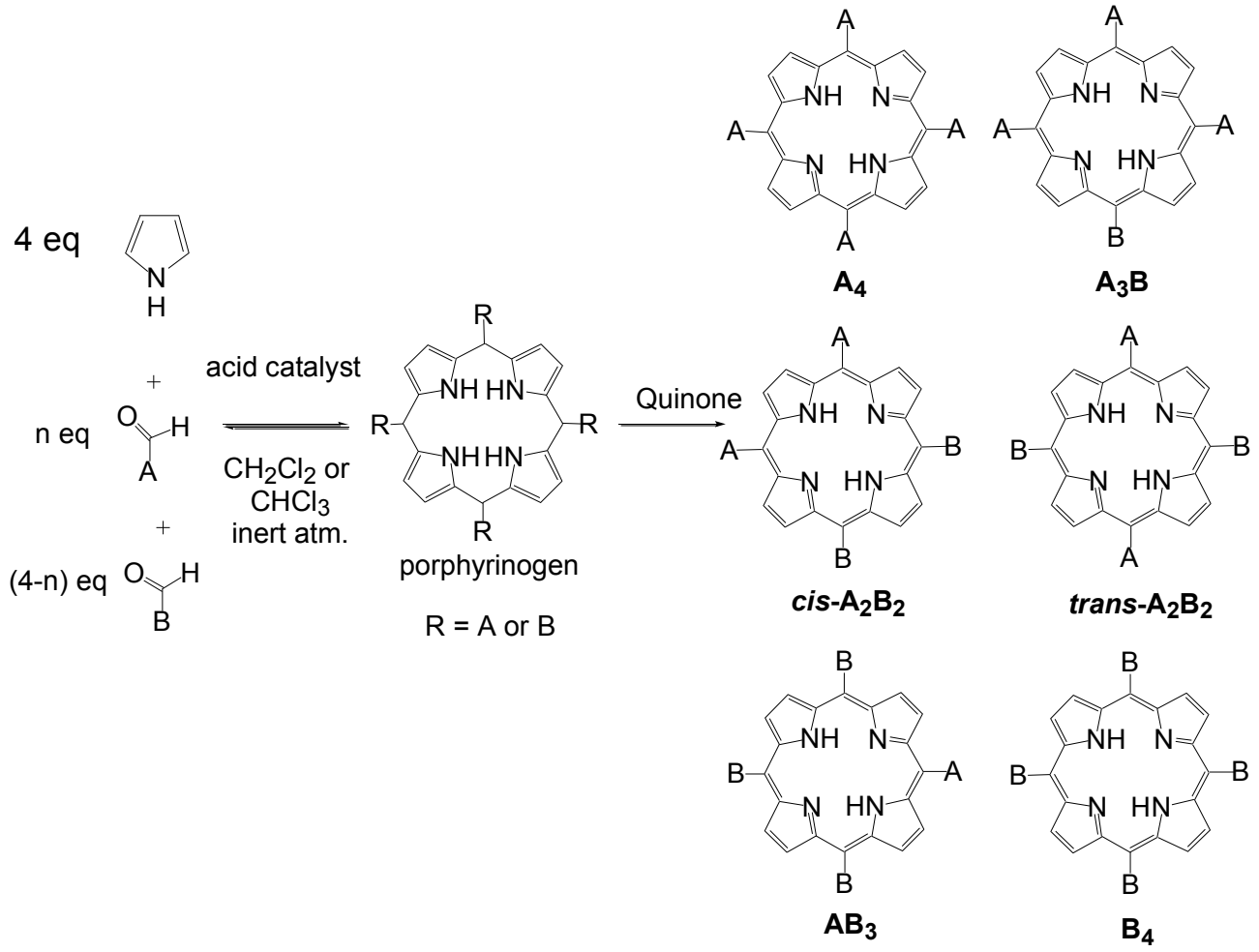

Scheme 2 : Synthesis of substituted porphyrins at *meso* positions

3. Characterization

As any organic or organometallic compound, a porphyrin is characterized by normal spectroscopies such as Nuclear Magnetic Resonance (NMR), proton (^{1}H), and carbon (^{13}C), UV-visible absorption (UV-vis), emission, and cyclic voltammetry (CV) as well. There will be standard features that identify and characterize a porphyrin structure in general. The characterization of porphyrins by the mentioned spectroscopies will be discussed in details in the following next part.

3.1. ^{1}H NMR

The first work on NMR studies of porphyrins was initiated by Becker *et coll.* in 1959.[11] As an aromatic cycle, the porphyrin macrocycle has an important cycle current that affects mainly the chemical shift of the protons (**Figure 5**). That is why the **^{1}H NMR** spectrum of a porphyrin is

characteristic. As presented in **Figure 5**, the protons in the porphyrin macrocycle are highly shielded. That explains their chemical shift which is around – 3 ppm. On the contrary, protons of the *beta* and *meso* carbons are highly deshielded and of chemical shifts around 7 ppm.[12]

In case of metallated porphyrins, the first signal observed in the **^{1}H NMR** spectrum is the absence of the signal at high field (– 3 ppm). Concerning the change of the chemical shifts of the other signals, it is highly dependent of the structure symmetry. No general rule could be drawn concerning the change of the chemical shift due to the metallation of porphyrin macrocycle.

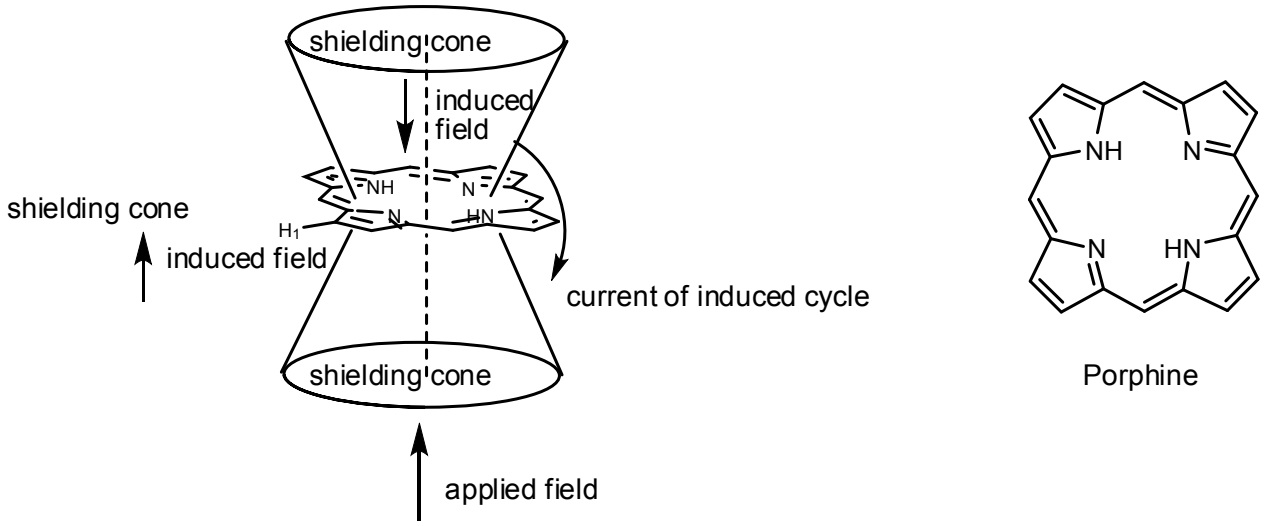

Figure 5 : Anisotropy magnetic cone of a porphyrin

3.2. ^{13}C NMR

The **^{13}C NMR** of a porphyrin could be divided into three different zones : *alpha* pyrrolic, *beta* pyrrolic and *meso* carbons. Concerning the first two types, *alpha* and *beta*, there is a problem in detecting clearly their corresponding peaks due to NH tautomerism.[13] These signals are clearer at low temperature since NH tautomerism is slow as temperature decreases.

Normally, *alpha* carbons are observed at around 145 ppm. In addition, there is a fairly constant chemical shift (about 17 ppm) difference between the *alpha* carbon signals. Concerning *beta* carbons, they are seen at around 130 ppm. The chemical shift difference between the *beta* carbons is smaller than that in case of *alpha*. It varies between 5.3 and 6.9 ppm. As for *meso* carbons, they are generally between 95 and 120 ppm.

If porphyrin core is metallated, the signals of *alpha* and *beta* carbons will be upshifted. In contrast, *meso* carbons show downfield shifts.

3.3. Absorption and Emission of Porphyrins

3.3.1. UV-Visible Spectroscopy

As mentioned in the introduction about porphyrins, the conjugation of these structures gave them the ability to absorb in the visible and near UV. Porphyrins present an interesting and characteristic visible spectrum due to two specific different types of bands :

a) **The Soret band** : this band is very intense and localized between 380 and 450 nm. It corresponds to the transition from the fundamental state $\mathbf{S_0}$ to the second singlet excited state $\mathbf{S_2}^*$. The extinction molar coefficient **ε,** of this transition is very high; in the order of 10^5 $M^{-1}.cm^{-1}$.

b) **The Q bands** : these bands are responsible for the intense color of the porphyrin compounds. Indeed they are localized in the visible region between 500 and 700 nm. These bands correspond to the transition from the fundamental state $\mathbf{S_0}$ to the first singlet excited state $\mathbf{S_1}^*$. The extinction molar coefficient **ε** of this transition is in the order of 10^4 $M^{-1}.cm^{-1}$.

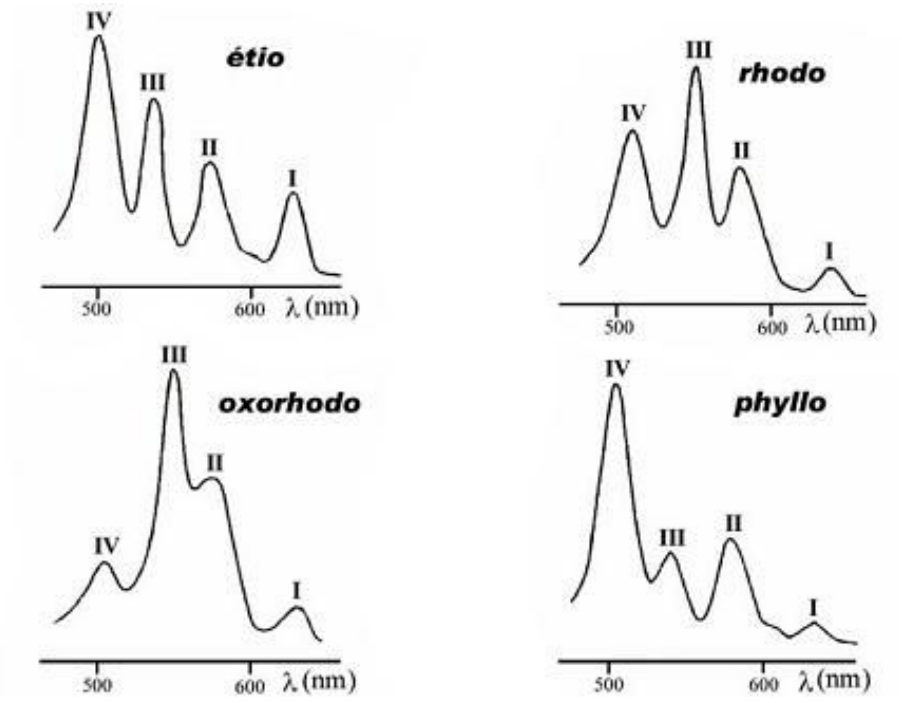

Figure 6 : Different Q bands of free base porphyrins

Since a porphyrin macrocycle can exist free (in D_2h symmetry), or metallated (in D_4h symmetry), it is worth to differentiate between their UV-visible spectra.

For **free base porphyrins**, we observe four Q bands. Knowing that the substituents of the porphyrin at its different possible positions have an effect on the molecule's photophysical properties,[14] then we define different spectra as seen in **Figure 6**. For example, *etio* type is observed in the case of substituted porphyrins at *beta* position with at least six groups. In case of *meso* substituted porphyrins, *phyllo* type is observed.[15]

On the other hand, if the **porphyrin macrocycle** is **metallated**, two Q bands instead of four are observed.

3.3.2. Luminescence of porphyrins

When a porphyrin is excited, it passes from the fundamental state $\mathbf{S_0}$ to the singlet $\mathbf{S_x}^*$. Then an internal conversion and a rapid relaxation take place to form the singlet state $\mathbf{S_1}^*$. Definitely, this state is of lower energy, an illustration is presented in **Figure 7**.

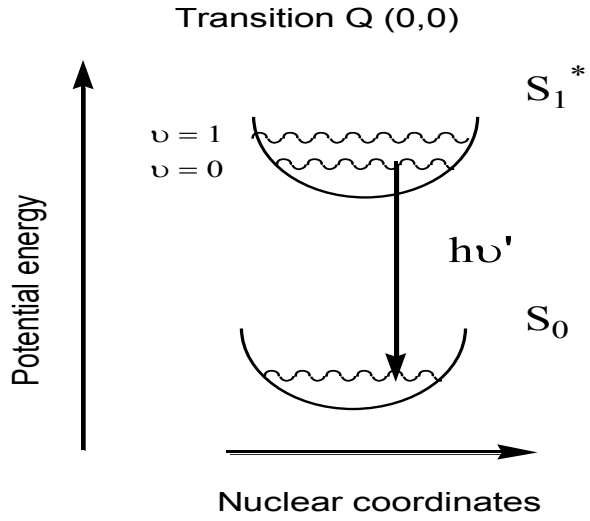

Figure 7 : Schematic representation of emission band of porphyrins

3.4. Cyclic Voltammetry

It is worth to mention that the redox potentials are affected by substituents of the porphyrins. The type of metal and its degree of oxidation (in case of metallated porphyrins) affect the redox potential as well.[16] Generalities about cyclic voltammetry will be discussed. For example, all of them could be

stepwise oxidized or reduced by two electrons at the π ring system to give π cation radicals and dications, and π-anion radicals and dianions[17] as presented in **Figure 8**.

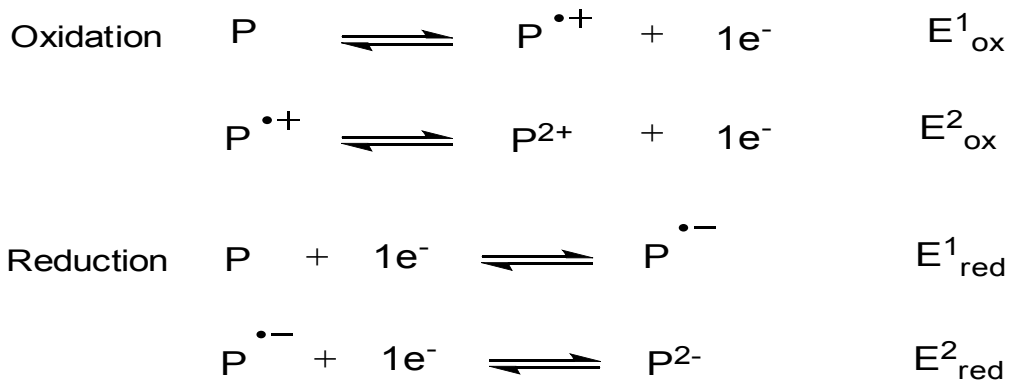

Figure 8 : Stepwise oxidation and reduction of a porphyrin macrocycle

Early electrochemical studies of tetraphenyl porphyrin **TPP** used a large part of cyclic voltammetry to measure half-wave potentials of each electrode reaction. Kadish demonstrated that most of the porphyrins exhibit a constant potential difference between the first and the second macrocycle centered oxidation, or the first and second macrocycle centered reductions.[18] This corresponds to a similar gap between the Highest occupied molecular orbital **HOMO** and the Lowest unoccupied mole

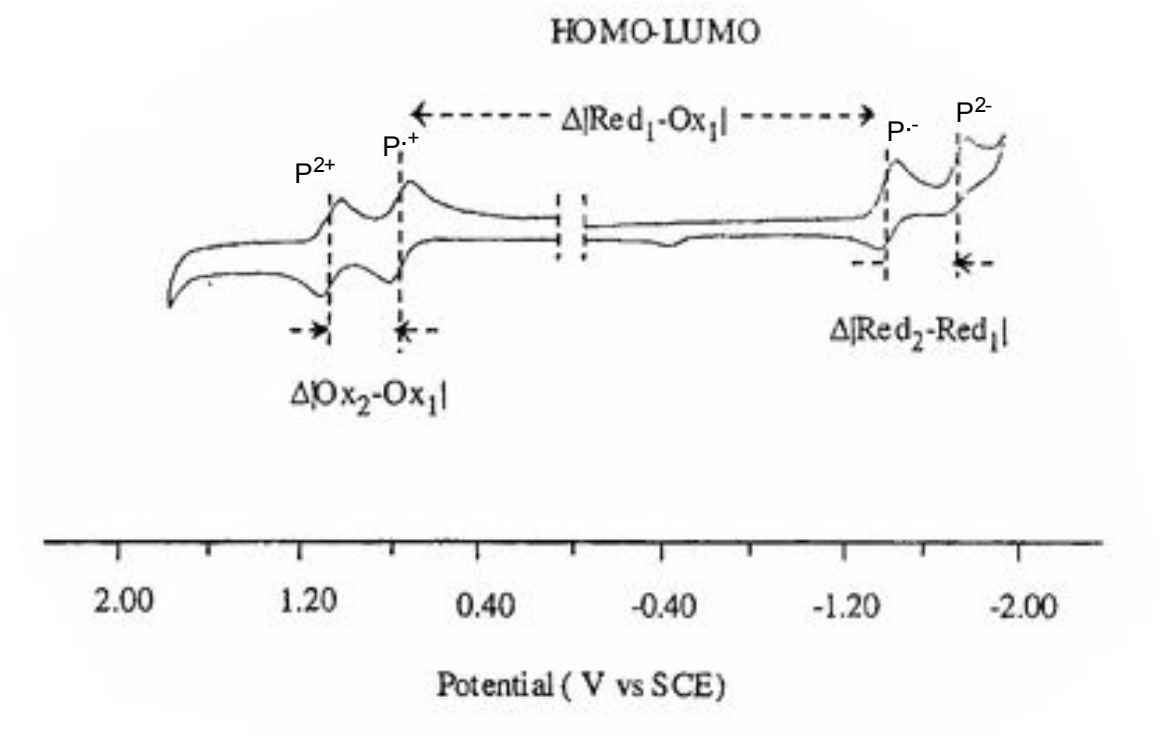

Figure 9 : Cyclic voltammetry of **TPP** in CH_2Cl_2

4. Quantum yield

By definition, the fluorescence quantum yield (Φ_F) is the ratio of photons emitted to photons absorbed through fluorescence. The most reliable method for recording Φ_F is the comparative method of Williams *et al.*[19]

This method involves the use of well characterized standard samples with known Φ_F values. We can assume that if the solutions of the standard and test samples are of identical absorbance at the same excitation wavelength, then they can be absorbing the same number of photons.

Then, a simple ratio of the integrated fluorescence intensities of the two solutions (measured under identical conditions) will yield the ratio of the quantum yield values. Since Φ_F for the standard sample is known, then it is easy to calculate the Φ_F for the test sample.

The fluorescence quantum yields of studied compounds (chapters 2 and 3) were determined with respect to a calibration standard of the reference (**TPP**). This compound (**TPP**) possesses fluorescence quantum yield of 0.12[20] in degassed toluene solution, and 0.13[21] in benzene solution. The quantum yield was calculated from the following equation :

$$\Phi_s = \Phi_{TPP} \times (F_s/F_{TPP}) \times (A_{TPP}/A_s) \times (n_{TPP}/n_s)^2$$

To simplify the equation, we define its terms as follows :

- $\mathbf{\Phi_s}$ is the fluorescent quantum yield of the new compound.
- **F** is the integration of the emission intensities.
- **n** is the index of refraction of the solution.
- **A** is the absorbance of the solution at the exciting wavelength.

The subscripts **TPP** and **s** denote the reference (**TPP**) and unknown samples, respectively.[22]

II. Fluorene unit

Given that an important part of the synthesis of porphyrins, which will be discussed in the next chapters, has **fluorene** as units or building blocks, it is worth to give a general presentation of these molecules. In fact, conjugated systems have called the attention of many chemists. Among the used monomers, fluorene was a remarkable unit due to its optical and electronic properties.[23] Fluorene has the chemical structure as shown in **Figure 10**.

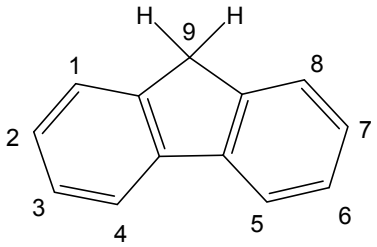

Figure 10 : Structure of fluorene

Many derivatives can be obtained easily starting from this molecule. That is, the structure could be easily modified at position 9. Moreover, positions 2 and 7 are considered to be the coupling sites. This means that many reactions can take place to achieve the target building block that serves one's need. These possible modifications give rise to different and diverse physical properties.

For example, Wong reported the synthesis of fluorene based molecules as presented in **Figure 11**. He showed the effect of substituents at position 9 on the photophysical properties.[24] All these facilities gave this precursor a great attention to be the center of research of many chemists. This was clear due to the application field observed, such as molecular electronics, linear,[25] and non linear optics.[26]

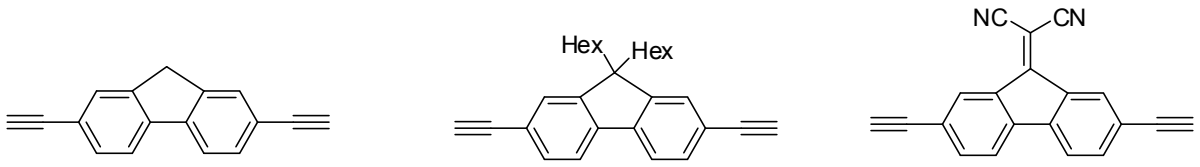

Figure 11 : Fluorene based molecules studied by **Wong**

In a general manner, fluorene and its derivatives possess characteristic luminescence in the blue region. This is explained to be due to $\pi \rightarrow \pi^*$ transition. Absorption and emission spectra that correspond to the transitions : (0 – 0), (0 – 1), (0 – 2) are shown in **Figure 12** below.

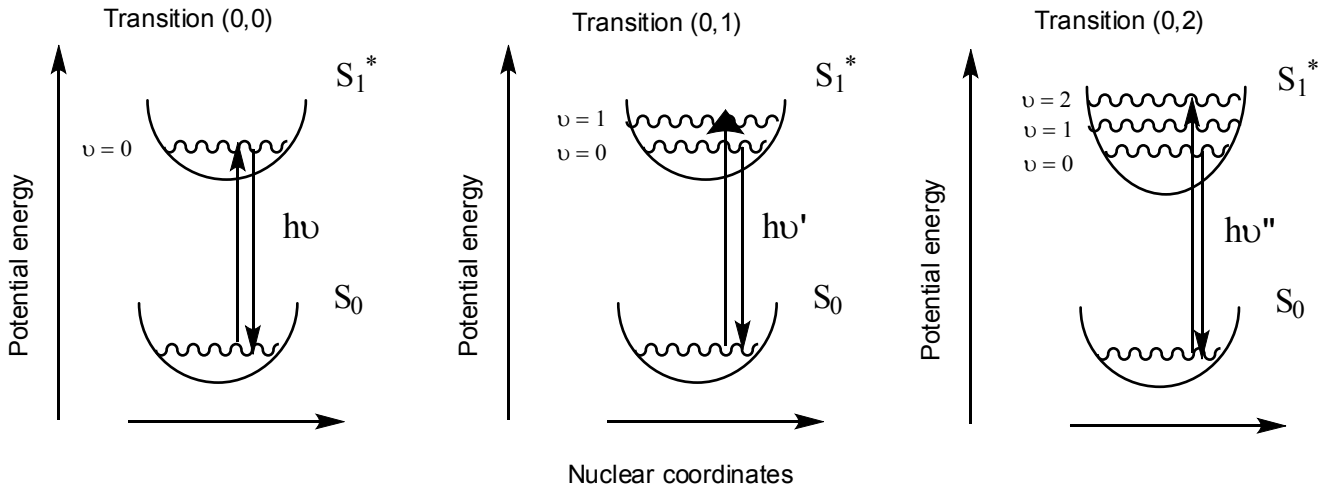

Figure 12 : Absorption and emission spectra of fluorene

Many groups have studied different series of molecules to understand the relation between the structure of the molecule and its two photon absorption (TPA) properties. We can cite Reinhardt *et coll.*[26] and Kim *et coll.*[27] who worked on the synthesis of many conjugated systems of different donors and acceptors. Finally, they were able to draw a conclusion about the effect of fluorene as units. In fact, the TPA was better for structure having **fluorene** units. Moreover, long chains at position 9 favored this process as well.

On the other hand, with the **fluorene** unit quadrupoles can be obtained. In addition, these molecules are fluorescent so two photon excited fluorescence (TPEF) can be studied. M. Blanchard-Desce *et al.* developed a molecular engineering strategy[28] to synthesize quadrupolar molecules (**Figure 13**) that are active for TPEF.

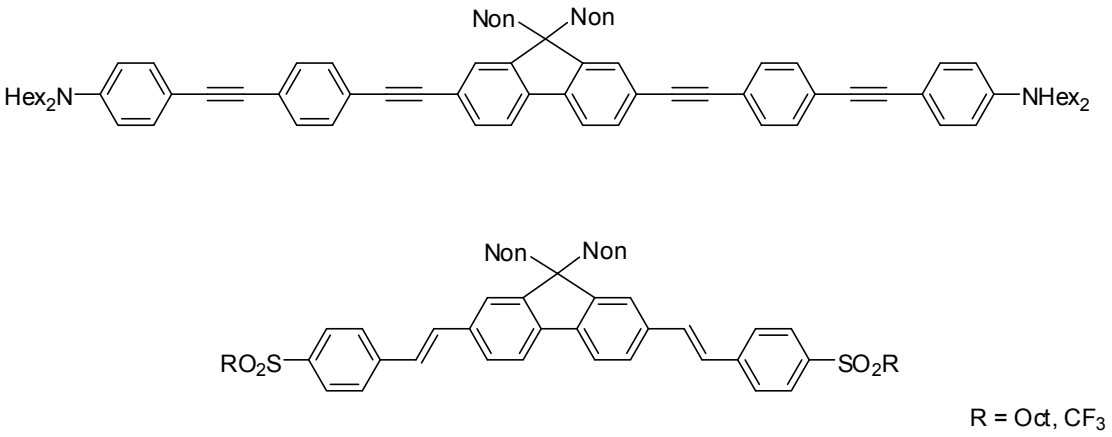

Figure 13 : Examples of TPEF active quadruploles

Furthermore, M. Blanchard-Desce *et al.* also synthesized two different fluorene based molecules (**Figure 14**), studied their TPA, and fluorescence at different pH.[29] They ended up by that fluorescence is strongly dependent of pH.

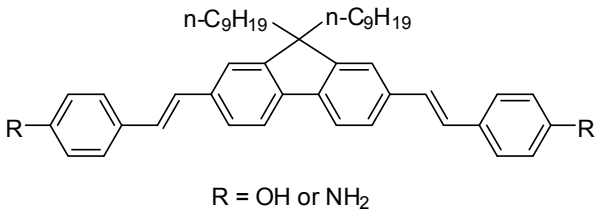

Figure 14 : Molecules studied by M. Blanchard-Desce

Based on these mentioned examples, we can tell that fluorenes are interesting as units to work with, having the advantage in modulating their physical properties by various functionalizations that serve one's target.

III. Electron and Energy transfer

Porphyrins by their nature and due to their spatial organization are responsible for energy and efficient electron transfer. To avoid mixing between these two mechanisms, it would be clearer if each is discussed separately.

1. Electron transfer

Simply, when a photosensible species is subjected to light, it passes from its fundamental state **P** to its excited state **P***. At the level of electrons, an electron migrates from the highest occupied molecular orbital (HOMO) to the lowest unoccupied molecular orbital (LUMO)[30] as presented in **Figure 15**.

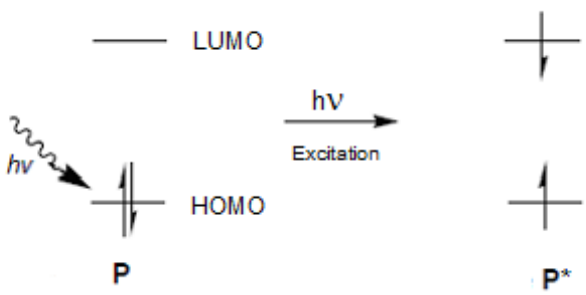

Figure 15 : Presentation of an excited chromophore

The fate of $\mathbf{P}^*$ depends on whether it will be in contact with electron rich or poor species. An electron transfer to the HOMO of $\mathbf{P}^*$ takes place in case of electron rich species. On the contrary, $\mathbf{P}^*$ loses an electron in case of electron poor species as presented in **Figure 16**.

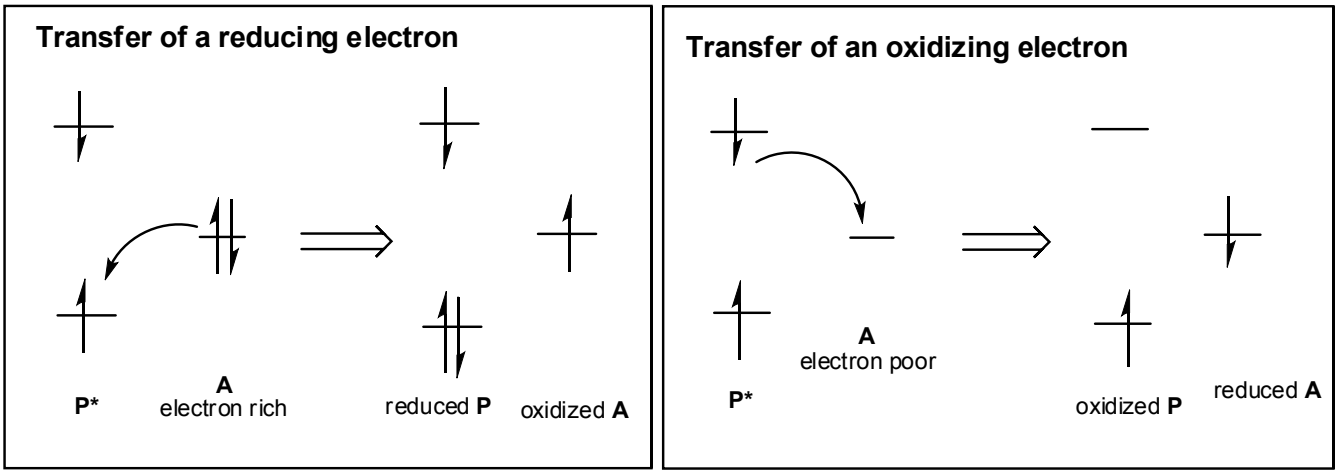

Figure 16 : Presentation of $\mathbf{P}^*$ trapped by a reducing or oxidizing electron

2. Energy transfer

When discussing energy transfer, we can differentiate between two different mechanisms : energy transfer can be dipole-induced (**Förster** or Coulombic)[31] or exchange-induced (**Dexter**).[32] The energy transfer could take place via the interaction between an excited chemical group, say **D*** (donor in its excited state), and a ground-state chemical group, say **A**, without emitting a photon when transferring energy.

In turn, after energy is transferred from **D*** to **A**, then **D*** goes back to its ground state **D** and **A** becomes in its excited state $\mathbf{A}^*$ as presented below in **Figure 17**.

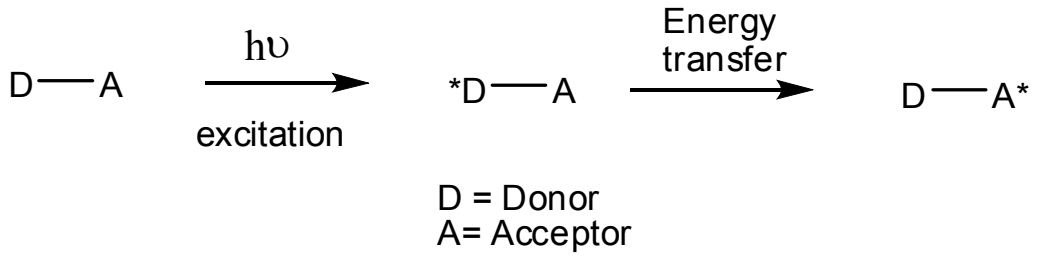

Figure 17 : Schematic presentation of **Energy Transfer** between **D*** and **A**

2.1. Dexter energy transfer

Dexter energy transfer is a process that two molecules (intermolecular) or two parts of a molecule (intramolecular) bilaterally exchange their electrons.[32] Dexter provided the mechanism that an excited donor group **D*** and an acceptor group **A** might indeed exchange electrons to accomplish the non-radiative process as seen in **Figure 18**. This exchange mechanism is also called the **short-range energy transfer**. That is because the reaction rate constant of Dexter energy transfer exponentially decays as the distance between these two species increases.

The exchange mechanism typically occurs within maximum 10 Angstroms.[32]

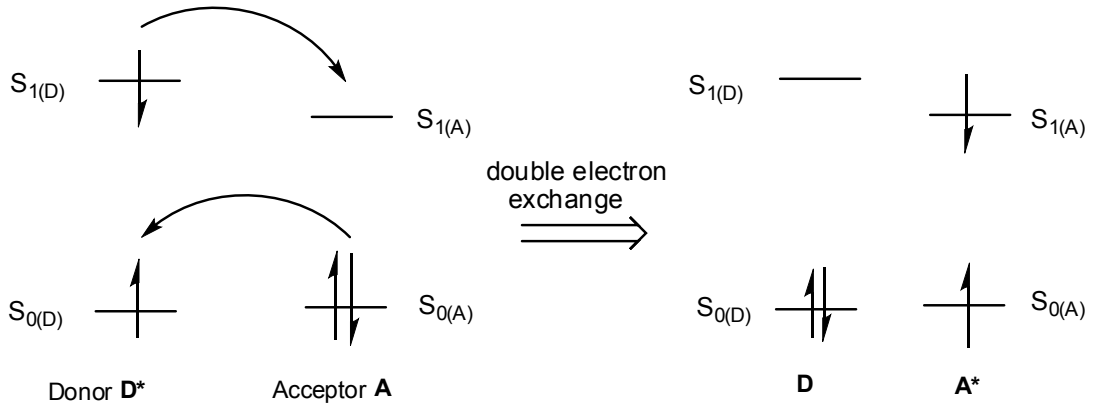

Figure 18 : Dexter type Energy Transfer

2.2. Förster energy transfer

Förster provided a model saying that the energy released from an excited donor **D*** could simultaneously excite the ground-state acceptor **A** based on the Coulombic interaction between these two chemical groups[31] as presented in **Figure 19**.

In more details, a donor chromophore **D**, initially in its electronic excited state **D***, may transfer energy to an acceptor chromophore **A** through nonradiative dipole–dipole coupling.

The efficiency of this energy transfer is inversely proportional to the sixth power of the distance between donor and acceptor.[31] So, the energy transfer rate depends on the strengths of the electronic transitions for donor and acceptor molecules, and requires resonance between donor fluorescence and acceptor absorption.

This mechanism occurs within 10 to 100 Angstroms.

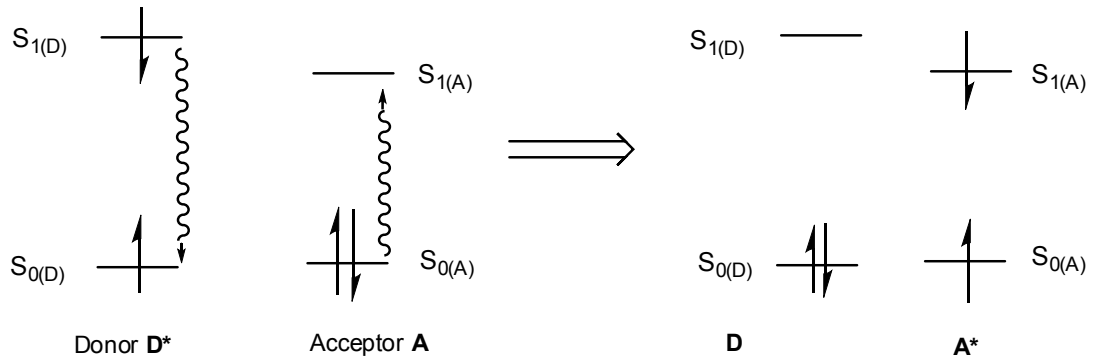

Figure 19 : Förster type energy transfer

IV. Conclusion

In this chapter, we present the two main monomers that constitute the center of the synthesis that will be presented in the next chapters : porphyrins and fluorene. State of art and history of synthesis, and synthetic strategies were discussed for porphyrins. In addition, porphyrin signatures in spectroscopic methods (NMR, CV, and UV) were mentioned as well. Since in the next chapters, there are many photophysical studies, the introduction includes the explanation of electron transfer and the two schools of energy transfer.

This thesis is mainly based on the synthesis of porphyrins for different objectives. In chapter two the target is to synthesize dendrimers having fluorenyl arms connected to porphyrin core to study photophysical properties.

In chapter three, the aim was to exploit the capacity of fluorene to exalt the luminescence. This target was achieved by the synthesis of a porphyrin dimer having six fluorenyl arms.

The third order of non linear optics is our concern for chapter four. So, synthesis of organometallic porphyrins assemblies bearing four ruthenium moieties is discussed. In addition, to benefit the dendritic effect for NLO measurements, an organometallic porphyrin dendrimer possessing twelve ruthenium species is reported as well.

The thesis is ended by chapter five where an interesting application of porphyrins in OLED fabrication is shown.

References :

1. Nencki, M.; Sieber, N. *Arch. Expt. Path. Pharmakol* **1884**, *18*, 401.
2. Kuster, W. *Physiol. Chem.* **1912**, *82*, 463.
3. Fischer, H.; Klarer, J. *Justus Liebigs Ann. Chem.* **1926**, *450*, 181.
4. Milgrom, L. R. *The Colours of Life: An Introduction to the Chemistry of Porphyrins and Related Compounds, Oxford University Press,* **1997**, *3*.
5. Rothemund, P. *J. Am. Chem. Soc.* **1935**, *57*, 2010.
6. Rothemund, P. J.; Menotti, A. R. *J. Am. Chem. Soc.* **1941**, *63*, 267.
7. Ball, R. H.; Dorough, G. D.; Calvin, M. *J. Am. Chem. Soc.* **1946**, *68*, 2278.
8. Adler, A. D.; Longo, F. R.; Finarelli, J. D.; Goldmacher, J.; Assour, J.; Korsakoff, L. *J. Org. Chem.* **1967**, *32*, 476.
9. Lindsey, J. S.; Hsu, H. C.; Schreiman, I. C. *Tetrahedron Lett.* **1986**, *27*, 4969.
10. Lindsey, J. S.; Schreiman, I. C.; Hsu, H. C.; Kearney, P. C.; Marguerettaz, A. M. *J. Org. Chem.* **1987**, *52*, 827.
11. Becker, E. D.; Bradley, R. B. *J. Chem. Phys.* **1959**, *31*, 1413.
12. Kadish, K. M.; Smith, K. M.; Guilard, R. *The Porphyrins Handbook,* **1999**, *5*, 7.
13. Kadish, K. M.; Smith, K. M.; Guilard, R. *The Porphyrins Handbook,* **1999**, *5*, 31.
14. Gouterman, M. *J. Mol. Spectrosc.* **1961**, *6*, 138.
15. Smith, K. M. *Porphyrins and Metalloporphyrins, Elsevier, Amsterdam* **1975**, 910.
16. Felton, R. H.; Linschitz, H. *J. Am. Chem. Soc* 1**966**, *88*, 1113.
17. Fajer, J.; Borg, D. C.; Forman, A.; Dolphin, D.; Felton, R. H. *J. Am. Chem. Soc.* **1970**, *92*, 3451.
18. Kadish, K. M.; Caemelbecke, E. V. *J. Solid State Electrochem.* **2003**, *7*, 254.
19. Williams, A. T. R.; Winfield, S. A.; Miller, J. N. *Analyst* **1983**, *108*, 1067.
20. Owens, J. W.; Smith, R.; Robinson, R.; Robins, M. *Inorg. Chim. Acta* **1998**, *279*, 226.
21. Zhang, X. H.; Xie, Z. Y.; Wu, F. P.; Zhou, L. L.; Wong, O. Y.; Lee, C. S.; Kwong, H. L.; Lee, S. T.; Wu, S. K. *Chem. Phys. Let.* **2003**, *382*, 561.
22. Demas, J. N.; Crosby, G. A. *J. Phys. Chem.* **1971**, *75*, 991.
23. Wong, W.-Y. *Coord. Chem. Rev.* **2005**, *249*, 971.
24. Wong, W.-Y.; Choi, K.-H.; Lu, G.-L.; Shi, J.-X.; Lai, P.-Y.; Chan, S.-M. *Organomettalics* **2001**, *20*, 5446.
25. Neher, D. *Macromol. Rapid. Commun.* **2001**, *22*, 1365.

26. Reinhardt, B. A.; Brott, L. L.; Clarson, S. J.; Dillard, A. G.; Bhatt, J. C.; Kannan, R.; Yuan, L.; He, G. S.; Prasad, P. N. *Chem. Mater.* **1998**, *10*, 1863.
27. Kim, O.-K.; Lee, K.-S.; Huang, Z.; Heuer, W. B.; Paik-Sung, C. S. *Opt. Mater.* **2002**, *21*, 559.
28. Mongin, O.; Porrès, L.; Charlot, M.; Katan, C.; Blanchard-Desce, M. *Chem. Eur. J.* **2007**, *13*, 1481.
29. Katan, C.; Charlot, M.; Mongin, O.; Ledroumaguet, C.; Jouikov, V.; Terenziani, F.; Badaeva, E.; Tretiak, S.; Blanchard-Desce, M. *J. Phys. Chem. B* **2010**, *114*, 3152.
30. Ward, M. D. *Chem. Soc. Rev.* **1997**, *26*, 365.
31. Förster, T. *Ann. Phys.* **1948**, *2*, 55.
32. Dexter, D. L. *J. Chem. Phys.* **1953**, *21*, 836.

Chapter 2

Synthesis of Porphyrin Dendrimers

I. The dendrimers

1. Introduction and generalities about dendrimers

A dendrimer is a hyper-branched molecule with well defined arborescent structure. It is composed of multiple branched monomers that elongate from a poly functionalized central core. Synthesis of dendrimers is based on repetitive reactions developing different and high generations. A generation is defined by the number of branch points encountered upon moving from the core to the periphery. After few generations, a dendrimer generally adopts a spherical form where steric hindrance becomes important. Since these molecules are prepared in a stepwise fashion, the products are theoretically monodisperse in size.[1] In fact, a monodisperse molecule is extremely desirable due to its synthetic reproducibility.

Detailing the structure of this class of macromolecules, we can define three basic important regions of the dendrimer. They are : the central functionalized core, the dendritic branches or the interior, and the periphery or end groups (**Figure 1**).

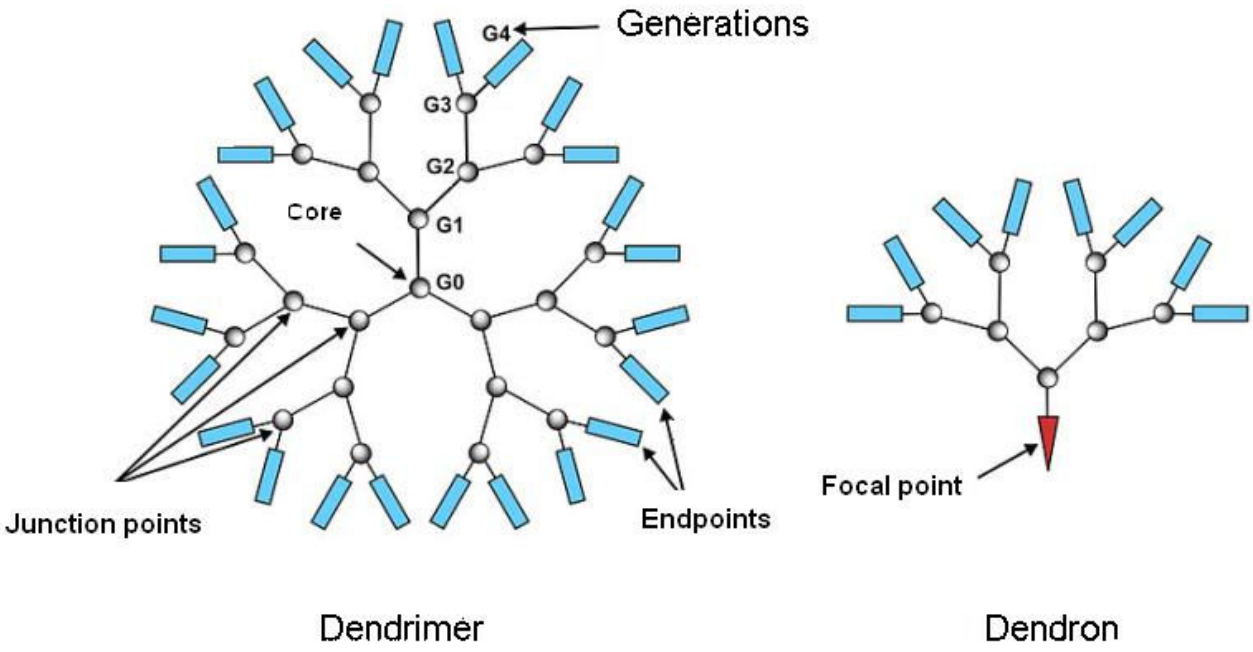

Figure 1 : The architecture of the dendrimer

2. History

Starting from the word itself, dendrimer comes from the greek language where it is the derivative of the words "*dendros*" and "*meros*". *Dendros* means tree or branch, and *meros* signifies a part of.

Going to chemistry, the first example of dendrimers was reported in 1978 by Vögtle and coworkers.[2] It was known as the cascade synthesis. This field developed slowly through the 1980s. In1981, Dekenwalter *et al.* described dendritic polylysine.[3] A few years later, Tomalia *et al.* reported the synthesis and the characterization of the first dendritic family which is now commercialized as PAMAM dendrimers.[1] In 1985, Newkome *et al.* reported initial results about the synthesis of tribranched dendritic amides.[4] Further developments occurred in the late 1980s till the review of Tomalia[5] refreshed the research that continued to the present including the synthesis of the polyester dendrimers.[6]

Two strategies have been formulated for dendrimer synthesis. One is the **divergent** synthesis (building from the core outwards) that was used by Tomalia,[1] Vögtle[2] and Newkome.[4] Another strategy is the **convergent** synthesis (building from the periphery inwards using wedges or dendrons) as it was used by Fréchet[7] and Miller[8] in the 1990s.

3. Synthetic strategies

3.1. Divergent Synthesis

Using this strategy, dendrimers grow outward from a multifunctional core. First the core reacts with monomeric molecules containing one reactive group. Then, for the next generation, the new periphery of the molecule reacts with more monomers as illustrated in **Scheme 1**. The presented compound is considered as the first example of polyester dendrimers[9] using divergent synthesis.

As the reaction is repeated as more generations are generated. Clearly, we can detect an advantage of this synthetic route which is the less steric problems due to the fact that small monomers are coupled each time. In addition, the excess of these monomers could be purified relatively easier due to the difference of sizes of the generation of this dendrimer and the monomer. In other words, a defect free product is guaranteed. On the other hand, as a disadvantage of this synthetic route is the difficulty to detect and to remove structurally impure dendrimers in which the added unit didn't react at every site.

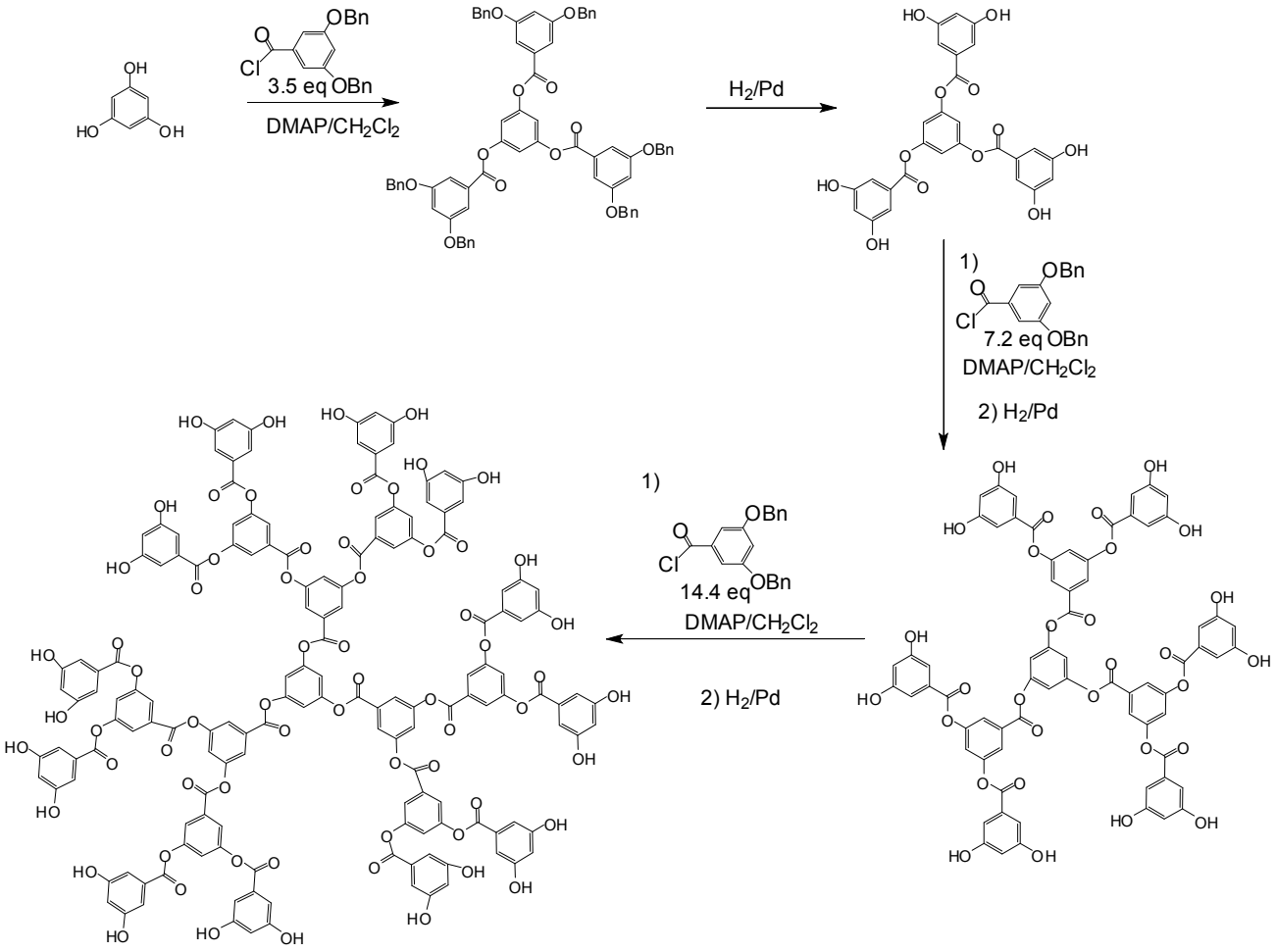

Scheme 1 : Example of divergent approach of dendrimer synthesis

3.2. Convergent Synthesis

Following this approach, the units, or the dendrons will be attached to the core which means that the dendrons must be synthesized first, then coupled to the porphyrin core. In other words, for every generation, a dendron of the desired size (depending on the generation) will be synthesized to be coupled to the core as it is shown in **Scheme 2**, that illustrates the first convergent synthesis of a polyester dendrimer.[10]

This means that fewer sites are reacted at each step. This fact lowers the chance to get structurally imperfect dendrimers, so it may be easier to purify them in case of having such

impurities. Moreover, the composition of the core doesn't need to tolerate all the reaction conditions since the core has to deal only with the final reaction of the dendrimer synthesis, which is grafting the desired dendron to the core. In other words, this method gives a flexibility to the used core. However, steric problems could be reached earlier in this method where a limit is obtained when big dendrons could not be grafted totally to the core.

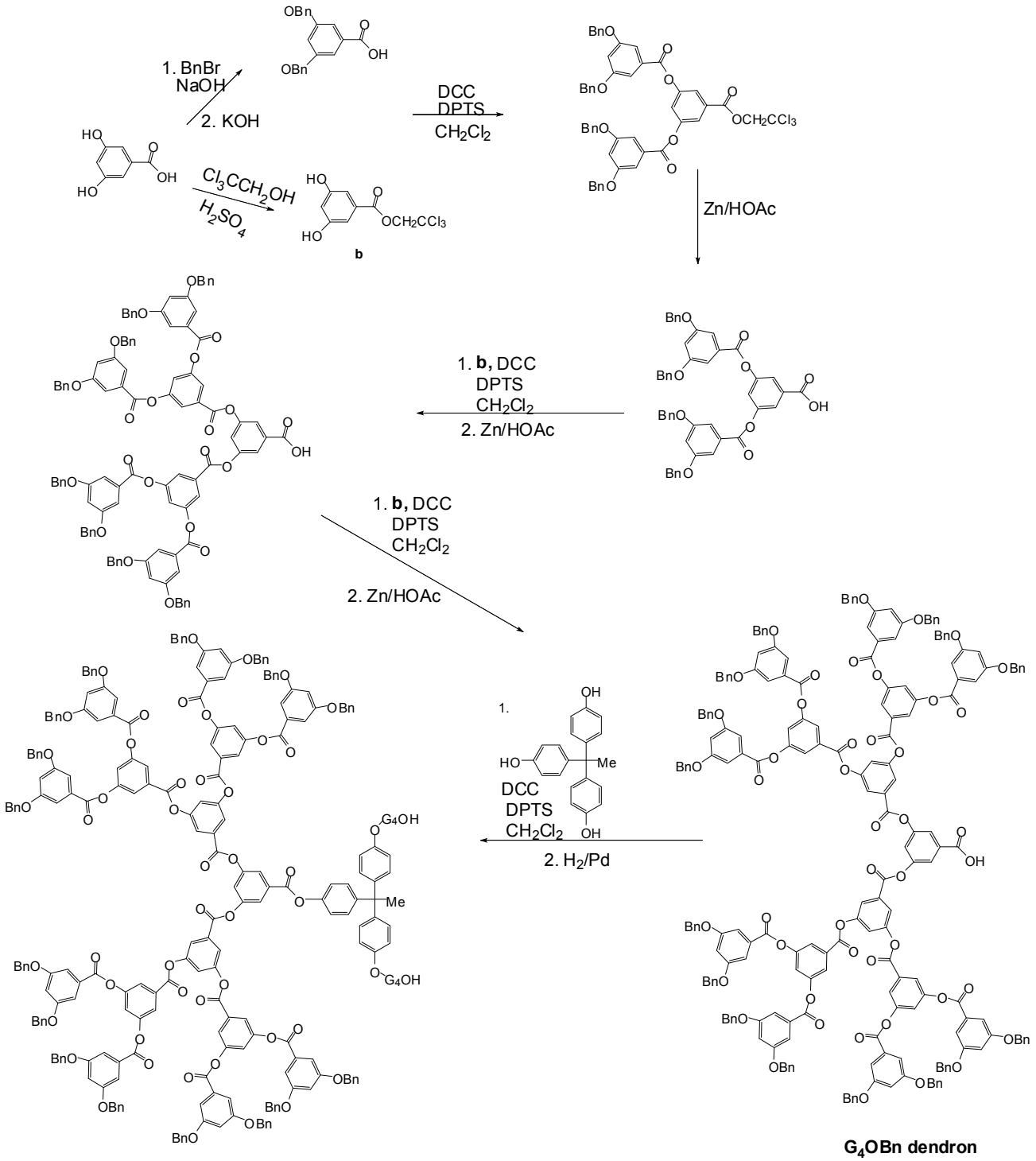

Scheme 2 : Example of convergent synthesis of polyester dendrimer

As one can see, both methods have their pros and cons and both are used in dendrimer synthesis. As a final point, the choice of the method is highly dependent on the size and the structure of the desired dendrimer.

4. Porphyrin dendrimers

After we had a general look on dendrimers, it is the time to spot the light on what concerns us which is a special class of these macromolecules: **The porphyrin dendrimers**.

The first example of porphyrin dendrimers was developed by Aida[11] in 1993. Six months later another example was demonstrated by Diederich *et al.*[12] who synthesized polyether amide porphyrin dendrimers. Then polyaryl ester porphyrin dendrimers were developed by Suslick *et coll.*[13] Concerning the reaction site, the majority of porphyrin dendrimers were synthesized by substituting the *meso* position by using either convergent or divergent synthesis. For example, Diederich adapted the divergent method to synthesize polyether amide dendrimer starting from the porphyrin core. On the other hand, Fréchet has developed the convergent synthesis by synthesizing the polyether benzyl dendron which can react with pyrrole to form the desired porphyrin. This method was useful enough so that it was applied later for porphyrin dendrimer synthesis based on carbazole[14] and truxene[15] units.

Although most of porphyrin core used for the synthesis of porphyrin dendrimers are substituted at the *meso* position, but we can still find examples of both *meso* and *beta* substitution at the same time as mentioned by Vinogradov *et coll*. in 2003[16] when the porphyrin core was substituted at both *meso* and *beta* positions by polyester amide dendrons. Moreover, in 2007, Zhao[17] presented porphyrin dendrimers where porphyrin core was substituted on its axial positions.

After detailing the synthesis of porphyrins, our interest is then to study the photophysical properties. Our choice of porphyrin dendrimers to achieve our target was based on the literature examples that support our choice. For example Aida[18] showed in 1998, the effect of the number of grafted dendrons on the porphyrin core *versus* the quantum yield. In other words, Aida showed that the tetra substituted porphyrin had the highest yield compared to the corresponding tri, di, and mono substituted porphyrin core. In addition, energy transfer from antennae (dendrons) to the porphyrin core was very efficient.

What confirms more the interest of the dendritic structure is the study made in 2002[19] where a comparative study of site isolation as a function of architecture was demonstrated for the first time.

This study shows that photophysical properties show significant differences based on architecture. In more details, a comparative photophysical study was carried on the following series shown in **Figure 2** below.

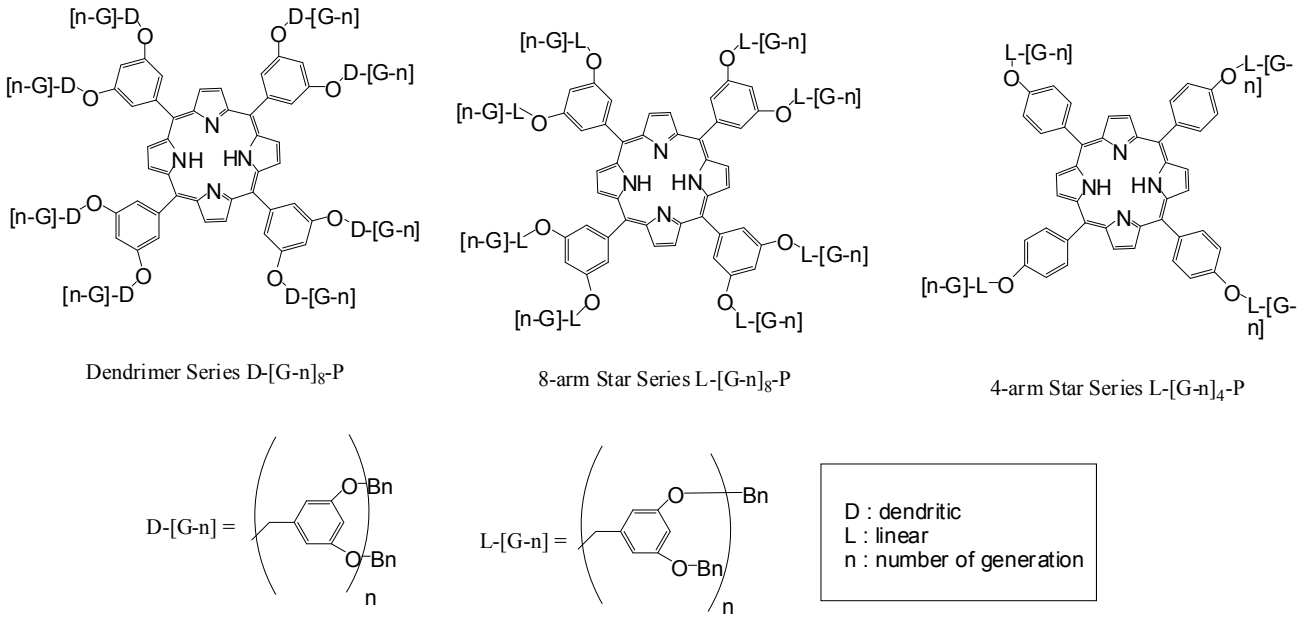

Figure 2 : Porphyrins of linear (L) and dendritic (D) substituents

As a summary of the photophysical study that was carried by Fréchet *et coll.*[19] on this series, it was shown that the energy transduction of the polybenzyl ether (the dendrons used in this case) to the core (porphyrin) was found to be facilitated in the dendritic case, whereas energy transfer decreases in the linear case at high molecular weights. Energy transfer was efficient in the case of dendrimers even in high generations. This observation was explained due to the relatively short distances that are maintained between the internal donor units and the acceptor core that suggests superior encapsulation properties of the dendritic structure.

Another study was done in 2005[20] where it was shown that the most efficient energy transfer was in the case of porphyrin dendrimers. In more details, light absorbed by the peripheral carbazole chromophores (dendrons in this case) was transferred to the porphyrin core and these new dendrimers were regarded as efficient light harvesting antenna systems having the porphyrin subunits as energy trap.

5. Conclusion

Based on what has been mentioned, we can conclude that the combination of the advantages of dendritic structure and the porphyrin as a core will be promising to expect efficient energy transfer. In summary, these molecules could be good candidates for further applications.

Since the porphyrin skeleton permits to attach easily four or more energy donors, it is possible to design and synthesize porphyrin dendrimers that contain a variety of organized chromophoric groups to expect efficient energy transfer. Consequently, the aim in this part of the thesis is to synthesize new porphyrin dendrimers and study their photophysical properties.

II. Synthesis and study of new porphyrin dendrimers for collecting light

1. Introduction

A series of new porphyrins has been recently synthesized in our group. One of these porphyrins is the tetrafluorenylporphyrin (**TFP**) where a porphyrin macrocycle is tetrasubstituted by fluorenyl groups at the *meso* position. **TFP** (**5**) has attracted the attention due to its interesting photophysical properties with respect to tetraphenylporphyrin (**TPP**) as a selected reference. The fluorescence quantum yield of **TFP** is 24% when measured in dichloromethane at room temperature.[21,22] This yield is surprisingly high for porphyrins[23] and is double than that of **TPP** (12%). To better understand the effect or the role of fluorene as substituents, it is worth to mention the following examples: difluorenyl-diphenylporphyrin (**DFDPP**), and difluorenyl-dihydrogenporphyrin (**DFDHP**) (**Figure 3**) synthesized by our group.

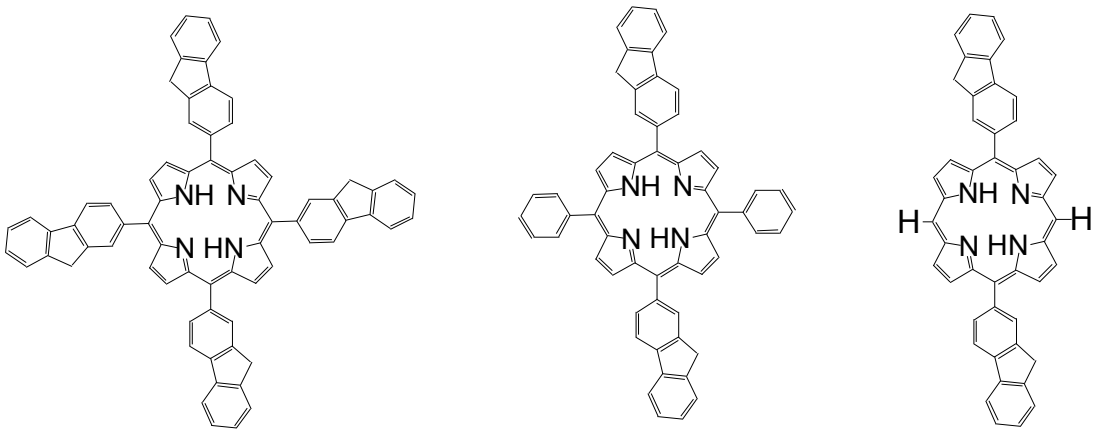

TFP (5) **DFDPP** **DFDHP**

Figure 3 : Porphyrins substituted by fluorenyl arms at *meso* position

Complete luminescence studies of **TFP**, **DFDPP**, and **DFDHP** were done in Durham University (UK) as a collaboration with **Pr. J. A. Williams**. It was shown that following selective excitation of the fluorene arms with UV light shows that the energy transfer process from the fluorene arms to the porphyrin cycle is very efficient.[24] Comparing these three compounds, mainly their excitation spectra, energy transfer is nearly complete in the case of **TFP** where residual emission from the fluorenyl chromophores was observed in the case of **DFDPP**, and **DFDHP**. As a result, energy transfer to the porphyrin core was not total in that case. Furthermore, it was noticed that the quantum

yield increases with the number of the fluorene groups. Eventually, what has been shown focuses on the influence of the presence of fluorene arms for improved luminescence properties.

Based on these interesting results, the objective in the laboratory is to obtain highly luminescent soluble organic compounds having a porphyrin core possessing fluorenyl arms since they could be promising candidates to access luminescent materials after electro-polymerization.[21] On the other hand, as mentioned before, Fréchet has demonstrated that the antennae effect is facilitated in dendritic case *versus* the corresponding linear case.[19]

So, combining all these previous mentioned factors, a new series of dendrimers of three different generations $\mathbf{G_0}$: tetra-oxyfluorenylphenylporphyrin (**TOFP**), $\mathbf{G_1}$: octa-oxyfluorenylphenylporphyrin (**OOFP**), and $\mathbf{G_2}$: sixteen-oxyfluorenylphenylporphyrin (**SOFP**) bearing four, eight,[25] and sixteen[26] fluorenyl arms, respectively (**Figure 4**) having functionalized porphyrin macrocyle as a core, was synthesized recently in our laboratory.

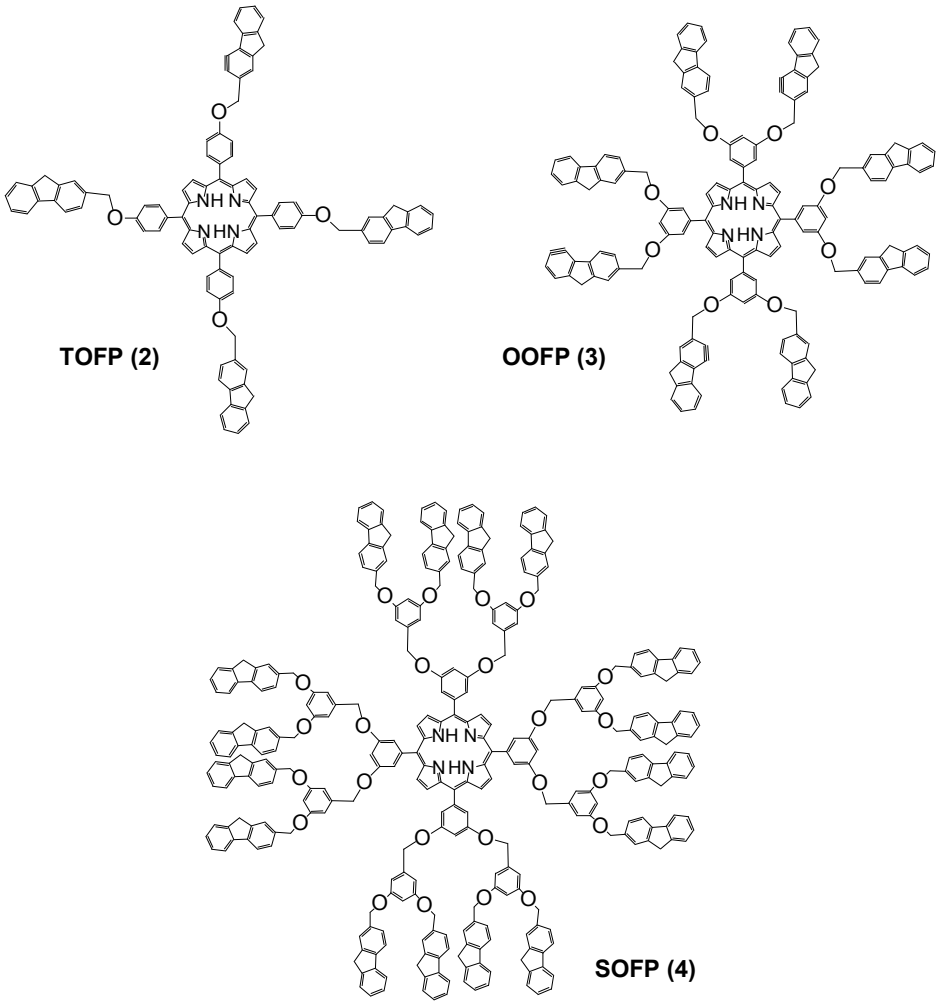

Figure 4 : Consecutive generation of porphyrin dendrimers

Concerning the UV-visible absorption spectra, we can see that the Soret bands of the compounds **2**, **3**, and **4** are similar and around 423 nm (**Figure 5**). Another thing to notice is that this band is slightly red shifted with respect to the reference **TPP** (417 nm) but not to the extent of **TFP** (426 nm). Similar red shift is observed for the Q bands as well. The π-π* absorption in the UV range is clearly apparent, due to the presence of fluorenyl arms. It is remarkable that the intensity of the absorption at around 270 nm is more important in the case of **4** : it is nearly as intense as that of the Soret band. So, here comes the positive effect of increasing the number of fluorenyl arms. Consequently, it is important for light–harvesting optimization to try to access to higher generation porphyrin dendrimer.

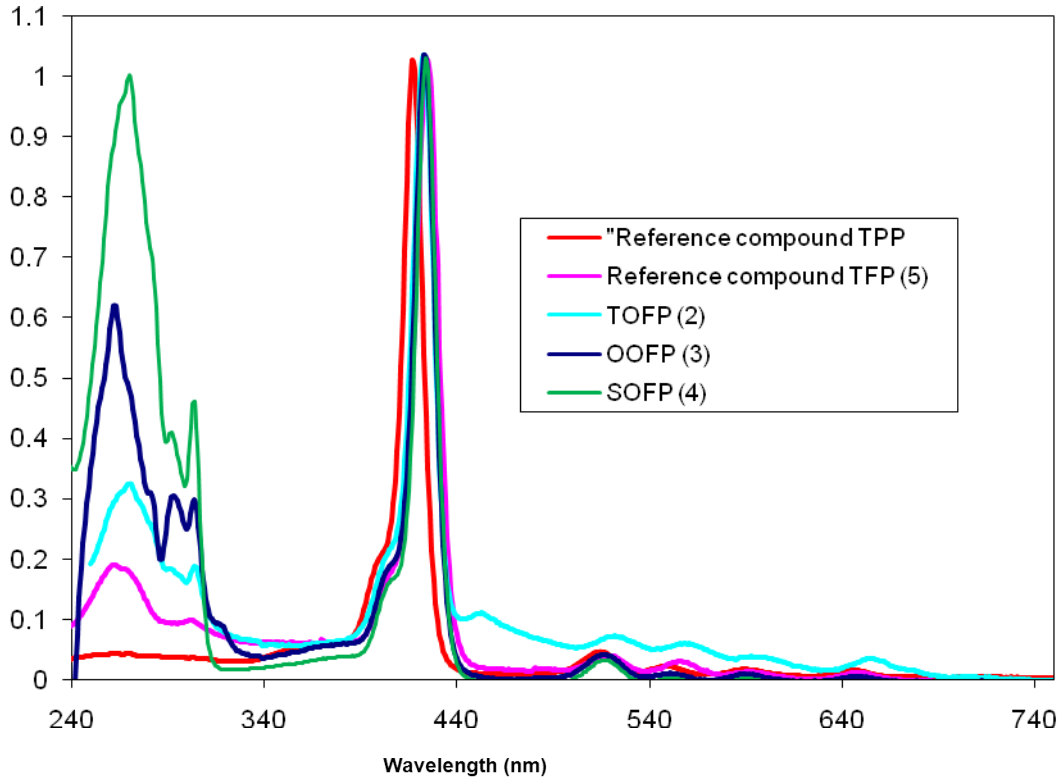

Figure 5 : Absorption spectra of **TPP** (red), **5** (pink), **2** (blue), **3** (dark blue) and **4** (green) in chloroform at room temperature. All the spectra are normalized to the spectrum of **the reference TPP** at 417 nm (concentration ~2.0 10^{-6} M).

In specific, the photophysical properties of these dendrimers were interesting proving the proportional increase of the quantum yield as a function of the number of fluorenyl arms. In specific, the luminescence quantum yield of **2**, **3**, and **4** is 12, 13, and 14% respectively.[26] In addition, the

energy transfer from the fluorene substituents to the porphyrin core was nearly complete.[26] Results were motivating to go on more synthesis reaching higher generations of these dendrimers to exploit the capacity of fluorine. So, the new target molecule is a porphyrin dendrimer with 32 fluorene arms (**Figure 6**) where the question is : will energy be transferred from the arms to the core, and what would be the quantum yield of this new high generation dendrimer?

2. Synthesis of the precursors of the porphyrin dendrimers

Based on the discussion of the synthetic modes of dendrimer synthesis, the **convergent** route is preferred in our case. The synthesis of such dendritic systems requires the preparation of dendritic fragments that could be coupled to a multifunctional core.

More precisely, to reach our target - the **32F** - a dendron bearing four fluorenyl groups **13** and a porphyrin core **7** with eight hydroxyl groups, that permit the grafting of the dendron, were synthesized (**Figure 6**).

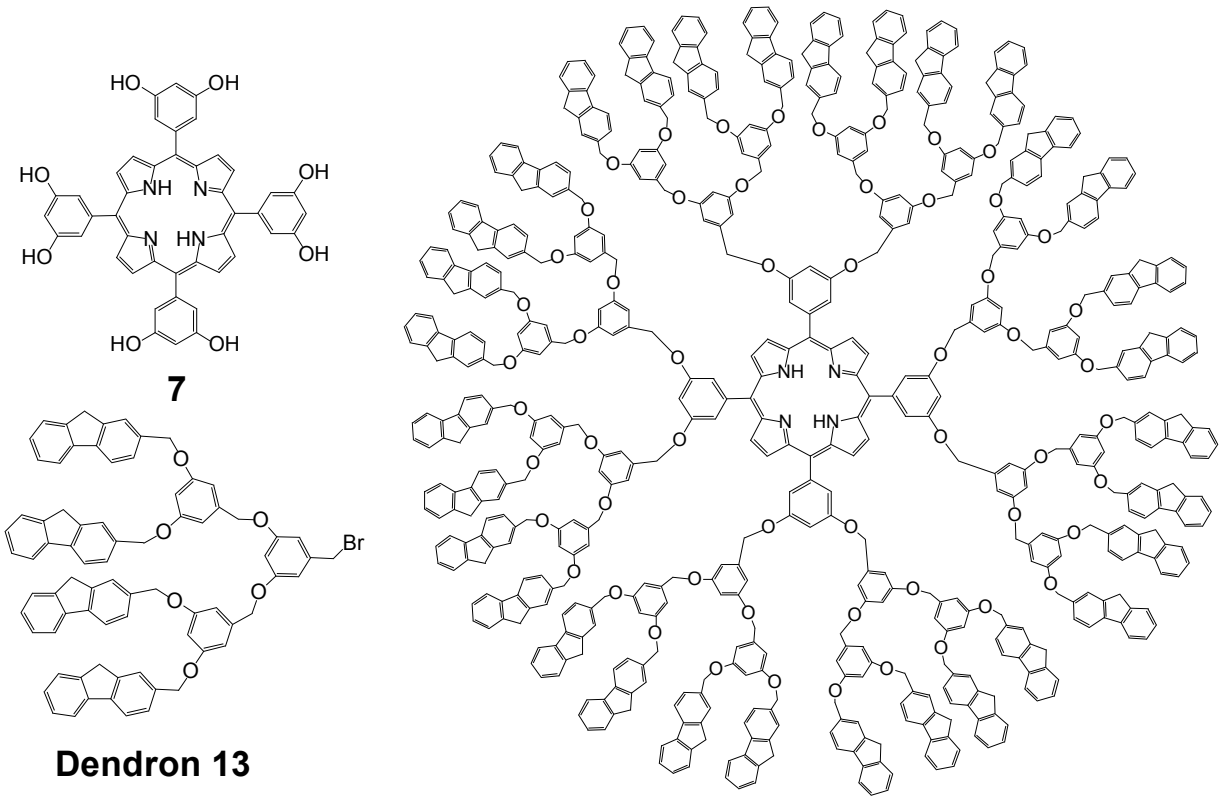

Figure 6 : New Dendron **13** and porphyrin **7** to be used for the synthesis of the **32F**

2.1. Synthesis of the tetrakis(3',5'-dihydroxyphenyl)-porphyrin (7)

This porphyrin core **7** was prepared in two steps. First the protected form - porphyrin **6** - was obtained using Adler et Longo's method[27] by refluxing the commercially available aldehyde (3,5-dimethoxybenzaldehyde) and pyrrole in propanoic acid. Then, the methoxy groups of **6** were deprotected under the action of tribromoborane in dichloromethane to give **7** with the eight hydroxyl groups (**Scheme 3**).

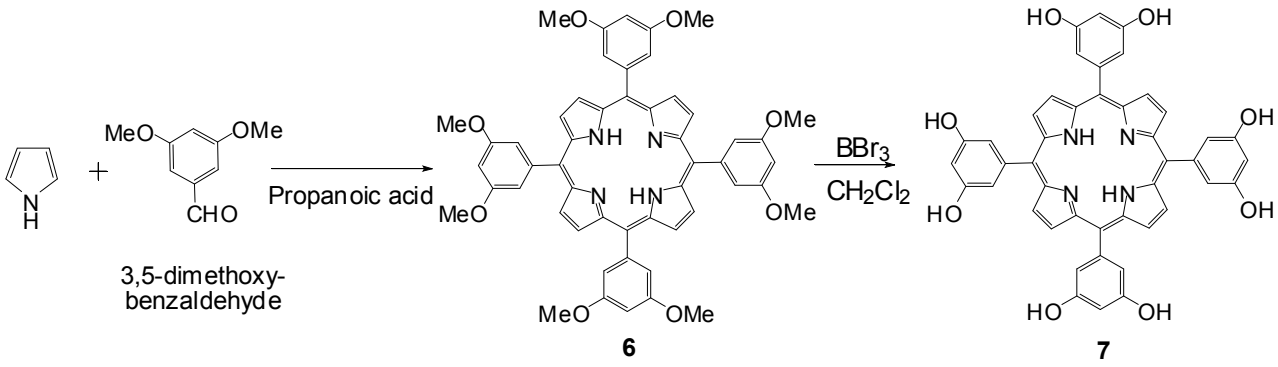

Scheme 3 : Synthesis of the porphyrin precursor **7**

Having the hydroxyl groups, on a phenyl at the *meso* position, proposes a Williamson coupling with bromo derived dendrons. So, as a next step comes the synthesis of the proposed dendron **13** with four fluorene groups to achieve the target : the **32F** porphyrin dendrimer.

2.2. Synthesis of the dendron 13

A key step in the synthesis of dendron **13** was repetitive reactions of Appel reaction[28] followed by Williamson condensation.[29] First, this series of reactions starts by reducing the fluorene-2-carboxaldehyde - which is a commercially available compound - into its corresponding alcohol **8** under the action of sodium borohydride in ethanol. Bromination of **8** was achieved using carbontetrabromide and triphenylphosphine in THF to get **9**. The detailed characterization and synthesis of **8** and **9** were reported earlier where **9** was used as the dendron to get **TOFP**.[25] As a next step is a Williamson condensation between **9** and 5-hydroxymethyl-benzen-1,3-diol in basic conditions to obtain **10** as a white solid. In turn, **10** was brominated using same conditions as for **8** and then purified over silica gel to yield **11** as a white solid (**Scheme 4**).

In addition, dendrons **10** and **11** were reported[26] since **11** was used to synthesize **OOFP** and **SOFP**, compounds **3** and **4** respectively.

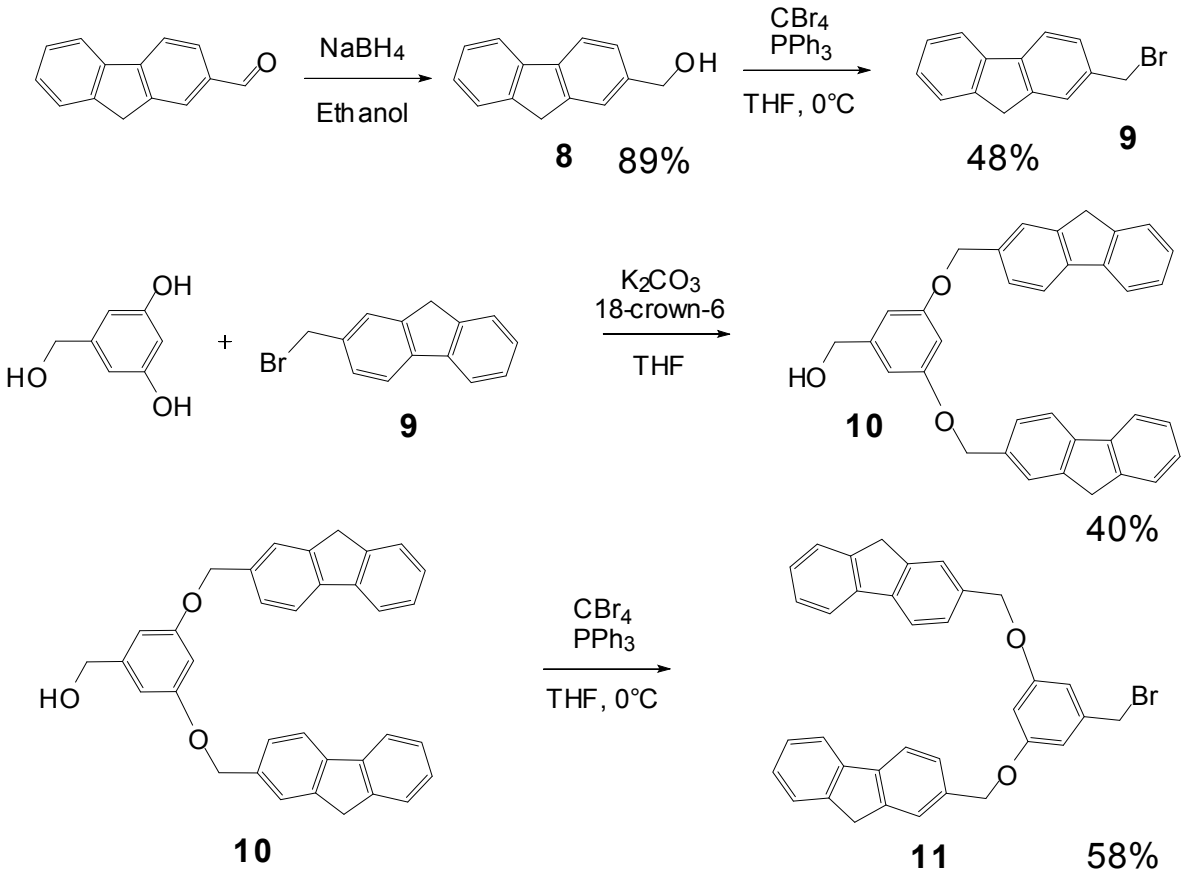

Scheme 4 : Synthesis of the dendrons **9**, **10**, and **11**

Consequently, the new tetrapod dendron **12** was obtained by the condensation of **11** with 5-hydroxymethyl-benzen-1,3-diol using potassium carbonate as a base in the presence of 18-crown-6 in dry THF. Purification of **12** over silica gel gave a pure white solid with 70% yield. In turn, **12** was brominated using carbon tetrabromide and triphenylphosphine in dry THF to get **13** (**Scheme 5**) as a yellow powder after purifying the crude product over silica gel.

It is worth to mention a point concerning the solubility, since normally alkyl chains are introduced on the position 9 of the fluorenyl arms to increase the solubility.[30] Since compounds **2**, **3**, and **4** are soluble and no problems were faced concerning this issue, alkyl groups are not introduced to the fluorenyl arms.

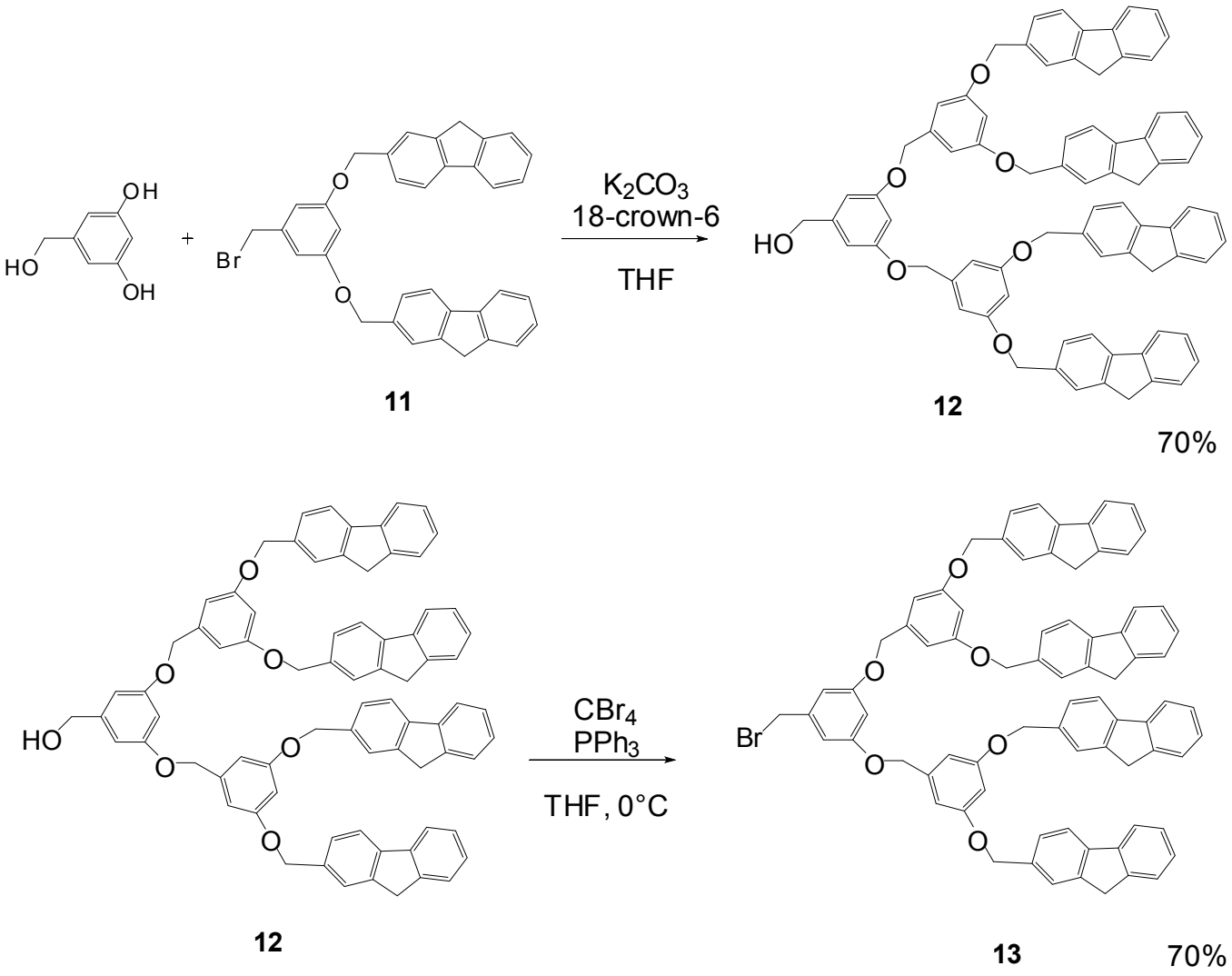

Scheme 5 : Synthesis of dendrons **12**, and **13**

3. Synthesis of the target dendrimer

Having the precursors prepared, here comes the final step to get our **32F** dendrimer which is grafting eight of the new dendron **13** to the functionalized porphyrin **7**. To do so, a classical Williamson reaction conditions is applied where 10 equivalents of **13** are reacted with one equivalent of **7** under basic conditions using potassium carbonate and 18-crown 6 in dry THF (**Scheme 6**).

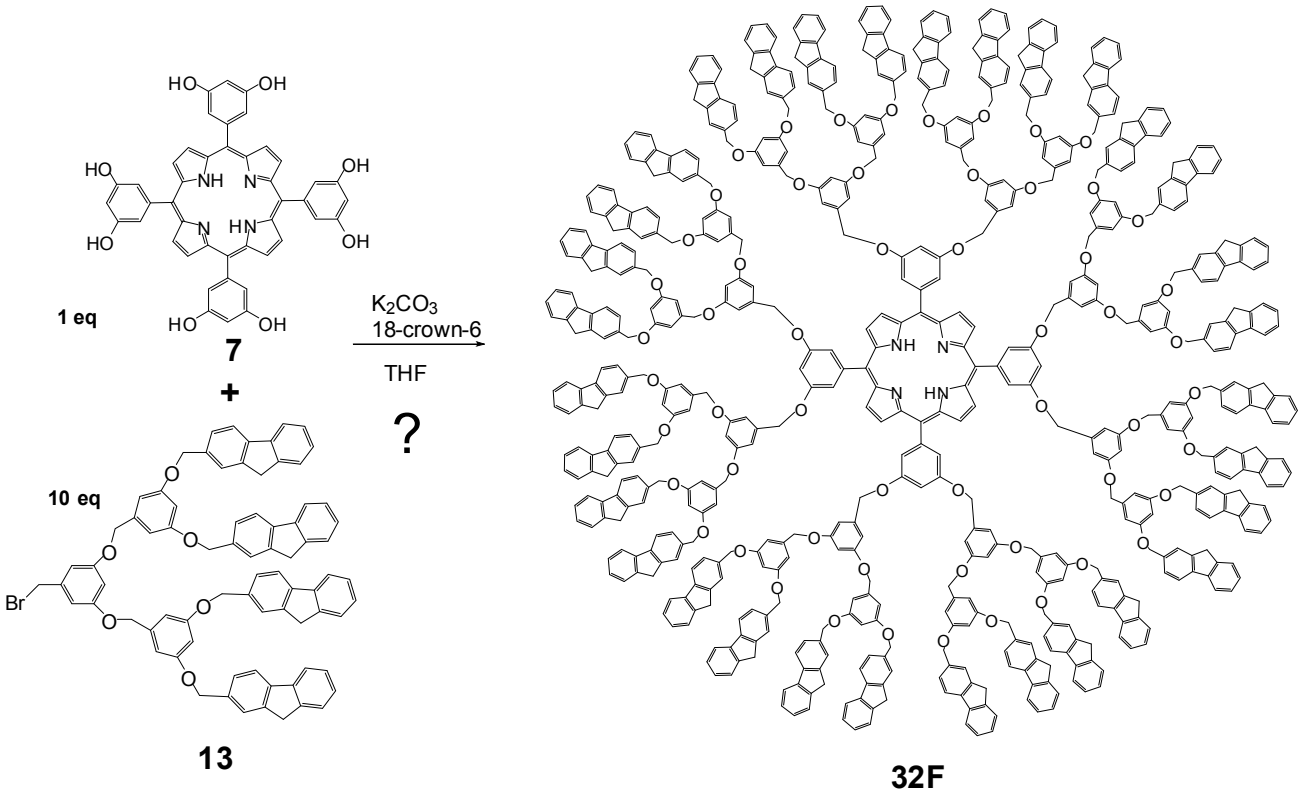

Scheme 6 : Attempt to synthesize dendrimer **32F**

Excess of **13** is used trying to favour total grafting and decreasing the possible by products. In such a reaction, we have the possibility to get mono, di, tri till total grafting of the Dendron to the macrocycle. The reaction progress was monitored by TLC spotting directly from the organic phase.

Furthermore, proton NMR showed that various number of donor chromophores was fixed but total grafting was not confirmed. A mixture of different substituted dendrimers was observed.

Unfortunately, repeating the reaction many times, and leaving it more time, gave the same results. Raising the 10 equivalents of dendron **13** to 20 equivalents to force complete grafting gave same results as well. Thinking about why the reaction is not complete and total grafting is not observed, even by analyzing the crude mixture by the aid of mass analysis, didn't show any value that corresponds to **32F**, spots the light on the dendrimer size, hindrance, and starbust limit effect.

In fact, concerning the dendrimer chemistry, it is known that in the generation synthesis, it gets to a point where a limiting generation is reached. After this point, no dendrimer perfect structure is possible to be obtained. Reaching this limiting generation in dendrimer growth is considered as a result of the starburst limit effect. That could go back to the steric hindrance during the dendrimer

formation.[31] The starburst point occurs at a well defined limit of each dendrimer system.[32] It seems that we have reached it in our case. As a result, the third generation in this dendrimer series is the limit, where higher generations are not possible to be formed. In other words, our target, the **32F** is not reachable.

On the other hand, it was observed that in the basic conditions used, as shown in **Scheme 6**, a new product was obtained which is different from all possible side products. In fact, one of the protons in position-9 of the non substituted fluorenyl arms (compound **13**), can react. The non-protected carbon, in position-9, will in an intramolecular way, react with the bromomethyl group to form cycle **1** (**Scheme 7**). This new compound **1** was obtained as a pale yellow solid (52%), very soluble in most organic solvents and can be purified by column chromatography (silica gel) followed by precipitation (THF, heptane).

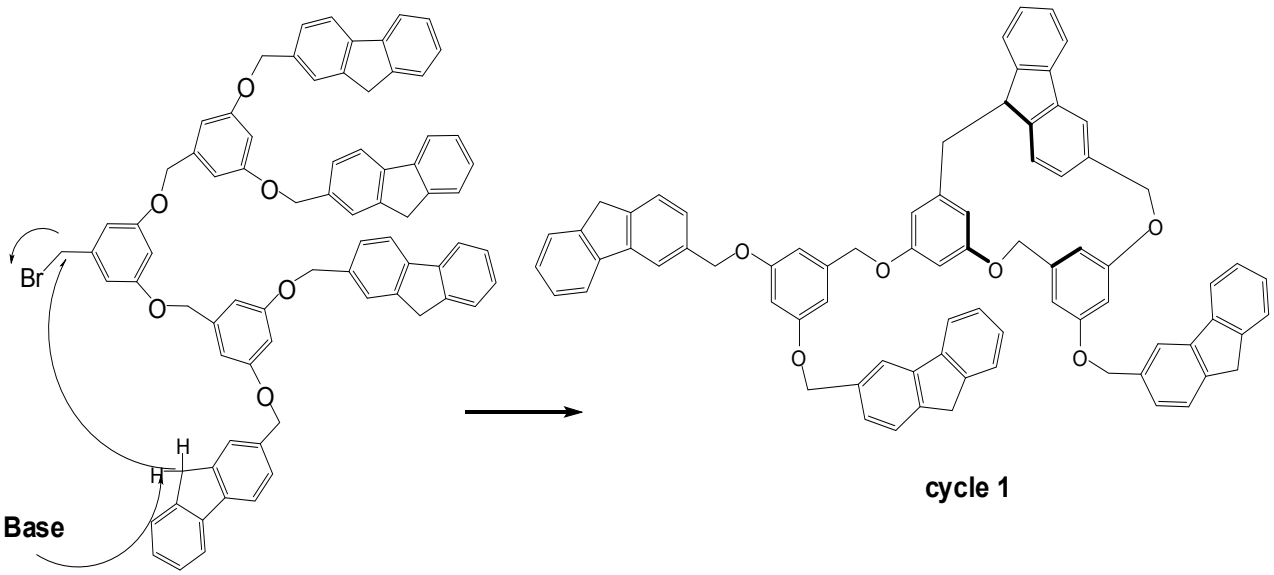

Scheme 7 : Mechanism of the formation of cycle **1**

Compound **1** was fully characterized by usual solution spectroscopies (NMR and mass spectrometry) and microanalysis.[33] The hydrogen and carbon atom-labeling scheme for this macrocycle **1** are shown in **Figure 7** for clear NMR analysis.

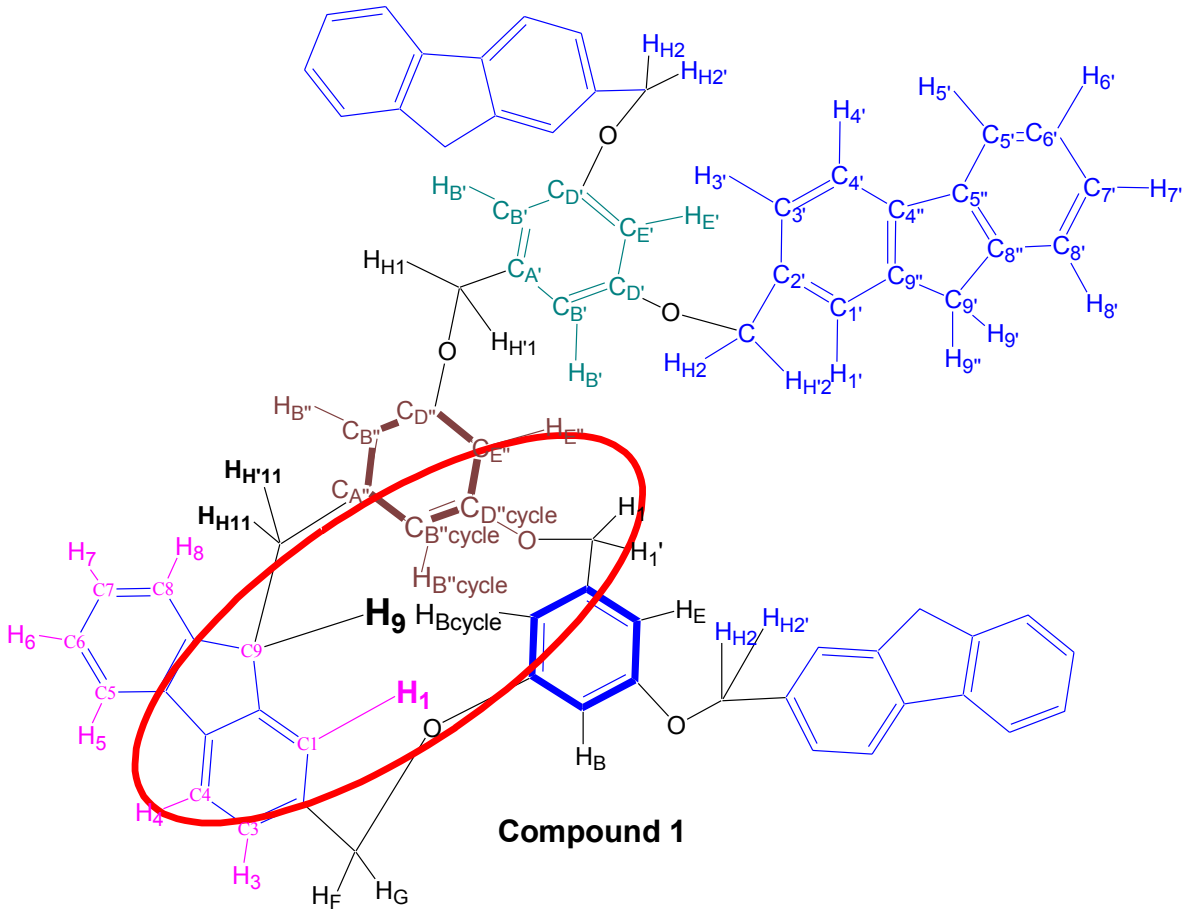

Figure 7 : Hydrogen and carbon atom-labeling for cycle **1**

3.1. NMR analysis

Starting with the dendrons, **12** and **13**, the **^{1}H NMR** signals obtained in deuterated chloroform for dendrons are fine and well resolved. For these two dendrons, there is only a clear difference in the shift of the protons of CH_2 group of the bromide ligand **13** $\underline{CH_2}Br$: $\delta = 4.38$ ppm and that of alcohol **12** $\underline{CH_2}OH$ at $\delta = 4.59$ ppm. As for the other peaks, they are quite similar.

As for the cycle **1**, the **^{1}H NMR** signals obtained in deuterated chloroform are fine and well resolved. A clear difference in shift is observed for the tetrapodal ligand **13** when free and in the corresponding tripodal cycle **1** (**Figure 8**). The latter is induced by the very close proximity of the benzyl groups shielding cone of the proton in the new formed cycle.

For example, the **^{1}H-NMR** spectrum of **1** reveals that the three ^{1}H resonances for proton in the position-9 of the fluorenyl (**H_9**-triplet) and CH_2 units (**H_{H11}** and **$H_{H'11}$** -doublet), are significantly up field of their positions in tetrapod ligand **12**, as expected for protons located within the shielding cone of benzyl groups (benzyl group in bold blue and brown, in **Figure 7**). This effect is particularly important for **H_9** (bold in **Figure 7**) with $\Delta\delta$ = -1.8 but weaker for **H_{H11}** and **$H_{H'11}$** (bold in **Figure 7**), with $\Delta\delta$ = -0.4 and $\Delta\delta$ = -0.7, these protons being on the CH_2 unit responsible for closing the cycle. These signals are also broader and less resolved, in line with the highly fluxional nature of the ligand at room temperature.

Similar shift is observed for **$H_{B"cycle}$** (δ at 6.02 ppm) but not for **H_{Bcycle}** (δ at 6.39 ppm), this difference is probably due to proximity to shielding cone of benzyl groups in the cycle.

Moreover, it is noticed that all the seven peripheral protons on the three non-cyclized fluorenyl arms are nearly equivalent, and in expected position : 7.80 ($H_{4'}$), 7.78 ($H_{5'}$), 7.59 ($H_{8'}$), 7.56 ($H_{3'}$), 7.33 ($H_{7'}$), 7.43-7.37 ($H_{1'}$ and $H_{6'}$).

On the contrary, the proton **H_1** (bold in **Figure 7**), on the cyclized fluorenyl group, is shifted to 6.44 ppm, so with an important up field of $\Delta\delta$ = -1.0, as before, due to be located within the shielding cone of benzyl groups (benzyl group in bold blue and brown in **Figure 7**). Whereas all the six other peripheral protons on the cyclized fluorenyl are in expected position : 7.72-7.62 (m, 3H, $H_{5\text{-}6\text{-}8}$) and 7.44 -7.36 (m, 3H, $H_{3\text{-}4\text{-}7}$).

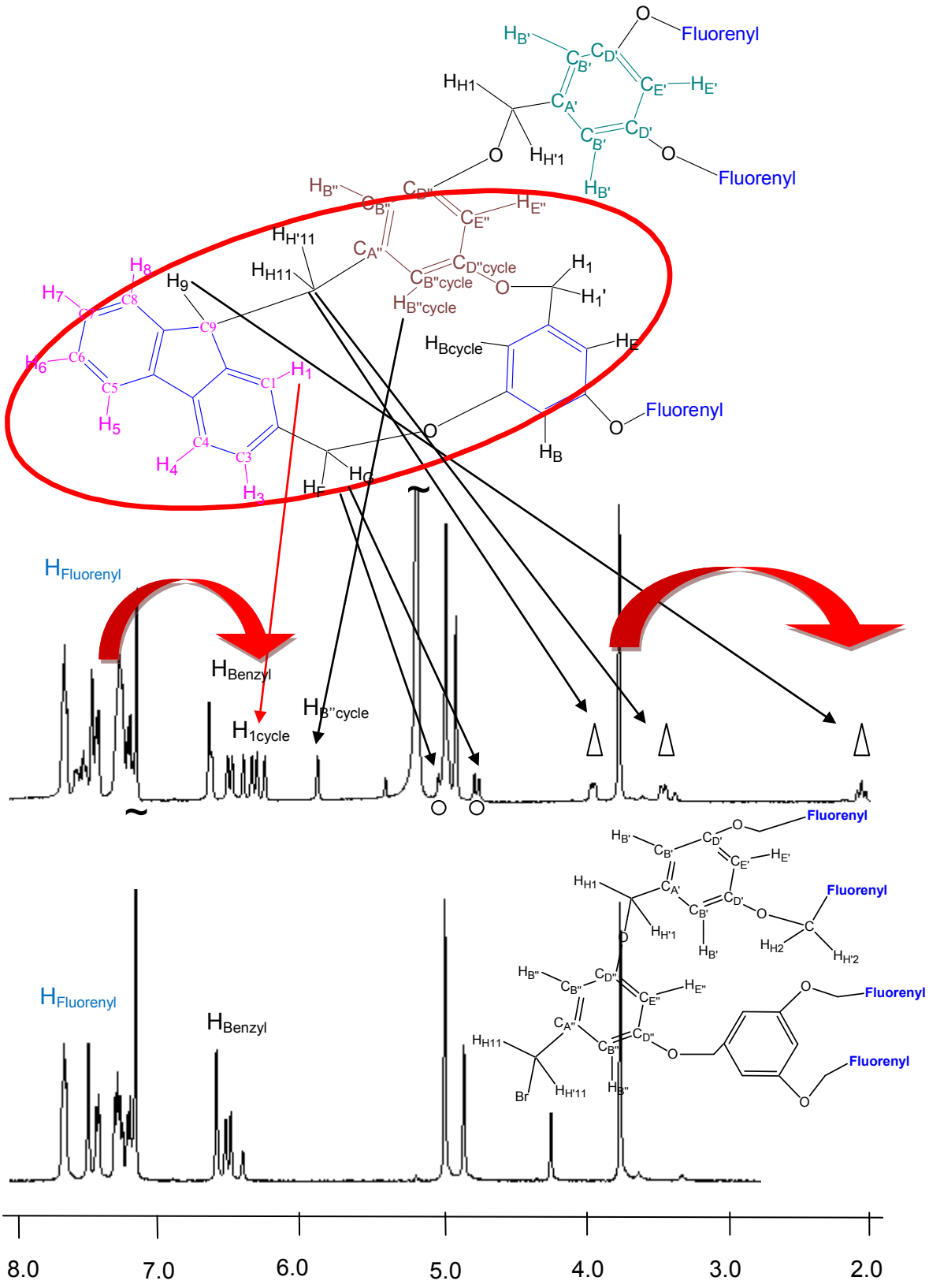

Figure 8 : ^{1}H-NMR studies (in $CDCl_3$) of free Dendron **13** in comparison to the cycle **1** (on the top with a CH_2Cl_2 pic), showing the shift for the cyclic fluorenyl as indicated by the arrows

III. Conclusion and perspectives

In conclusion, although the target **32F** - the dendrimer of higher generation - was not achieved, but it is still interesting to know the limit of this series. In addition, we can tell that the porphyrin dendrimers are of interesting photophysical properties. These dendrimers called the attention of many application fields (seen in chapter 5).

Since the mechanism of the formation of cycle **1** was known and understood, so it is worth to try the reaction another time trying to push the reaction toward the formation of **32F** if possible. In other words, it is to modify the dendron in a way to prevent the formation of this macrocycle. It is to synthesize protected fluorenyl arms, as seen in **Figure 9**. By this way, the formation of cycle **1** will be avoided. In addition, we might be able to force the reaction to go forward to the formation of **32F**. On the other hand, this will enhance the steric hindrance.

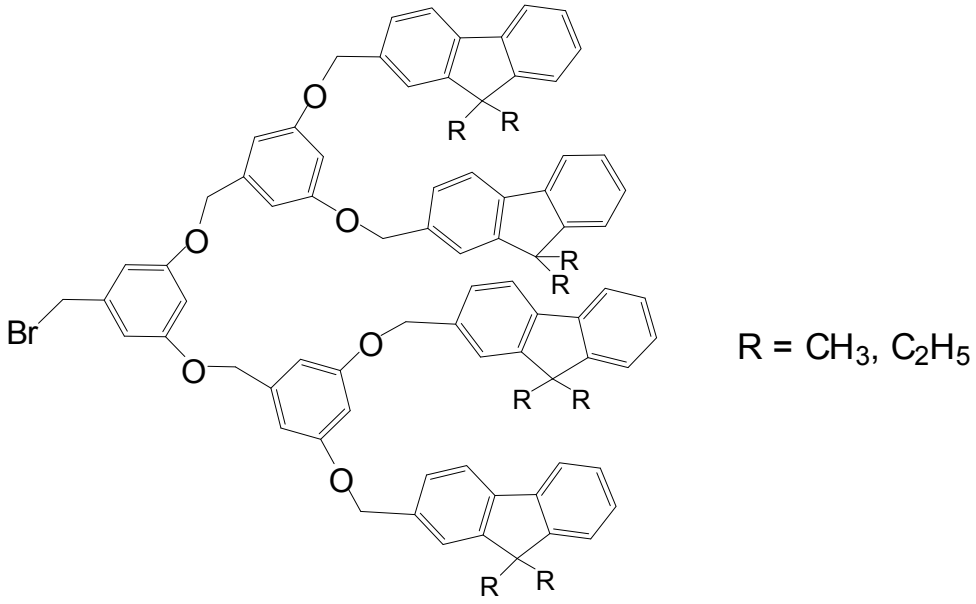

Figure 9 : Protected fluorenyl dendron

It is true that the work to get higher generations of this series is not achieved since the starburst point was reached, but our group is still working on porphyrin dendrimers.

A new project has been initiated in our laboratory, and is currently developed concerning the synthesis of **conjugated dendrimers**. In this case, advantages of the dendrimer effect and the conjugation properties will be mixed. This favors the use of these future compounds in different fields of applications.

Experimental Section

General experimental procedure

All reactions were performed under argon and were magnetically stirred. Solvents were distilled by using the appropriate drying agents. For example, THF was distilled using sodium/benzophenone system. The rest of the solvents used were of HPLC grade. Commercially available reagents were used without any purification. 2-Fluorenecarboxaldehyde -purchased from Aldrich- was used as received. **^{1}H NMR** and **^{13}C NMR** were done in $CDCl_3$ using Bruker 300 DPX, 400 DPX and 500 DPX spectrometers. The chemical shifts are referenced to internal TMS.

The assignments were performed by 2D NMR experiments: COSY (Correlation Spectroscopy), HMBC (Heteronuclear Multiple Bond Correlation) and HMQC (Heteronuclear Multiple Quantum Coherence). UV spectra were recorded on UVIKON XL from Biotek instruments. PL emission was recorded on a Photon Technology International (PTI) apparatus coupled on an 814 Photomultiplier Detection System, Lamp Power Supply 220B and MD-5020.

The following references: tetrafluorenylporphyrin (**TFP**), and tetraphenylporphyrin (**TPP**) were used as references for luminescence studies.

Synthesis of *9H*-(fluoren-2-yl)methanol : 8

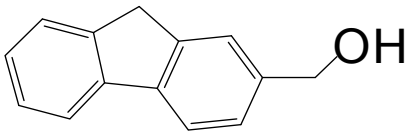

In a round bottom flask, sodium borohydride (1.168 g, 0.031 mmol) was added at 0°C to a solution of the commercial fluorene-2-carboxaldehyde (5.00 g, 0.026 mmol) in ethanol (180 mL). After 30 minutes, the reaction mixture was stirred at room temperature for two hours. Then, water was added, and the obtained mixture was extracted with DCM. The organic layer was washed with brine, dried over anhydrous $MgSO_4$, filtered, and then taken to dryness to yield a white solid (4.5 g, 89%).

^{1}H NMR (200 MHz, $CDCl_3$, δ in ppm) : 7.81 (d, $^3J_{HH}$ = 8.0 Hz, 1H), 7.75 (d, $^3J_{HH}$ = 7.7 Hz, 1H), 7.59 (d, $^3J_{HH}$ = 8.8 Hz, 2H), 7.43 (d, $^3J_{HH}$ = 7.9 Hz, 1H), 7.38 (d, $^3J_{HH}$ = 8.0 Hz, 1H), 7.33 (s, 1H), 4.80 (s, 2H, CH_2-OH), 3.94 (s, 2H, $CH_{2fluorene}$).

Synthesis of 2-(bromomethyl)-*9H*-fluorene : 9

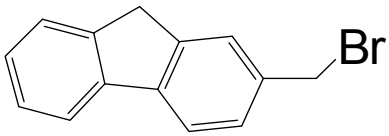

Carbon tetrabromide (5.07 g, 0.0156 mmol) was added to a solution of alcohol **8** (2.5 g, 0.013 mmol) in freshly distilled THF (25 mL) under argon. Then, triphenylphosphine (4.09 g, 0.0156 mmol) was added in a portionwise manner at 0°C. The reaction mixture was stirred at 0°C for 1 hour then at room temperature for 3 hours. Then, water was added, and the obtained mixture was extracted with DCM. The organic layer was washed with brine, dried over anhydrous $MgSO_4$, filtered, and then taken to dryness. The crude product was precipitated in methanol and filtered to yield a white solid (1.57 g, 48%).

^{1}H NMR (200 MHz, $CDCl_3$, δ in ppm) : 7.81 (d, $^3J_{HH}$ = 8.0 Hz, 1H), 7.75 (d, $^3J_{HH}$ = 7.7 Hz, 1H), 7.59 (d, $^3J_{HH}$ = 8.8 Hz, 2H), 7.43 (d, $^3J_{HH}$ = 7.9 Hz, 1H), 7.38 (d, $^3J_{HH}$ = 8.0 Hz, 1H), 7.37 (s, 1H), 4.61 (s, 2H, CH_2-Br), 3.94 (s, 2H, $CH_{2fluorene}$).

Synthesis of (3,5-bis(*9H*-fluoren-2-yl)methoxy)phenyl)methanol : <u>10</u>

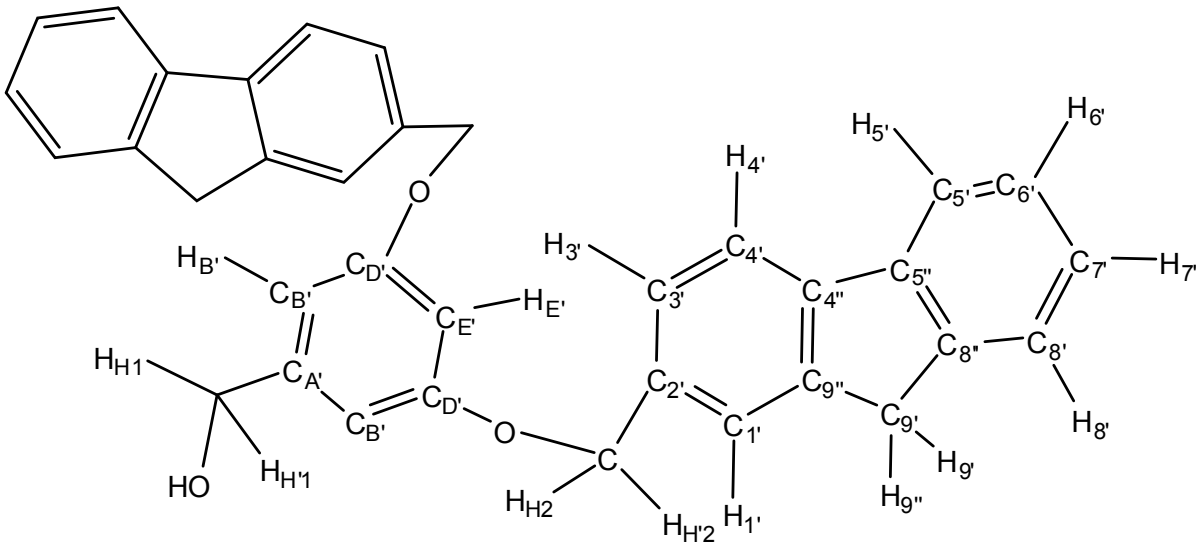

Potassium carbonate (0.359 g, 2.6 mmol), and 18-crown-6 (0.171 g, 0.65 mmol) were added to a solution of the commercial 5-hydroxymethyl-benzen-1,3-diol (0.091 g, 0.65 mmol) in freshly distilled THF (9 mL). Then, the brominated species **9** (0.480 g, 1.85 mmol) was added to the reaction mixture. The reaction mixture was refluxed for 6 hours, cooled at room temperature, filtered, and taken to dryness. The crude product was then extracted with dichloromethane, washed with water, dried over anhydrous $MgSO_4$, and taken to dryness. The residue was purified by column chromatography on silica gel using dichloromethane as an eluent to yield a white solid (0.129 g, 40%).

^{1}H NMR (200 MHz, $CDCl_3$, δ in ppm) : 7.81 (d, $^3J_{HH}$ = 7.5 Hz, 4H, $H_{4'-5'}$), 7.64 (s, 2H, $H_{1'}$), 7.57 (d, $^3J_{HH}$ = 7.1 Hz, 2H, $H_{8'}$), 7.46-7.26 (m, 6H, $H_{3'-6'-7'}$), 6.69 (broad s, 2H, $H_{B'}$), 6.63 (broad s, 1H, $H_{E'}$), 5.15 (s, 4H, $H_{H2, 2'}$), 4.68 (d, $^3J_{HH}$ = 3.7 Hz , 2H, $H_{1-1'}$), 3.95 (s, 4H, $H_{9'-9''}$).

Synthesis of 2,2'–(((5-(bromomethyl)-1,3-phenylene)bis(oxy))bis(methylene))bis(*9H*-fluorene) : 11

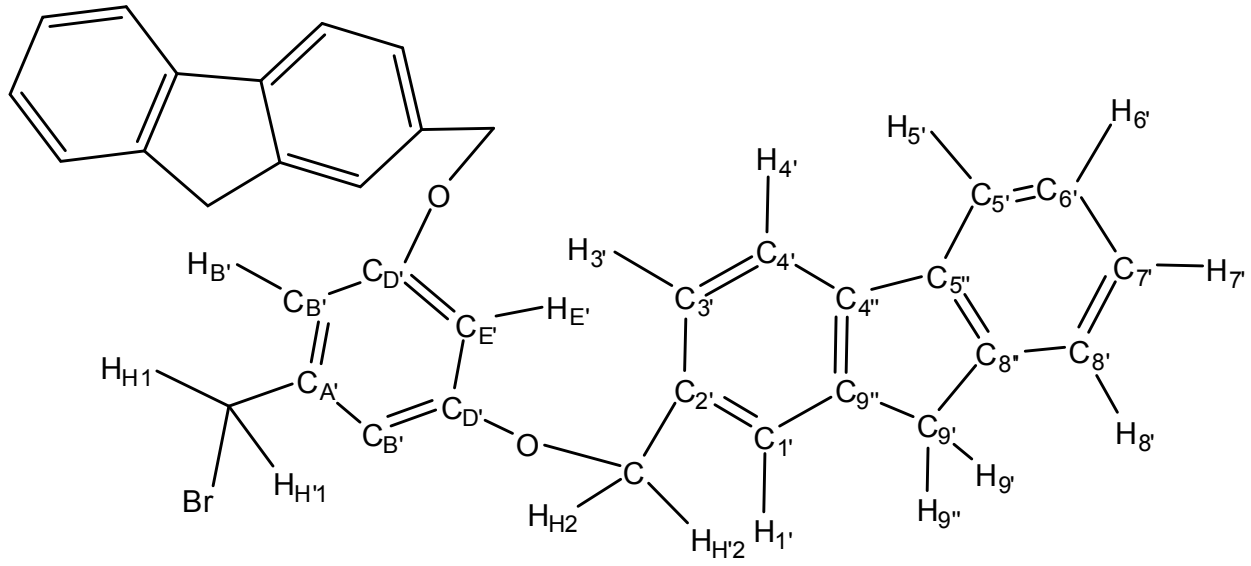

Carbon tetrabromide (0.431 g, 1.30 mmol) was added to a solution of alcohol **10** (0.4 g, 0.81 mmol) in freshly distilled THF (28 mL) under argon. Then, triphenylphosphine (0.341 g, 1.3 mmol) was added in a portion wise manner at 0°C. The reaction mixture was stirred at 0°C for 1 hour then at room temperature for 22 hours. Then, water was added, and the obtained mixture was extracted with DCM. The organic layer was washed with brine, dried over anhydrous $MgSO_4$, filtered, and then taken to dryness. The residue was purified by column chromatography on silica gel using heptane/dichloromethane (70/30) as eluent then the percentage of DCM was increased to 100% to yield a white solid (0.264 g, 58%).

^{1}H NMR (400 MHz, $CDCl_3$, δ in ppm) : 7.79 (d, $^3J_{HH}$ = 7.6 Hz, 4H, $H_{4'-5'}$), 7.61 (s, 2H, $H_{1'}$), 7.55 (d, $^3J_{HH}$ = 7.6 Hz, 2H, $H_{8'}$), 7.43-7.30 (m, 6H, $H_{3'-6'-7'}$), 6.69 (s, 2H, $H_{B'}$), 6.63 (s, 1H, $H_{E'}$), 5.10 (s, 4H, $H_{H2, 2'}$), 4.44 (s, 2H, $H_{1-1'}$), 3.91 (s, 4H, $H_{9'-9''}$).

Synthesis of the tetrapod : 12

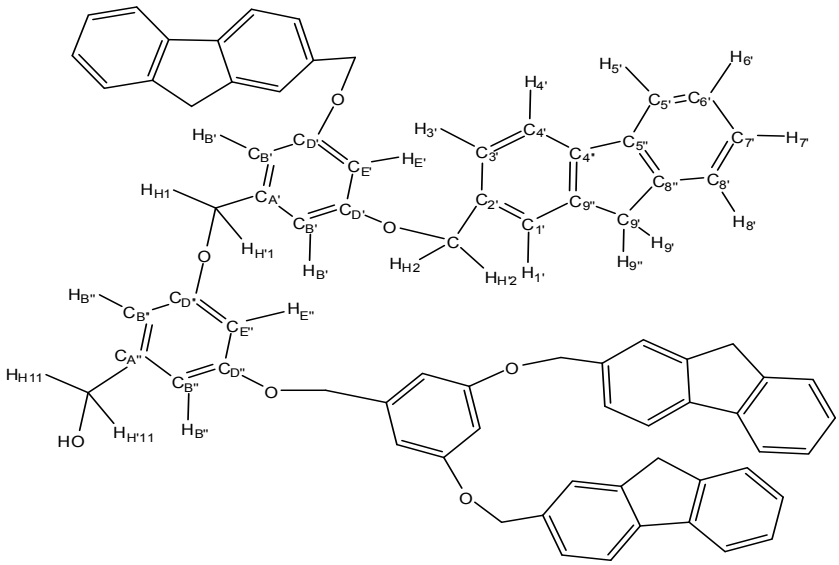

5-hydroxymethyl-benzen-1,3-diol (0.021 g, 0.15 mmol) was added to a solution of the brominated compound **11** (0.175 g, 0.31 mmol) in freshly distilled THF (20 mL) under argon. Then, Potassium carbonate (0.083 g, 0.6 mmol), and 18-crown-6 ether (0.04 g, 0.15 mmol) were added. The reaction mixture was refluxed for 15 hours, cooled at room temperature, filtered, and taken to dryness. The crude product was then extracted with dichloromethane, and washed with water. The organic layer was washed with saturated solution of sodium chloride, dried over anhydrous $MgSO_4$, and taken to dryness. The obtained oil was purified by column chromatography on silica gel using dichloromethane as eluent. The expected compound **11** was obtained as a thin white powder (0.115 g, 70%). This new dendron was characterized by the usual spectroscopy (NMR, UV-vis), mass, and elemental analysis.

^{1}H NMR (400 MHz, $CDCl_3$, δ in ppm) : 7.78 (d, 4H, $H_{4'}$, $^3J_{HH}$ = 6.4 Hz), 7.77 (d, 4H, $H_{5'}$, $^3J_{HH}$ = 7.2 Hz), 7.61 (s, 4H, $H_{1'}$), 7.55 (d, 4H, $H_{8'}$, $^3J_{HH}$ = 7.2 Hz), 7.42 (d, 4H, $H_{3'}$, $^3J_{HH}$ = 7.6 Hz), 7.39 (t, 4H, $H_{6'}$, $^3J_{HH}$ = 7.6 Hz), 7.32 (t, 4H, $H_{7'}$, $^3J_{HH}$ = 7.2 Hz), 6.72 (s, 4H, $H_{B'}$,), 6.65 (s, 2H, $H_{E'}$), 6.59 (s, 2H, $H_{B''}$), 6.54 (s, 1H, $H_{E''}$), 5.12 (s, 8H, OCH_2, $H_{H2\text{-}H2'}$), 5.00 (s, 4H, OCH_2, $H_{H1\text{-}H1'}$), 4.59 (d, 2H, CH_2-OH, $H_{H11\text{-}H11'}$, $^3J_{HH}$ = 5.6 Hz), 3.89 (s, 8H, $CH_{2fluorene}$, $H_{9'\text{-}9''}$).

Analysis : calcd for $C_{77}H_{60}O_7 \cdot 1CH_2Cl_2$: C, 79.24; H, 5.29; N, 0.00; found : C, 80.29; H, 5.56; N, 0.00.

MS (ESI) : calcd for $C_{77}H_{60}O_7$: 1119.4339 $[MNa]^+$, found : 1119.1800 $[MNa]^+$.

Melting point : 130.1°C.

Synthesis of the brominated tetrapod : 13

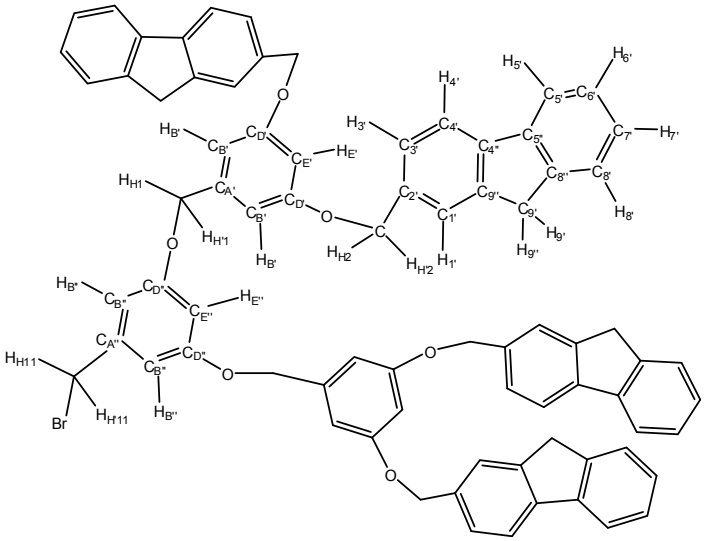

Carbon tetrabromide (37 mg, 0.11 mmol) was added to a solution of alcohol **12** (75 mg, 0.07 mmol) in distilled THF (1.5 mL) under argon. The reaction was cooled to 0°C, and triphenylphosphine (29 mg, 0.11 mmol) was added portion wise. The reaction mixture was stirred at 0°C for 1 h, then at room temperature for 3 h. Repetitive additions of 4 eq of carbon tetrabromide, 1.5 mL of THF followed by addition of 4 eq of triphenylphosphine were done twice every 12 hours. Reaction progress was followed by TLC, spotting directly from the organic layer. The solution was transferred in a separating funnel with distilled water. The aqueous layer was extracted three times with DCM. Organic layers were combined and dried over $MgSO_4$ and taken to dryness. The light brownish oil obtained was subjected to column chromatography over silica with DCM as eluent. The expected compound tetrafluorenyl dendron **13**, was obtained as a yellow powder to yield 60 mg (70%). This new dendron **13** was characterized by NMR, UV-visible, microanalysis and mass spectrometry.

^{1}H NMR (300 MHz, $CDCl_3$, δ in ppm) : 7.77 (d, 4H, $H_{4'}$, $^3J_{HH}$ = 7.5 Hz), 7.74 (d, 4H, $H_{5'}$, $^3J_{HH}$ = 7.5 Hz), 7.59 (s, 4H, $H_{1'}$), 7.52 (d, 4H, $H_{8'}$, $^3J_{HH}$ = 7.2 Hz), 7.39 (d, 4H, $H_{3'}$, $^3J_{HH}$ = 7.6 Hz), 7.36 (t, 4H, $H_{6'}$, $^3J_{HH}$ = 7.6 Hz), 7.31 (t, 4H, $H_{7'}$, $^3J_{HH}$ = 7.2 Hz), 6.69 (s, 4H, $H_{B'}$), 6.63 (s, 2H, $H_{E'}$), 6.60 (s, 2H, $H_{B''}$), 6.51 (s, 1H, $H_{E''}$), 5.10 (s, 8H, OCH_2, $H_{H2\text{-}H2'}$), 4.97 (s, 4H, OCH_2, $H_{H1\text{-}H1'}$), 4.36 (s, 2H, $C\underline{H_2}$-Br, $H_{H11\text{-}H11'}$), 3.88 (s, 8H, $CH_{2fluorene}$, $H_{9'\text{-}9''}$).

Analysis : calcd for $C_{77}H_{59}BrO_6{\cdot}4CH_2Cl_2$: C, 64.97; H, 4.72; N, 0.00; found : C, 65.72; H, 4.28; N, 0.00.

MS (ESI) : calcd for $C_{77}H_{59}BrO_6$: 1181.33927 $[MNa]^+$, found : 1181.33860 $[MNa]^+$.

Melting point : 126.0°C.

Attempt to synthesis porphyrin 32F- Formation of cycle : 1

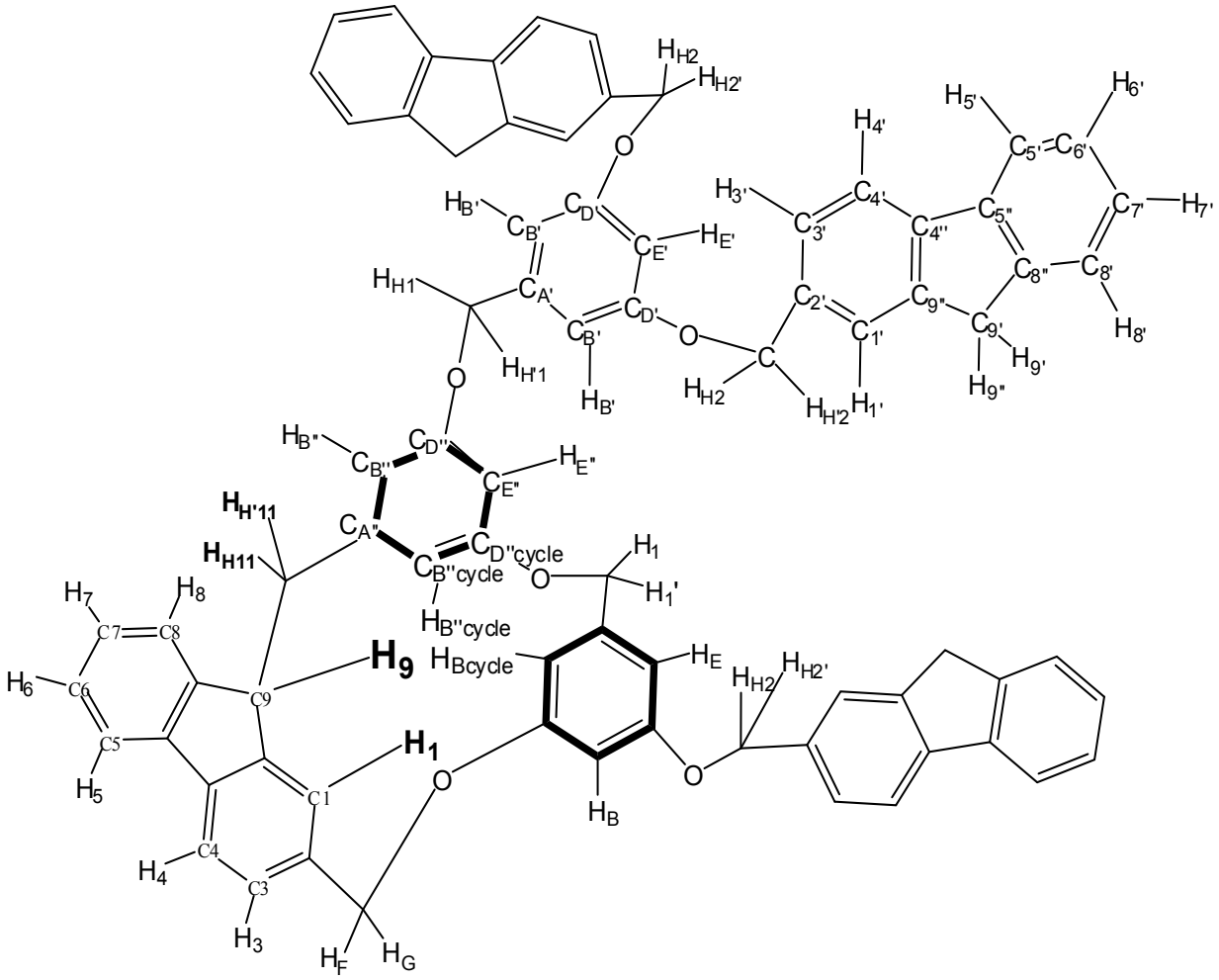

Potassium carbonate (11 mg, $7.7.10^{-5}$ mol), 18-crown-6 ether (1.3 mg, $4.8.10^{-6}$ mol), and the bromide dendron **13** (50 mg, $4.3.10^{-5}$ mol) were added to a solution of the tetrakis (3,5-dihydroxyphenyl)-porphyrin **7** (3.6 mg, $4.8.10^{-6}$ mol) in distilled THF (3 mL) under argon. The reaction mixture was heated to reflux for two days. Repetitive additions of 16 equivalent of K_2CO_3 (11 mg, $7.7.10^{-5}$ mol) and 18-crown-6 ether (1.3 mg, $4.8.10^{-6}$ mol) were done every 2 days. Reaction progress was monitored by TLC, spotting directly from the organic layer. Then, at the end of the reaction (8^{th} day), the mixture was cooled to room temperature and THF was evaporated in vacuum. The residue was dissolved in DCM and transferred into a separating funnel. The organic layer was washed with brine, dried over anhydrous $MgSO_4$, filtered, and then taken to dryness. The brown

product obtained was subjected to column chromatography over silica with 100% DCM as eluent and then a mixture of DCM/acetone gradient and finally; 100% acetone.

Two products were obtained : cycle **1** as a pale yellow product (24 mg, yield : 52%) and a dark red product; a mixture of differently substituted porphyrins (12 mg, yield around 40%). Separation of these porphyrins was unsuccessfully tried but compound **1** was isolated pure.

This new cycle **1** was characterized by NMR, microanalysis and mass spectrometry.

^{1}H NMR (assignments aided by COSY; 300 MHz, $CDCl_3$, δ in ppm) : 7.80 (d, 3H, $H_{4'}$, $^{3}J_{HH}$ = 7.3 Hz), 7.78 (d, 3H, $H_{5'}$, $^{3}J_{HH}$ = 7.3 Hz), 7.72-7.62 (m, 3H, $H_{5\text{-}6\text{-}8}$), 7.59 (d, 3H, $H_{8'}$, $^{3}J_{HH}$ = 5.1 Hz), 7.56 (d, 3H, $H_{3'}$, $^{3}J_{HH}$ = 5.1 Hz), 7.43-7.37 (m, 6H, $H_{1'\text{-}6'}$), 7.44 -7.36 (m, 3H, $H_{3\text{-}4\text{-}7}$), 7.33 (t, 3H, $H_{7'}$, $^{3}J_{HH}$ = 7.0 Hz), 6.78 (d, $^{3}J_{HH}$ = 2.2 Hz, 2H, $2H_{B'}$), 6.75 (m, 1H, $H_{B''}$), 6.65 (t, $^{4}J_{HH}$ = 2.2 Hz, 1H, $H_{E'}$), 6.61 (t, $^{4}J_{HH}$ = 2.2 Hz, 1H, $H_{E''}$), 6.54 (m, 1H, H_E), 6.48 (t, $^{4}J_{HH}$ = 2.2 Hz, 1H, H_B), 6.44 (t, $^{3}J_{HH}$ = 2.2 Hz, 1H, H_9), 6.39 (m, 1H, H_{Bcycle}), 6.02 (m, 1H, $H_{B''cycle}$), 5.14 (d, 1H, H_F, $^{2}J_{HH}$ = 13.1 Hz), 5.12 (s, 6H, OCH_2, $H_{H2\text{-}H2'}$), 5.05 (s, 4H, OCH_2, $H_{H1\text{-}H1'}$), 4.91 (d, 1H, H_G , $^{2}J_{HH}$ = 13.1 Hz), 4.08 (dd, 1H, H_{H11} , $^{2}J_{HH}$ = 11.09 Hz, $^{3}J_{HH}$ = 4.1 Hz), 3.89 (s, 6H, $3CH_{2fluorene}$, $H_{9'\text{-}9''}$), 3.59 (dd, 1H, $H_{H11'\ (cycle)}$, $^{2}J_{HH}$ = 13.0 Hz, $^{3}J_{HH}$ = 4.7 Hz), 2.21 (dd, 1H, H_9, $^{2}J_{HH}$ = 13.1 Hz, $^{3}J_{HH}$ = 11.4 Hz).

^{13}C-NMR (assignments aided by COSY; 300 MHz, $CDCl_3$, δ in ppm) : 160.3 (C_q), 160.0 ($C_{D''}$), 159.8 (C_q), 159.4 ($C_{D''cycle}$), 158.9 (C_q), 147.3 (C_q), 145.3 ($C_{A''}$), 143.7, 143.6, 143.4, 142.2, 141.7, 141.6, 141.3 (C_q), 140.7 (C_2), 140.3, 139.8, 139.4 (C_q), 135.3, 135.2, 134.7, 127.8 (C_1), 127.4-127.3-127.1 ($C_{5\text{-}6\text{-}8}$), 126.8 ($C_{3'}$), 126.7 ($C_{4'}$), 126.4 ($C_{8'}$), 125.0 ($C_{7'}$), 124.4 ($C_{5'}$), 124.1 ($C_{3\text{-}4\text{-}7}$), 120.1, 120.0, 119.9, 119.8 (C_q), 108.9 ($C_{B''}$), 108.6 ($C_{B''cycle}$), 106.5, 105.45, 104.7, 103.9, 102.1 ($C_{E''}$), 101.6 (C_t), 70.50, 70.33, 70.1, 69.9, 69.1, 49.3 (C_9), 40.8 ($C_{H11\text{-}H11'}$), 36.8, 29.7, 29.3, 22.7.

Analysis : calcd for $C_{77}H_{58}O_6$·Na : C, 83.90; H, 5.30; N, 0.00; found : C, 83.91; H, 6.02; N, 0.00.

MS (ESI) : calcd for $C_{77}H_{58}O_6$: 1101.41311 $[MNa]^+$, 1117.38705 $[MK]^+$; found : 1101.41150 $[MNa]^+$, 1117.37140 $[MK]^+$.

References :

1. Tomalia, D. A.; Baker, H.; Dewald, J.; Hall, M.; Kallos, G.; Martin, S.; Roeck, J.; Ryder, J.; Smith, P. *Polym. J.* **1985**, *17*, 117.
2. Buhleier, E.; Wehner, W.; Vogtle, F. *Synthesis* **1978**, 155.
3. Denkewalter, R. G.; Kolc, J.; Kukasavage, W. J. *U.S. Patent* **1981**, 4289872.
4. Newkome, G. R.; Yao, Z. Q.; Baker, G. R.; Gupta, V. K. *J. Org. Chem.* **1985**, *50,* 2003.
5. Tomalia, D. A.; Naylor, A. M.; Goddard, W. A. *Angew. Chem. Int. Ed.* **1990**, *29*, 138.
6. Hawker, C. J.; Fréchet, J. M. J. *J. Am. Chem. Soc.* **1992**, *114*, 8405.
7. Hawker, C. J.; Fréchet, J. M. J. *J. Am. Chem. Soc.* **1990**, *112*, 7638.
8. Macor, K. A.; Su, Y. O.; Miller, L. A.; Spiro, T. G. *Inorg. Chem.* **1987**, *26*, 2594.
9. Haddleton, D. M.; Sahota, H. S.; Taylor, P. C.; Yeates, S. G. *J. Chem. Soc. Perkin Trans.* **1996**, *1*, 649.
10. Hawker, C. J.; Fréchet, J. M. J. *J. Chem. Soc. Perkin Trans.* **1992**, *1*, 2459.
11. Jin, R. H.; Aida, T.; Inoue, S. *J. Chem. Soc. Chem. Commun.* **1993**, 1260.
12. Dandliker, P. J.; Diedrich, F.; Gross, M.; Knobler, C. B.; Louati, A. *Angew. Chem., Int. Ed. Engl.* **1994**, *33*, 1739.
13. Bhyrappa, P.; Young, J. K.; Moore, J. S.; Suslick, K. S. *J. Am. Chem. Soc.* **1996**, *118*, 5708.
14. Xu, T. H.; Lu, R.; Qiu, X. P.; Liu, X. L.; Xue, P. C.; Tan, C. H.; Bao, C. Y.; Zhao, Y. *Eur. J. Org. Chem.* **2006**, 4014.
15. Duan, X.-F.; Wang, J. L.; Pei, J. *Org. Lett.* **2005**, *7*, 4071.
16. Finikova, O.; Galkin, A.; Rozhkov, V.; Cordero, M.; Hägerhäll, C.; Vinogradov, S. *J. Am. Chem. Soc.* **2003**, *125*, 4882.
17. Xu, T. H.; Lu, R.; Liu, X.; Zheng, X.; Qiu, X. P.; Zhao, Y. *Eur, Org. Lett.* **2007**, *9*, 797.
18. Jiang, D.-L.; Aida, T. *J. Am. Chem. Soc.* **1998**, *120*, 10895.
19. Harth, E. M.; Hecht, S.; Helms, B.; Malmstrom, E. E.; Fréchet, J. M.; Hawker, C. J. *J. Am. Chem. Soc.* **2002**, *124*, 3926.
20. Loiseau, F.; Campagna, S.; Hameurlaine, A.; Dehaen, W. *J. Am. Chem. Soc.* **2005**, *127*, 11352.
21. Paul-Roth, C. O.; Simonneaux, G. *Tetrahedron Lett.* **2006**, *47*, 3275.
22. Paul-Roth, C. O.; Simonneaux, G. *C.R. Acad. Sci., Ser. IIb: Chim.* **2006**, *9*, 1277.
23. George, R. G.; Padmanabhan, M. *Polyhedron* **2003**, *22*, 3145.
24. Paul-Roth, C.; Williams, G.; Letessier, J.; Simonneaux , G. *Tetrahedron Lett.* **2007**, *48*, 4317.

25. Drouet, S.; Paul-Roth, C.; Simonneaux, G. *Tetrahedron* **2009**, *65*, 2975.
26. Drouet, S.; Paul-Roth, C. O. *Tetrahedron* **2009**, *65*, 10693.
27. Adler, A. D.; Longo, F. R.; Finarelli, J. D.; Goldmacher, J.; Assour, J.; Korsakoff, L. *J. Org. Chem.* **1967**, *32*, 476.
28. Appel, R. *Angew. Chem. Int. Ed. Engl.* **1975**, *87*, 863.
29. Williamson, A. W. *J. Chem. Soc.* **1852**, *4*, 229.
30. Li, B.; Li, J.; Fu, Y.; Bo, Z. *J. Am. Chem. Soc.* **2004**, *126*, 3430.
31. Nicholson, J. W. *The Chemistry of Polymers-Education* **2006**, *Royal Society of Chemistry (Great Britain)*.
32. Vögtle, F.; Richardt, G.; Werner, N. *Dendrimer Chemistry: Concepts, Syntheses, Properties, Applications -Science* **2009**.
33. Merhi, A.; Drouet, S.; Kerisit, N.; Paul-Roth, C. O. *Tetrahedron* **2012**, *68*, 7723.

Chapter 3

Multiporphyrin Arrays

Multiporphyrin Arrays : State of art

Recently, modular synthetic approaches called great attention for the preparation of multicomponent systems. The synthesis of photosynthetic or related model systems requires strategies for joining large number of components into functional arrays. In turn, the ability to design and construct molecular architectures where energy flow is controlled becomes a great challenge. One modular approach employs **organic porphyrin building blocks** bearing peripheral functional groups that can be joined *via* specific coupling methods.[1]

There are many ways to link porphyrins together. One of the first examples was the synthesis of diporphyrins and triporphyrins by an ester bond. It was developed by Anton in 1976[2] as shown in **Figure 1**. These compounds were used for energy and electron transfer in biological processes.

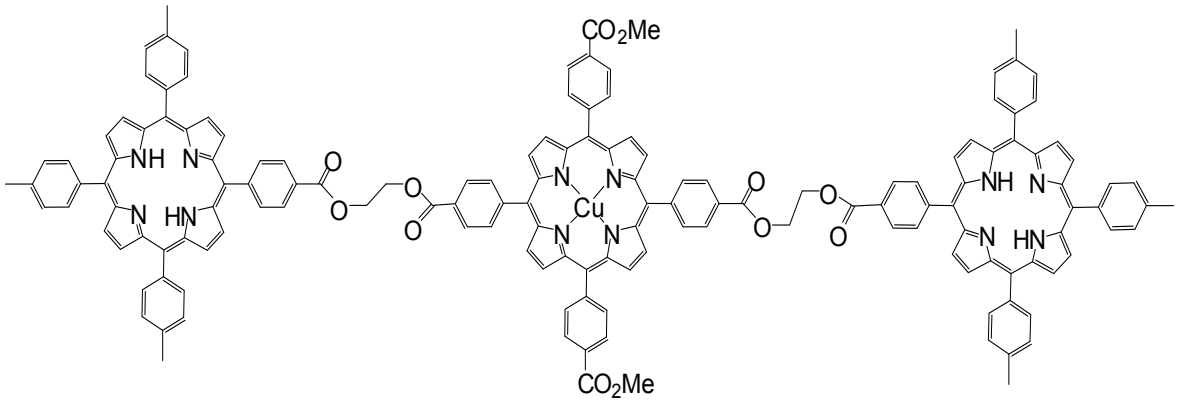

Figure 1 : Trimer presented by **Anton**

Porphyrins linked by ether bond were then presented in 1983,[3] these porphyrin arrays were used for light collecting. Few years later, many other examples were shown; Therien *et al.*[4] published a porphyrin dimer linked at *meso* position by two triple bonds, and a trimer linked by triple bonds; these assemblies were used as models for light collecting antenna (**Figure 2**).

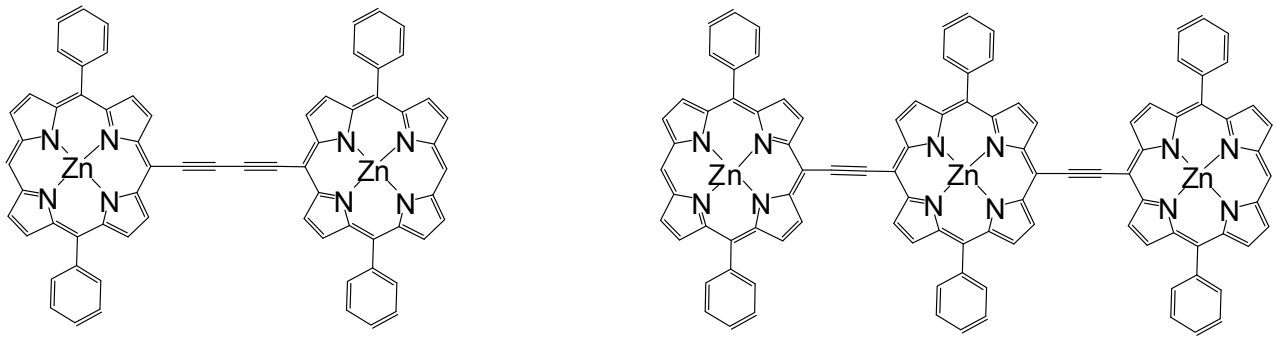

Figure 2 : Dimer and trimer synthesized by **Therien**

Later, the target was the study of absorption and emission properties and factors that affect them. For this reason, synthesis of dimers and trimers linked by ethynyl bond at positions like *meso-meso*, or *meso-beta* were proposed.[5] Many other examples were presented by Lindsey's group[6] as well; studies of efficient electronic energy transfer were applied on some of their dimers and trimers.[7]

On the other hand, certain trimer arrays formed a self-assembled monolayer that exhibit multiple and reversible oxidation waves.[8] Synthesis was not limited to form trimers : bigger assemblies were synthesized such as pentamers and hexamers. For example, Lindsey presented an interesting hexamer in 2001.[9] It was used for the study of flow of excited state energy in self assembled light harvesting systems.

After considering organic arrays, we have to notice that certain type of **organometallic porphyrins** called the attention due to their interesting applications. That is due to the combination of the properties of porphyrin from one side, and that of the organometallic part from another side. For example, in 2008, the first conjugation between a porphyrin and areneruthenium was presented.

The evaluation of such complexes in photodynamic therapy in human cancer was reported as well.[10] It is worth to mention that the success of the application of these complexes was due to the combination of photosensitizing properties of porphyrins and chemotherapeutic effects of ruthenium.

Another example was about achieving **on/off switching** of porphyrin fluorescence through the use of the ferrocene/ferrocenium redox couple[11] as presented in **Figure 3**.

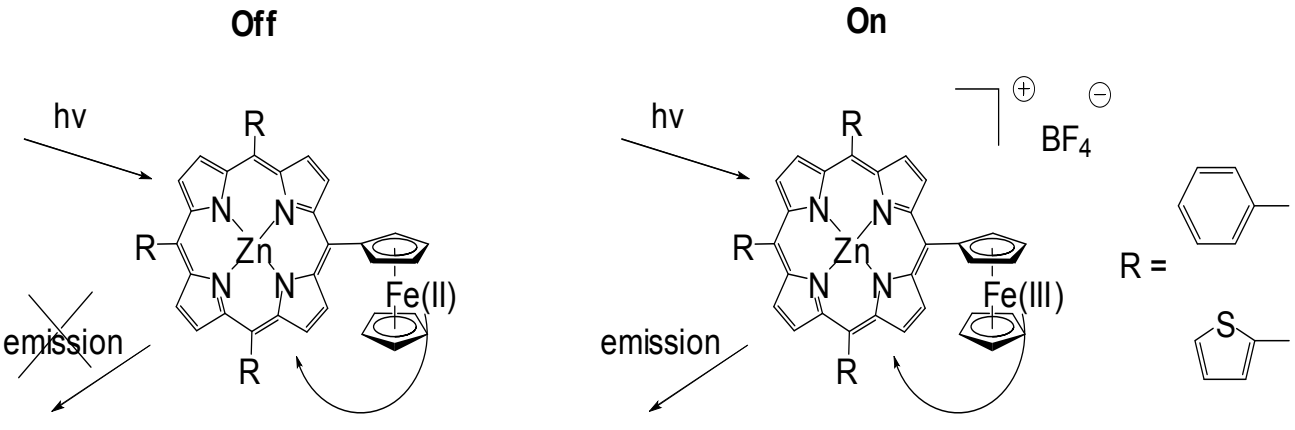

Figure 3 : Example of switching porphyrin fluorescence

Based on all what has been mentioned, **Organic multiporphyrin arrays** (dimers, trimers, etc.) and **Organometallic porphyrin assemblies** seem to be an interesting subject, especially concerning applications. Since they constitute two different fields, to clarify our objectives, this chapter will be divided into two parts :

I. Organic multiporphyrin Arrays

As it has been mentioned earlier in chapter 2, the fluorescence quantum yield of **TFP**[12] was surprisingly high (24%). So, our target is to exploit highly efficient fluorenyl based antenna by coupling porphyrin monomers substituted by fluorenyl units, at the *meso* position.

In other words, we intend to develop porphyrin dimers and trimers, having six and eight fluorenyl arms, respectively.

II. Organometallic porphyrin Assemblies

The other part of the chapter will be concerning the synthesis of organometallic porphyrins having one ruthenium moiety as well as fluorenyl arms. The target is to exploit the capacity of the fluorenyl arms to exalt the luminescence of these complexes combined with another objective. That is by trying to switch these luminescence properties by the oxidation or reduction of single ruthenium.

I. Organic multiporphyrin Arrays :

As it has been mentioned, the target is to synthesize porphyrins with fluorenyl arms. To achieve this, porphyrin monomers that will be used, possess three fluorenyl groups connected at the *meso* position. The fourth *meso* position will be functionalized for coupling conditions.

The dimer (coupling of two porphyrin monomers) will be the first target in this series. For the coupling conditions, it is proposed to have a **halogenated porphyrin** from one hand, and a **terminal alkyne porphyrin** from the other hand. Then a copper-free Sonogashira reaction can be applied (**Scheme 1**).

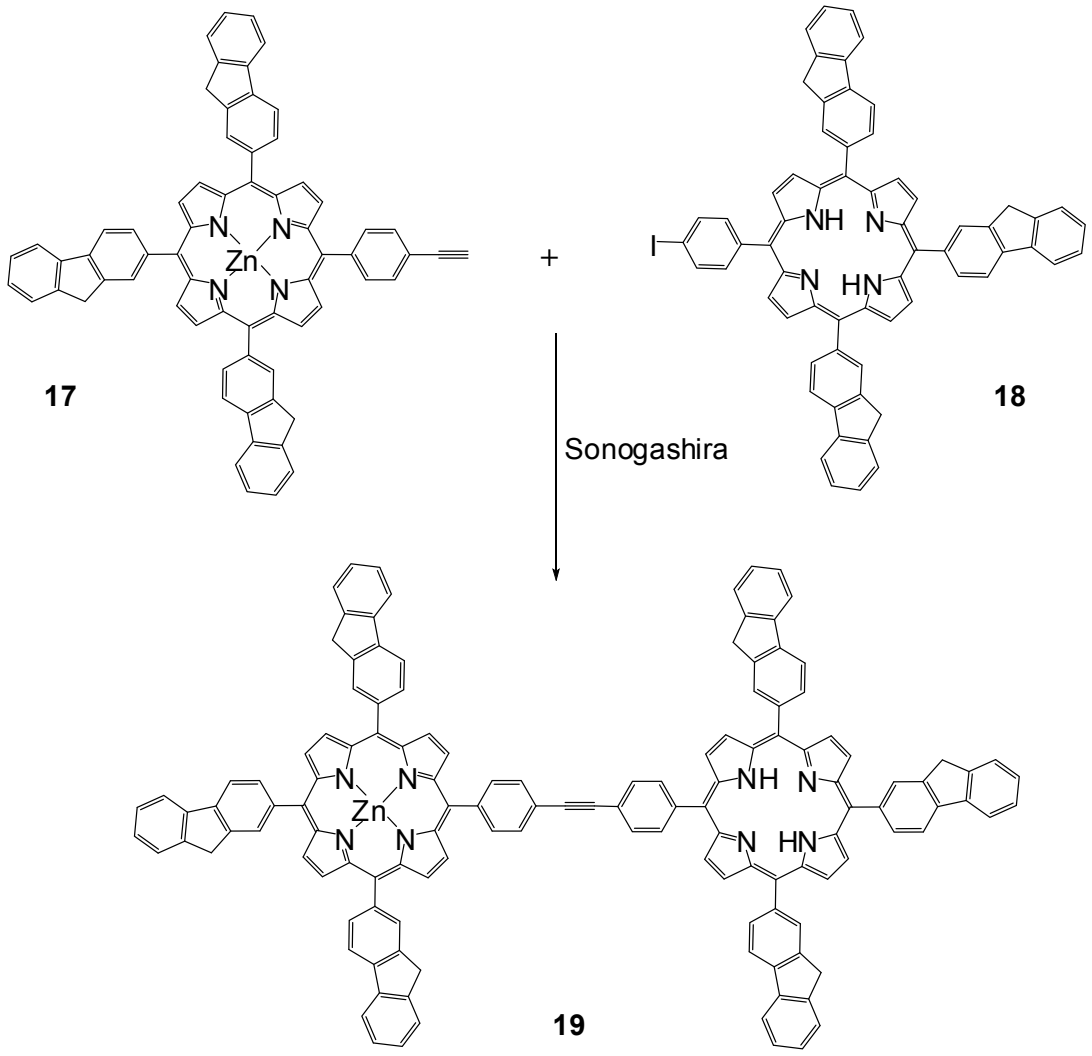

Scheme 1 : Synthesis of the dimer **19**

1. Synthesis of the precursor Zn porphyrin complex 17

Porphyrin **17** is of **A_3B** type, so it could be synthesized starting from its free based protected derivative **15** (**Scheme 2**). In turn, **15** could be synthesized by Lindsey's method.[13]

This strategy is used by reacting the pyrrole with two aldehydes : 2-fluorenecarboxaldehyde (commercially available), and trimethylsilyl benzaldehyde **14**. Then, the protected porphyrin **15** could be deprotected and metallated by zinc. So, to get the precursor zinc porphyrin complex **17**, it is worth to start the synthesis of aldehyde **14**.

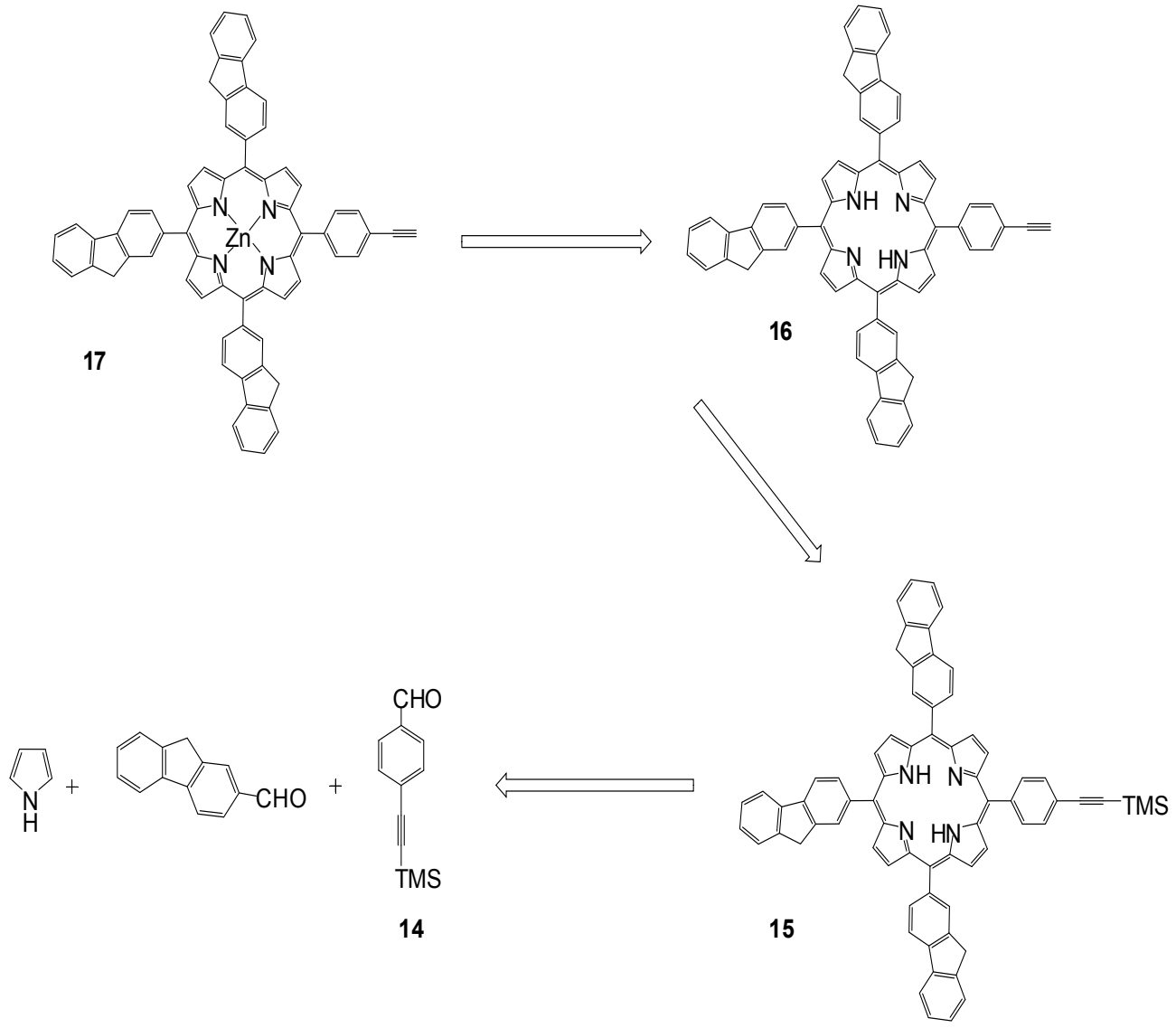

Scheme 2 : Retrosynthesis of porphyrin **17**

1.1. Synthesis of trimethylsilyl benzaldehyde 14

This aldehyde **14** is synthesized by a classical Sonogashira coupling between bromobenzaldehyde and trimethylsilylacetylene using triethylamine as a base in THF (**Scheme 3**). Palladium(II) is used as a catalyst and copper iodide as a cocatalyst. Aldehyde **14** is obtained as a pale yellow solid with 92% yield.

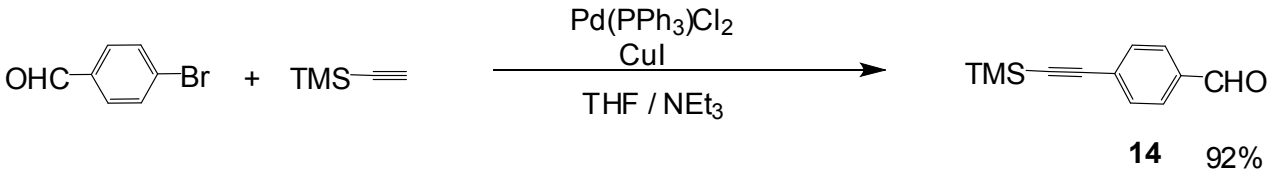

Scheme 3 : Synthesis of the protected aldehyde **14**

1.2. Synthesis and characterization of the free base porphyrin 15

This porphyrin is synthesized by following Lindsey's method.[13] It is done by the condensation of pyrrole with the two aldehydes : **14** and fluorenylcarboxylaldehyde. It is catalysed by the Lewis acid $BF_3.OEt_2$ in distilled chloroform (**Scheme 4**). After three hours, *p*-chloranil is added to oxidize the formed porphyrinogen. The reaction is refluxed for one more hour. Then, the reaction mixture is neutralized by triethylamine.

Treatment of the reaction was done by two columns. The first column was to separate the porphyrin mixture from the polymer, and the second was to separate the different formed porphyrins. Monomer **15** was obtained pure as a result of the second column with 15% yield, and was characterized by the usual spectroscopies (NMR, UV-vis), mass, and elemental analysis.

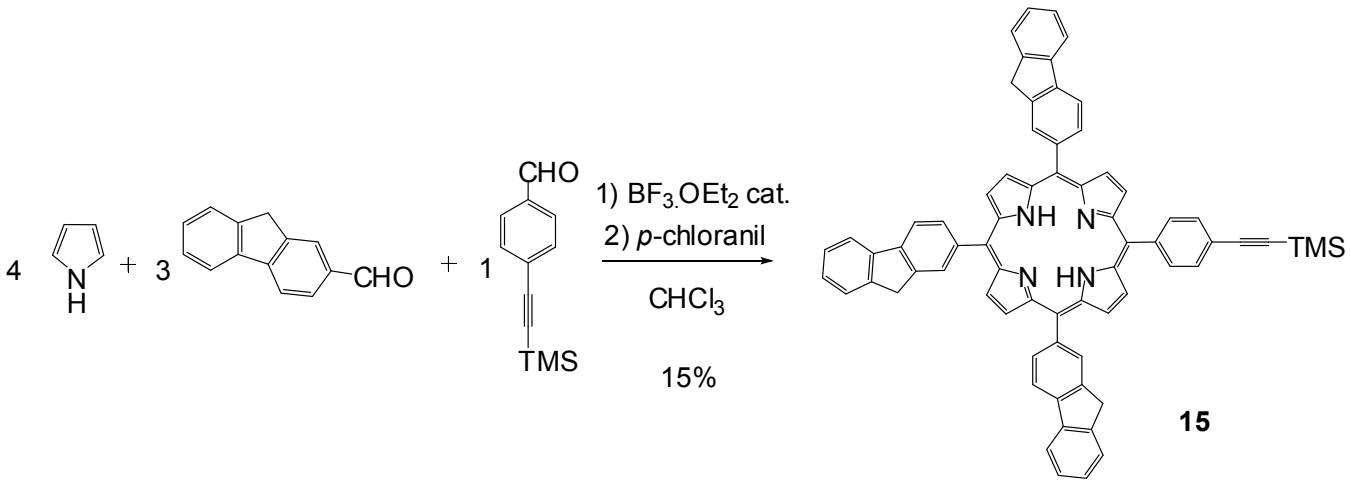

Scheme 4 : Synthesis of the porphyrin precursor **15**

Proton **NMR** of **15** exhibits signatures of porphyrin; for example, the protons of the macrocycle (NH) were observed at around – 2.7 ppm. The peak at 4.2 ppm characterizes the ($C\underline{H_2}$) of fluorenyl groups. In addition, the β pyrrolic protons are identified by the peaks around 9 ppm.

Moreover, the UV-visible studies of **15**, done at room temperature in dichloromethane, show the presence of the Soret band at 424 nm, and four Q bands at 518, 555, 594, 649 nm. Having four Q bands is characteristic for free-base (nonmetallated) porphyrin. On the other hand, a band at 274 nm is observed which corresponds to the three fluorene arms absorption.

1.3. Synthesis and characterization of the deprotected porphyrin 16

The trimethylsilyl group of **15** was deprotected by using potassium carbonate in dichloromethane and methanol. The reaction took place at room temperature (**Scheme 5**). It was then purified by extraction, followed by a column, to afford **16** as a product of 98% yield. This new porphyrin was fully characterized.

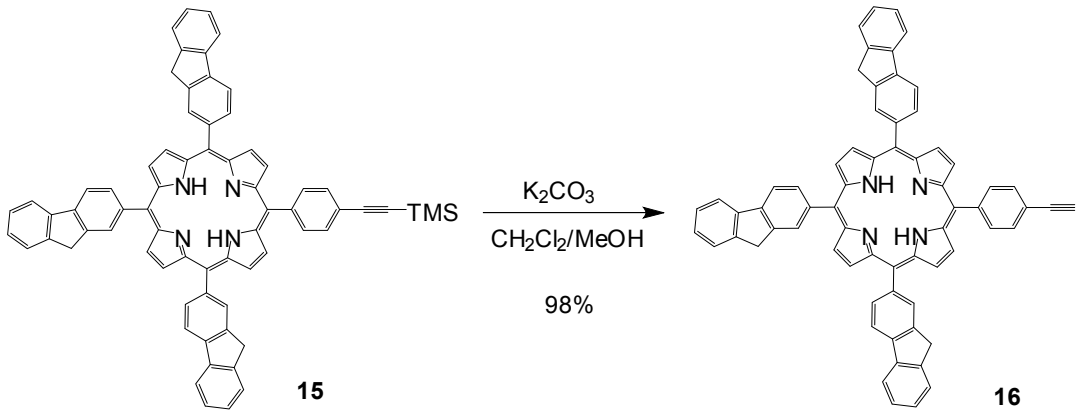

Scheme 5 : Deprotection of the TMS group of **15**

The **^{1}H NMR** of **16** is similar to that of **15** except for the absence of TMS protons at 0.27 ppm. In addition, the new signal at 3.3 ppm is observed; it corresponds to the terminal alkyne proton that characterizes the reaction.

The **UV-visible** spectrum of **16** is similar to that of **15** with slight shift. The Soret band is observed at 425 nm and the Q bands as follows: 518, 555, 594, and 649. In addition, the band at 275 ppm shows the absorption of fluorene arms.

1.4. Synthesis and characterization of the zinc metallated porphyrin 17

The porphyrin **16** was metallated by adding zinc acetate in dichloromethane and methanol (**Scheme 6**). The reaction was monitored by both UV-visible absorption and TLC. It was complete after 48 hours at room temperature.

The indication of the complete metallation of the porphyrin macrocycle cavity was also proved by **^{1}H NMR**. For example, the absence of the signal at high field: at –2.7 ppm (N<u>H</u>) indicates that the macrocycle cavity is yet occupied by a metal.

In addition, concerning UV-visible studies, there is an important difference between the Q bands of free-base and metallated porphyrin. For example, the UV-visible study of **17** that was done at room temperature in dichloromethane, shows the Soret band at 426 nm, which is slightly shifted from that of free base **16** (425). Moreover, two Q bands at 554, 595 nm are observed instead of four which is characteristic for metallated porphyrins.

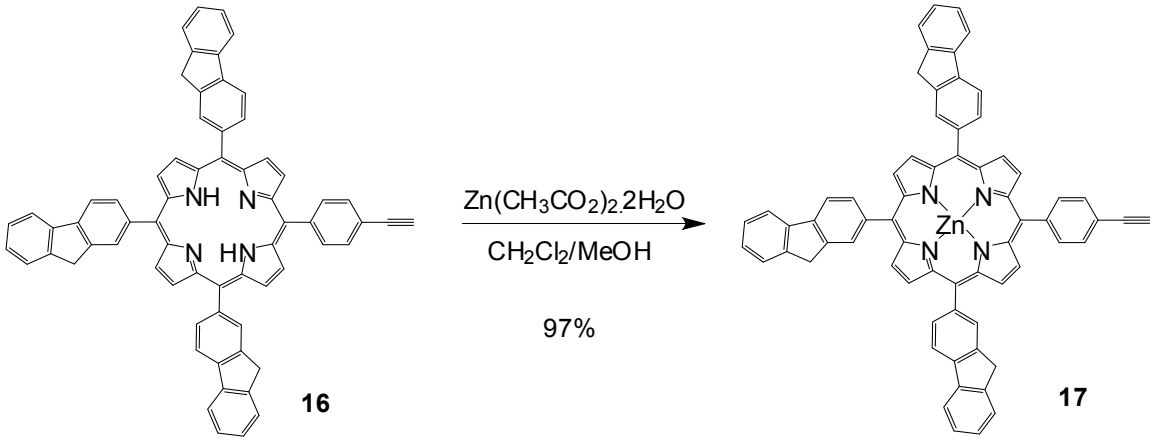

16 **17**

Scheme 6 : Metallation of porphyrin **16**

2. Synthesis and characterization of the iodo-porphyrin 18

Another monomer is needed for the dimer synthesis, which is the proposed iodo porphyrin **18**. It is of **A_3B** type, so the synthesis will be similar to that of **15** using Lindsey's method. It is achieved by the condensation of pyrrole and the two commercially available aldehydes : iodobenzaldehyde and 2-fluorenylcarboxaldehyde (**Scheme 7**).

Then, a similar procedure, as mentioned for **15**, is applied. The porphyrin **18** was obtained pure as violet solid with a yield of 8%. It was fully characterized.

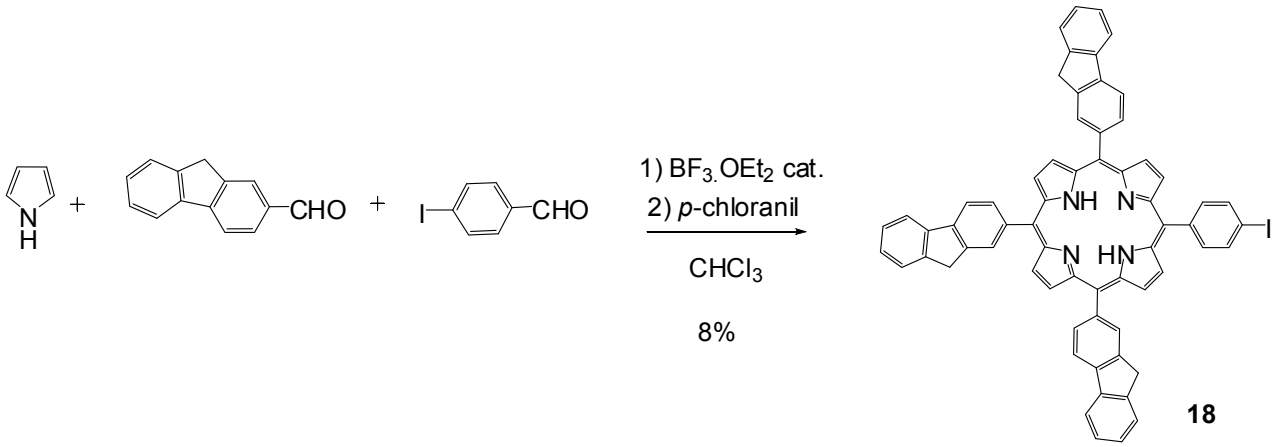

Scheme 7 : Synthesis of the iodo porphyrin **18**

^{1}H NMR of **18** shows the protons of the macrocycle (NH) at around – 2.7 ppm. The peak at 4.2 ppm characterizes the ($C\underline{H_2}$) of fluorenes. In addition, the β pyrrolic protons are identified by the peaks around 9 ppm.

The **UV-visible** study of **18**, which was done at room temperature in dichloromethane, shows the presence of the Soret band at 424 nm, and four Q bands at 519, 555, 593, 649 nm. Having four Q bands is characteristic for free-base (nonmetallated) porphyrin. In the UV region, a band at 275 nm is observed which corresponds to the fluorene absorption.

3. Synthesis of the dimer 19

3.1. Attempt to dimer synthesis using triphenylarsine as a catalytical ligand

To obtain our target molecule : the dimer, a Sonogashira coupling is proposed. It is worth to mention that it should be done as a copper free reaction, this is to avoid the insertion of the copper in the porphyrin macrocycle and as a consequence, the catalytic cycle will be interrupted. Even if copper is used in excess, the removal of the copper from the macrocycle is difficult.[14]

Another thing to be mentioned is that such reactions shouldn't be done at high temperature, otherwise, palladium insertion in the porphyrin macrocycle is observed.

Based on the literature, Lindsey's group did a study on the ligand effect and deduced that triphenylarsine ($AsPh_3$) was selected as the best ligand.[6,15] The first trial to obtain our target was tried using the conditions shown in **Scheme 8**.

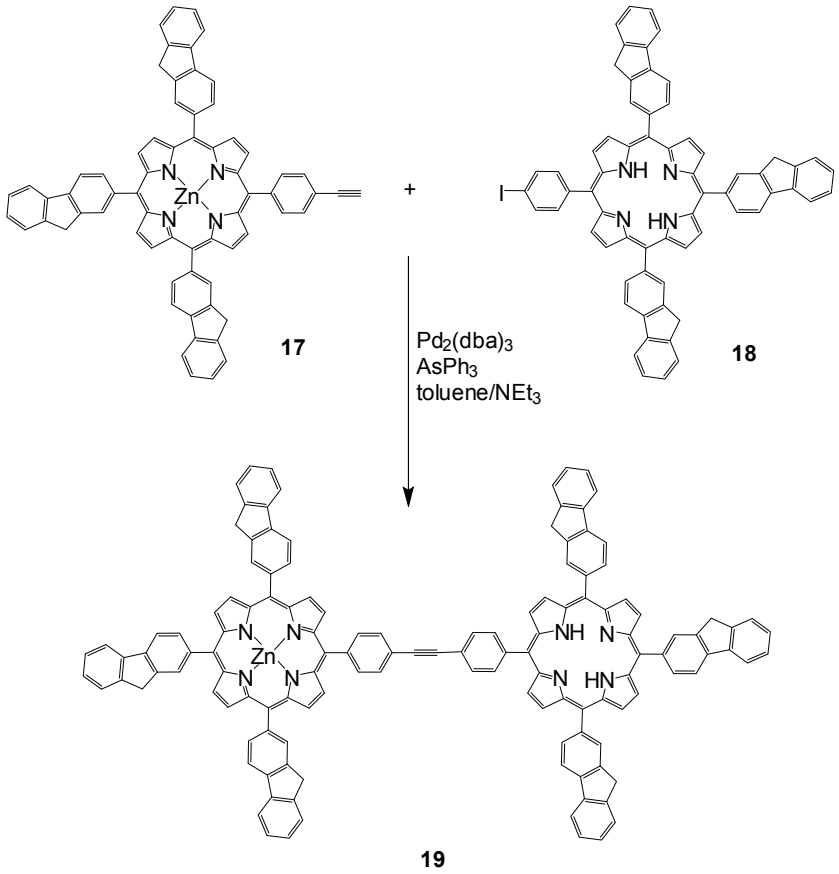

Scheme 8 : Synthesis of **19** using triphenylarsine as a ligand

The reaction was done at 35°C under argon and it was monitored by TLC and finally stopped after 72 hours. The solvent was taken to dryness. The residue was dissolved in dichloromethane, and then purified twice by column chromatography.

Purification was accompanied by mass analysis to check what products are obtained. As mentioned in the literature, high molecular weight molecules were observed as well. The fraction containing our product mixed with other impurities was subjected to several purification techniques such as : columns, washing, and precipitation in heptane.

Unfortunately, dimer **19** was always obtained accompanied with the by-products **20** and **21** (**Figure 4**). Similar case has been reported in 1999.[16]

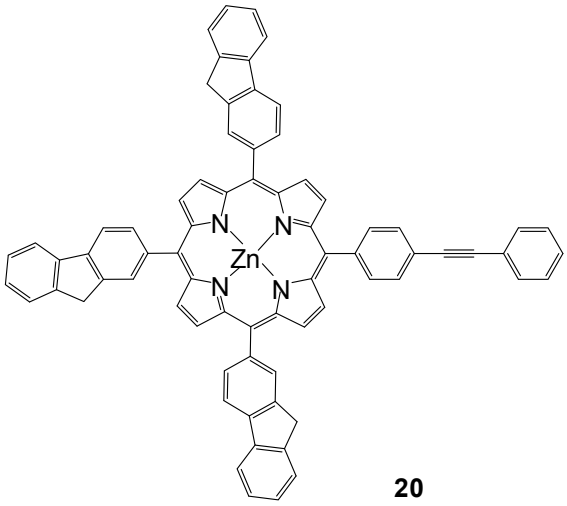

20

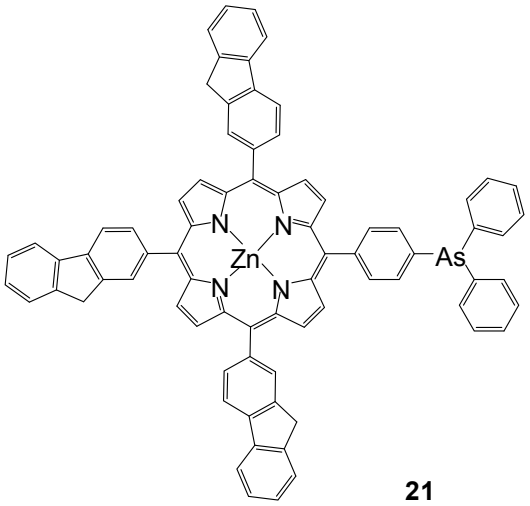

21

Figure 4 : Side products obtained during **dimer** formation

The reason of by-products (**20** and **21**) formed in this reaction could be referred to a phenyl aryl exchange as shown in the proposed catalytic cycle shown in **Figure 5**. This cycle is adapted from Novak *et al.*[17] Compound **20** was obtained pure as the first fraction of the column and it was characterized by **^{1}H NMR** and mass analysis as well.

On the contrary, **21** was always found as a fraction mixed with the iodo porphyrin **18**, or as another fraction mixed with the dimer **19**. As a result, only mass analysis was done.

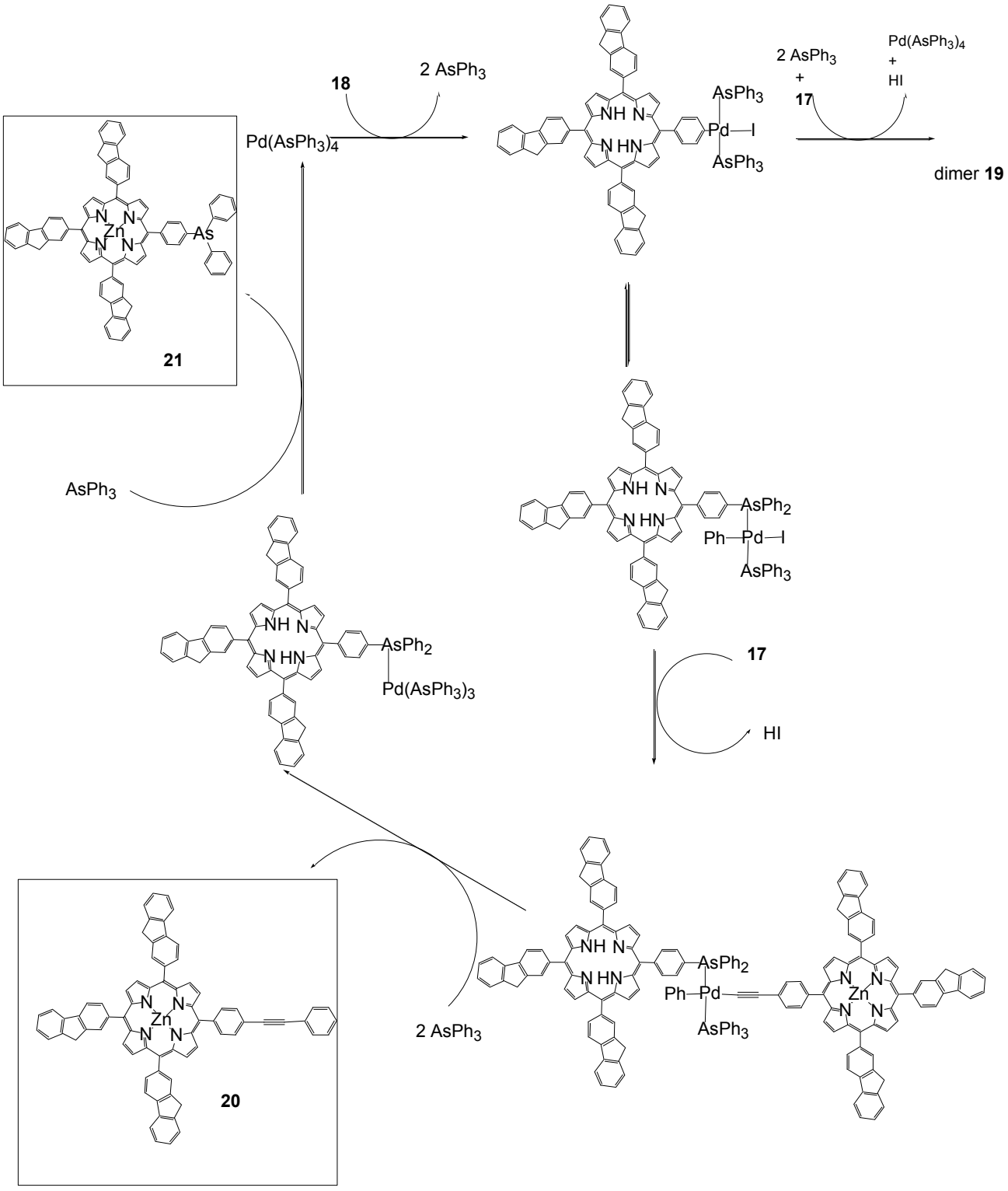

Figure 5 : Proposed mechanism for the formation of **20** and **21**

3.2. Synthesis of dimer 19 using tri(ortho-tolyl)phosphine as a catalytic ligand

It is clear that the target now is to get the dimer **19** as a pure compound and in acceptable quantities. To achieve that, a new synthetic strategy must be used. Since the triphenylarsine was the source of the impurities obtained (**Figure 5**) so the solution is to use another ligand. As a result, the tri(ortho-tolyl)phosphine was used instead.[16,18]

In other words, the reaction was repeated using exactly the same conditions as mentioned above. The only difference was the replacement of $AsPh_3$ by the tri(ortho-tolyl)phosphine $P(o\text{-}tol)_3$. After 72 hours, the crude mixture was purified twice by column chromatography followed by precipitation in heptane. Dimer **19** was obtained as a dark red powder with 25% yield.

The coupling was confirmed by matrix-assisted laser desorption ionization time-of-flight mass spectrometry (MALDI-TOF MS) and UV-Visible spectrometry. In addition, the overlap of the *beta* pyrrolic protons seen in the ^1H NMR was another indication as seen below. Dimer **19** is very soluble in most organic solvents, it was fully characterized by usual solution spectroscopies (NMR and mass spectrometry) and microanalysis.

4. Characterization of the dimer 19

4.1. ^1H NMR :

The 2 protons carried by the nitrogen atoms of the porphyrin-free base in the dimer could not be observed at high field. The singlet at 4.2 ppm, corresponds to the 12 protons of the CH_2 protons of the 6 fluorenyl groups. The aromatic protons (fluorenyl and phenyl) resonate in the region between 7.5 and 8.5 ppm. The signals of the seven protons on the six fluorenyl arms are large. They are at expected positions in comparison to the monomers: 8.42 (s, 6H); 8.29 (m, 6H); 8.18 (m, 6H); 8.06 (d, 6H); 7.71 (d, 6H); 7.54 (t, 6H) and 7.43 (t, 6H).

Around 9 ppm, there are five signals assigned to the *beta* pyrrolic protons: 9.09 (s, 4H), 9.07 (d, 2H), 9.05 (s, 4H), 9.04 (s, 4H), 9.02 (d, 2H). Three of these signals are singlets integrating for four protons each. Two signals are an AB system integrating in totally for four protons, due to the symmetry of this molecule.

An additional sign to be mentioned is the disappearance of the singlet at 3.3 ppm that corresponds to the terminal alkyne of porphyrin **17**.

4.2. UV-Visible :

The recording of the UV-visible absorption spectra of the dimer **19** was carried out at room temperature in dichloromethane. Compound **19** shows the presence of a Soret band at 428 nm. As for the Q bands, this dimer contains a free and a metallated porphyrinic macrocycle. So, it is expected to have certain overlapping of the bands. That is because metallated porphyrins are characterized by two Q bands where the free base porphyrins by four. The following bands located at 513 nm (very weak), 555 nm (strong), 597 nm (strong) and 643 nm (weak) are identified. They correspond to the superposition of UV-Vis absorption of free base porphyrin and zinc complex. In addition, there is a wide band at 280 nm corresponding to the absorption of the six fluorenyl arms.

5. Synthesis of the free dimer 22

As mentioned at the beginning of this chapter, the target is to synthesize dimers of porphyrins as a model for the effect of light collecting antenna. Having zinc in one of the macrocycles (**19**), will quench the luminescence.

So now comes the step to get the free dimer **22**, starting from its analogue **19**. This was done by adding acid (TFA) to zinc complex **19**. This experiment was monitored by UV-visible (**Figure 6**).

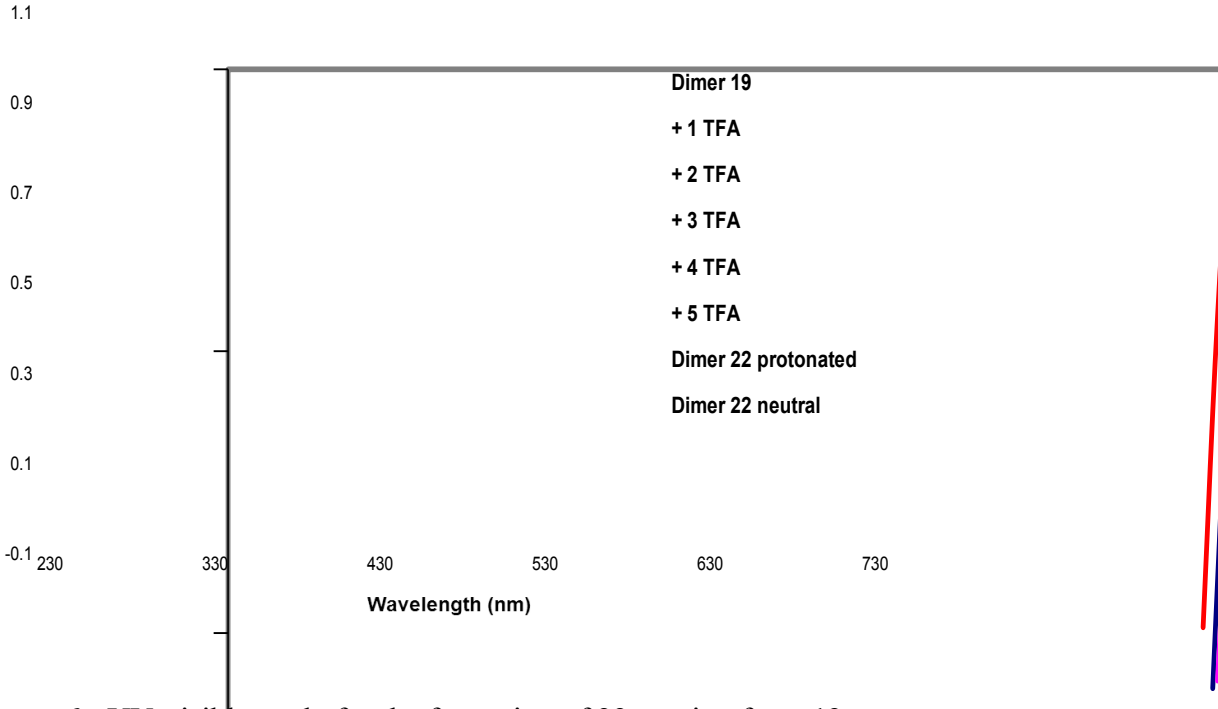

Figure 6 : UV-visible study for the formation of **22** starting from **19**

During a porphyrin titration experiment, going from basic to acidic conditions, the porphyrin macrocycle passes in the following stages as shown in **Figure 7**. It is also worth to define the stability constants since they will be used when we discuss the titration; for example, the acidity constant values of our reference are as follows : $pK_3 = 4.38$ and $pK_4 = 3.85$.[19,20]

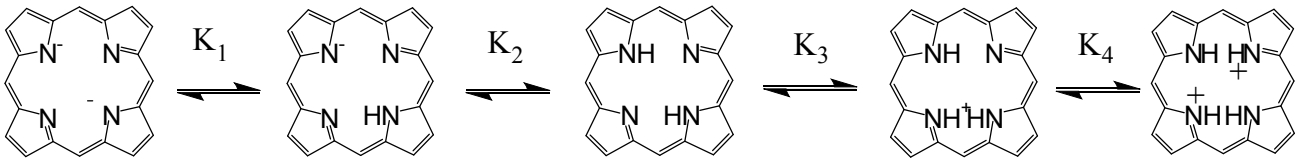

Di-Anion	Mono-Anion	Free Base	Mono-Cation	Di-Cation
Por^{2-}	**$HPor^{-}$**	**H_2Por**	**H_3Por^{+}**	**H_4Por^{2+}**

Figure 7 : Porphyrin macrocycle during titration

Concerning the titration of dimer **19**, the Soret band, initially at 428 nm, is red shifted to 463 nm due to protonation and the loss of encapsulated zinc. While protonating a porphyrin monomer, there exists a difference between stability constants K_3 and K_4. This difference is due to cooperative protonation, so only two forms are observed by spectral methods:[21] the neutral free base **H_2Por** and the dication **H_4Por^{2+}**.

In our work, dimer **19** is called **ZnPor-H_2Por** because composed of a zinc complex (**ZnPor**) and a free base (**H_2Por**). Dimer **19** has the Soret band at 428 nm as mentioned previously. Upon adding TFA to a DCM solution of dimer **19**, the following species will be formed :

$$[\textbf{ZnPor-H}_2\textbf{Por}] \longrightarrow [\textbf{ZnPor-H}_4\textbf{Por}]^{2+} \longrightarrow [\textbf{H}_4\textbf{Por-H}_4\textbf{Por}]^{4+}$$

In this specific case, the dication form **$[ZnPor\text{-}H_4Por]^{2+}$** was not observed, probably due to the small difference between stability constant. On the other hand, only the starting form [**ZnPor-H_2Por**] and the tetraprotonated form **$[H_4Por\text{-}H_4Por]^{4+}$** are observed by UV-Visible. So, we observe an isosbestic point at 432 nm; illustrating the formation of a distinct species: **$[H_4Por\text{-}H_4Por]^{4+}$**. For this tetracation porphyrin dimer, we observe the presence of a band at 463 nm and large band which is located at 684 nm corresponding to the superposition of UV-Vis absorption of two similar protonated porphyrins.[21] No evolution of the spectrum is observed if more acid is added.

Then, we neutralize this tetracation **[H_4Por-H_4Por]$^{4+}$**, by adding NEt_3 :

[H_4Por-H_4Por]$^{4+}$ $\xrightarrow{\text{Base}}$ **[H_2Por-H_2Por]**

Adding a base to this species **[H_4Por-H_4Por]$^{4+}$** means the deprotonation and the transformation of **[H_4Por-H_4Por]$^{4+}$** into the free base. The UV-visible spectrum showed that the band at 462 nm disappeared and an isosbestic point at 432 nm was observed again. In other words, the original spectrum was not restored because of the irreversible loss of zinc. No partial degradation was observed. A new form is obtained corresponding to the neutral species **[H_2Por-H_2Por]** named free dimer **22**.

6. Characterization of free dimer 22

6.1. ^{1}H NMR :

At high field, a singlet at – 2.70 ppm is observed: it integrates for four protons. These protons correspond to the 4 protons carried by the nitrogen atoms of the two porphyrin-free bases of **22**. This signal confirms the removal of zinc from the macrocycle.

In addition, another singlet that integrates for 12 protons is observed at 4.22 ppm. This singlet refers to the 12 protons of the CH_2 protons of the 6 fluorenyl groups.

The aromatic protons (fluorenyl and phenyl) resonate in the region between 7.4 and 8.9 ppm. All the seven protons on the six fluorenyl arms are equivalent, and in expected positions in comparison to the monomers : 8.32 (s, 6H), 8.18 (m, 6H), 8.08 (m, 6H), 7.98 (d, 6H), 7.68 (d, 6H), 7.52 (t, 6H) and 7.43 (t, 6H). At around 8.9 ppm, there is a large signal for the 16 *beta* pyrrolic protons.

6.2. UV-Visible :

The free dimer **22** shows the presence of a Soret band at 426 nm. This band is considered to be slightly blue shifted compared to 428 nm for dimer **19**. This could be referred to the loss of zinc.

This tendency in blue shifting is not observed for the Q bands. Instead, they are slightly red shifted compared to dimer **19**. They are located at 521 nm (strong), 557 nm (strong), 595 nm (strong) and 650 nm (weak).

Having four Q bands is characteristic to UV-Vis absorption of a free porphyrin. In addition, there is exaltation in UV absorption: a wide band at 268 nm corresponding to the absorption of the six fluorenyl arms is observed. We can notice (**Figure 8**) that in this conjugated system possessing 6 fluorenyl arms and two porphyrin macrocycles, the antenna absorption is stronger for dimer **22**, than for **TFP** possessing 4 arms per porphyrin core.

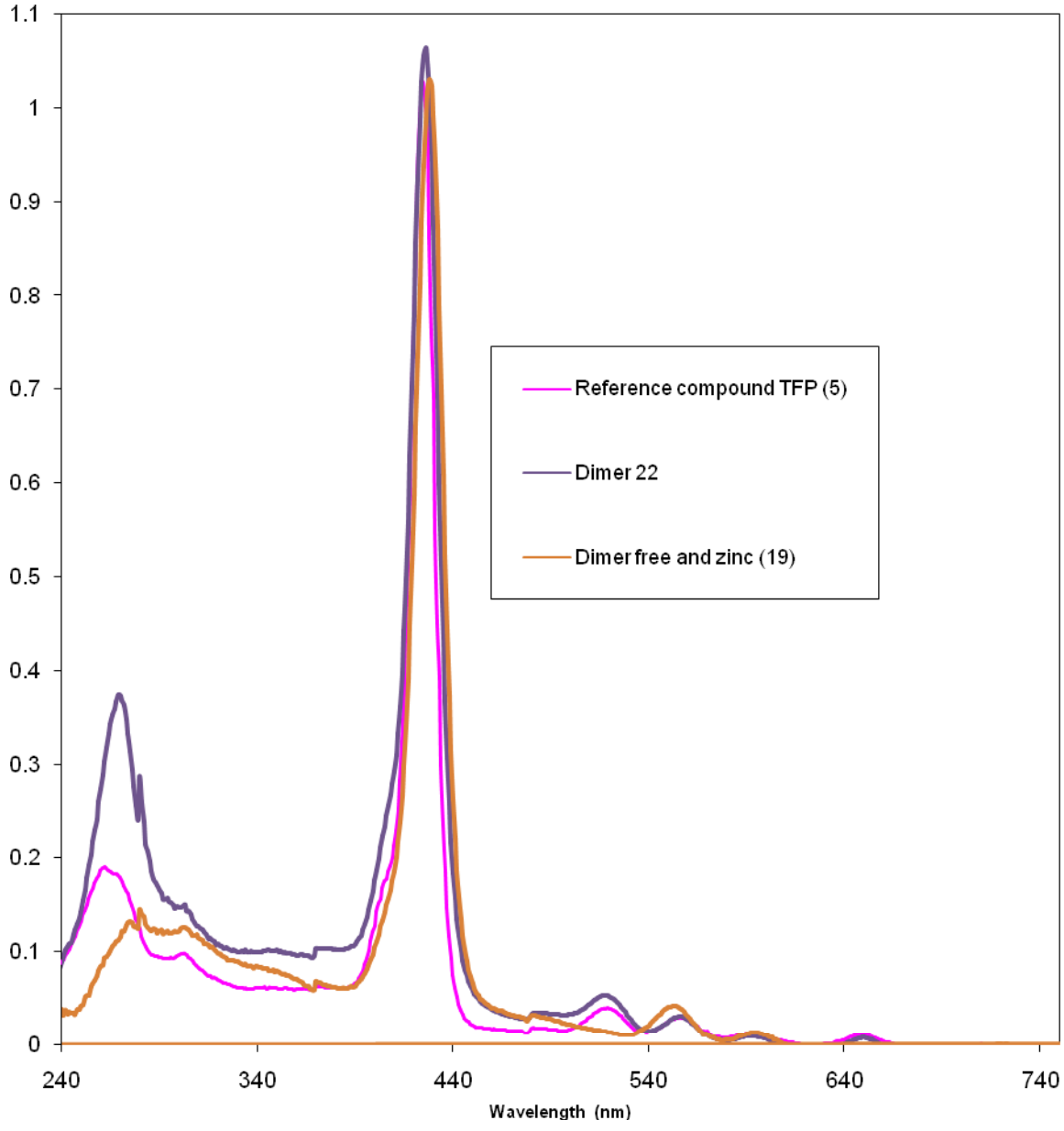

Figure 8 : Absorption spectra of **TFP** (pink), metallated dimer **19**, and free dimer **22** in DCM at room temperature. All the spectra are normalized to the spectrum of the reference **TPP** at 417 nm (concentration ~2.0 10^{-6} M)

7. Photophysical studies :

7.1. Emission Spectroscopy

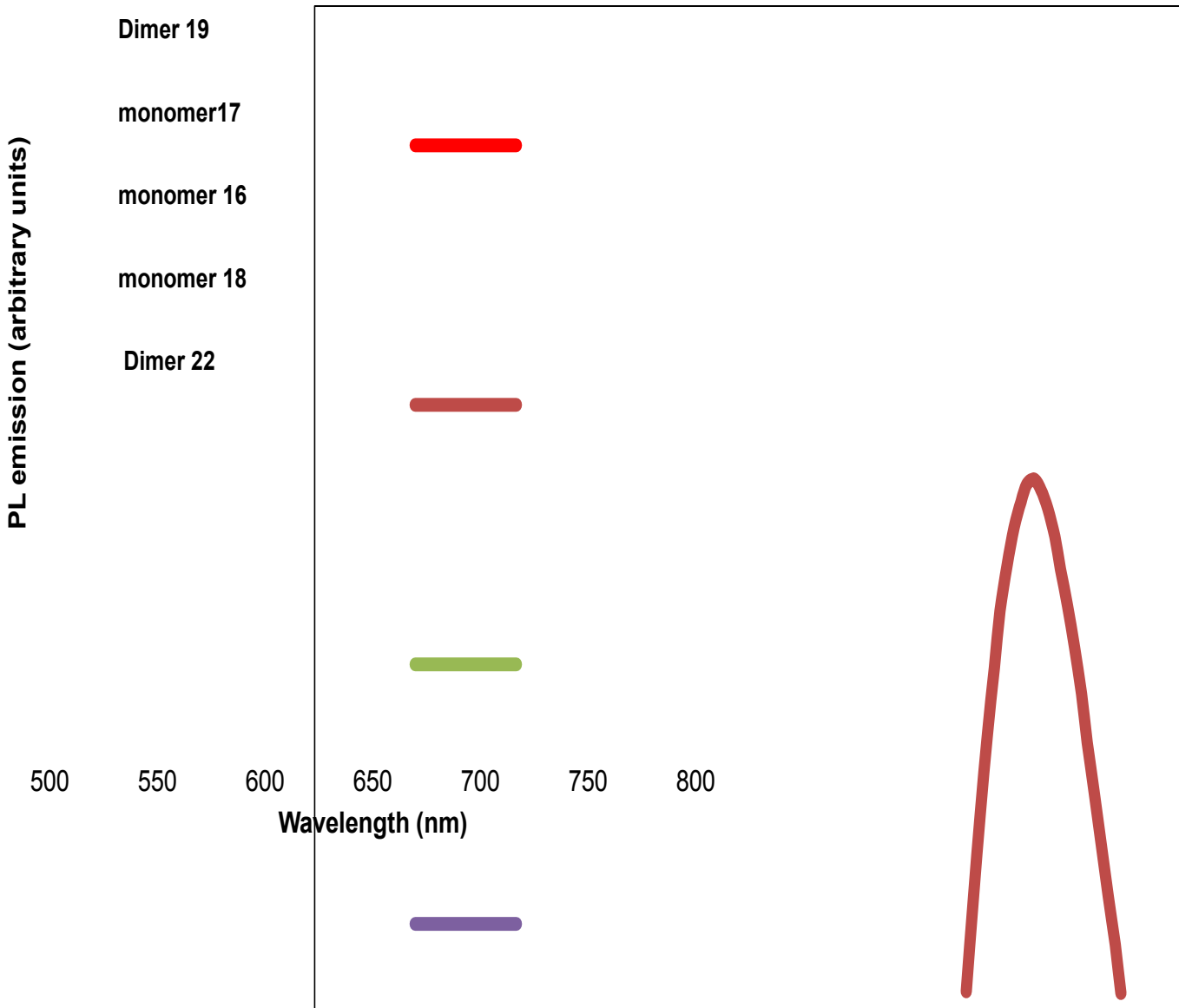

Figure 9 : Emission spectra of monomers **16**, **17** and **18** compared to dimers **19** and **22** in DCM at room temperature. All the spectra are normalized to the spectrum of dimer **19** at 657 nm (concentration ~2.0 10^{-6} M).

To better understand and compare the emission of dimers **19** and **22**, the emission of the monomers **16**, **17**, and **18** are presented (**Figure 9**) as well. The emission spectrum of compound **17**, after excitation in the Soret band reveals a strong red fluorescence with a peak maximum at 607 nm and a big band at 655 nm. The emission spectrum of compound **18** shows a strong red emission at 663 nm and a weak band at 728 nm, after excitation in the Soret band. In other words, by emission

spectroscopy, we should be able to clearly identify the free base moiety, and the zinc complex moiety of the dimer molecule.

Concerning, dimer **19**, effectively; after excitation in the Soret band, a weak emission at 600 nm, a strong red emission at 657 nm and a weaker shoulder at 720 nm are observed. In conclusion for this compound **19**, the free base part and the zinc complex part of the dimer molecule are identified. On the contrary, for demetallated dimer **22**, which is composed of two similar free base moieties, two peaks : at 657 and 720 nm are observed. In conclusion, the emission profile for free monomers **16**, **18** and free dimer **22** is quite similar.

7.2. Energy Transfer

The interest in this part is to discuss the efficiency of energy transfer from the fluorenyl arms (donors) to the porphyrin core (acceptor). Upon the excitation of dimers **19** and **22** in the antenna (at 280 nm) a red emission of porphyrins with a maximum at 657 nm is observed in both cases. Another thing to mention is that the blue fluorenyl emission is partly quenched for **19**, but almost completely quenched for **22**. In addition, red emission is seen predominantly from the porphyrin.

It is remarkable that, when excited directly at 425 nm, dimers **19** and **22** show a strong red emission in comparison to the indirect excitation at 280 nm. This couldn't be considered as inefficient energy transfer. Instead, it is considered as a complicated process.[22]

The excitation spectrum of compound **19** around 657 nm (**Figure 10**) reveals that the strong emission from the Soret state is populated when the fluorenyl band is excited. This indicates that excitation over all the 200-650 nm region leads to the population of the fluorescent excited states of the porphyrin, as the fluorene absorption becomes apparent under such excitation conditions.

For comparison, the corresponding excitation spectrum of free dimer **22** is also shown in (**Figure 10**). We can see an enhancement in the UV region due to the fluorenyl arms for the latter. In conclusion, the luminescence of **19** and **22** can be modulated in a large range of excitation wavelengths from UV to red, to finally obtain the desired red emission.

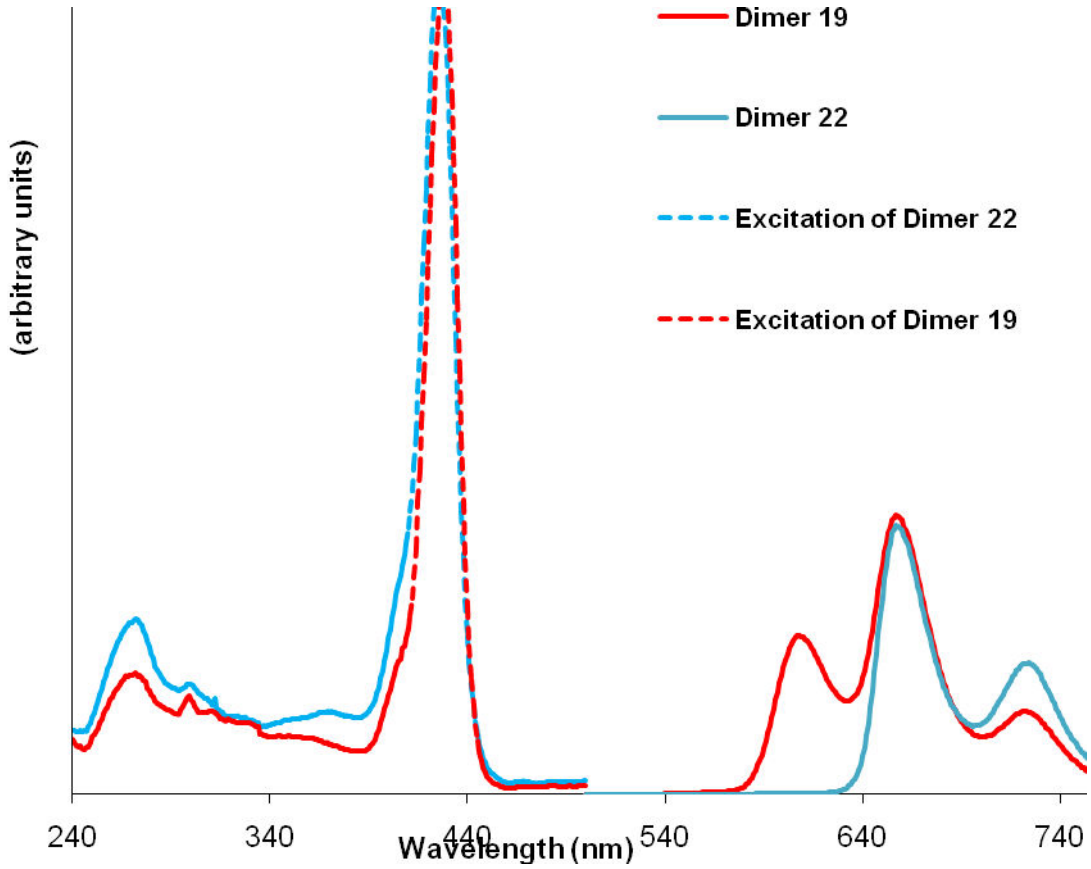

Figure 10 : Photoluminescence spectra of dimer **19** (red) and **22** (blue) in CH_2Cl_2 solution (~1.0 10^{-6} M), at 25°C, the emission spectra were cut above 800 nm. Excitation spectra of compounds **19** (dashed red) and **22** (dashed blue) at 650 nm

7.3. Fluorescence quantum yield

The fluorescence quantum yields of these compounds were next determined with respect to a calibration standard of the reference (**TPP**). This reference possesses fluorescence quantum yield of 0.12[23] in degassed toluene solution, and 0.13[24] in benzene solution. The quantum yield was calculated using the equation mentioned in the introduction (**Chapter 1**).

Monomer **17** and dimer **19** have low luminescence quantum yield (around 5-7%), which is higher than this of the reference compound **ZnTPP**. Monomer **18** has low yield as well, and that could be referred to the halogen effect.[25] Whereas the luminescence quantum yield of monomer **16** is relatively high (21%). As for the free dimer **22**, the yield is 17% which is high compared to **TPP** but not higher than **TFP**. Still it is considered an interesting result compared to non conjugated dendrimers.[26]

8. Synthetic strategies to obtain porphyrin Trimers

Based on the interesting photophysical properties of the free dimer **22**, it was motivating to go forward in coupling more porphyrin units to get assemblies with higher fluorenyl arms. As a next step was the synthesis of porphyrin trimer **24** possessing 8 fluorenyl units. This could be achieved in two ways from a retrosynthetic point of view (**Figure 11**).

One pathway is by reacting two equivalents of ethyne porphyrin **17** with bis-iodo porphyrin **23**. Another proposition is the reaction between mono iodo porphyrin with bis-ethynyl porphyrin. Following this method, the probability to get high molecular weight materials (HMWM) is more important. As a result, the first proposition is adapted. It is worth to mention that bis-iodo **23** is obtained as a fraction of the reaction mixture for the preparation of mono-iodo **18**.

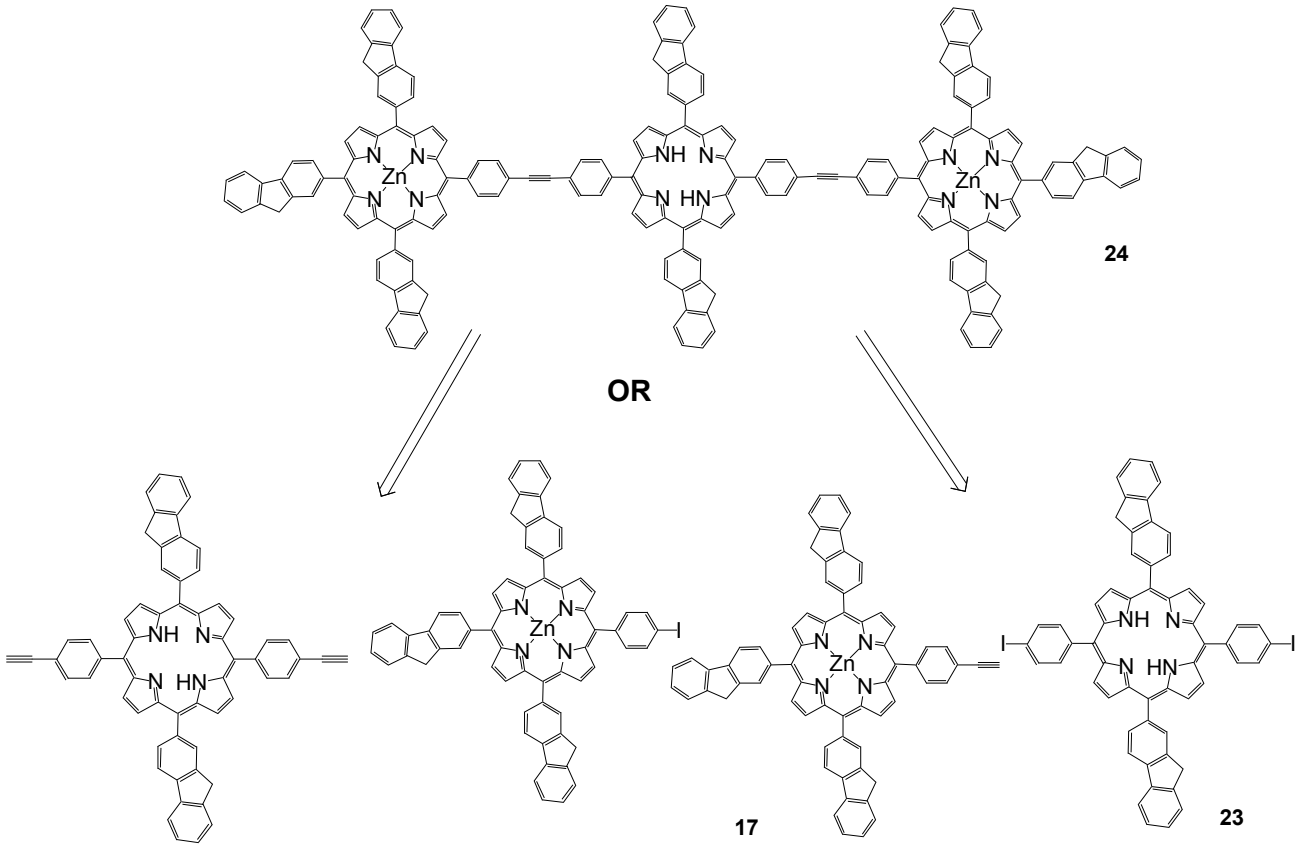

Figure 11 : Two possible synthetic routes for the preparation of trimer **24**

9. Synthesis of the Trimer 24

To synthesize trimer **24**, the coupling conditions that were used for dimer **22** are adapted. So, the ligand used was the triorthotolylphosphine since it worked well in the case of dimer synthesis.

In other words, the reaction was done at 35°C under argon. It was monitored by TLC and stopped after 72 hours. The solvent was taken to dryness. The residue was dissolved in dichloromethane, and then purified by 2 column chromatographies. Purification was accompanied by mass analysis to check what products are obtained.

Unfortunately, trimer **24** was obtained with a very low yield (less than 5%). In addition **24** is always obtained accompanied with HMWM comprised as undefined porphyrin oligomers.[16]

It was clear that the conditions used were not the optimized ones to get such low yield and impurities. Another trial to get **24** was done using $AsPh_3$ as a ligand. This time, reaction conditions were used as mentioned in the literature.[6] So, reaction was done at 35°C for 72 hours (**Scheme 9**).

In these conditions, the yield was better (25%), and the purification was easier in a way that **24** was obtained as a pure violet powder.

Trimer **24** was characterized by **^{1}H NMR**, but still we need a bigger quantity of the product for NMR peaks to be assigned precisely. At least, **^{1}H NMR** shows a singlet at 4.2 ppm that corresponds to the 16 protons of the CH_2 protons of the 8 fluorenyl groups. The aromatic protons (fluorenyl and phenyl) resonate in the region between 7.5 and 8.5 ppm. The signals of the seven protons on the eight fluorenyl arms are large and more NMR experiments are needed to assign these protons. Around 9 ppm, there are signals assigned to the *beta* pyrrolic protons.

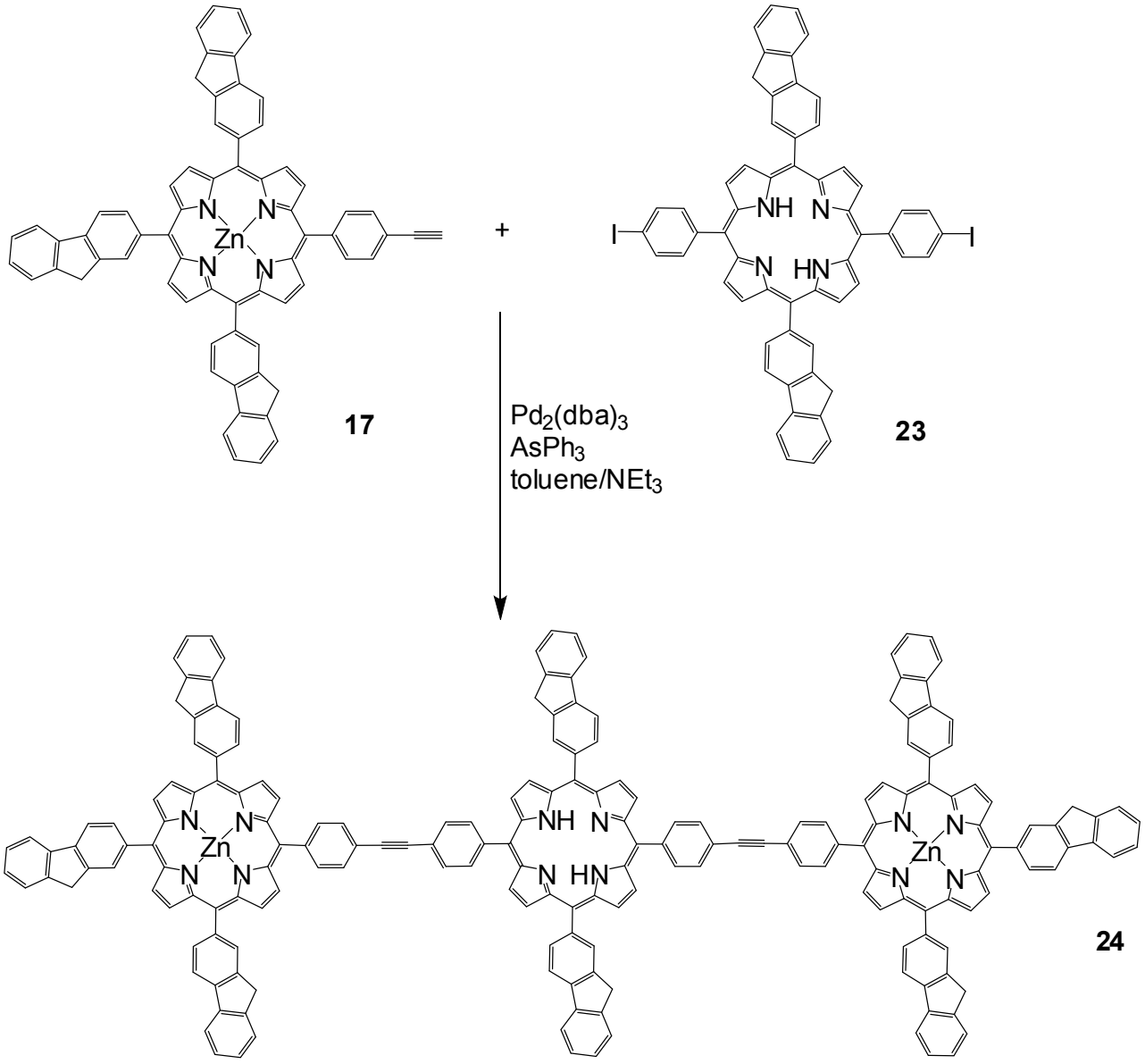

Scheme 9 : Synthesis of the trimer 24

The reaction was tried on a small scale so only few mg were collected, and they weren't sufficient to do all the needed analysis.

For the moment, the work on this optimized synthesis is still in progress.

II. Organometallic porphyrin assemblies

As it was mentioned at the beginning of this chapter, the second part will be concerning the synthesis of organometallic porphyrins having ruthenium moiety, and using the benefit of high luminescence due to fluorenyl arms. The target is to study the luminescent properties of these new complexes and then to try to switch these properties by the oxidation of ruthenium. The two proposed complexes are presented in **Figure 12**.

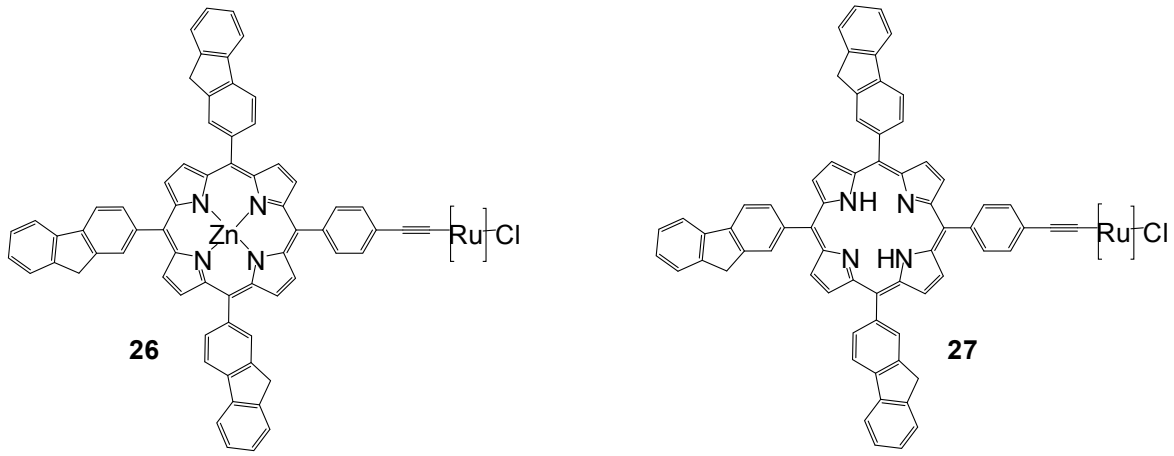

Figure 12 : Proposed target molecules **26** and **27**

1. Synthesis and characterization of zinc porphyrin ruthenium complex 26

To synthesize **26**, a solution of **17**, and excess of the 16 electron Ru species (**25**) was prepared in distilled dichloromethane under argon (**Scheme 10**) at room temperature. Ruthenium salt (**25**) was used in excess to avoid a mixture of the starting material and the desired product **26**. This is because the separation will be difficult since **26** decomposes on silica.

In addition, **26** and **17** have nearly same solubility, so purification by precipitation couldn't be used. The reaction mixture was stirred at room temperature and followed by **^{31}P** and **^{1}H NMR**. The ruthenium species (**25**) is characterized by two triplets at 55.8 and 83.7 ppm for **^{31}P NMR**. The vinylidene formed is expected to have a singlet at around 37 ppm. In other words, **^{31}P NMR** was able to tell the progress of the reaction but not the completion since the ruthenium species is used in excess.

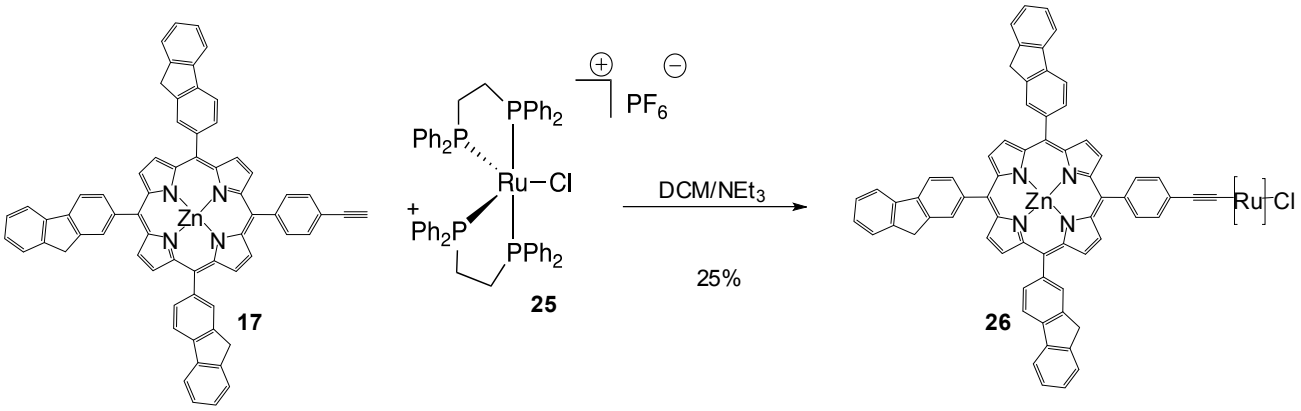

Scheme 10 : Synthesis of **26**

The disappearance of the two triplets will not be observed. On the contrary, the ^{1}H NMR can be significant in this case. Compound **17** must be totally consumed, so the singlet of the terminal alkyne at 3.3 ppm must disappear. After 72 hours, the reaction was complete, and concentrated under reduced pressure.

The desired vinylidene was precipitated in ether to remove the excess of **25**. The obtained vinylidene was dissolved in 10 mL of dichloromethane, and deprotonated by adding triethylamine (0.25 mL) dropwise.

The brown green solution was concentrated and filtered over few centimeters of basic alumina using dichloromethane and 2% triethylamine as eluent. In turn, the solution was concentrated and the desired product **26** was precipitated in ether to yield a greenish brown solid (yield 25%).

The new complex **26** was characterized by the usual spectroscopies (NMR, UV-vis), mass, and elemental analysis. The **^{31}P NMR** showed a singlet at 50 ppm. This singlet corresponds to the four equivalent phosphorus atoms from the two dppe ligands coordinated to the ruthenium group.

^{1}H NMR of **26** shows a broad singlet at 2.8 ppm that corresponds to the eight- equivalent CH_2 protons of the dppe. It exhibits signatures of porphyrin as well. For example, two peaks, a singlet at 4.2 ppm, and another at 4.22 ppm characterize $C\underline{H_2}$ protons of fluorenes. Between 7 and 8.5 ppm, the seven peaks that correspond to the fluorene groups are identified. In addition, the β pyrrolic protons are identified by the peaks at around 9 ppm.

The **UV-visible** study was done in dichloromethane at room temperature. It shows the presence of the Soret band at 424 nm. Two Q bands are observed at 550, and 596 nm respectively. In addition, a band at 258 nm is observed which corresponds to the absorption of the three fluorenyl units.

2. Synthesis and characterization of the free base porphyrin complex 27

To synthesize **27**, the procedure of **26** is exactly adapted except using the free base porphyrin **16** instead of zinc complex **17** as a starting material. Same NMR signals were observed as well. The only difference was in the **^{1}H NMR**, where an additional singlet was observed at – 2.6 ppm characterizing the NH protons. This is to prove that the porphyrin macrocycle is free.

The **UV-visible** spectrum was done in dichloromethane at room temperature. It shows the presence of the Soret band at 422 nm. Normally, it is expected to get 4 Q bands that characterize a free base porphyrin. In our case, three Q bands are observed at 513, 569, and 657 nm. It is important to mention that the band at 569 is large, which could be the overlap of more than one band. On the other hand, a band at 259 nm is observed which corresponds to the fluorenyl absorption.

3. Emission Spectroscopy

The emission spectrum of the free base complex **27** after excitation in the Soret band reveals a strong red fluorescence with a peak maximum at 659 nm and a weaker band at 724 nm (**Figure 13**). Whereas, the emission spectrum of the zinc metallated ruthenium complex **26** after excitation in the Soret band reveals a weaker red fluorescence with a peak maximum at 612 nm and a weaker band at 659 nm. In conclusion, the emission profile of the free porphyrin (**27**) complex is more red shifted in comparison to its metallated analogue (**26**).

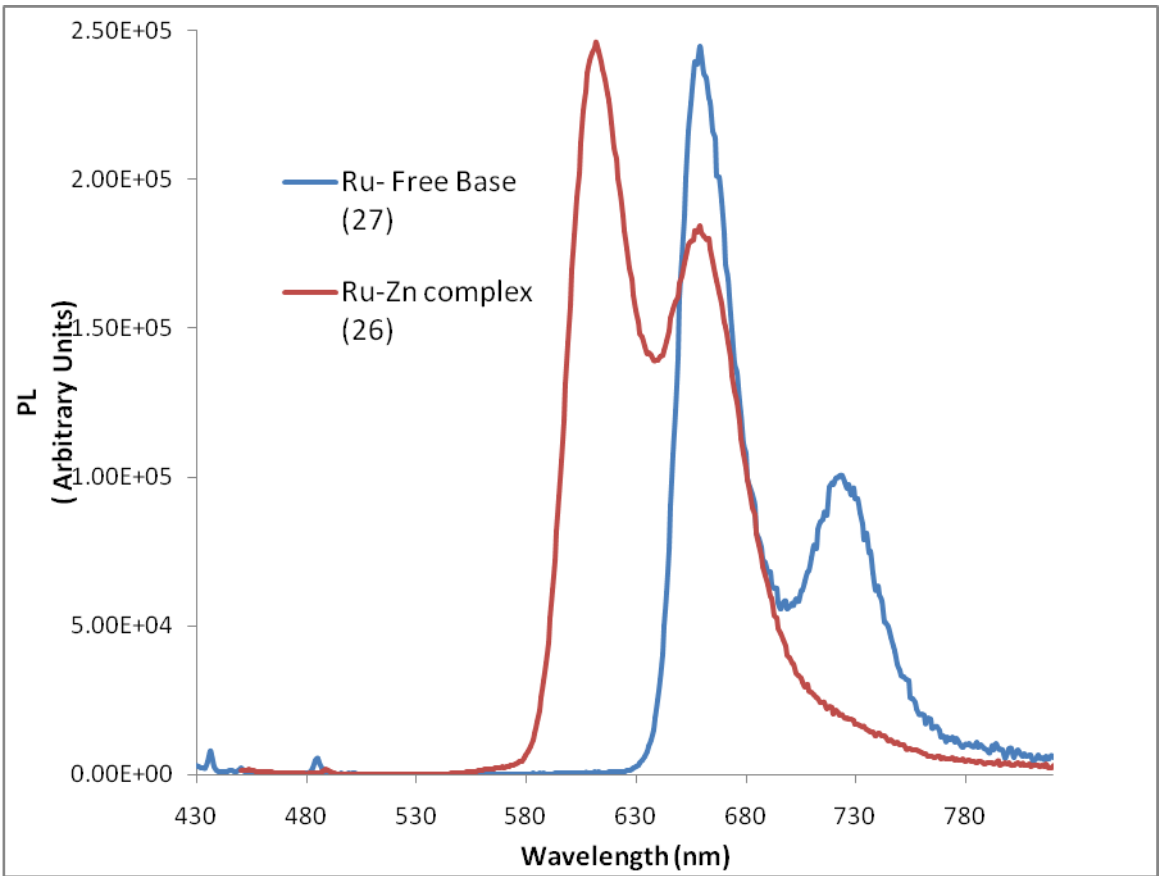

Figure 13 : Emission spectra of monomers **26** (red) and **27** (blue) in DCM solution (~1.0 10^{-6} M for **27** and ~1.0 10^{-5} M for **26**) at room temperature after excitation at 420 nm

4. Fluorescence quantum yield

As mentioned in this chapter (part **7.3.**), the fluorescence quantum yield of these compounds are measured with respect to a calibration standard of the reference **TPP**.

These ruthenium complexes (**26** and **27**) possess low luminescence quantum yields (0.02 and 1.54%) respectively. These values are less than that of the reference **TPP** (12%)[23] and its metallated analogue **ZnTPP** (3.3%).[27]

III. Conclusion and perspectives

For the first part of this chapter, a new organic dimer **22** was synthesized and fully characterized. Luminescence studies were promising with respect to the references **TPP** and **TFP**. The synthesis of corresponding trimer was optimized, but still more quantity is needed to fully characterize and study this new complex. Perspectives can be modifying the **bridge** connecting the two porphyrins of the assembly to optimize the luminescence as proposed in **Figure 14**.

Another thing is to extend the synthesis to tetramer and pentamer synthesis as well. We can also consider grafting fluorenyl dendrons at the periphery of these new dimers, to have more antenna around the porphyrin core for light collection.

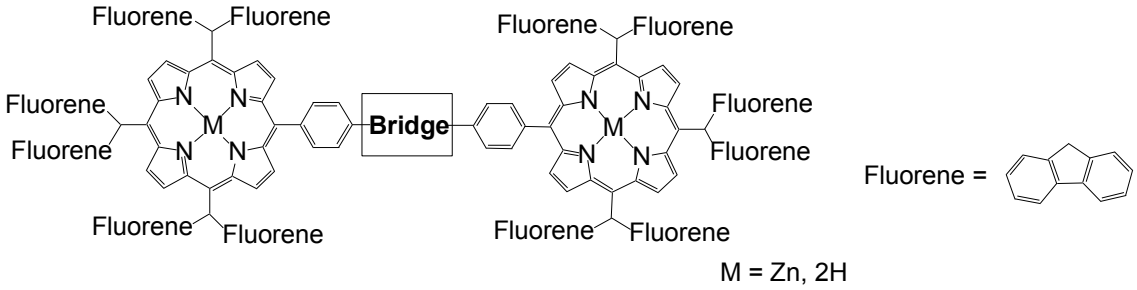

Figure 14 : Perspective dimer with fluorene dendrons and modified bridge

For the next part of the chapter, concerning the organometallic assemblies, new complexes, **26** and **27** were synthesized and characterized. Preliminary luminescence studies are promising. Further work is to try to oxidize the ruthenium moitey and check if the concept of switch can be applied. Based on the results obtained, the bis acetylide as shown in **Figure 15** can be a future target molecule. It would be interesting then to compare mono organometallic assemblies to their corresponding bis acetylides.

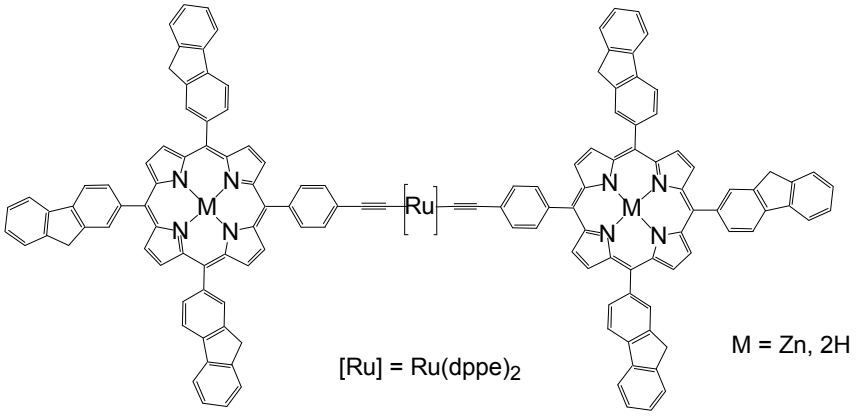

Figure 15 : The bis acetylide as a target molecule

Experimental Section

Synthesis of 4-((trimethylsilyl)ethynyl)benzaldehyde : 14

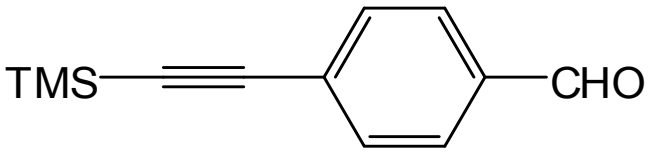

Trimethylsilylacetylene (5 mL, 4.03 g, 41.0 mmol), was added to a solution of 4-bromobenzaldehyde (5.00 g, 27.0 mmol), $Pd(PPh_3)_2Cl_2$ (50 mg, 0.07 mmol) and CuI (25 mg, 0.13 mmol) in distilled THF (40 mL) under argon. Then, triethylamine (6.5 mL) was added and the reaction mixture was heated at 40°C overnight. The solvent was evaporated under reduced pressure. The obtained residue was extracted in dichloromethane, washed in water, dried with $MgSO_4$, and then taken into dryness. The solid was then purified by column chromatography on silica gel using a mixture of heptane/DCM (1 : 1) as eluent.

The compound **14** was obtained as a pale yellow solid to yield 5.04 g (92%).

^{1}H NMR (400 MHz, $CDCl_3$, δ in ppm) : 10.01 (s, 1H, CHO), 7.83 (d, 2H, H_{phenyl}, $^3J_{HH}$ = 7.6 Hz), 7.62 (d, 2H, H_{phenyl}, $^3J_{HH}$ = 7.2 Hz), 0.29 (s, 9H, $(C\underline{H_3})_3Si$).

Synthesis of 5,10,15-(trifluorenyl)-20-(4-((trimethylsilyl)ethynyl)phenyl)porphyrin : <u>15</u>

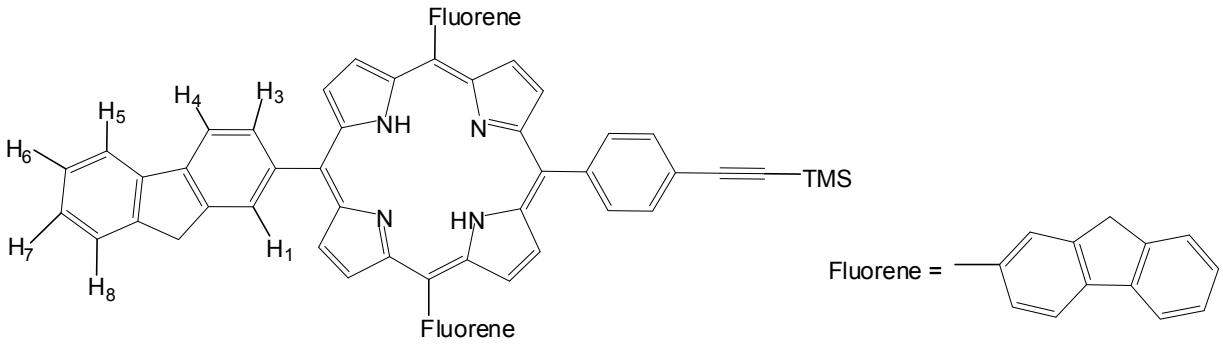

2-Fluorenylcarboxylaldehyde (3.00 g, 15.4 mmol), 4-((trimethylsilyl)ethynyl)benzaldehyde (1.00 g, 5.0 mmol) and pyrrole (1.4 mL, 20.0 mmol) were added to distilled chloroform (1.5 L) in a double necked round bottom flask under argon. The flask was covered with aluminium foil since the reaction is light sensitive at this stage. Boron trifluoride diethyl etherate, $BF_3.OEt_2$ (560 µL) was added, and the reaction was kept at room temperature for three hours. Then, three equivalents of *p*-chloranil (3.78 g, 15.4 mmol) were added and the solution was heated to reflux (light protection was removed). After 1 h, the solution was cooled to room temperature. Two pipettes of triethylamine were added to neutralize the reaction mixture. Solvent was evaporated and the residue was filtered over silica with heptane/DCM (65 : 35) and then (45 : 55). The solid obtained was subjected to a second column chromatography of silica using the eluent heptane/DCM (70 : 30). The expected compound **15** was obtained as a purple solid to yield 756 mg (15%). This new porphyrin was fully characterized by usual solution spectroscopies (NMR and mass spectrometry) and microanalysis.

^{1}H NMR (400 MHz, $CDCl_3$, δ in ppm) : 8.92 (d, 2H, $^3J_{HH}$ = 5.0 Hz, $H_{\beta\text{-pyrrolic}}$), 8.91 (s, 4H, $H_{\beta\text{-pyrrolic}}$), 8.82 (d, 2H, $^3J_{HH}$ = 4.4 Hz, $H_{\beta\text{-pyrrolic}}$), 8.38 (s, 3H, $H_{fluorenyl}$, H_1), 8.25 (d, 3H, $^3J_{HH}$ = 7.6 Hz, $H_{fluorenyl}$, H_4), 8.17 (m, 5H, $2H_{phenyl}$ and $3H_{fluorenyl}$ H_3), 8.06 (d, 3H, $^3J_{HH}$ = 8.0 Hz, $H_{fluorenyl}$, H_5), 7.87 (d, 2H, $^3J_{HH}$ = 8.4 Hz, H_{phenyl}), 7.70 (d, 3H, $^3J_{HH}$ = 7.2 Hz, $H_{fluorenyl}$, H_8), 7.52 (m, 3H, $H_{fluorenyl}$, H_6), 7.44 (m, 3H, $H_{fluorenyl}$, H_7), 4.20 (s, 6H, $3CH_{2\text{-fluorenyl}}$), 0.29 (s, 9H, $Si(CH_3)_3$), - 2.61 (broad s, 2H, NH).

Analysis : calcd for $C_{70}H_{50}N_4Si.0.5CHCl_3$: C, 81.82, H, 4.92, N, 5.14, found : C, 81.88, H, 6.06, N, 4.71.

MALDI TOF-MS : calcd for $C_{70}H_{50}N_4Si$: 975.38047 $[MH]^+$, found $[MH]^+$: 975.43900.

Synthesis of 5,10,15-(trifluorenyl)-20-(4-ethynylphenyl)porphyrin : <u>16</u>

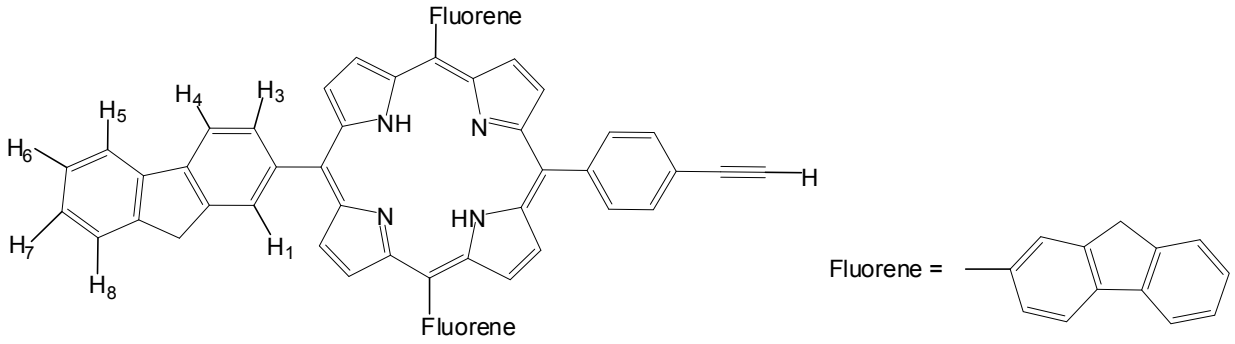

Potassium carbonate (145 mg, 1.05 mmol) was added to a solution of porphyrin **15** (200 mg, 0.21 mmol) in distilled DCM (36 mL) and methanol (12 mL) under argon. The reaction mixture was stirred at room temperature for 47 hours. Then, solvent was evaporated under reduced pressure. The obtained residue was extracted in dichloromethane, washed with 10% (v/v) aqueous solution of sodium hydrogen carbonate, dried with $MgSO_4$, and then taken into dryness. The solid obtained was filtered over silica with DCM as an eluent. The deprotected porphyrin **16** was fully characterized and was obtained as a purple powder to yield 187 mg (98%).

^{1}H NMR (400 MHz, $CDCl_3$, δ in ppm) : 8.94 (d, 2H, $^3J_{HH}$ = 5.0 Hz, $H_{\beta\text{-pyrrolic}}$), 8.92 (s, 4H, $H_{\beta\text{-pyrrolic}}$), 8.84 (d, 2H, $^3J_{HH}$ = 4.4 Hz, $H_{\beta\text{-pyrrolic}}$), 8.39 (s, 3H, $H_{fluorenyl,}$ H_1), 8.25 (d, 3H, $^3J_{HH}$ = 7.6 Hz, $H_{fluorenyl,}$ H_4), 8.17 (m, 5H, $2H_{phenyl}$ and $3H_{fluorenyl,}$ H_3), 8.06 (d, 3H, $^3J_{HH}$ = 7.6 Hz, $H_{fluorenyl,}$ H_5), 7.89 (d, 2H, $^3J_{HH}$ = 8.0 Hz, H_{phenyl}), 7.70 (d, 3H, $^3J_{HH}$ = 7.2 Hz, $H_{fluorenyl,}$ H_8), 7.53 (m, 3H, $H_{fluorenyl}$, H_6), 7.44 (m, 3H, $H_{fluorenyl}$, H_7), 4.21 (s, 6H, $3CH_{2\text{-fluorenyl}}$), 3.31 (s, 1H, C_{alkyne}-H), - 2.65 (broad s, 2H, NH).

FT-IR (n, KBr, cm^{-1}) : 2106 (C≡ C).

UV-vis (λ max, (ε, 10^{-3} $M^{-1}.cm^{-1}$), CH_2Cl_2, nm) : 275 (83), 425 (624), 519 (24), 556 (14), 593 (4.7), 649 (4.9).

Analysis : calcd for $C_{67}H_{42}N_4.CH_3OH$: C, 87.34, H, 4.96, N, 5.99, found : C, 87.51, H, 5.08, N, 5.70.

MALDI TOF-MS : calcd for $C_{67}H_{42}N_4$: 903.34877 $[MH]^+$, found 903.3400 $[MH]^+$.

MS (ESI) : calcd for $C_{67}H_{42}N_4$: 925.33072 $[MNa]^+$, 903.34877 $[MH]^+$, found : 925.3305 $[MNa]^+$, 903.3471 $[MH]^+$.

Synthesis of Zn(II)-5,10,15-(trifluorenyl)-20-(4-ethynylphenyl)porphyrinato : 17

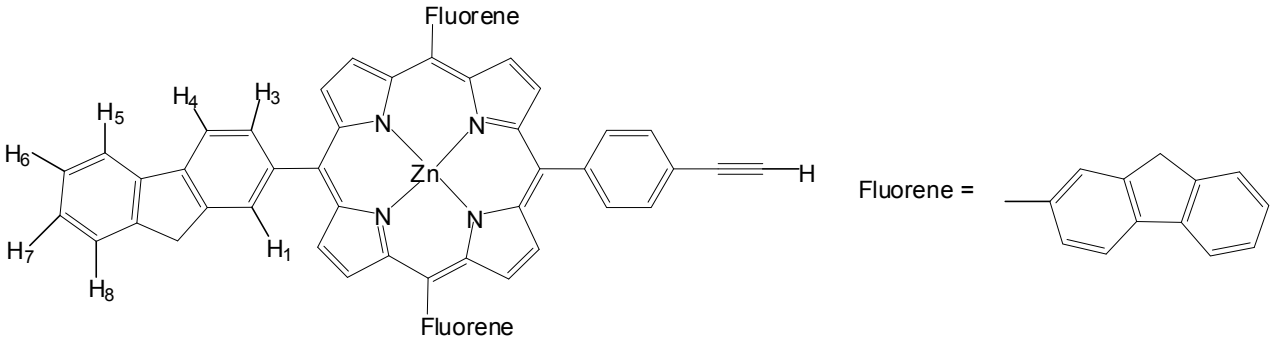

$Zn(CH_3CO_2)_2.2H_2O$ (220 mg, 1.0 mmol) was added to a solution of porphyrin **16** (185 mg, 0.2 mmol) in distilled DCM (127 mL) and methanol (63 mL) under argon. The reaction mixture was stirred during 24h at room temperature. The reaction progress was monitored by UV-visible spectroscopy and by TLC, spotting directly from the organic layer. Solvent was evaporated under reduced pressure. The obtained residue was extracted in dichloromethane, washed with 10% (v/v) aqueous solution of sodium hydrogen carbonate, dried with $MgSO_4$, and then taken into dryness. The solid obtained was filtered over silica with DCM as an eluent. The metallated porphyrin **17** was obtained as a purple solid to yield 188 mg (97%). The new intermediate porphyrin **17** was fully characterized.

^{1}H NMR (400 MHz, $CDCl_3$, δ in ppm) : 9.04 (d, 2H, $^3J_{HH}$ = 5.0 Hz, $H_{\beta\text{-pyrrolic}}$), 9.02 (s, 4H, $H_{\beta\text{-pyrrolic}}$), 8.93 (d, 2H, $^3J_{HH}$ = 4.4 Hz, $H_{\beta\text{-pyrrolic}}$), 8.39 (s, 3H, $H_{fluorenyl,}$ H_1), 8.25 (d, 3H, $^3J_{HH}$ = 8.0 Hz, $H_{fluorenyl,}$ H_4), 8.17 (m, 5H, $2H_{phenyl}$ and $3H_{fluorenyl:}$ H_3), 8.05 (d, 3H, $^3J_{HH}$ = 7.2 Hz, $H_{fluorenyl,}$ H_5), 7.89 (d, 2H, $^3J_{HH}$ = 8.0 Hz, H_{phenyl}), 7.69 (d, 3H, $^3J_{HH}$ = 7.6 Hz, $H_{fluorenyl,}$ H_8), 7.53 (m, 3H, $H_{fluorenyl,}$ H_6), 7.44 (m, 3H, $H_{fluorenyl,}$ H_7), 4.20 (s, 6H, $3CH_{2\text{-fluorenyl}}$), 3.30 (s, 1H, C_{alkyne}-H).

FT-IR (n, KBr, cm^{-1}) : 2106 (C≡C).

UV-vis (λ max, (ε, 10^{-3} $M^{-1}.cm^{-1}$), CH_2Cl_2, nm) : 273 (36), 303 (19), 428 (316), 554 (11), 596 (3).

Analysis : calcd for $C_{67}H_{40}N_4Zn.CH_3OH$: C, 81.80, H, 4.44, N, 5.61, found : C, 81.22, H, 4.75, N, 5.18.

MALDI TOF-MS : calcd for $C_{67}H_{40}N_4Zn$: 965.25444 $[MH]^+$, found : 965.90810 $[MH]^+$.

MS (ESI) : calcd for $C_{67}H_{40}N_4Zn$: 987.24421 $[MNa]^+$, found : 987.2432 $[MNa]^+$.

Synthesis of 5, 10, 15-(trifluorenyl)-20-(4-iodophenyl)porphyrin : <u>18</u>

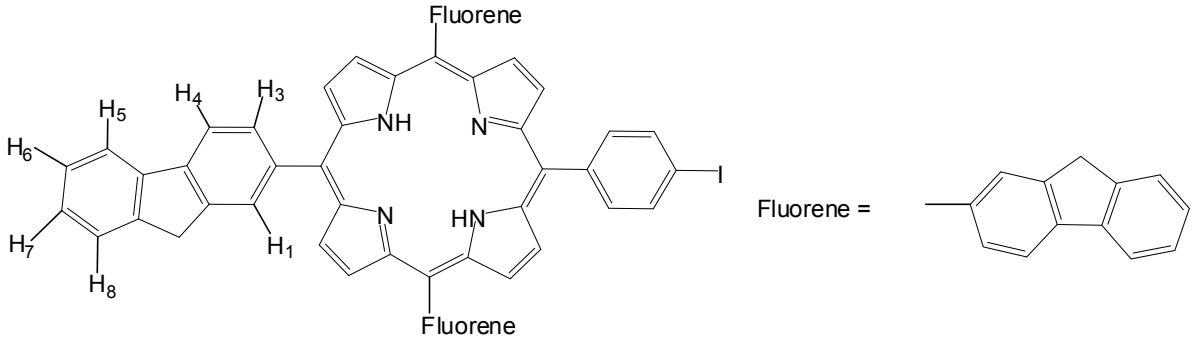

A solution of *p*-iodobenzaldehyde (1.00 g, 4.3 mmol), 2-fluorenecarboxaldehyde (2.52 g, 12.9 mmol) and pyrrole (1.18 mL, 17.2 mmol) in distilled chloroform (1.5 L) was placed in a two necked flask under argon. The chloroform solution was degassed by argon bubbling for 20 minutes. The flask was covered with aluminium foil since the reaction is light sensitive at this stage. Boron trifluoride diethyl etherate, $BF_3.OEt_2$ (690 µL) was added with a syringe. The solution was stirred for three hours at room temperature. Then, the oxidant, *p*-chloranil (3.44 g, 14 mmol) was added, and the reaction mixture was refluxed for one hour (light protection was removed). After neutralization of the acid catalyst by adding two pipettes of triethylamine, the solvent was removed. The resulting black solid was purified twice by column chromatography (column 1 : CH_2Cl_2/heptane 1 : 1, and then column 2 : CH_2Cl_2/heptane 1 : 4) affording 330 mg (8%) of the desired porphyrin **18** as a purple solid. The new intermediate porphyrin **18** was fully characterized.

^{1}H NMR (400 MHz, $CDCl_3$, δ in ppm) : 8.94 (d, 2H, $^3J_{HH}$ = 5.0 Hz, $H_{\beta\text{-pyrrolic}}$), 8.92 (s, 4H, $H_{\beta\text{-pyrrolic}}$), 8.84 (d, 2H, $^3J_{HH}$ = 4.4 Hz, $H_{\beta\text{-pyrrolic}}$), 8.39 (s, 3H, $H_{fluorenyl,}$ H_1), 8.24 (d, 3H, $^3J_{HH}$ = 8.0 Hz, $H_{fluorenyl,}$ H_4), 8.15 (m, 5H, $2H_{phenyl}$ and $3H_{fluorenyl,}$ H_3), 8.05 (d, 3H, $^3J_{HH}$ = 7.6 Hz, $H_{fluorenyl,}$ H_5), 7.96 (d, 2H, $^3J_{HH}$ = 7.6 Hz, H_{phenyl}), 7.70 (d, 3H, $^3J_{HH}$ = 7.2 Hz, $H_{fluorenyl,}$ H_8), 7.52 (m, 3H, $H_{fluorenyl,}$ H_6), 7.44 (m, 3H, $H_{fluorenyl,}$ H_7), 4.20 (s, 6H, $3CH_{2\text{-fluorenyl}}$), - 2.60 (s, 2H, NH).

UV-vis (λ max, (ε, 10^{-3} $M^{-1}.cm^{-1}$), CH_2Cl_2, nm) : 275 (34), 424 (287), 519 (11), 556 (5), 593 (1.5), 649 (1.6).

Analysis : calcd for $C_{65}H_{41}IN_4.0.5CH_2Cl_2$: C, 75.11, H, 4.04, N, 5.35, found : C, 74.60, H, 4.40, N, 5.17.

MALDI TOF-MS : calcd for $C_{65}H_{41}IN_4$: 1027.22737 $[MNa]^+$, found : 1027.22640 $[MNa]^+$ and 1005.24542 $[MH]^+$, found : 1005.24460 $[MH]^+$.

Attempt to synthesis of the dimer 19 using $AsPh_3$ as a ligand :

A solution of **17**, zinc(II)-5,10,15-(trifluorenyl)-20-(4-ethynylphenyl)porphyrinato (52 mg, 0.053 mmol), free base **18**, 5,10,15-(trifluorenyl)-20-(4-iodophenyl)porphyrin (50 mg, 0.050 mmol), $Pd_2(dba)_3.CHCl_3$ (16 mg, 0.015 mmol), and $AsPh_3$ (37 mg, 0.12 mmol) was prepared in 18 mL of freshly distilled THF under argon. Then, triethylamine (3.5 mL) was added to this solution. This reaction mixture was stirred for 72 hours at 35°C under argon. Then, it was cooled at room temperature, filtered and evaporated to dryness. The residue was purified by column chromatography on silica gel using DCM/heptane (1 : 1) as eluent then increasing the proportion of DCM till 100% affording the product **19**, as a dark red impure powder with a yield around 5%. Two side products (**20**, and **21**) were isolated and characterized as shown below.

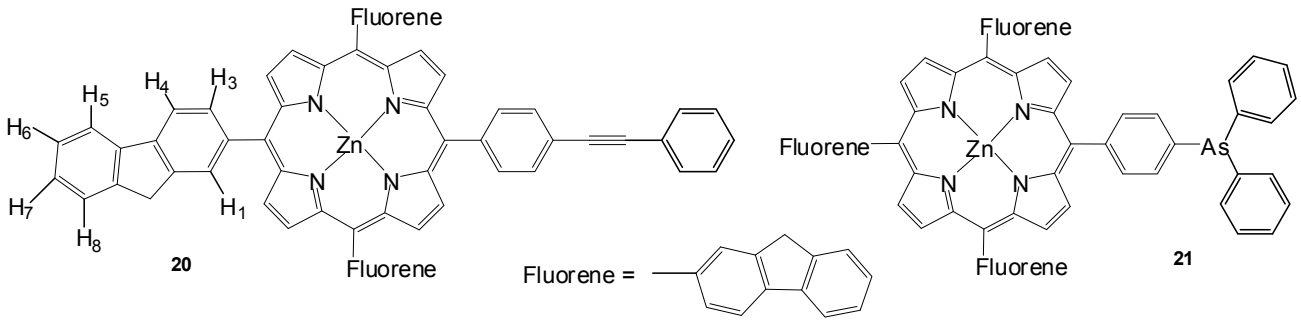

The porphyrin **20** was obtained pure as a first fraction of the column when using DCM/heptane (1 : 1), and was isolated as a purple solid and characterized by ^1H NMR and Mass.

^1H NMR (400 MHz, $CDCl_3$, δ in ppm) : 9.01 (d, 2H, $^3J_{HH}$ = 4.8 Hz, $H_{\beta\text{-pyrrolic}}$), 9.00 (s, 4H, $H_{\beta\text{-pyrrolic}}$), 8.95 (d, 2H, $^3J_{HH}$ = 4.8 Hz, $H_{\beta\text{-pyrrolic}}$), 8.38 (s, 3H, $H_{fluorenyl,}$ H_1), 8.22 (m, 5H, $2H_{phenyl}$ and $3H_{fluorenyl,}$ H_4), 8.14-8.11 (m, 3H, $H_{fluorenyl,}$ H_3), 8.05-8.02 (m, 3H, $H_{fluorenyl,}$ H_5), 7.92 (d, 2H, $^3J_{HH}$ = 8.0 Hz, H_{phenyl}), 7.69-7.66 (m, 5H, $2H_{phenyl}$ and $3H_{fluorenyl,}$ H_8), 7.54-7.50 (m, $3H_{fluorenyl,}$ H_6), 7.44-7.40 (m, 5H, $2H_{phenyl}$ and $3H_{fluorenyl,}$ H_7), 4.18 (s, 6H, $3CH_{2\text{-fluorenyl}}$).

MALDI TOF-MS : calcd for $C_{73}H_{44}N_4Zn$: 1043.54742 $[MH]^+$, found : 1043.0360 $[MH]^+$.

As for the porphyrin **21**, among the obtained fractions from the column chromatography, the arsine porphyrin **21** was obtained in a purple solid, always mixed with non-reacted iodo compound **18** or dimer **19**. This by-product **21** was characterized by Mass:

MALDI TOF-MS : calcd for $C_{77}H_{51}AsN_4$: 1108.17740 $[MH]^+$, found : 1108.04600 $[MH]^+$.

Synthesis of dimer 19 using $P(o\text{-}tol)_3$ as a ligand :

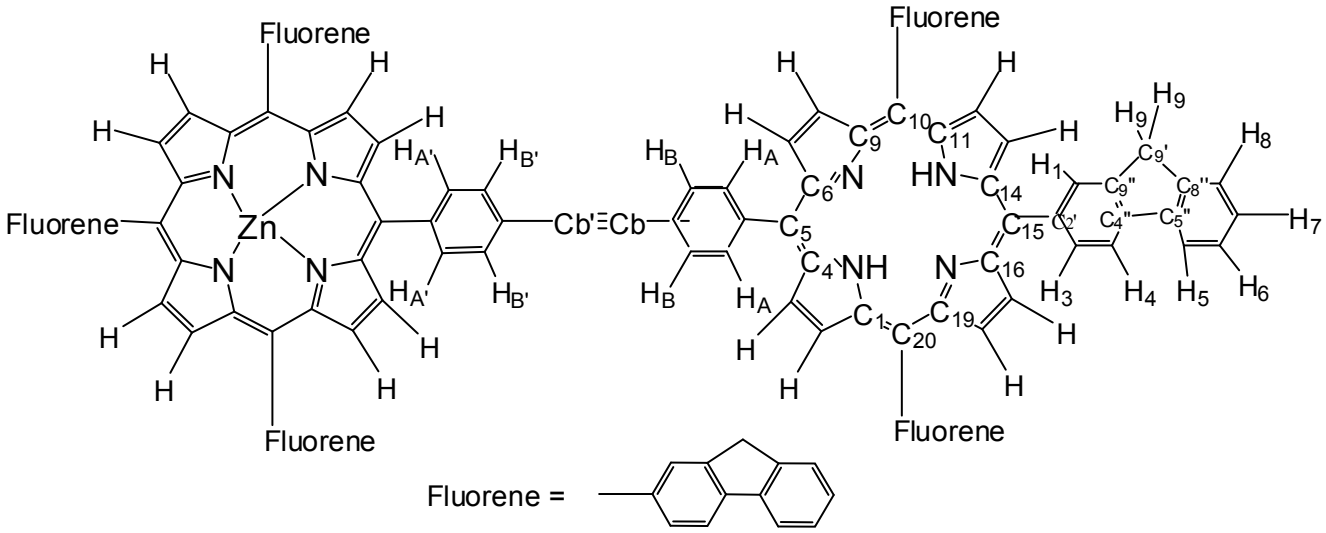

A solution of one equivalent of **17**, zinc(II)-5,10,15-(trifluorenyl)-20-(4-ethynylphenyl) porphyrinato (48 mg, 0.05 mmol), one equivalent of free base **18**, 5,10,15-(trifluorenyl)-20-(4-iodophenyl)porphyrin (50 mg, 0.05 mmol), $Pd_2(dba)_3.CHCl_3$ (7.8 mg, 0.007 mmol), and $P(o\text{-}tol)_3$ (18 mg, 0.06 mmol) in 18 mL of freshly distilled toluene was prepared under argon. Finally, triethylamine (3.5 mL) was added to this solution.

The reaction mixture was stirred for 24 hours at 35°C under argon. Then, it was cooled at room temperature, filtered and evaporated to dryness. The residue was purified twice by column chromatography on silica gel using DCM/heptane (1 : 1) as eluent then increasing the proportion of DCM. Product **19** was isolated as a dark red powder when DCM/heptane (3 : 1) were used. Then, the obtained product was precipitated in heptane to afford **19** as a pure product with 25% yield.

The reaction was followed by MALDI-TOF MS as well as by NMR. This new compound **19** is very soluble in most organic solvents and can be purified by precipitation (DCM/heptane). Compound **19** behaved well on silica gel chromatography and was fully characterized by usual solution spectroscopies (NMR, mass spectrometry) and microanalysis.

^{1}H NMR (500 MHz, $CDCl_3$, δ in ppm) : 9.09 (s, 4H, $H_{\beta\text{-pyrrolic}}$), 9.07 (d, $^{3}J_{HH}$ = 5.7 Hz, 2H, $H_{\beta\text{-pyrrolic}}$), 9.05 (s, 4H, $H_{\beta\text{-pyrrolic}}$), 9.04 (s, 4H, $H_{\beta\text{-pyrrolic}}$), 9.02 (d, $^{3}J_{HH}$ = 5.6 Hz, 2H, $H_{\beta\text{-pyrrolic}}$), 8.42 (s, 6H, $H_{fluorenyl}$, H_1), 8.35 (m, 2H, H_{phenyl}), 8.29 (m, 6H, $H_{fluorenyl}$, H_4), 8.26 (m, 2H, H_{phenyl}), 8.18 (m, 6H, $H_{fluorenyl}$, H_3), 8.06 (d, 6H, $^{3}J_{HH}$ = 7.8 Hz, $H_{fluorenyl}$, H_5), 8.05 (m, 2H, H_{phenyl}), 7.71 (d, 6H, $^{3}J_{HH}$ = 7.6 Hz, $H_{fluorenyl}$, H_8), 7.54 (t, 6H, $^{3}J_{HH}$ = 6.9 Hz, $H_{fluorenyl}$, H_6), 7.43 (t, 6H, $^{3}J_{HH}$ = 6.5 Hz, $H_{fluorenyl}$, H_7), 7.42 (m, 2H, $H_{phenyl,}$ $H_{B'}$), 4.22 (s, 12H, $6CH_{2\text{-fluorenyl}}$).

^{13}C-NMR ($CDCl_3$) : 150.4 (m, C_q, $C_{1\text{-}4\text{-}6\text{-}9\text{-}11\text{-}14\text{-}16\text{-}19}$), 143.7 ($C_q$, $C_{9''}$), 141.7 (C_q, $C_{4''}$), 141.6 (C_q, $C_{8''}$), 141.5 (C_q, $C_{5''}$), 134.7 (C_B), 134.5 (C_A), 134.0 (C_q, $C_{2'}$), 133.4 ($C_{4'}$), 132.1 (m, CH, $C_{2\text{-}3\text{-}7\text{-}8\text{-}12\text{-}13\text{-}17\text{-}18}$), 131.3 ($C_{1'}$), 130.0 ($C_{B'}$), 127.0 ($C_{6'}$ and $C_{7'}$), 126.8 ($C_{A'}$), 125.2 ($C_{8'}$), 121.6 (m, C_q, $C_{5\text{-}10\text{-}15\text{-}20}$), 120.2 ($C_{5'}$), 117.8 ($C_{3'}$), 37.1 ($C_{9'}$).

UV-vis (λ max, (ε, 10^{-3} $M^{-1}.cm^{-1}$), CH_2Cl_2, nm) : 281 (150), 428 (479), 513 (10), 555 (37), 597 (16), 643 (w).

Analysis : calcd for $C_{132}H_{80}N_8Zn.3CH_2Cl_2$: C, 77.27, H, 4.13, N, 5.34, found : C, 77.31, H, 4.82, N, 5.02.

MALDI TOF-MS : calcd for $C_{132}H_{80}N_8Zn$: 1841.57974 $[MH]^+$, found : 1841.18810 $[MH]^+$.

Synthesis of free dimer : 22

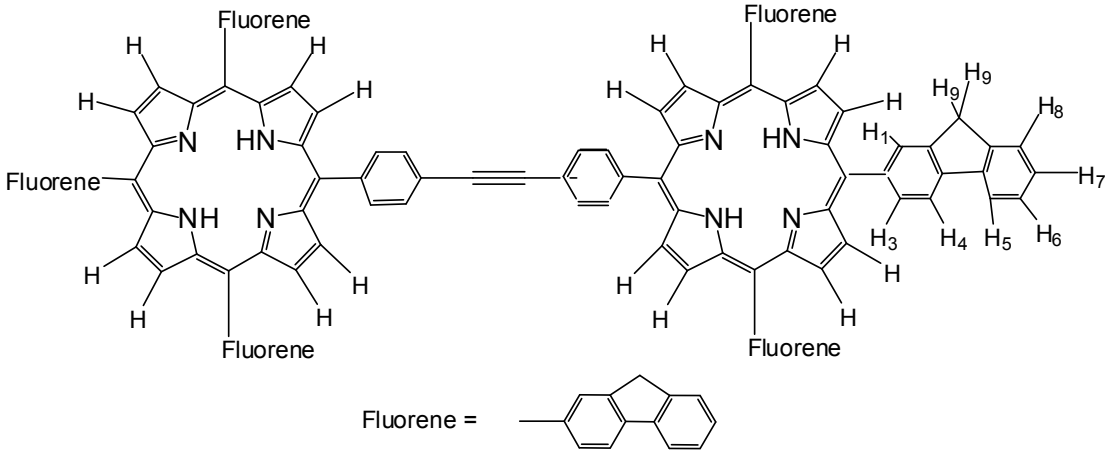

This new free dimer **22** was obtained from the mono zinc complex **19** by acidic treatments. To a solution of one equivalent of dimer **19** (10 mg, 0.005 mmol), in 5 mL of freshly distilled DCM under argon, was added trifluoroacetic acid in large excess (TFA, 0.05 mL, 75 mg, 0.66 mmol). Immediately, the dark red solution (in DCM) turned green. The reaction mixture was stirred for 30 minutes at room temperature and was controlled by UV-Vis. spectrometry to be sure that zinc was entirely eliminated from the porphyrin macrocycle, to obtain the totally free and protonated porphyrin dimer. Finally, potassium carbonate was added to neutralize this dark green solution, to obtain the free but non protonated porphyrin dimer **22**. The red solution was stirred for 30 minutes at room temperature. Then, the residue was filtrated on silica gel using DCM as eluent to afford neutral **22**, as a pure product : a dark red powder with 95% yield.

^{1}H NMR (500 MHz, $CDCl_3$ δ in ppm) : 8.94 (m, 16H, $H_{\beta\text{-pyrrolic}}$), 8.62 (m, 4H, H_{phenyl}), 8.32 (s, 6H, $H_{fluorenyl}$, H_1), 8.18 (m, 6H, $H_{fluorenyl}$, H_4), 8.08 (m, 6H, $H_{fluorenyl}$, H_3), 7.98 (d, 6H, $^3J_{HH}$ = 7.8 Hz, $H_{fluorenyl}$, H_5), 7.78 (m, 4H, H_{phenyl}), 7.68 (d, 6H, $^3J_{HH}$ = 7.6 Hz, $H_{fluorenyl}$, H_8), 7.52 (t, 6H, $^3J_{HH}$ = 6.9 Hz, $H_{fluorenyl}$, H_6), 7.43 (t, 6H, $^3J_{HH}$ = 6.5 Hz, $H_{fluorenyl}$, H_7), 4.22 (s, 12H, $6CH_{2\text{-fluorenyl}}$), - 2.70 (4H, NH).

UV-vis (λ max, (ε, 10^{-3} $M^{-1}.cm^{-1}$), CH_2Cl_2, nm) : compound **22** as a tetra cation **[H_4Por-H_4Por]$^{4+}$** : 268-280, 461, 681; compound **22** as a double free base **[H_2Por-H_2Por]** : 268 (181), 426 (522), 521 (26), 557 (15), 595 (5), 650 (4).

MALDI TOF-MS : calcd for $C_{132}H_{82}N_8$: 1779.66624 $[MH]^+$, found : 1778.95120 $[MH]^+$.

Synthesis of 26 :

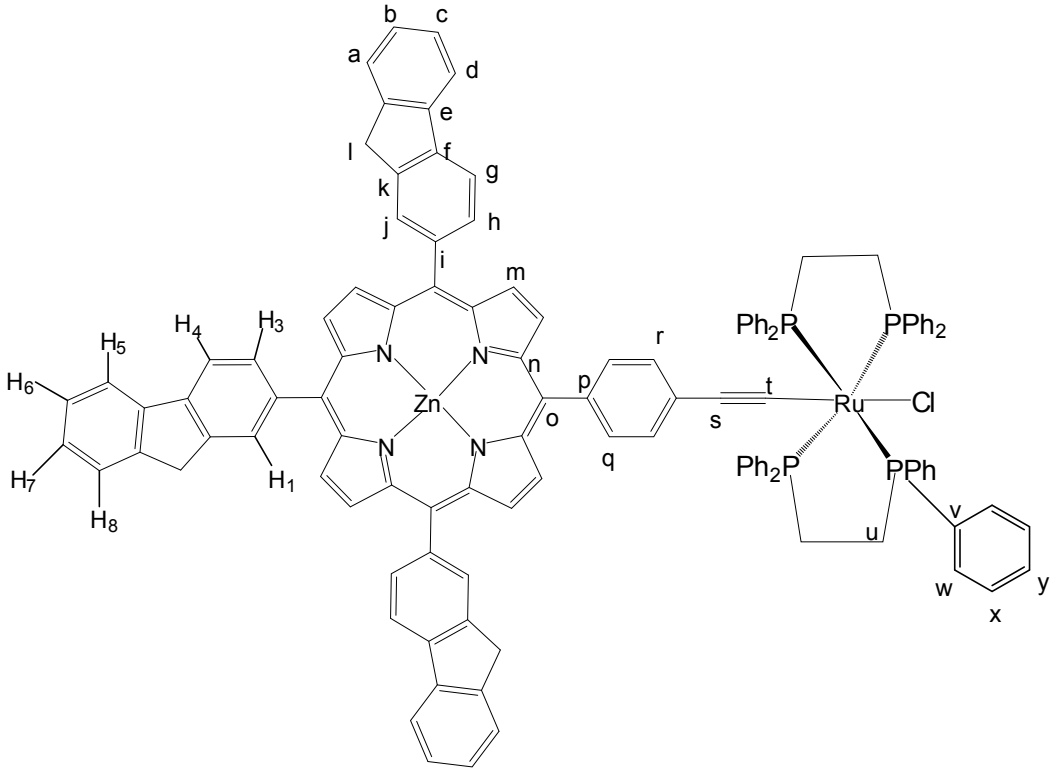

In a schlenk tube, a solution of **17** (0.040 g, 0.041 mmol) and 16 electron Ru species **25** (0.049 g, 0.0455 mmol) in distilled dichloromethane (20 mL) was prepared under argon. The reaction mixture was stirred at room temperature. Following the reaction by ^{31}P and ^{1}H NMR, and judged it was complete after 72 hours. The reaction mixture was concentrated under reduced pressure and the desired vinylidene was precipitated in ether to remove the excess of **25**. The obtained vinylidene was dissolved in 10 mL of dichloromethane, and deprotonated by adding triethylamine (0.25 mL) dropwise. The brown green solution was concentrated and filtered over few centimeters of basic alumina using dichloromethane and 2% triethylamine as eluent. In turn, the solution was concentrated and the desired product **26** was precipitated in ether to yield a greenish brown solid (yield 25%).

This new complex was fully characterized by usual solution spectroscopies (NMR, mass spectrometry) and microanalysis.

^{1}H NMR (400 MHz, $CDCl_3$, δ in ppm) : 9.11 (d, 2H, $^{3}J_{HH}$ = 4.4 Hz, $H_{\beta\text{-pyrrolic}}$), 9.08 (d, 2H, $^{3}J_{HH}$ = 4.4 Hz, $H_{\beta\text{-pyrrolic}}$), 9.03 (s, 4H, $H_{\beta\text{-pyrrolic}}$), 8.42 (m, 3H, $H_{fluorenyl,}$ H_1), 8.28 (m, 3H, $H_{fluorenyl,}$ H_4), 8.17 (m, 3H, $H_{fluorenyl,}$ H_3), 8.06 (d, 3H, $^{3}J_{HH}$ = 7.2 Hz, $H_{fluorenyl,}$ H_5), 7.97 (d, 2H, $^{3}J_{HH}$ = 8.0 Hz, H_{phenyl}), 7.71 (m, 12H, 3H, $H_{fluorenyl,}$ H_8, $9H_{phenyl}$), 7.53 (m, 3H, $H_{fluorenyl,}$ H_6), 7.44 (m, 3H, $H_{fluorenyl,}$ H_7), 7.33 (m, 9H, H_{phenyl}), 7.20 (d, 3H, $^{3}J_{HH}$ = 7.2 Hz, H_{phenyl}) 7.11 (t, 9H, $^{3}J_{HH}$ = 7.6 Hz, H_{phenyl}), 7.03 (t, 12H, $^{3}J_{HH}$ = 7.6 Hz, H_{phenyl}), 4.22 (s, 4H, $2CH_{2\text{-fluorenyl}}$), 4.20 (s, 2H, $1CH_{2\text{-fluorenyl}}$), 2.80 (s, 8H, $CH_{2/dppe}$).

^{31}P NMR (81 MHz, $CDCl_3$, δ in ppm) : 50.00 (s 4P, $(dppe)_2Ru$).

^{13}C NMR (125 MHz, $CDCl_3$, δ in ppm) **:** 150.3 (C_n), 141.7 ($C_{e'}$), 141.5 (C_k), 141.4 (Ce), 141.0 (C_f) 137.1 ($C_{p,v}$), 136.7 ($C_{b,i}$), 135.8 (C_h), 134.4 (C_t), 134.1 ($C_{q,w}$), 131.9 (C_j), 131.8 (C_m), 128.6 ($C_{r,y}$), 128.1 (C_c), 127.1 (C_x), 122.5 (C_o), 121.2(C_a), 120.0 (C_d), 117.8 (C_g), 114.0 (C_s), 37.1 (C_l), 30.8 (C_u).

UV-vis (λ max, (ε, 10^{-3} $M^{-1}.cm^{-1}$), CH_2Cl_2, nm) : 264 (107), 425 (524), 557 (26.6), 602 (20.4).

Analysis : calcd for $C_{119}H_{87}ClN_4P_4ZnRu.0.5CHCl_3$: C, 73.29, H, 4.50, N, 2.86, found : C, 73.29, H, 4.54, N, 2.92.

Synthesis of 27 :

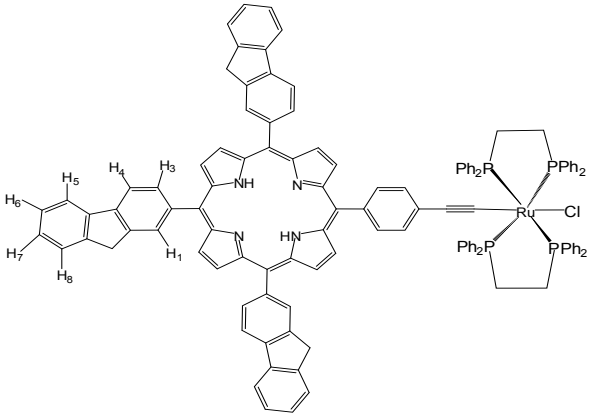

In a schlenk tube, a solution of **16** (0.045 g, 0.0498 mmol) and the 16 electron Ru species **25** (0.059 g, 0.548 mmol) in distilled dichloromethane (18 mL) was prepared under argon. The reaction mixture was stirred at room temperature. Following the reaction by ^{31}P and ^{1}H NMR, and judged it was complete after 72 hours. The reaction mixture was concentrated under reduced pressure and the desired vinylidene was precipitated in ether to remove the excess of **25**. The obtained vinylidene was dissolved in 10 mL of dichloromethane, and deprotonated by adding triethylamine (0.25 mL) dropwise. The brown green solution was concentrated and filtered over few centimeters of basic alumina using dichloromethane and 2% triethylamine as eluent. In turn, the solution was concentrated and the desired product **27** was precipitated in ether to yield a greenish brown solid (yield 22%).

^{1}H NMR (400 MHz, $CDCl_3$, δ in ppm) : 9.00 (d, 2H, $^{3}J_{HH}$ = 4.8 Hz, $H_{\beta\text{-pyrrolic}}$), 8.97 (d, 2H, $^{3}J_{HH}$ = 4.8 Hz, $H_{\beta\text{-pyrrolic}}$), 8.93 (s, 4H, $H_{\beta\text{-pyrrolic}}$), 8.41 (m, 3H, $H_{fluorenyl,}$ H_1), 8.28 (m, 3H, $H_{fluorenyl,}$ H_4), 8.17 (m, 3H, $H_{fluorenyl,}$ H_3), 8.06 (d, 3H, $^{3}J_{HH}$ = 7.2 Hz, $H_{fluorenyl,}$ H_5), 7.97 (d, 2H, $^{3}J_{HH}$ = 8.0 Hz, H_{phenyl}), 7.71 (m, 12H, 3H, $H_{fluorenyl,}$ H_8, $9H_{phenyl}$), 7.53 (m, 3H, $H_{fluorenyl,}$ H_6), 7.44 (m, 3H, $H_{fluorenyl,}$ H_7), 7.33 (m, 9H, H_{phenyl}), 7.20 (t, 4H, $^{3}J_{HH}$ = 7.2 Hz, H_{phenyl}) 7.11 (t, 9H, $^{3}J_{HH}$ = 7.6 Hz, H_{phenyl}), 7.03 (t, 11H, $^{3}J_{HH}$ = 7.6 Hz, H_{phenyl}), 4.22 (s, 4H, $2CH_{2\text{-fluorenyl}}$), 4.20 (s, 2H, $1CH_{2\text{-fluorenyl}}$), 2.80 (s, 8H, $CH_{2/dppe}$), - 2.60 (s, 2H, NH).

^{31}P NMR (81 MHz, $CDCl_3$, δ in ppm) : 50.00 (s 4P, $(dppe)_2Ru$).

UV-vis (λ max, (ε, 10^{-3} $M^{-1}.cm^{-1}$), CH_2Cl_2, nm) : 263 (104), 423 (511), 520 (21), 568 (18), 590 (15.1), 657 (10.5).

Analysis : calcd for $C_{119}H_{89}ClN_4P_4Ru$: C, 77.87, H, 4.89, N, 3.05, found : C, 77.31, H, 4.98, N, 2.96.

References :

1. Lindsey, J. S.; Prathapan, S.; Johnson, T. E.; Wagner, R. W. *Tetrahedron* **1994**, *50*, 8941.
2. Anton, J. A.; Kwong, J.; Loach, P. A. *J. Heterocycl. Chem.* **1976**, *13*, 717.
3. Milgrom, L. R. *J. Chem. Soc., Perkin Trans.* **1983**, *1*, 2535.
4. Lin, V. S.-Y.; Di Magno, S. G.; Therien, J. M. *Science* **1994**, *264,* 1105.
5. Lin, V. S.-Y.; Therien, J. M. *Chem. Eur. J.* **1995**, *1*, 645.
6. Wagner, R. W.; Johnson, T. E.; Li, F.; Lindsey, J. S. *J. Org. Chem.* **1995**, *60*, 5266.
7. Nishino, N.; Wagner, R. W.; Lindsey, J. S. *J. Org. Chem.* **1996**, *61*, 7534.
8. Clausen, C.; Gryko, D. T.; Dabke, R. B.; Dontha, N.; Bocian, D. F.; Kuhr, W. G.; Lindsey, J. S. *J. Org. Chem.* **2000**, *65*, 7363.
9. Yu, L.; Lindsey, J. S. *J. Org. Chem.* **2001**, *66*, 7402.
10. Schmitt, F.; Govindaswamy, P.; Suss-Fink, G.; Ang, W. H.; Dyson, P. J.; Juillerat-Jeanneret, L.; Therien, B. *J. Med. Chem.* **2008**, *51*, 1811.
11. Rochford, J.; Rooney, A. D.; Pryce, M. T. *Inorg. Chem.* **2007**, *46*, 7247.
12. Paul-Roth, C. O.; Simonneaux, G. *Tetrahedron Lett.* **2006**, *47*, 3275.
13. Lindsey, J. S.; Hsu, H. C.; Schreiman, I. C. *Tetrahedron Lett.* **1986**, *27*, 4969.
14. Smith, K. M.; Criag, G. W. *J. Org. Chem.* **1983**, *48*, 4302.
15. Wagner, R. W.; Johnson, T. E.; Lindsey, J. S. *J. Am. Chem. Soc.* **1996**, *118*, 11166.
16. Wagner, R.; Ciringh, Y.; Clausen, C.; Lindsey, J. S. *Chem. Mater.* **1999**, *11*, 2974.
17. Goodson, F. E. I.; Wallow, T. I.; Novak, B. M. *J. Am. Chem. Soc.* **1997**, *119*, 12441.
18. Thamyongkit, P.; Speckbacher, M.; Diers, J. S.; Ling Kee, H.; Kirmaier, C.; Holten, D.; Bocian, D. F.; Lindsey, J. S. *J. Org. Chem.* **2004**, *69*, 3700.
19. Aronoff, S. *J. Phys. Chem* **1958**, *62*, 428.
20. Lavallee, D. K.; Gebala, A. E. *Inorg. Chem.* **1973**, *13*, 2004.
21. Falk, J. E. *Porphyrins and Metalloporphyrins, Elsevier, Amsterdam* **1964**, *4*, 398.
22. Drouet, S.; Ballut, S.; Rault-Berthelot, J.; Turban, P.; Paul-Roth, C. *Thin Solid Films* **2009**, *517*, 5474.
23. Owens, J. W.; Smith, R.; Robinson, R.; Robins, M. *Inorg. Chim. Acta* **1998**, *279*, 226.
24. Zang, X. H.; Xie, Z. Y.; Wu, F. P.; Zhou, L. L.; Wong, O. Y.; Lee, C. S.; Kwong, H. L.; Lee, S. T.; Wu, S. K. *Chem. Phys. Lett.* **2003**, *382*, 561.
25. Serra, A.; Pineiro, M.; Santos, C. E.; Gonsalves, A. M.; Abrantes, M.; Laranjo, M.; Botelho, M. F. *Photochemistry and Photobiology* **2010**, *86*, 206.
26. Drouet, S.; Paul-Roth, C. O. *Tetrahedron* **2009**, *65*, 10693.

27. Paul-Roth, C. O.; Simonneaux, G. *C. R. Chimie* **2006**, *9*, 1277.

Chapter 4

Porphyrin Organometallic Assemblies for Nonlinear Optics of Third Order

I. Nonlinear Optics Theory

There has been a great interest in the Nonlinear Optical (NLO) properties of materials over the last 30 years. Studies of the NLO response of organic molecules have been carried out with many materials having large NLO coefficients and rapid response.[1] Although organic molecules allow for more structural diversity, but as many of them pack in a centrosymmetric way, the NLO properties are limited and the commercial applications are reduced. Organometallic complexes were first investigated in the mid-1980s.[2] Before considering NLO measurements of molecular architecture, we will first introduce the NLO theory.

When matter interacts with strong electromagnetic fields, the NLO phenomenon is a result. Concerning molecules (organic or organometallic), interactions at the molecular level are considered. As a detailed description, when a light beam, *via* its associated electric field **E**, interacts with the polarizable electrons of a molecule, it generates a distortion in the molecule's electron density distribution $\rho(r)$. Then, as a result an *induced dipole moment* $\boldsymbol{\mu}$ is created. The changes in the dipole moment, induced by a relatively weak field are proportion in a **linear** relationship to the magnitude of the field.

However, if the intensity of the electric field, **E** increases strongly (such as with lasers) and is comparable in strength to the internal electric fields within the molecule, the linear relationship is no longer valid. The variation of the dipole moment is now not proportional to the intensity of fields, but involves quadratic, cubic, etc…, terms dependant of **E**; this is the field of Nonlinear Optics.[3] This dependence of the dipole moment on the electric field can be represented as a power series (**Equations 1a** and **1b**). The values of β and γ are expressed in electrostatic units (esu).

$$\boldsymbol{\mu} = \boldsymbol{\mu}_0 + \alpha\mathbf{E} + \beta\mathbf{EE} + \gamma\mathbf{EEE} + \ldots \quad (\mathbf{1a})$$

$$\boldsymbol{\mu} = \boldsymbol{\mu}_0 + \alpha\mathbf{E} + \beta\mathbf{E}^2 + \gamma\mathbf{E}^3 + \ldots \quad (\mathbf{1b})$$

The terms of the equations are defined as :

μ_0 : static dipole moment

α : linear polarizability

β : quadratic hyperpolarizability (second-order polarizability)

γ : cubic hyperpolarizability (third-order polarizability)

Interactions between molecular contributions are translated to the **macroscopic scale** in the form of a polarization equation (**Equation 2**) :

$$\mathbf{P} = \mathbf{P}_0 + \chi^{(1)}\mathbf{E} + \chi^{(2)}\mathbf{E}^2 + \chi^{(3)}\mathbf{E}^3 + \ldots \quad (\mathbf{2})$$

The terms of the equations are defined as :

P : induced polarization

P_0 : permanent polarization

$\chi^{(1)}$: linear susceptibility

$\chi^{(2)}$ and $\chi^{(3)}$: quadratic and cubic susceptibility

It is important to mention that in these equations, α and $\chi^{(1)}$, correspond to the linear contribution whereas β, γ, $\chi^{(2)}$ and $\chi^{(3)}$ represent the nonlinear contributions of second- and third-order. As **μ**, **E** and **P** are vectors, the polarizabilities and susceptibilities are tensors of the appropriate ranks : α, $\chi^{(1)}$ are second-rank tensors, β, $\chi^{(2)}$are third-rank tensors and γ, $\chi^{(3)}$are fourth-rank tensors.

The electric field of a light wave can be expressed from its frequency ω at a given instant *t* as seen in **Equation 3** :

$$\mathbf{E}(t) = \mathbf{E_0}\cos(\omega t) = \frac{\mathbf{E_0}}{2}\left[\exp(i\omega t) + \exp(-i\omega t)\right] \quad (\mathbf{3})$$

Substituting this into (**1**), one obtains (**Equation 4**) :

$$\boldsymbol{\mu}(t) = \boldsymbol{\mu}_0 + \alpha\,\mathbf{E}_0\cos(\omega t) + \frac{1}{2}\beta\mathbf{E}_0^2 + \frac{1}{2}\beta\mathbf{E}_0^2\cos(2\omega t) + \frac{3}{8}\gamma E_0^3\cos(\omega t) + \frac{1}{8}\gamma E_0^3\cos(3\omega t) + \ldots \quad (\mathbf{4})$$

In equation **4**, appear terms derived from $\cos^2(\omega t)$, $\cos^3(\omega t)$.… Terms in which the quadratic hyperpolarization coefficient β (or the quadratic susceptibility $\chi^{(2)}$ on the macroscopic scale) are involved are at the origin of second-order NLO phenomena. Whereas, third-order phenomena are related to terms in which the cubic hyperpolarizability coefficient γ appears (or the cubic susceptibility coefficient $\chi^{(3)}$). Further development of **Equation 4** leads to the appearance of terms containing 2ω, 3ω, corresponding to frequency doubling and tripling, responsible for second- and third-harmonic generation.

Furthermore, as the values are dependent on the frequency of the incident laser beam, it is necessary to compare second- and third-order NLO activities of different molecules at the same wavelength, for a given experimental measurement technique. We define α, β and γ as complex numbers, with real and imaginary parts. For second-order NLO effects, only the real part is

important, but for third-order NLO performance, both real and imaginary parts have to be taken into consideration.

As the target of our project is to study the third order of NLO, we will detail precisely this class of NLO.

1. Third-order phenomena

At a given wavelength, third-order properties are related to the cubic hyperpolarizability coefficient γ (or the cubic susceptibility χ^3 on a macroscopic scale). This coefficient γ is complex, so it is divided into real and imaginary parts (**Equation 5**) :

$$\gamma = \sqrt{\gamma_{real}^2 + \gamma_{imag}^2} \qquad (5)$$

The real part, γ_{real} is called the refractive part. It is responsible for the modifications of the refractive properties of the molecule or medium. The modifications of the absorptive properties are related to the imaginary part γ_{imag} of γ[4,5]. As a consequence, the refractive part concerns instantaneous electronic effects or frequency tripling while the imaginary part is responsible for absorptive phenomena (two- or more photon absorption, saturable absorption).

Since these phenomena have different response times, so time of these phenomena is the key. In other words, time-resolved measurements have to be undertaken so that we can tell which mechanisms are involved in the third-order NLO response of a given molecule or material.

The two photon absorption (TPA), saturable absorption (SA), and reverse saturable absorption (RSA) will be mentioned in the discussion of our NLO studies. It is worth to define these phenomena briefly as follows.

2. Two-photon absorption

As the name tells, two-photon absorption (TPA) corresponds to the simultaneous absorption, by a compound, of two photons. This phenomenon was theoretically predicted by Maria Goeppert-Mayer in 1931[6] and demonstrated experimentally in the early 1960s.[7,8] Two types of TPA are possible : in the **degenerate case**, the two-photon absorbed are of the same energy, whereas in the **non-degenerate case**, their energies are different. This NLO effect can be imagined as the stepwise

absorption of two photons : in the first step, a photon is absorbed by the compound, enabling it to reach a "virtual" excited state, usually from the ground-state. In this "virtual" excited state the compound can then absorb a second photon (of the same or different energy than the first one) to reach a real excited state (**Figure 1**).

However, this explanation is to simplify the phenomenon but in the reality, the virtual state doesn't exist. In fact, the two photons are absorbed at the same time and a sufficient density of photon is needed for this to happen, which can only be attained with the use of lasers.

The TPA cross-section is expressed in cm^4/GW or, more conveniently, in Goeppert-Mayer units ($1\ GM = 10^{-50}\ cm^4 \cdot s \cdot photon^{-1} \cdot molecule^{-1}$). In principle, the direct process of two-photon absorption is suitable for optical limiting.

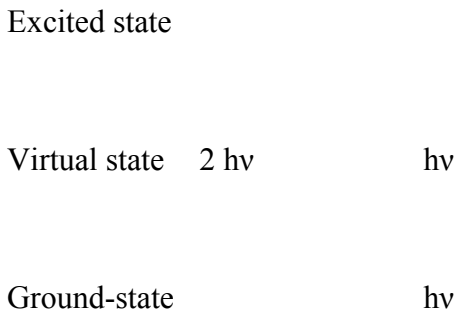

Figure 1 : Presentation of **TPA** phenomena

3. Saturable absorption and reverse saturable absorption

Saturable absorption (SA) and reverse saturable absorption (RSA) are, similar to TPA, absorptive phenomena related to the imaginary part of γ in which two photons are absorbed. The difference with TPA is temporal; the two photons are absorbed one after another, in contrast to TPA in which the process is simultaneous.

Due to this stepwise process, a real excited state of the molecule is involved from where the second photon is then absorbed in a process called excited state absorption (ESA). These phenomena are presented in **Figure 2**.

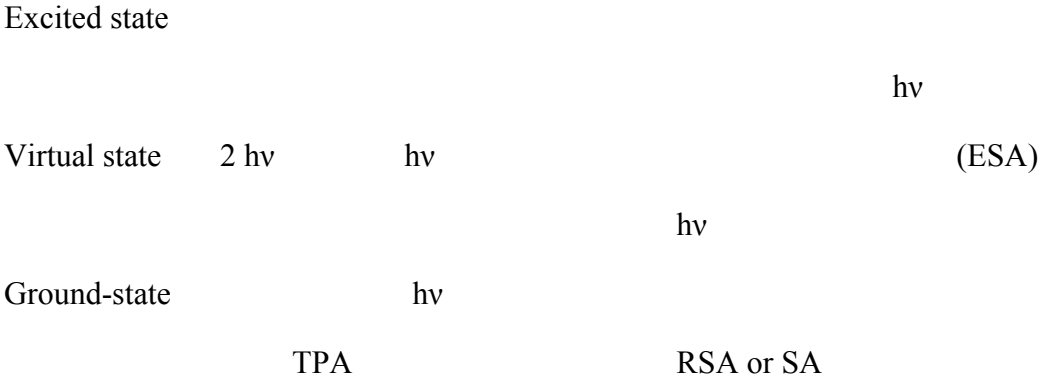

Figure 2 : Presentation of **TPA**, **SA**, and **RSA** phenomena

For RSA, a "photodarkening" effect is observed: the transmission of the medium is decreased as the compound in this excited state has greater absorptivity than in the ground-state at a given wavelength.

In contrast, if the excited state had a lower absorptivity than the ground-state, the transmission of the sample will be increased, as ground-state molecules are depleted : an absorption bleaching will be observed (SA). In other words, if the absorption cross-section of the medium in the excited state is lower than in the ground-state, the transmission of the system increases once the medium is excited.

It should be noted that when $\gamma_{im} > 0$, the compound acts as a two-photon absorber, whereas when $\gamma_{im} < 0$, the compound has saturable absorber properties.

4. Experimental techniques

A large number of techniques had been used for measurement of second- and third-order responses of molecules.[9,10] The following discussion only covers techniques used for organometallic alkynyl and related complexes. In more specific, **Z-scan** will be more detailed than other techniques since it is the used method to study our complexes.

4.1. Third-harmonic generation

Third-harmonic generation (THG) is a NLO process occurring in all materials, because they all possess a χ^3 susceptibility. The THG experiment is used to determine the electronic contribution of χ^3 for centrosymmetric compounds, on solid samples. This technique is frequently difficult to use.

However, the THG experiment is sometimes used in addition to EFISH (electric field-induced second harmonic generation) for dipolar molecules, to determine the γ value and then, the value of β.[5]

4.2. Degenerate four-wave mixing

Degenerate four-wave mixing (DFWM) has been used to measure the cubic nonlinearities of various organometallic complexes. Despite its complexity to use, DFWM is applied for neutral and charged organic or organometallic compounds, to determine the electronic part of the response.

4.3. Two-photon excited fluorescence

Normally, when a molecule absorbs two-photon, there are two ways for the molecule to return to its ground-state : by radiative or non-radiative relaxation. If the relaxation is radiative, that is by emission of light, a fluorescence or phosphorescence phenomenon is observed (**Figure 3**). By analogy to the linear process, the nonlinear process is termed two-photon excited fluorescence (**TPEF**).

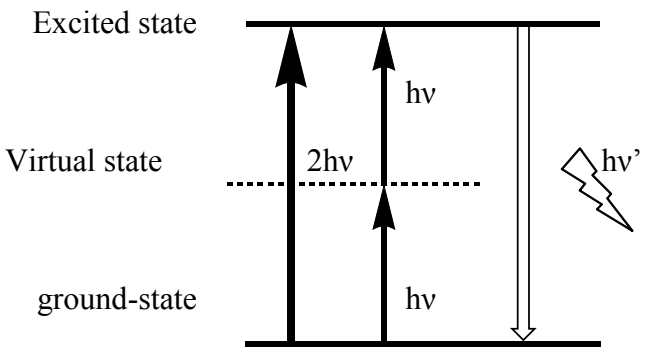

Figure 3 : Representation of **TPEF**

The global efficiency of the process is $\zeta_{TPA}.\varphi$, with φ the quantum yield of fluorescence. By measuring the intensity of the emitted fluorescence, it is possible to determine ζ_{TPA} if the quantum yield of fluorescence of the measured compound is known.

This technique requires that the molecule possesses both TPA and fluorescence properties, and preliminary fluorescence studies have to be carried out in order to determine φ.[11]

4.4. Z-Scan

Z-scan is a simple and convenient technique to measure nonlinear refractive (self-focusing and defocusing phenomena) as well as nonlinear absorptive properties of a given compound. The value of χ^3 and γ can be determined from the variation of the nonlinear refractive index n_2. It is noted that most of the cubic NLO responses of organometallic complexes have been measured using the Z-scan technique. A simplified representation of the Z-scan set-up is shown in **Figure 4**.

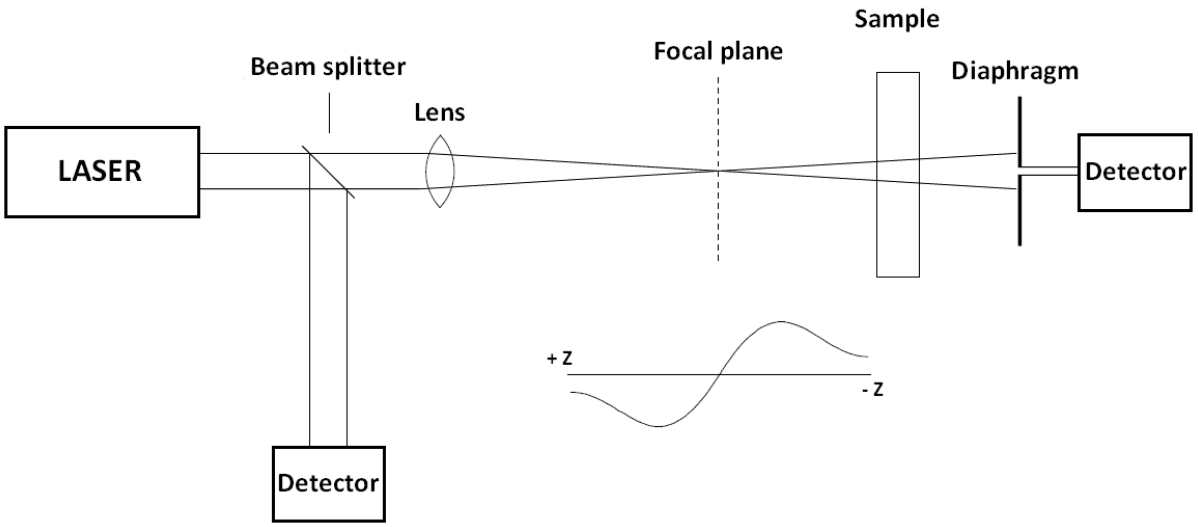

Figure 4 : Z-scan technique

A laser beam is focussed with a lens, with the focal point at Z = 0. The sample, a solution of the nonlinear active material in a thin cell, is moved along the Z axis which is also the axis of the lens. The transmitted intensity is measured as a function of the position of the sample on the axis, after the transmitted beam has passed through a diaphragm. Two types of measurements can be undertaken: with the diaphragm in place (closed aperture to measure the real part) or removed (open aperture to measure the imaginary part).

Due to the presence of the intensity-dependent absorption coefficient, absorption phenomena happen close to the focal plane, modifying the transmitted intensity. Both TPA and saturable absorption can be measured with the open aperture set-up, the differentiation between both reside in nature of the sign of the nonlinear absorption coefficient.

Once the variation of the intensity had been measured, the value of n_2, γ and χ^3 are calculated using mathematical relationships. Using this technique, the sign and magnitude of the nonlinear refractive index n_2 can be established as well as the imaginary and real parts of χ^3.

II. Synthesis and Characterization of New Organometallic Porphyrin Assemblies

1. Objective of the project

There has been an increasing interest on multi-photon absorbing materials because of their technological applications such as photonic devices,[12] optical data storage,[13] microfabrication, [14,15] fluorescence imaging and photodynamic therapy.[16] Organometallic compounds are more attractive candidates than that of organic alternatives for nonlinear optics due to metal-to-ligand or ligand-to-metal charge transfer, which are related to improved optical nonlinearities.[17] In addition, modifying the ligand environment around the metal center affords the possibility of tuning the NLO performance.[18,19] More specifically, many examples of d^6 alkynyl complexes featuring an equatorial $Ru(dppe)_2$ core have been explored.[18,20]

On the other hand, large metallated pi compounds such as porphyrins and phthalocyanines were also identified as efficient and robust cubic NLO- phores.[21,22] For example, Rao *et al.* showed in 2000 that various metallated tetra-*p*-tolylporphyrins (**TTP**), as shown in **Figure 5**, could exhibit quite high cubic optical nonlinearities at 532 or 600 nm.[23] These porphyrins showed important values of nonlinearity in the nanosecond scale.

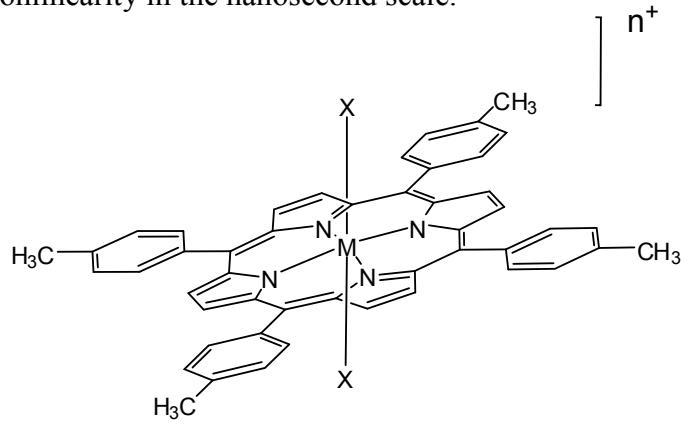

M = **2H,** n = 0

M = **Co, Ni, Cu, Zn, Ag, Cd ou Hg**, n = 0

M = **Cr, Mn, Fe ou Au**, n = 1, X = O

M = **In**, n = 1, X = OH

M = **Ge ou Sn**, n = 2, X = OH

M = **V,** n = 2, X = O

M = **P**, n = 3, X = OH

Figure 5 : Metallated tetra-*p*-tolylporphyrins

Moreover, large nonlinearities were observed at 532 nm for electron releasing *para*-substituents on *meso* phenyl in related tetraphenyl tetrabenzyl porphyrins.[24]

Recently, some of us reported multi stable d^6-alkynyl complexes exhibiting large and redox-switchable third-order (cubic) nonlinearities.[25] Others have reported the synthesis and properties of tetrafluorenyl porphyrin derivatives.[26] In addition, they evidenced the determining role of the *meso*-substituents on the photophysical properties of these porphyrins.[27]

However, to the best of our knowledge, only a few porphyrins featuring alkynyl metal complexes as peripheral substituents have been reported so far,[28] with very few constructed around a **TPP**-core, such as in **56** (**Figure 6**).[29] Moreover, none were studied from the perspective of their cubic NLO properties. We have consequently pursued the synthesis and third-order NLO responses of a series of new **ZnTPP** derivatives functionalized with electron-releasing d^6-alkynyl Ru(II) complexes at the *para*-location of their *meso*-aryl groups.[30]

By using the controlled stepwise reactivity of the *cis*-$[RuCl_2(dppe)_2]$ and *trans*-$Ru(C{\equiv}CAr)Cl(dppe)_2]$ complexes,[31,32] derivatives with organoruthenium termini possessing differently functionalized terminal arylalkynyl ligands were targeted, in order to evidence the effect of electron-releasing or electron-attracting *para*-substituents on their cubic NLO response.

Based on all what has been mentioned, the target was to synthesize a new series of organometallic porphyrin assemblies starting from the precursor **31**. Then, as a next step, is to functionalize the endgroups by different substituents -**32-X** (NO_2, H, OMe) - and fully characterize them. Based on what we will obtain as results and analysis, we might draw out conclusions concerning the effect of the substituents. In addition, we can judge the interest of this series at the level of the third order of NLO since Z-scan measurements of their cubic nonlinear absorption properties will be studied.

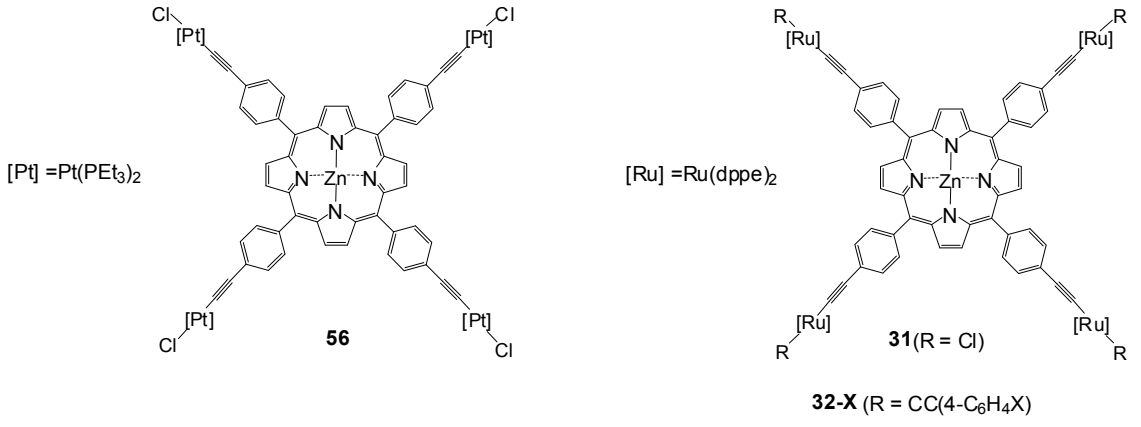

Figure 6 : Selected **TPP**-based porphyrins substituted with alkynyl complexes

2. Synthesis of a new series of porphyrin organoruthenium complexes

To achieve the synthesis of the new series **32-X**, it is worth to start the preparation of the porphyrin core. In specific, it is a derivative of the tetraphenyl porphyrin **TPP** possessing four alkyne terminals **30**. These terminals permit the coupling to ruthenium species to get the organometallic precursor **31**. Then, as a final step will be the functionalizalion of the terminal groups by different substituents (**32-X**).

2.1. Synthesis of the zinc porphyrin precursor 30

Porphyrin **30**[29] was prepared starting from its precursor **28**. In turn, porphyrin **28** was prepared using Lindsey's method.[33] Maybe it is worth to mention that this tetra-alkyne Zn porphyrin **28** has been previously synthesized in fair yields (29%).[29] But, using Lindsey's method[33] the yield (45%) was improved by using the $BF_3(OEt_2)$ complex as a Lewis-acid promoter. The reaction was done by condensation of pyrrole with prepared aldehyde **14** by acid catalysis as shown in **Scheme 1**.

In a typical experimental procedure, the pyrrole compound (1 eq) and the aldehyde **14** (1 eq) dissolved in 1L of distilled and degassed CH_2Cl_2 were stirred in the presence of a catalytical amount of $BF_3(OEt_2)$ under argon. After three hours, *p*-chloranil was added, and the mixture was refluxed for one hour. Then, the dark green solution was basified by the addition of triethylamine. After removing the solvent, the black red residue was chromatographed on silica gel column (dichloromethane) to separate our desired porphyrin **28** from the polymer formed.

The tetra TMS-phenylporphyrin **28** was obtained with a yield of 45%. **^{1}H NMR** of **28** exhibits signatures of porphyrin. For example, the protons of the macrocycle (NH) were observed at high field (– 2.7 ppm). In addition, the β pyrrolic protons are identified by the peaks around 9 ppm.

As a next step, the trimethylsilyl groups of **28** were deprotected by using potassium carbonate in dichloromethane and methanol. Extraction and filtration were done to afford **29** as a pure compound with 98% yield. The characteristic change in the **^{1}H NMR** was the absence of TMS protons at 0.27 ppm and the presence of the new signal at 3.3 ppm. This signal corresponds to terminal alkyne proton that characterizes the reaction.

As a last step, comes the metallation[34] of **29** as shown in **Scheme 1**. After that the metallation was complete, **30** was obtained pure after extraction and filtration were done with 95% yield. The absence of the protons of the macrocycle (NH) at around – 2.7 ppm was a sign that the macrocycle

was metallated. Another indication was the UV-visible that showed two Q bands instead of four. Having two Q bands is characteristic for metallated porphyrins.

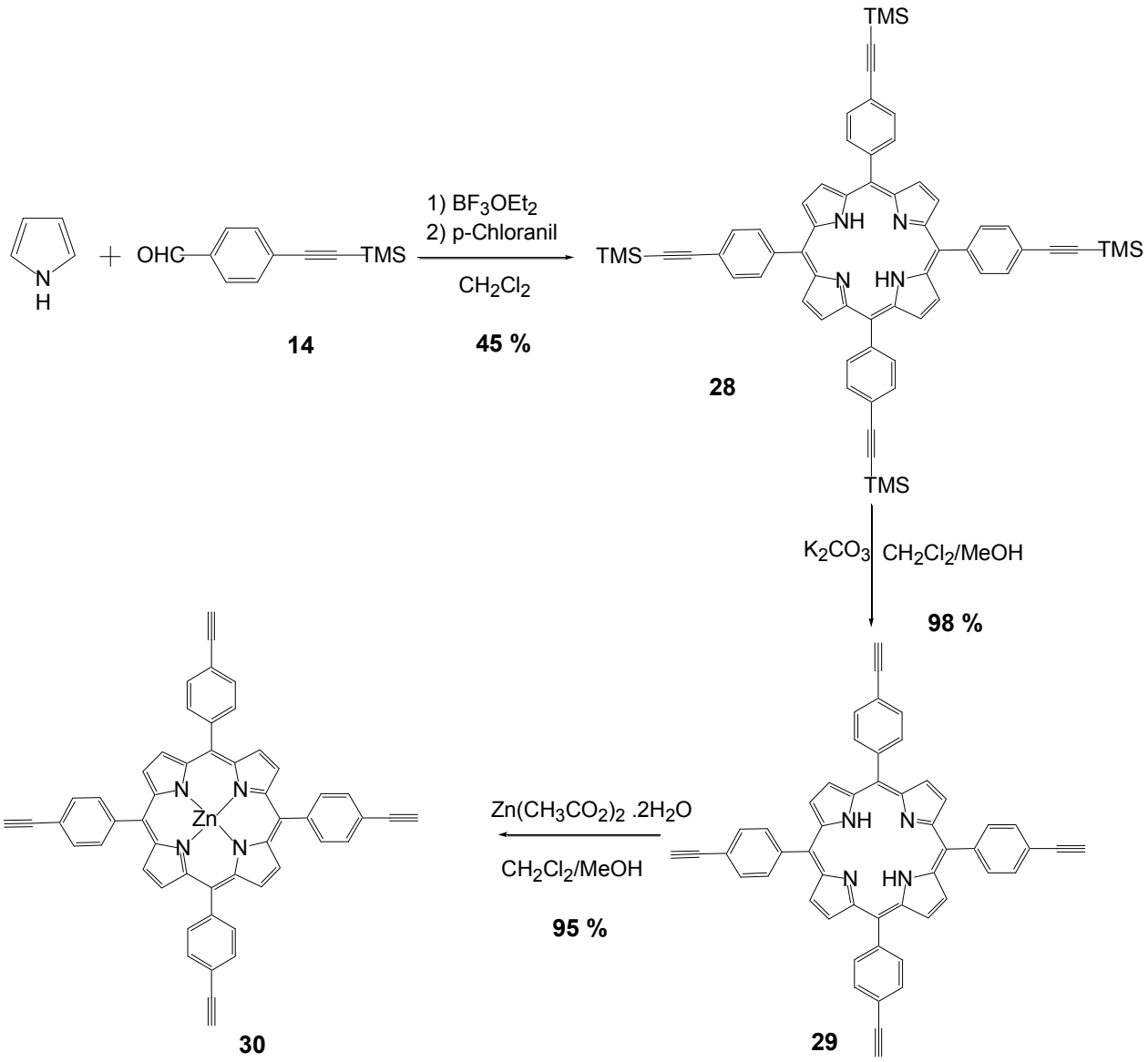

Scheme 1 : Synthesis of the zinc porphyrin **30**

2.2. Synthesis and characterization of the pentametallic precursor 31

After that our porphyrin precursor **30** was synthesized, it is now the time to prepare our pentametallic species **31**. A reaction was carried between the tetra-alkyne Zn porphyrin **30** with the known *cis* ruthenium(II) organometallic precursor complex.

It is worth to mention that the *cis* ruthenium complex was prepared as reported in the literature.[35] As it is shown in **Scheme 2**, the reaction to get **31** is of two steps.

The first step of is the formation of the vinylidene species by a 1,2-hydrogen shift which is stabilized by the large PF_6^- counter ions. This formed vinylidene is identified by a singlet in the **^{31}P NMR** at 37 ppm, and was not characterized.[36]

Instead, it was deprotonated *in situ* by excess triethylamine to give **31**. Completion of the reaction forming **31** was confirmed by the **^{31}P NMR**, which gave a sharp singlet corresponding to the sixteen equivalent phosphorus atoms from the eight dppe ligands coordinated to the ruthenium terminal groups. The chemical shift of this signal (50 ppm) is characteristic of monosubstituted sigma alkynyl ruthenium complexes of this type.[37]

This new complex was characterized by the usual spectroscopies (NMR, UV-Vis and IR), microanalysis and electrospray mass spectrometry (ESI-MS).

^{1}H NMR spectrum of **31** exhibits both the spectral signatures of the porphyrin core and signals typical of the ζ-alkynylRu(II) endgroups. For example, a characteristic singlet at 9 ppm was observed. It corresponds to the eight equivalent β-pyrrolic protons. In addition, a broad singlet at around 3 ppm was detected as well. It corresponds to the thirty-two equivalent CH_2 protons of the ruthenium-coordinated dppe. Between 6.5 and 9 ppm are the signals of the various aromatic protons of the porphyrin and of the dppe.

Further evidence for the structure of this compound comes from the **^{13}C NMR** spectrum. All carbon atoms of **31** can be observed and assigned by polarization transfer studies, except for the weak quintuplet corresponding to the C_α-alkyne carbon atoms which escaped detection. The presence of the four alkynyl bonds in **31** is nevertheless revealed by a broad singlet near 115 ppm, corresponding to the equivalent C_β carbon atoms.[32,38]

The presence of these alkynyl bonds is more clearly revealed by **infrared**, since **31** displays an intense absorption band at around 2050 cm^{-1} (**Table 1**), characteristic of the $\nu_{C\equiv C}$ mode of these Ru(II) ζ-alkynylcomplexes.[32,38]

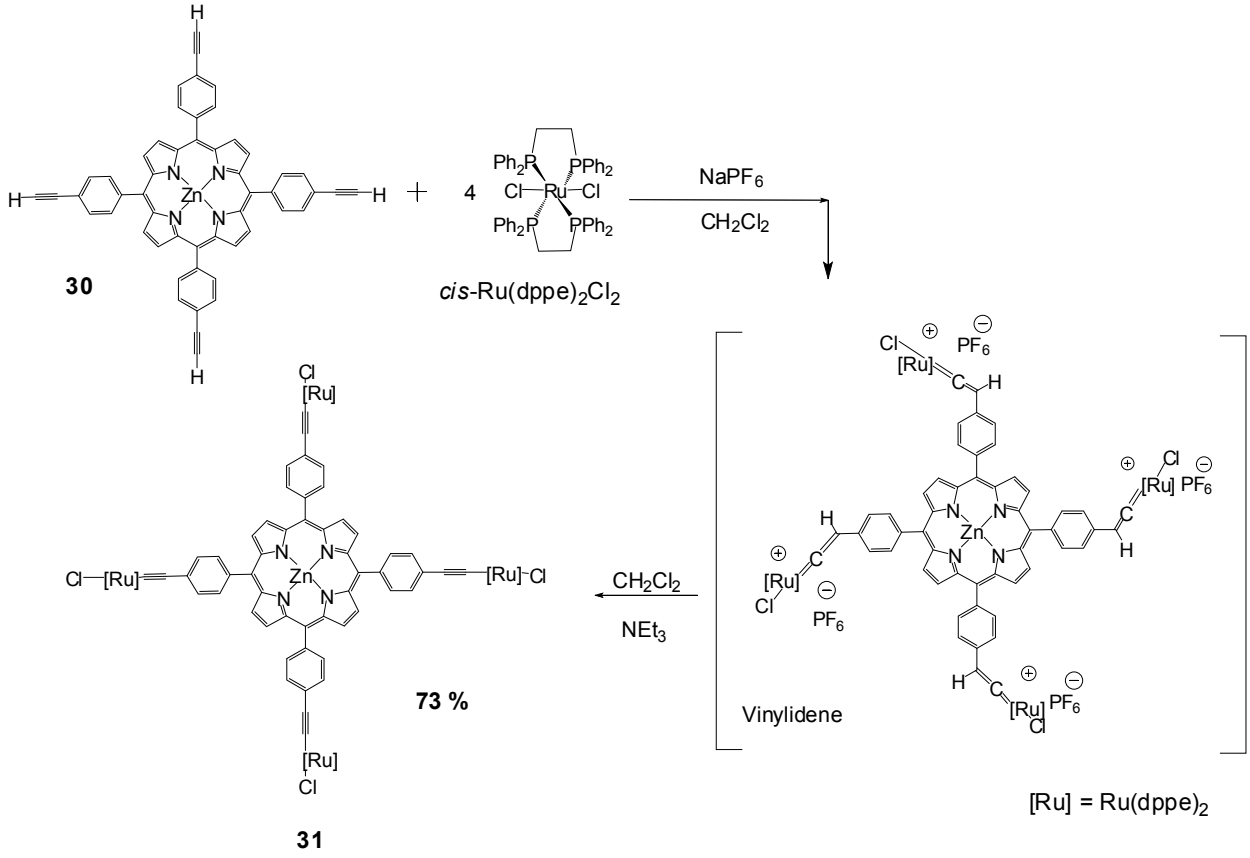

Scheme 2 : Synthesis of substituted tetra(ruthenium-chloride) **ZnTPP 31**

2.3. Synthesis and characterization of the tetra ruthenium-bis(alkynyl) Zn(II) porphyrins

By using the pentametallic porphyrin **31** as a starting material, three new derivatives **32-X** (X = NO_2, H, OMe) were synthesized by ligand metathesis (**Scheme 3**). This reaction was performed in the presence of sodium hexafluorophosphate and with an excess of the corresponding functional arylethyne. Reaction protocols developed for the *trans*-[Ru(C≡CAr)Cl(dppe)$_2$] complexes were used as shown in **Scheme 3**.[39]

The synthesis of these tetra-substituted porphyrins featuring bis-alkynyl ruthenium endgroups was achieved in one pot, without attempt to isolate the intermediate vinylidene species. Triethylamine was added to the reaction mixture with the other reactants. The desired complexes **32-X** were obtained in good yields from **31** after 72 h of reflux.

These new complexes were fully characterized by means of IR, UV and NMR spectroscopies, microanalyses, and CV. Attempts to detect the molecular ions of these species by ESI-MS or MALDI-MS were unsuccessful. Instead, constituent fragments were observed in each case. It may be that these complexes undergo extensive fragmentation in the mass spectrometer.

Both **^{1}H** and **^{13}C NMR** spectra of **32-X** presented signals that resemble those previously observed for **31**. Additional signals that correspond to the presence of the terminal arylethynyl fragments in **32-X** are also observed. These signals are seen with the correct integrations, confirming the presence of the tetra-ruthenated porphyrin core. In particular, NMR is diagnostic of the high symmetry of the various compounds isolated, indicating that the chloride metathesis occurs at all of the Ru(II) centers of **31**.

The unique singlet observed in the **^{31}P NMR** spectrum is now located at 54 ppm (**Table 1**). This shift to lower field, relative to the same signal in **31**, is diagnostic of the presence of the bis-alkynyl Ru(II) moieties in **32-X**.[40]

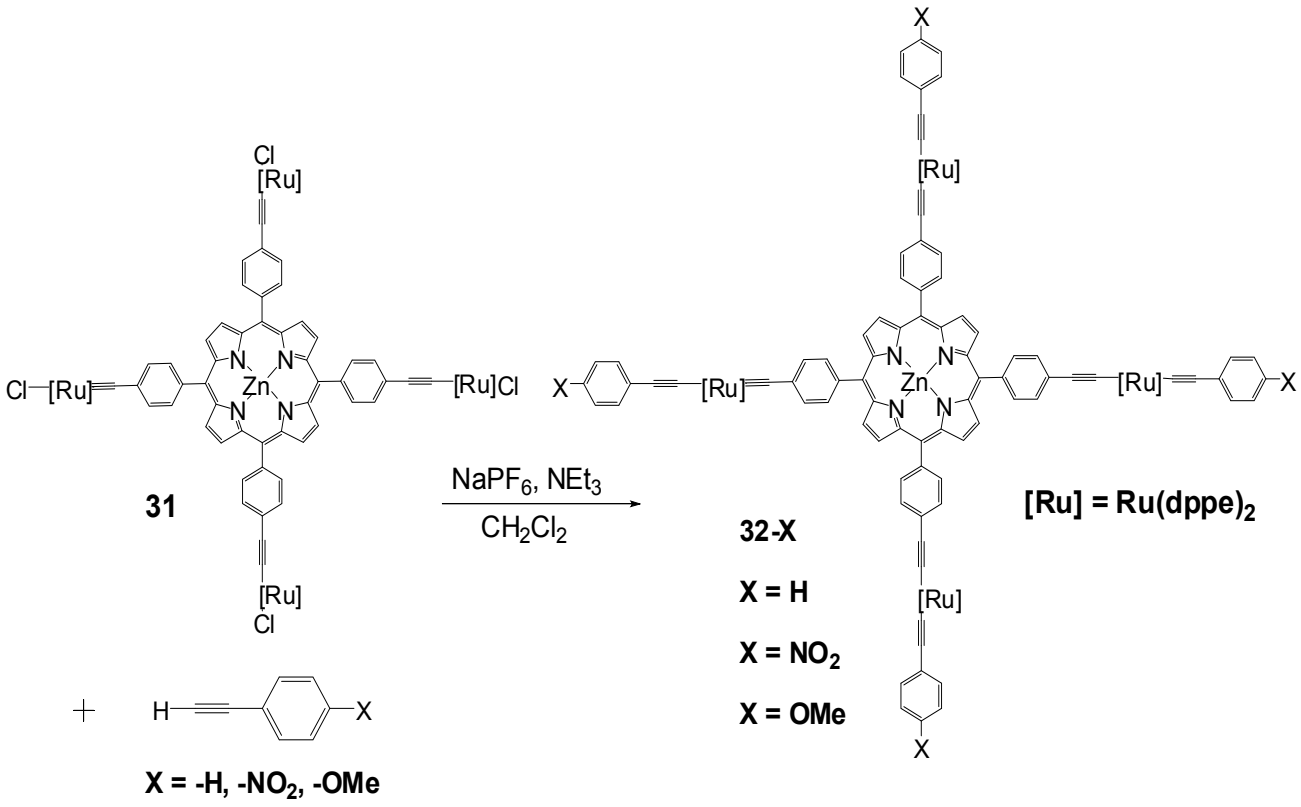

Scheme 3 : Synthesis of the series **32-X**

2.4. Infrared studies

It is often observed for bis-alkynyl Ru(II) complexes,[30] that both $\nu_{C\equiv C}$ modes appear as a single and broad absorption at ca 2050 cm^{-1} (**Table 1**). This characteristic vibration is shifted to slightly lower energies (2042 cm^{-1}) for the nitro compound **32-NO_2**, in comparison to the other **32-X** compounds,[41] which exhibit this broad $\nu_{C\equiv C}$ band at 2056 cm^{-1}.[38]

As seen previously with closely related bis-alkynyl Ru(II) compounds,[30] only one broad $\nu_{C\equiv C}$ band is observed for **32-NO_2** in spite of the presence of two dissimilar alkynyl ligands at the Ru(II) center.[36]

As for **32-OMe**, its vibration band was unchanged with respect to the precursor **31**. So, it seems that the donating group Phenyl-OMe had no effect on this vibration band.

Compound	$\upsilon_{C\equiv C}$ [a]	^{31}P NMR [b]
31	2057	51.0
32-NO_2	2042	54.7
32-H	2056	55.2
32-OMe	2056	55.1

[a]IR pellet in KBr. [b]In $CDCl_3$.

Table 1 : Selected spectral signatures for **31** and **32-X** complexes

2.5. UV-visible Spectroscopy

A slight hypsochromic shift of the Soret band is observed for **31** and the **32-X** derivatives, relative to **30** ($\Delta\nu$ = 167-395 cm^{-1}). As for the two Q bands, they are bathochromically shifted (**Table 2**). No other absorption bands could be detected at longer wavelengths (until 2000 nm). In total, the energies of the Soret and Q bands are weakly influenced by the change in the terminal X substituent. The weakness of their shifts within the **32-X** series (**Figure 7**) is consistent with the porphyrin core experiencing only a weak influence of the peripheral electron-rich Ru(II) endgroups. It is noteworthy that a larger bathochromic shift ($\Delta\nu$ = 486 cm^{-1}) of the Soret band relative to **30** had been observed in

earlier work upon complexation of platinum(II) to the terminal ethynyl groups,[29] suggesting a slightly different interaction between the porphyrin core and the peripheral metal alkynyl fragments relative to **30** or **32-X**.

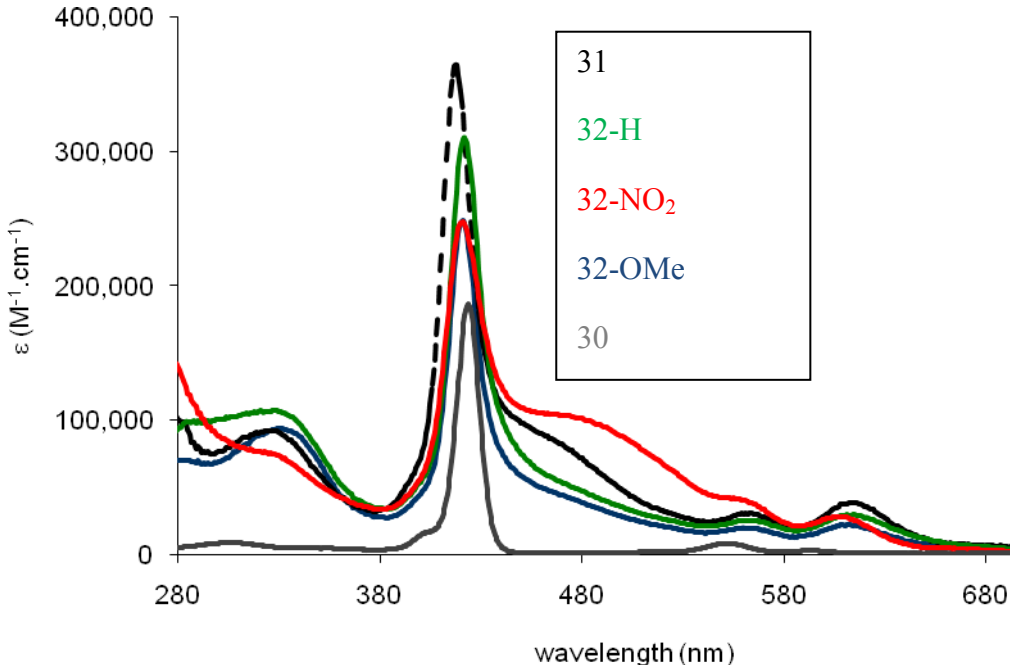

Figure 7 : UV-Visible absorption spectra of the zinc porphyrins **31** and **32-X** (X = NO_2, H, OMe) in CH_2Cl_2 at 25°C. For comparison, the compound **30** (with ε/ values divided by three, for the figure) is also reported under the same conditions.

A new absorption band appears near 330 nm upon functionalization of the pendant ethynyl substituents of **30** by organoruthenium groups. Normally, this is a spectral region where $d_{Ru} \rightarrow \pi^*_{C\equiv C}$ transitions are often observed with Ru(II) alkynyl complexes.[42] Knowing that such an absorption is also observed for *cis*-[Ru(dppe)$_2$Cl$_2$], we tentatively propose that it corresponds to a $d_{Ru} \rightarrow \pi^*_{C\equiv CTPP}$ MLCT transition. Consistent with such an assignment, its energy across the **32-X** series seems poorly influenced by the change in the terminal arylalkynyl ligand.

For these bis-alkynyl complexes, a second band corresponding to a $d_{Ru} \rightarrow \pi^*_{C\equiv C(4\text{-}C6H4X)}$ MLCT transition is also observed in the same spectral region,[42] except for **32-NO$_2$**, for which it appears as a shoulder on the Soret band, at 466 nm. This might be due to its strong $d_{Ru} \rightarrow \pi^*_{NO2}$ character. Such a

transition is quite specific to *trans*-[Ru(dppe)$_2$] fragments with 4-nitroarylalkynyl ligands. Similar case has been previously mentioned in the literature, and the band was then observed at 484 nm.[38]

Compounds	λ in nm (ε in 10^3 L. mol^{-1}.cm^{-1})
31	327 (93); 418 (364); 452 (sh, 97); 563 (31); 615 (39)
32-NO$_2$	322 (77); 420 (248); 466 (sh,104); 553 (sh,42); 607 (30)
32-H	330 (94); 421 (249); 460 (sh, 50); 563 (20); 612 (39)
32-OMe	321 (107); 422 (310); 460 (sh, 61); 562 (26); 611 (30)
30	302 (27); 424 (556); 552 (28); 594 (10)

Table 2 : UV-Visible data for complexes **30**, **31**, and **32-X**

2.6. Cyclic voltammetry

The cyclic voltammetry (CV) studies of the different complexes synthesized, were performed in dichloromethane, with a concentration of 0.1 M [NBu$_4$] [PF$_6$] used as supporting electrolyte. Reported potentials were measured and are expressed relative to saturated calomel electrode (SCE). For greater accuracy, the reference electrode was routinely calibrated by measuring the potential of a solution containing the complex Cp*(dppe)Fe-C≡C-Ph with ($\mathbf{E°_{Fe(III)/Fe(II)}}$ = - 0.15 V *vs.* SCE), since the oxidation wave of ferrocene, internal reference usually used, overlaps with that of ruthenium.

The electrochemical oxidation of a porphyrin involves two-electron processes, which are characterized by cyclic voltammetry by two reversible waves named $\mathbf{E^1Ox}$ and $\mathbf{E^2Ox}$.[26,43] To determine these two specific oxidation potentials of the porphyrin macrocycle, compared to that of ruthenium, we studied the starting monometallic zinc porphyrin **30**. The voltammogram of zinc porphyrin **30**, as expected, shows two oxidation waves $\mathbf{E^1Ox}$ at 0.87 V and $\mathbf{E^2Ox}$ to 1.14 V *vs.* SCE.

Substitution by organoruthenium complexes, that are electron donating groups, of the parent zinc porphyrin **30,** might make oxidation of the macrocycle easier and thus move the oxidation potentials at lower values. One can speculate that the first oxidation wave observed for these type of

organometallic complexes, will be the oxidation of the four ruthenium on the periphery, called $\mathbf{E°_{Ru(III)/Ru(II)}}$ lower than the oxidation wave, $\mathbf{E^1Ox}$, corresponding to the porphyrin macrocycle. This hypothesis is confirmed by the voltammetry studies performed on compounds **31** and **31-X**. For example, for compound **31**, after the ruthenium oxidation wave $\mathbf{E°_{Ru(III)/Ru(II)}}$ at 0.49 V, there are two well-defined oxidation waves at 0.87 V and 1.16 V corresponding respectively to $\mathbf{E^1Ox}$ and $\mathbf{E^2Ox}$ of the porphyrin.

To better analyze the CV results, studies were performed for both the precursor **31** and the **32-X** derivatives (**Table 3**). Starting with **31**, a reversible electrochemical process is observed at 0.48 V (**Table 3**). This value corresponds to the simultaneous oxidation of the four organoruthenium (II) termini. This mentioned value is not far from that of 0.44 V observed for the corresponding chlorido-phenylalkynyl Ru(II) complex **33-H** (**Figure 8**).[30]

The difference between the two values of the oxidation potential indicates that the oxidation of the four Ru(II) centers in **31** is slightly more difficult than for the unique Ru(II) center in **33**. Two additional pseudo-reversible processes at 0.87 V and near 1.16 V *versus* SCE were seen in the voltammogram of **31**. They were decreased in intensity by approximatively 25%. These redox waves are attributed to the stepwise one-electron oxidations of the metallated porphyrin macrocycle. Indeed, **ZnTPP** (**34**; **Figure 8**) usually undergoes two chemically reversible one-electron processes at 0.92 V and 1.18 V vs. SCE.[44]

In addition, the voltammogram of the precursor porphyrin **30** (used to synthesize **31**) shows two pseudo-reversible oxidation waves at 0.87V and 1.14V *versus* SCE. The present data indicate that *para*-substitution of the porphyrin phenyl groups with ruthenium alkynyl moieties has a weak effect on the oxidation of the porphyrin core. This observation is consistent with previous statements pertaining to substituent effects on the *meso*-aryl groups.[44] In the present system, the decrease of the chemical reversibility of the porphyrin-centered oxidations at room temperatures, may be referred to the well known kinetic instability of Ru(III) alkynyl complexes in solution.[45,46]

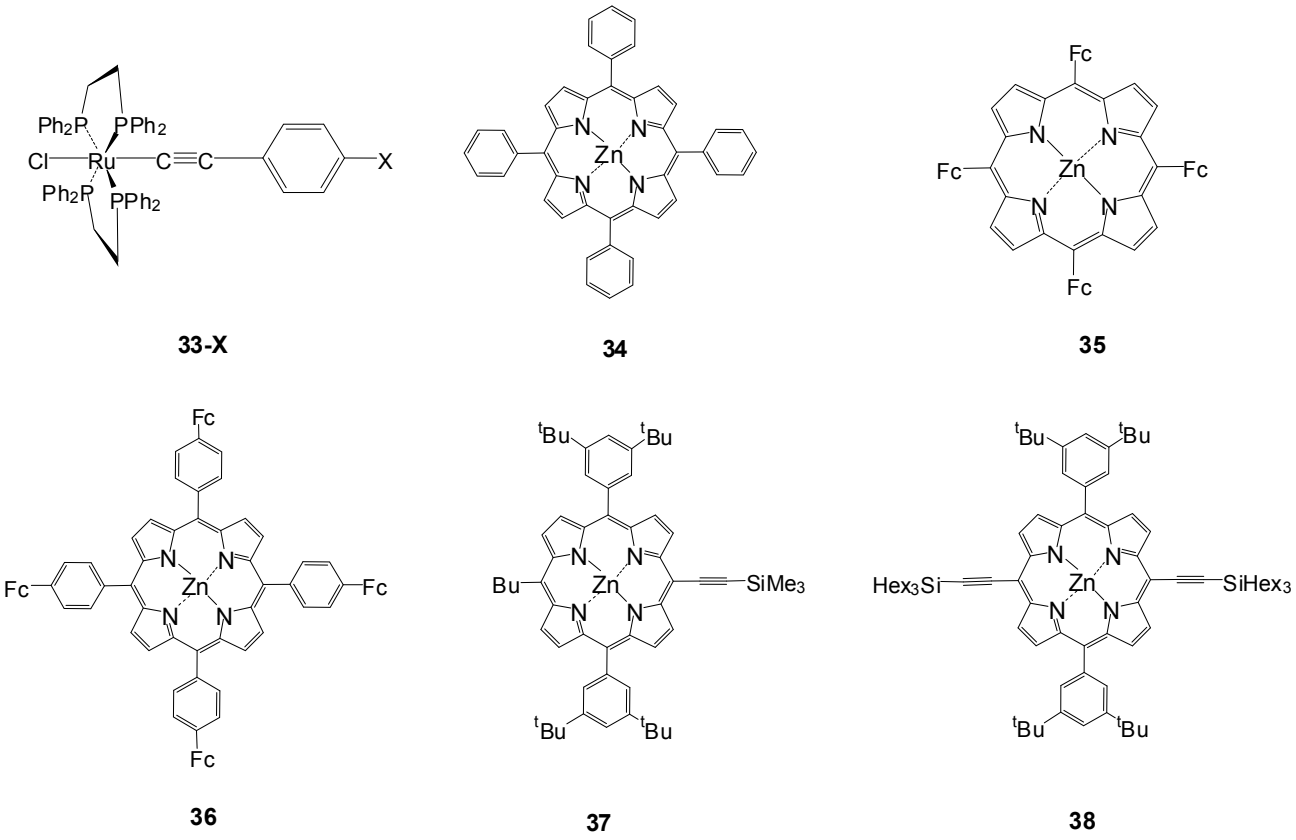

Figure 8 : Selected Ru(II) alkynyl complexes and porphyrins

The voltammograms of **32-NO_2** and **32-H** are similar to that of **31**. They are obtained in the 0-1.3 V range, exhibiting three waves in a 4:1:1 ratio. The most intense process occurs at the lowest potential, again corresponding to the simultaneous oxidation of the Ru(II) centers. The higher potential processes correspond to the first two oxidations of the **ZnTPP** core. For **32-OMe,** an additional irreversible process masks the second porphyrin-based oxidation. As for **32-NO_2**, another strong irreversible wave is observed at - 0.96 V, which corresponds to the multi-electron reduction of the nitroaryl groups.[38,47,48]

In comparison to **31**, the Ru(III/II) potentials of **32-H** are slightly lower (0.46 V vs. 0.49 V), as expected from the more electron-donating character of the arylalkynyl ligand relative to the chlorido ligand.[42] Within the **32-X** series, classic substituent effects control the Ru-centered oxidation potentials.[45,38] As expected, the potential is lowered for the compound **32-OMe** with four peripheral electron-donating methoxy groups. On the contrary, the opposite is found for **32-NO_2** with strongly electron-withdrawing nitro groups (**Table 3**). In contrast, the porphyrin-based oxidations appear only weakly affected by modifications in the *trans*-ligand at the peripheral ruthenium centers (**Table 3**).

To confirm our obtained results, a comparison to other symmetrically-functionalized porphyrins bearing redox-active substituents on their periphery is presented. Thus, the Zn(II) porphyrin **35** (**Figure 8**), which has four ferrocenyl groups appended to its *meso*-positions, exhibits several resolved Fc-based oxidations.[49] In the present system, the observation of a single wave for the oxidation of the peripheral organometallic substituents in **31** or **32-X** is indicative of a weaker electronic interaction between them. Similar case was observed for **36** with the four ferrocenyl substituents on the *para*-positions of the *meso*-phenyl groups.[50]

The observation of a chemically reversible and simultaneous oxidation of the four metal-alkynyl substituents in **31** or **32-X** is of interest in possible redox-switching of the NLO properties,[25,17,51] since this oxidation will preserve the symmetry of the compound, and thereby facilitate our analysis of the physics underlying the switching phenomenon.

Compounds	$E°_{Ru(III)/Ru(II)}$ (V)[a,b]	$E°_{ZnTPP/ZnTPP^{+}/ZnTPP^{2+}}$ (V)[a,b]
31	0.49[c]	0.87, 1.16
32-NO_2	0.57[c]	0.86, 1.21
32-H	0.46[c]	0.88, 1.21
32-OMe	0.34[c]	0.84[d]
30	/	0.87, 1.14

[a]V vs SCE. [b]Conditions: CH_2Cl_2, 0.1 M$[NBu_4][PF_6]$, scan rate 0.1 $V.s^{-1}$. [c]$Fe(C{\equiv}CPh)(dppe)(\eta^5\text{-}C_5Me_5)$ was used as an internal calibrant ($E°_{Fe(III)/Fe(II)}$=-0.15Vvs. SCE).[42]

[d] An irreversible oxidation occurs at 1.16 V.

Table 3 : Oxidation potentials for complexes **30**, **31**, and **32-X**[a,b]

2.7. NLO measurements

Standard femtosecond Z-scan measurements were carried out on our organometallic porphyrin series **32-X** in dichloromethane. Measurements could not be done for the precursor **31** since it was insufficiently soluble for performing such measurements. They were performed in the spectral range between 530 and 1600 nm, with simultaneous recording of the open- and closed-aperture signals. It

should be emphasized that this region partly overlaps the one-photon absorptions of all the compounds (the Q bands) and so two-photon transitions to many states can be expected in this range.

It must be kept in mind that different selection rules govern one-photon and two-photon transitions. Due to the presence of various resonances, the NLO properties in the investigated wavelength range are likely to contain several contributions, including that of saturation of absorption (SA), so the NLO parameters need to be treated as "effective" responses (as well as contributions from SA, the NLO parameters may be laser pulse width- and pulse energy-dependent).

The Z-scan traces obtained from these studies were used to calculate the effective values of the real and imaginary part of the cubic hyperpolarizability γ of the chromophores.

However, the **real parts** of $\boldsymbol{\gamma}$ were found to exhibit complex behaviour which, together with inherently large errors in their determination (they are calculated from differences between scans for a solution and that for the solvent alone), has rendered it impossible to analyze them at the present stage. We therefore focus here on the absorptive nonlinearities, represented by the **imaginary parts** of $\boldsymbol{\gamma}$ which were determined and subsequently converted into **two-photon absorption cross-sections** ($\boldsymbol{\sigma_{2eff}}$) as presented in **Table 4**.

The data reveal that all **32-X** complexes behave as two-photon absorbers around 1100 nm and 710 nm. For the nitro- and methoxy-containing complexes, a third two-photon absorption (TPA) peak is found at higher energies, near 530 nm. In addition, all **32-X** complexes show SA behaviour near 600 nm, in a spectral range which roughly corresponds to their second Q band.

The best TPA performances were obtained near 710 nm for **32-NO_2** and **32-H**, with effective cross-sections exceeding 4500 GM. However, since these processes partly overlap with the SA process near 600 nm, the measured ζ_{2eff} values result from a competition between these two processes, a situation that likely leads to an underestimation of the actual cross-section of the pure TPA process. Also, the presence of ultrafast reverse saturable absorption (RSA) processes that contributes to the effective TPA cross-sections near 710 nm found cannot be disregarded at this stage.[23] However, these appear unlikely due to the poor overlap with the second Q-band. This must also be considered when attempting any comparison between the ζ_{2eff} values near 710 nm for the different compounds.

This organometallic porphyrin series is of centrosymmetric nature. So, selection rules predict that excited states to which transitions are allowed for one-photon processes should be forbidden for two-

photon processes, and vice-versa.[22] Thus, examination of the one photon absorption (OPA) spectra is at best indicative of the nature of the excited state involved in the TPA process.

The poor match between the OPA and TPA peaks suggests that none of the observed TPA bands can be ascribed to a reduction in symmetry due to the presence of conformers in solution. It is especially interesting that the one-photon Soret band near 400 nm does not have a two-photon analogue at 800 nm. In contrast, there seems to be some antiresonant behaviour in this region.

The small TPA peaks observed at 1100 nm can be tentatively associated with excited states similar to those at the origin of the Q-bands. Their poor X-substituent dependency is consistent with such an assignment.

The main TPA peaks near 710 nm roughly correspond to the onset of OPA peaks at 350 nm. It may be that a "dark" MLCT state is involved in this process. Consistent with such a hypothesis, a more pronounced dependence of the ζ_{2eff} values on the nature of the X-substituent is suggested by the data (keeping in mind the experimental error margins), the strongest effective cross-section being obtained for the most electron-withdrawing substituents. This is reminiscent of the fact that related 4-nitroarylalkynyl Ru(II) complexes are often found to present larger effective TPA cross-sections than their unsubstituted counterparts.[47,52]

However, as mentioned above, the comparison between effective TPA cross-sections determined for **32-X** compounds must be undertaken with care due to the occurrence of a SA process in the same spectral range, as manifested by the presence of negative values for the effective cross-section around 600 nm.[23]

Compound	**σ_{2eff} (1st max.) [GM]**	**λ (1st max.) [nm]**	**σ_{2eff} (2nd max.) [GM]**	**λ (2nd max.) [nm]**	**σ_{2eff} (1st min.) [GM]**	**λ (1st min.) [nm]**
32-NO_2[a]	6000 ± 3000	770	1500 ± 500	1000	-4500 ± 200	620
32-H	4800 ± 500	710	1400 ± 500	1300	-2800 ± 600	595
32-OMe[a]	4200 ± 500	710	1300 ± 100	1000	-1400 ± 400	620

[a]An additional maximum is apparent at $\lambda < 530$ nm with $\zeta_{2eff} \geq 6400$ GM.

Table 4 : Comparison of extremal values of the effective two-photon absorption cross-sections (ζ_{2eff}) for given wavelengths between 600 and 1600 nm for **32-X** complexes

Finally, comparison with the literature data reveals that related porphyrins such as **37**[53] or **38**[54] (**Figure 8**) possess very weak TPA (< 50 GM) above 700 nm, behavior. That was also predicted by independent DFT calculations conducted on Zn(II) porphyrins modeling **38**.

These calculations also suggested that, for **38**, a more efficient TPA process may occur at higher energy, just below 600 nm. It would originate from a dark porphyrin-based excited state with an energy just above that of the Soret band.[55]

With **32-X** derivatives, similar states could be at the origin of the TPA peak detected near 700 nm. However, the effective cross-sections found for these compounds are much larger than the theoretical predictions for the porphyrin modelling **38**.

Instead, as discussed above, we believe that the state at the origin of this two-photon absorption process corresponds to a $d_{Ru} \rightarrow \pi^*_{C\equiv C}$ MLCT state, in line with the slight substituent-dependency seen for the cross-sections.

In conclusion, a new series of organometallic porphyrin assemblies possessing four ruthenium moieties was synthesized and fully characterized. In addition, preliminary Z-scan measurements seem to be promising.

3. Synthesis of organometallic porphyrin dendrimers

As seen in chapter 2, dendrimers, comprised of **dendrons** that are attached in turn to a **central core** could be obtained by either **convergent** or **divergent** synthesis.

We reported in chapter 2, a convergent route exploited by Vögtle and co-workers[56] where the dendron is synthesized by stepwise repetition of two types of reactions and then used to react with a central core to get the target dendrimer as a final step (see **Scheme 2** chapter 2).

As we mentioned earlier, this method can induce steric problems leading to less possible generations, but on the other hand purifying the desired dendrimer from other impurities is much more facile.

Whereas in the case of **divergent synthesis**, there are less chances of steric problems but purification of the wanted dendrimer is hard or even impossible due to the close sizes of the dendrimer to the impurities.

More specifically, concerning **organometallic dendrimers**, Takahashi, Stang, and their co-workers presented the synthesis of alkynylmetal dendrimers using metal dihalides *trans*-[$PtX_2(PR_3)_2$] and alkynes.[57,58] In addition, the first electron rich examples were synthesized by Humphrey's group.[59]

Motivating NLO response was obtained from the alkyl ruthenium dendrimer **1a** which was synthesized using the sterically controlled organometallic dendron or wedge **46**.[31] The latter was extended by one phenyl **48**, as a compound to be used in the preparation of another generation of organometallic dendrimer **2a**[31] (**Scheme 4**).

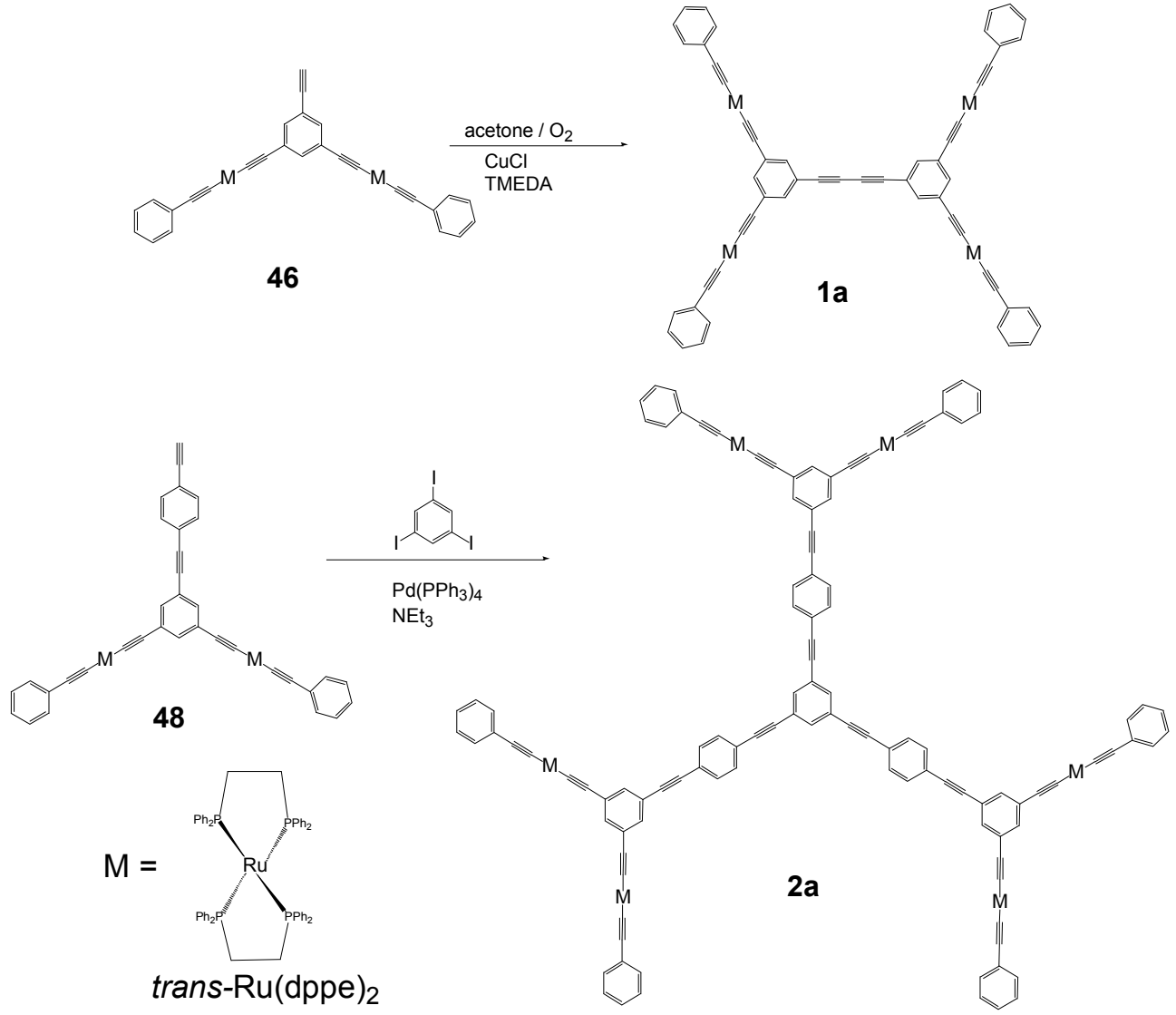

Scheme 4 : Selected examples of organometallic dendrons and their corresponding dendrimers

Moreover, due to steric hindrance, compound **46** was extended by two phenyls **50** to prepare the N-core dendrimer **3a** by convergent synthesis[19] as seen in **Scheme 5**.

This convergent synthesis proved the dramatic increase in the NLO response going from one generation to another. This increase could be related to the dendritic effect.

Furthermore, active NLO organometallic dendrimers synthesized via divergent route were also reported by M. Humphrey's group.[60]

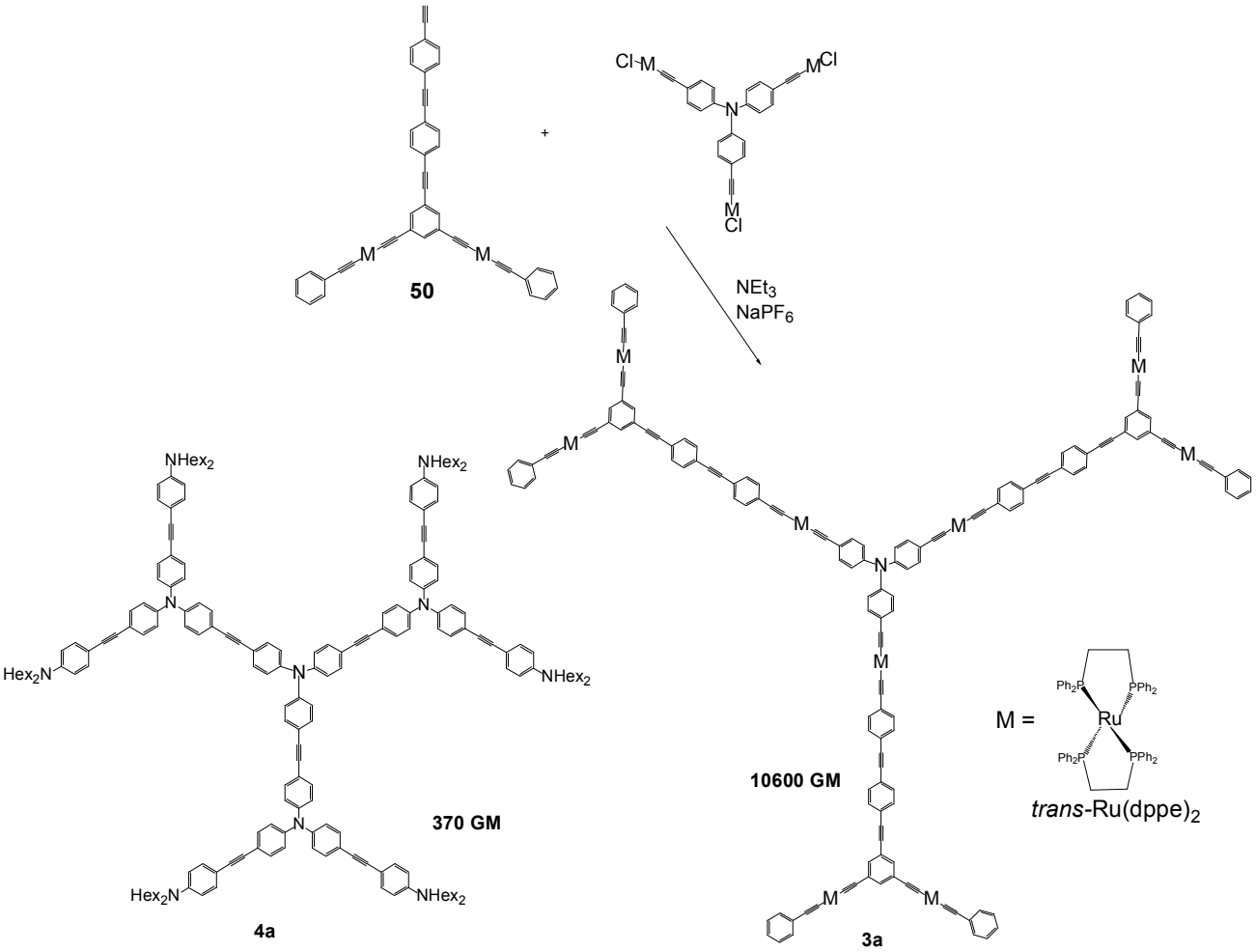

Scheme 5 : Organometallic dendrimer **3a** and organic dendrimer **4a**

Another important thing to focus on, is the influence of organometallic complexes versus organic analogues on the NLO response.

For example, a comparative study was done recently between the organometallic dendrimer **3a** and its organic analogue **4a**[61] as seen in **Scheme 5**. The performance of **3a** is an order of magnitude greater than of its similar organic dendrimer **4a** even when scaled for molecular weight. That is probably due to incorporation of metal centers at appropriate sites in the molecular architecture.[62]

So, based on all what has been mentioned, a project was elaborated combining all the driving factors to theoretically obtain better NLO response. In other words, the target was to use the porphyrin precursor **31**, increase the number of metals and exploit the dendritic effect. So, the proposal was to synthesize **organometallic dendrimers** having porphyrin precursor as a core, and use organometallic dendrons (**Figure 9**).

During my stay in Canberra (Australia) in the ANU for three months, last year, as collaboration between the two laboratories, this project was developed. The short organometallic dendron **46** was not used directly, due to steric hindrance, it was extended by a one phenyl linker to get **48**. So, during discussion, the synthesis of this linker comes first, then followed by the coupling to the porphyrin core.

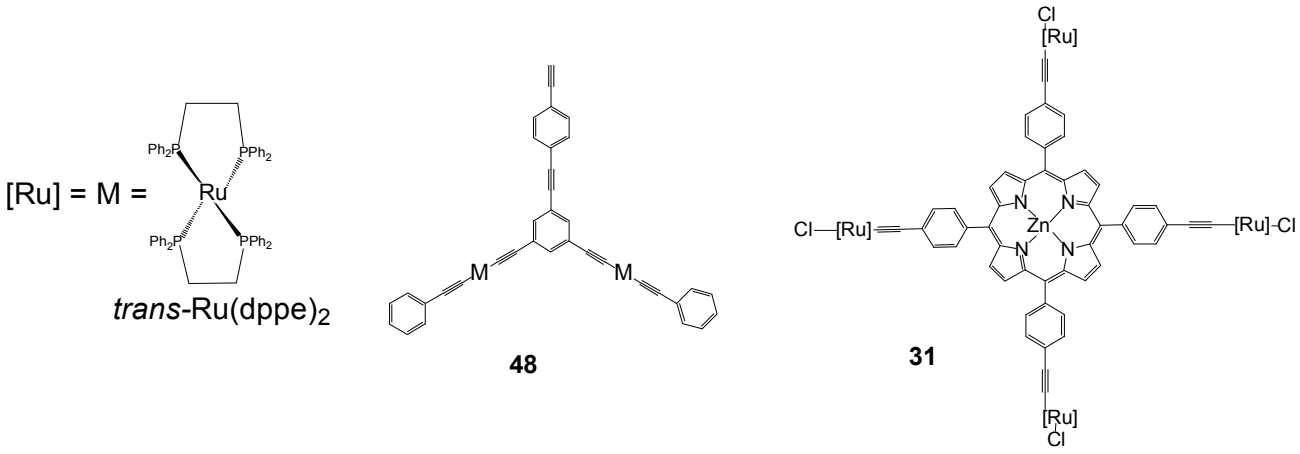

Figure 9 : Precursors (**48** and **31**) to synthesize the desired organometallic dendrimer

3.1. Synthesis of the one phenyl linker

The synthesis of ((4-iodophenyl)ethynyl)trimethylsilane **40**, was achieved in two steps. First, a Sonogashira couling was carried between 1-bromo-4-iodobenzene (commercially available) and trimethylsilylacetylene in triethylamine (**Scheme 6**).

The crude product was purified over few centimetres of silica to get **39** as a pure colourless compound as 94% yield. Then, a lithium-halogen exchange was applied for **39**. The obtained mixture was extracted with DCM, dried over $MgSO_4$, filtered, and then taken to dryness. The resulting solid was purified by column chromatography on silica gel using hexane as an eluent to yield a colourless compound **40** as a pure product with 57% yield.

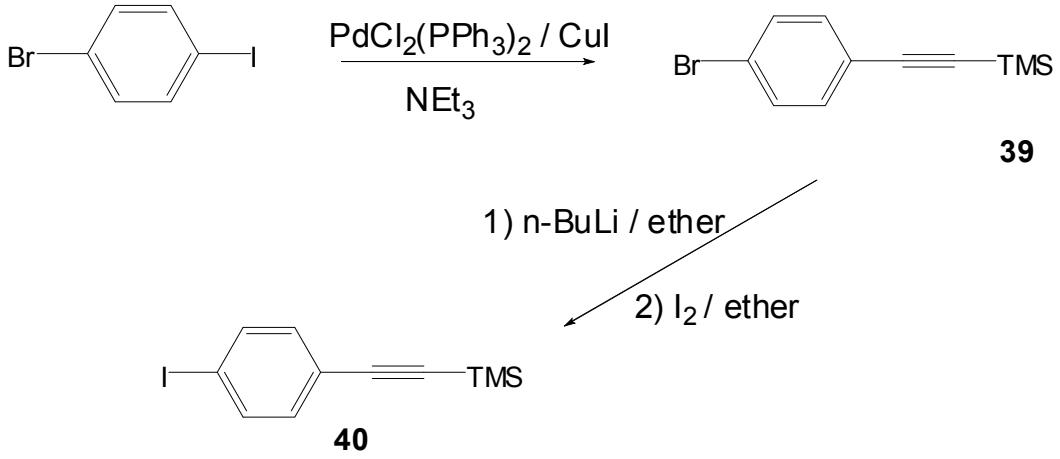

Scheme 6 : Synthesis of the one phenyl linker **40**

3.2. Synthesis of the organometallic wedge 46

Humphrey's group[63] and Long's group[64] have demonstrated that 1,3,5 triethynylbenzene reacts with *cis*-$[RuCl_2(dppm)_2]$ to give 1,3-{trans$[(dppm)_2ClRuC{\equiv}C]\}_2$-5-$HC{\equiv}CC_6H_3$. It proved impossible for the tris product to be formed even if excess ruthenium reagent was used and in addition, a structural studies confirmed that steric crowding was the reaction limiting factor.[63] Although it is possible to form bis acetylide using $Ru(dppm)_2$ unit,[65,66] the $Ru(dppe)_2$ building block provides a more convenient group to afford bis-acetylides and hence facilitates dendrimer constructions. For these reasons the synthesis and characterisation of **46** was reported,[31] we have adapted the synthesis mentioned in the literature with some modifications.

The synthesis of **46** starts by reacting the known complex *cis*-$[RuCl_2(dppe)_2]$ with triethynyl benzene followed by reaction with NEt_3, to get cleanly under steric control an intermediate **45** which was characterized by a singlet for the **^{31}P NMR** at 50.5 ppm corresponding to the eight equivalent phosphorus atoms from the four dppe ligands coordinated to the two ruthenium terminal groups.

^{1}H NMR gave another evidence about the structure of this intermediate for the integration of the terminal alkyne proton, at 3.02 ppm was one relative to other peaks. Ethynylbenzene was then added

to this intermediate **45** to get **46** which was identified by a singlet for the **^{31}P NMR** at 54.5 ppm, consisting to a bis-alkynyl ruthenium unit.[67] Triethynylbenzene was the result of a Sonogashira coupling between the commercially available compound 1,3,5 tribromobenzene and trimethylsilylacetylene followed by classical deprotection of the trimethylsilyl groups using potassium carbonate (**Scheme 7**).

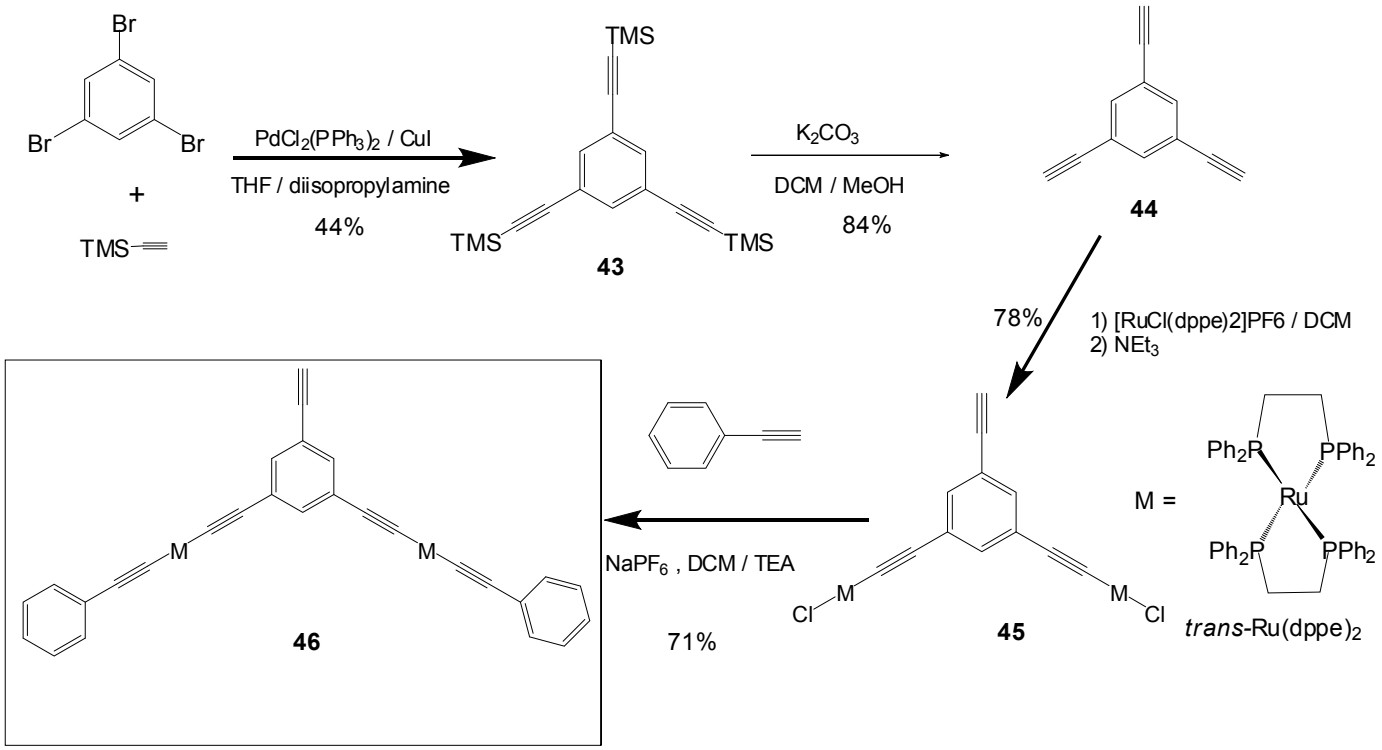

Scheme 7 : Synthesis of the organometallic wedge **46**

3.3. Synthesis of the one phenyl extended organometallic wedge 48

Since our interest is to synthesize a dendrimer using our zinc porphyrin **5** by convergent synthesis, the used dendrons need to be extended. To reduce the hindrance resulting from the dendron **46** due to the dppe on the ruthenium atoms as endgroups of the mentioned porphyrins, and that of **46**, so dendron **46** needs to be extended.

First, it was suggested to extend **46** by one phenyl group and then to do the final reaction between dendron **48** (**46** extended by one phenyl) and porphyrin **31** expecting to get the dendrimer

51. The organometallic wedge **48** was already reported in literature with full characterization.[31] We adapted the synthesis mentioned in literature with some modifications.

In short, **48** was obtained as a result of a classical Sonogashira coupling between **46** and ((4-iodophenyl)ethynyl)trimethylsilane **40** followed by deprotection of TMS group using tetrabutylammonium fluoride (TBAF) as presented in **Scheme 8**.

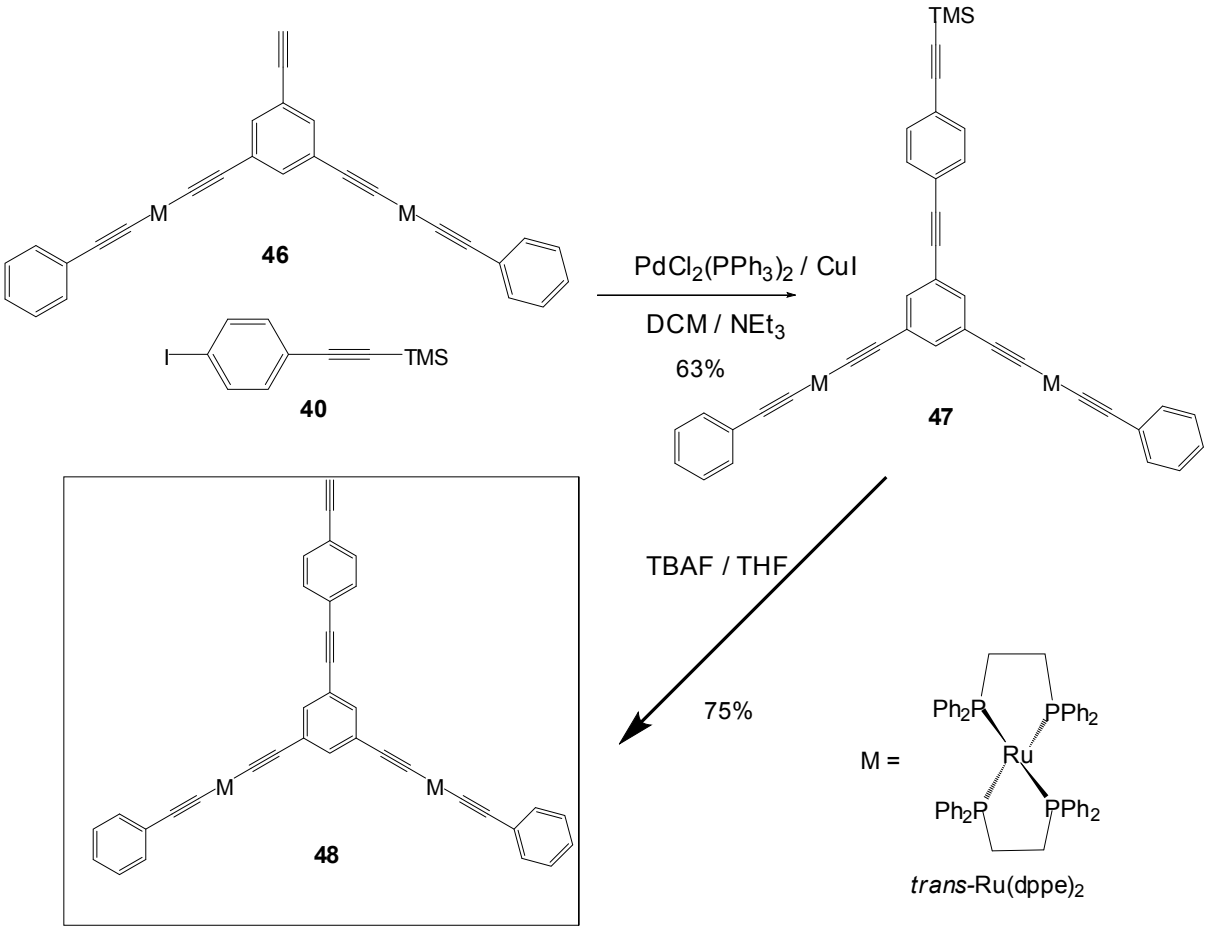

Scheme 8 : Synthesis of the one phenyl extended dendron **48**

3.4. Attempt to synthesize the organometallic porphyrin

As in our case, we proceeded to the substitution of chloride ions by more electron rich ligands, having a large π electron system. We expect that this substitution in the ruthenium *trans* position, is possible by reaction with a large excess of functionalized dendrons.

After synthesizing the teraruthenated Zn porphyrin **31** and the organometallic dendron extended by one phenyl **48**, comes the final step to react both species using $NaPF_6$, triethylamine as a base in dichloromethane at room temperature expecting to get the desired dendrimer **51** (**Scheme 9**).

The reaction was monitored by **^{31}P NMR** since the reaction will be accompanied by changes in the chemical shifts in comparison to the starting materials. Unfortunately, no changes in the phosphorus chemical shifts were observed : a singlet at 54 ppm, and another at 50 ppm were observed after 24, 48, and 72 hours. That means that no reaction took place. Many trials were done trying to obtain the dendrimer **51**; the mixture was heated at different temperatures and finally refluxed. Dichloromethane was then replaced by THF where the reaction was tested at both room temperature and heated to reflux.

Unfortunately, nothing but the starting materials could be observed and identified by **^{31}P NMR**. As a result, it seems that it is not possible to insert the one-phenyl extended wedge **48** in the porphyrin core due to steric hindrance.

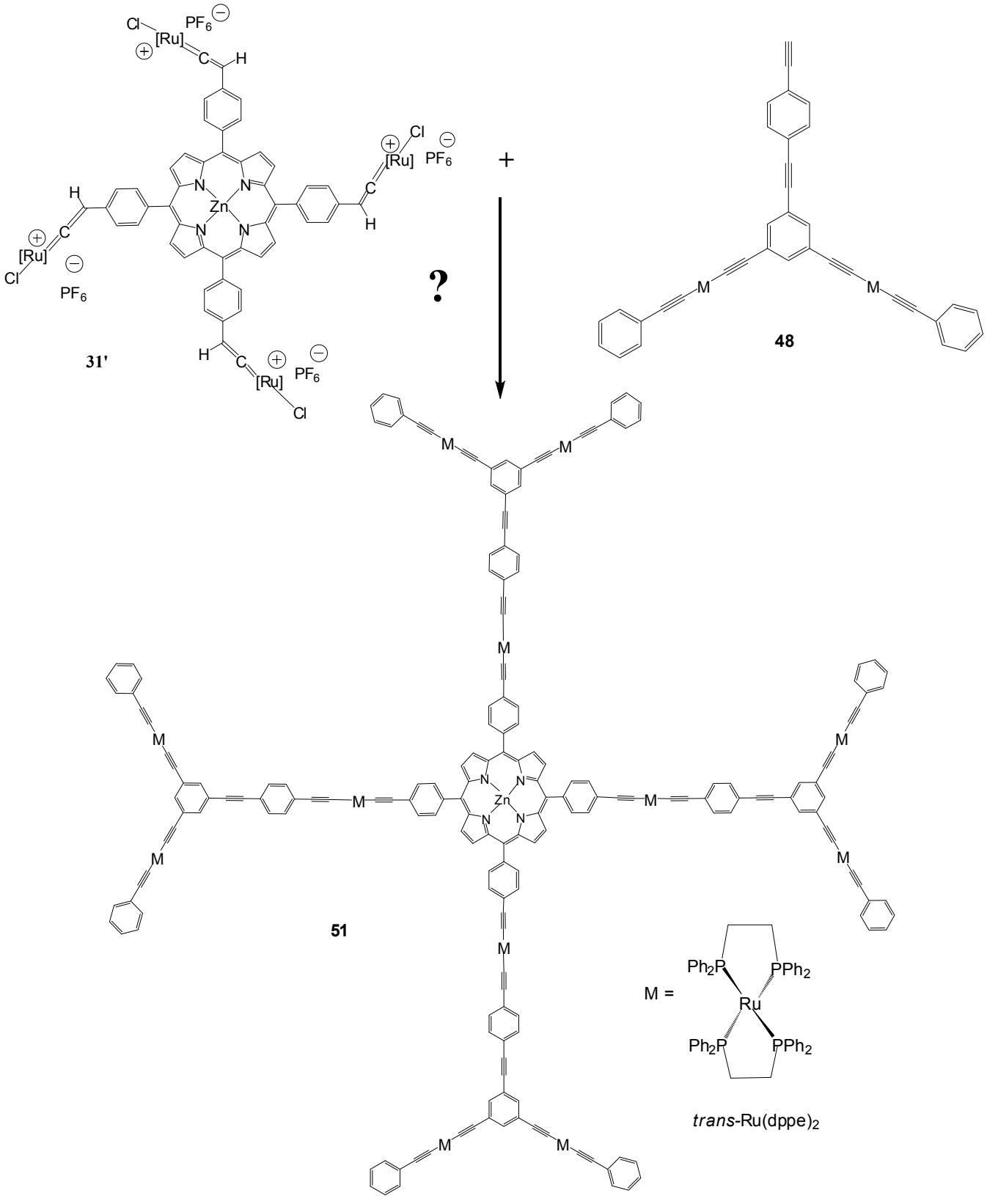

Scheme 9 : Attempt to synthesize the organometallic dendrimer **51**

It is worth to mention that our case is very similar to that in K. Green's honors (**Scheme 10**) where the target molecule couldn't be obtained in case of **48** but it was obtained when **48** was replaced by **50**. This result was considered to be surprising due to many reasons. One reason is that this molecule has an arene branching point with one ruthenium directly bound by an ethynyl group and two ruthenium attached by ethynyl-phenylethynyl links. Another important reason is that no significant steric problems appeared to be from the SPARTAN modelling. This same modelling has been used before to accurately estimate the size of similar molecules,[40] and was thought to provide a reasonable estimate of the size and geometry.

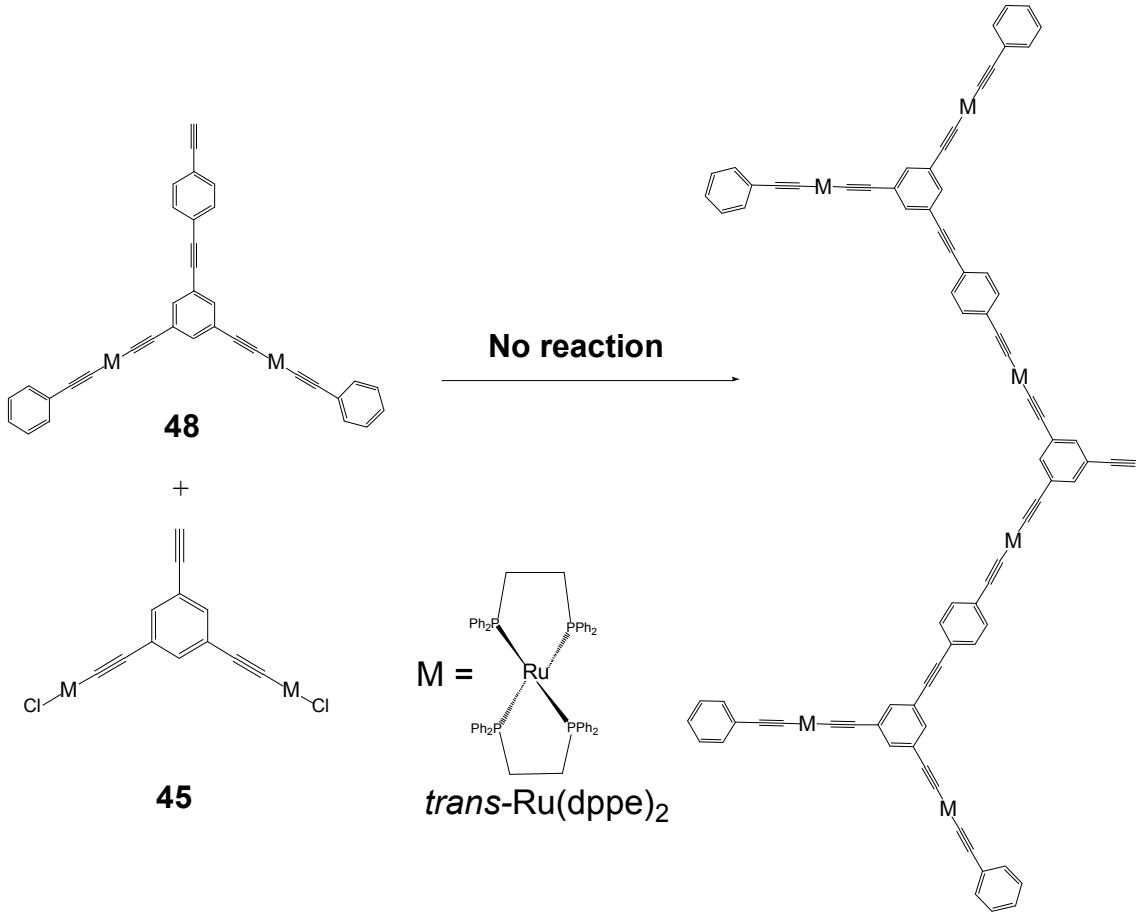

Scheme 10 : Selected example of K. Green's honors

3.5. Synthesis of the two phenyl linker

The synthesis of the two phenyl linker **42** was achieved in two steps. A Sonogashira coupling between iodoaniline and ((4-ethynylphenyl)ethynyltrimethylsilane was done to obtain **41** as a pure white solid with 83% yield. As a next step, Sandmayer reaction was applied on **41** as seen in **Scheme**

11. The organic phase of the crude mixture was washed with thiosulfate, dried over $MgSO_4$, and taken into dryness. It was then purified by column chromatography on silica gel using hexane as an eluent, and crystallized in $MeOH/CHCl_3$ to obtain **42** as a pure white solid product.

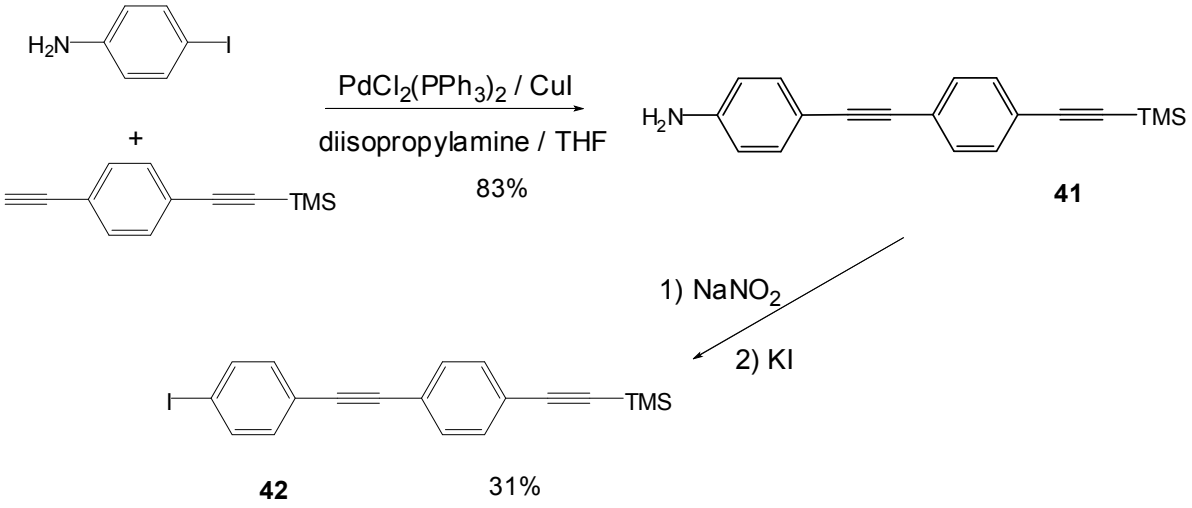

Scheme 11 : Synthesis of the two phenyl linker **42**

3.6. Synthesis of the extended organometallic wedge

To efficiently synthesize porphyrin dendrimers, dendrons need to be extended, probably at a longer size than medium length dendron **48**, so we suggested to extend it by one more phenyl group.

Dendron **50** was already reported in literature with full characterization[62] but we adapted the synthesis mentioned in literature with some modifications. Extended wedge **49** was obtained as a result of a classical Sonogashira coupling between **46** and ((4-((4-iodophenyl)ethynyl)phenyl)trimethylsilane **42**.

Then deprotection of TMS group using TBAF (**Scheme 12**) in THF was done. The deprotection was confirmed by **^{1}H NMR** due to the absence of TMS protons at 0.26 ppm replaced by the singlet at 3.19 ppm proving the terminal alkyne proton. Finally, reaction will be tried between the two-phenyl extended wedge **50** and porphyrins salt **31'** expecting to get the new organometallic dendrimer **52**.

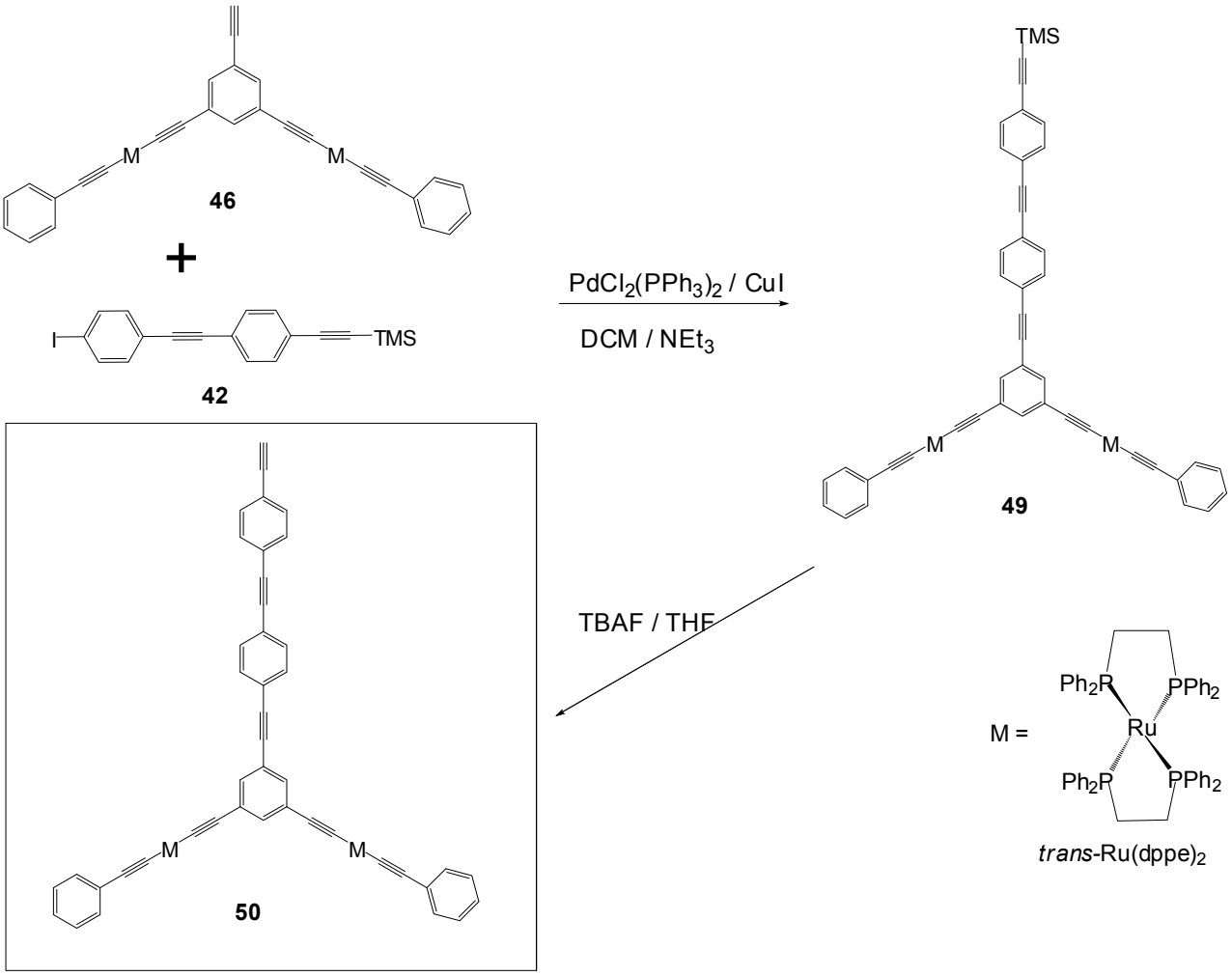

Scheme 12 : Synthesis of the two phenyl extended organometallic dendron **50**

3.7. Synthesis of the organometallic dendrimer 52

In this case, steric hindrance is avoided by the length of the dendrons. So substitution of the chloride ion, in the ruthenium *trans* position, should be done easily by reaction with an excess of extended dendrons **50**.

We can notice that the synthesis of tetraacetylide disubstituted ruthenium type complex is performed (i) directly without isolating the vinylidene intermediate species **31'** (ii) as well as with the neutral species **31**, triethylamine being added to the reaction mixture together with the other reactants in both cases.

This highly organized 12 ruthenium assembly is prepared by reacting vinylidene salt **31'** with long size dendron **50** to afford the new dendrimer **52** in good yields (**Scheme 13**).

In more details, dendron **50** and porphyrin salt **31'** were reacted in dichloromethane using $NaPF_6$, and triethylamine as a base at room temperature. The reaction was monitored by **^{31}P NMR**, and after 48 hours, chemical shift changes of the starting materials were observed. For example, a singlet at 54.34 ppm and another doublet at 54.57 appeared. No more singlet of the starting material at 51 ppm was observed indicating the total consumption of porphyrin. The desired dendrimer **52** was precipitated in hexane as a green solid.

This new organometallic dendrimer **52** was fully characterized by means of NMR spectroscopy, microanalysis, IR, UV and CV. Mass analysis could not be done since the molar mass of this complex exceeds the limit of the machine.

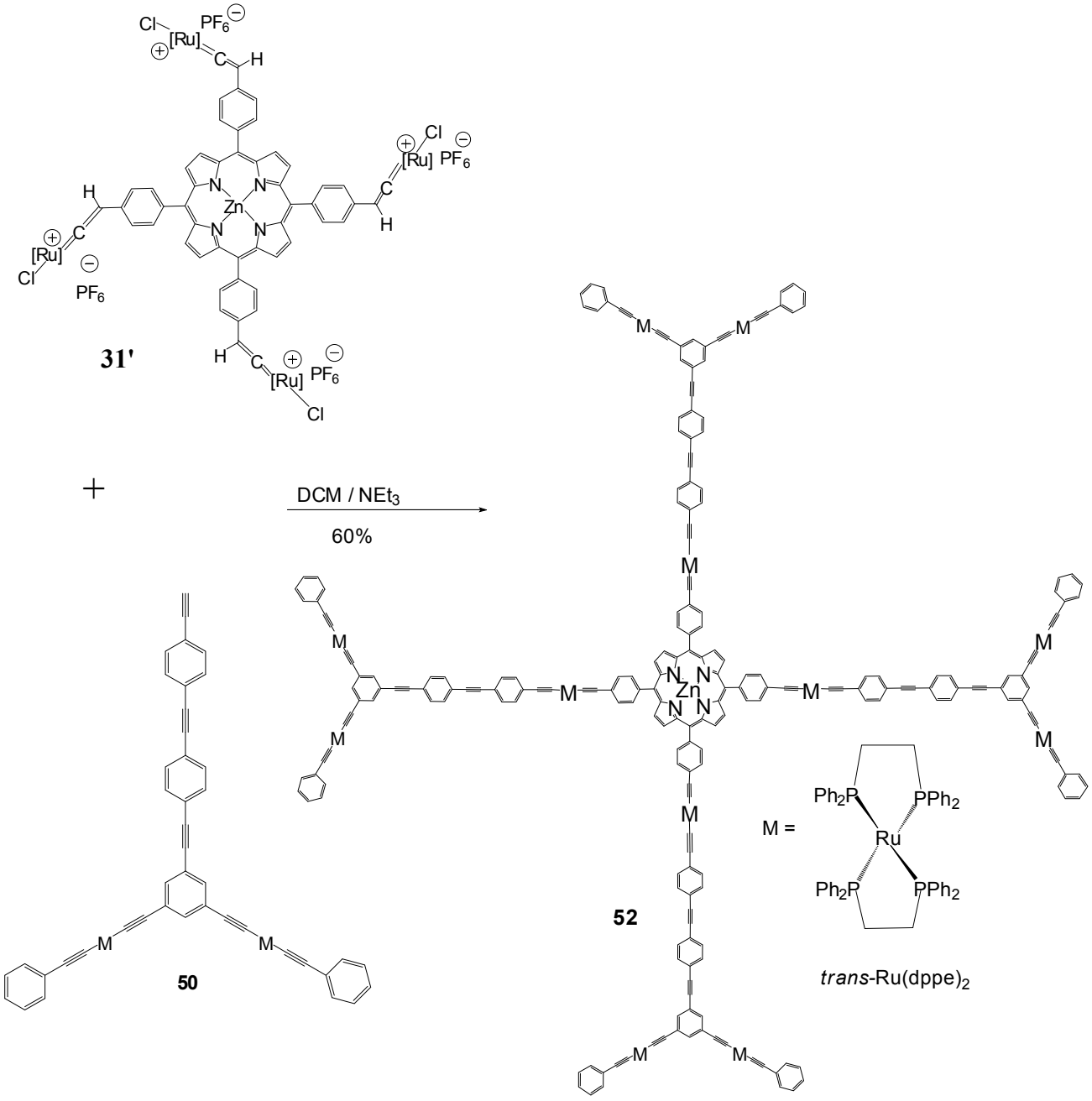

Scheme 13 : Synthesis of the new organometallic dendrimer **52**

3.8. NMR Spectroscopy

The **^{1}H NMR** spectrum of the organometallic dendrimer **52** exhibits both the characteristic signals of porphyrin and ζ-acetylide complex of ruthenium. For example, a broad singlet corresponding to the CH_2 protons of the ruthenium dppe is observed at around 3 ppm. The signals of aromatic protons of the benzene groups and of the dppe are identified between 6.5 and 9 ppm.

Another singlet around 9 ppm is associated to the eight equivalent β-pyrrole protons of the porphyrin macrocycle.

The **^{31}P NMR** spectrum, shows signals that corresponds to the phosphorus from the ligand dppe of the ruthenium. The chemical shifts of these signals at 54 ppm are characteristic of disubstituted ζ-acetylide ruthenium complexes.[40]

3.9. Infrared studies

As seen before, it is known for bis-alkynyl Ru(II) complexes, that both $\nu_{C\equiv C}$ modes appear as a single and broad absorption at around 2050 cm^{-1} (**Table 1**).[68] The infrared spectra of both complexes **31** and dendrimer **52** are presented to be able to compare both values. The organometallic precursor **31** has an intense vibration band at 2057 cm^{-1}. As for the porphyrin dendrimer **52** presents an intense band characteristic of complex ζ-acetylide ruthenium around 2050 cm^{-1}. As expected, for these characteristic vibration bands, for compound **52**, with the terminal organometallic dendrons, this band is slightly lowered to in comparison to the precursor compound **31**.

3.10. Cyclic voltammetry studies

The CV's of the new ruthenium dendrimer **52** presents four oxidation waves in a 8:4:1:1 ratio. The two first waves $\mathbf{E°_{Ru(III)/Ru(II)}}$ and $\mathbf{E°_{Ru(III)/Ru(II)}}$ are easily identified because the intensity is eight and four times stronger than $\mathbf{E^1Ox}$ and $\mathbf{E^2Ox}$ of the porphyrin.

These first and second reversible oxidation waves, with an intensity of eight and four, correspond to simultaneous oxidation of all eight peripheral ruthenium ($\mathbf{E°_{Ru(III)/Ru(II)}}$) and the four internal organoruthenium groups ($\mathbf{E°_{Ru(III)/Ru(II)}}$), the third, with an intensity of one, corresponds to the first oxidation of the porphyrin ($\mathbf{E^1Ox}$) and the fourth to the second oxidation of the porphyrin ($\mathbf{E^2Ox}$).

As expected, for the oxidation of all eight peripheral ruthenium in compound **52**, the potential $\mathbf{E°_{Ru(III)/Ru(II)}}$, is slightly lowered to 0.45 V, in comparison to the precursor compound **31** with $\mathbf{E°_{Ru(III)\,/\,Ru(II)}}$ = 0.49 V.

We can conclude from these studies, that in theory, new compound **52**, with twelve groups of organometallic ruthenium, can be studied in electro commutation. Indeed, like the waves of the ruthenium oxidation ($\mathbf{E°_{Ru(III)/Ru(II)}}$) and oxidation of the porphyrin ($\mathbf{E^1Ox}$) do not overlap, the oxidation of ruthenium can occur without selectively oxidize the macrocycle.

3.11. UV-Visible Spectroscopy

To better understand the absorption of new dendrimer **52**, we report the UV-visible absorption spectra of the complete series.

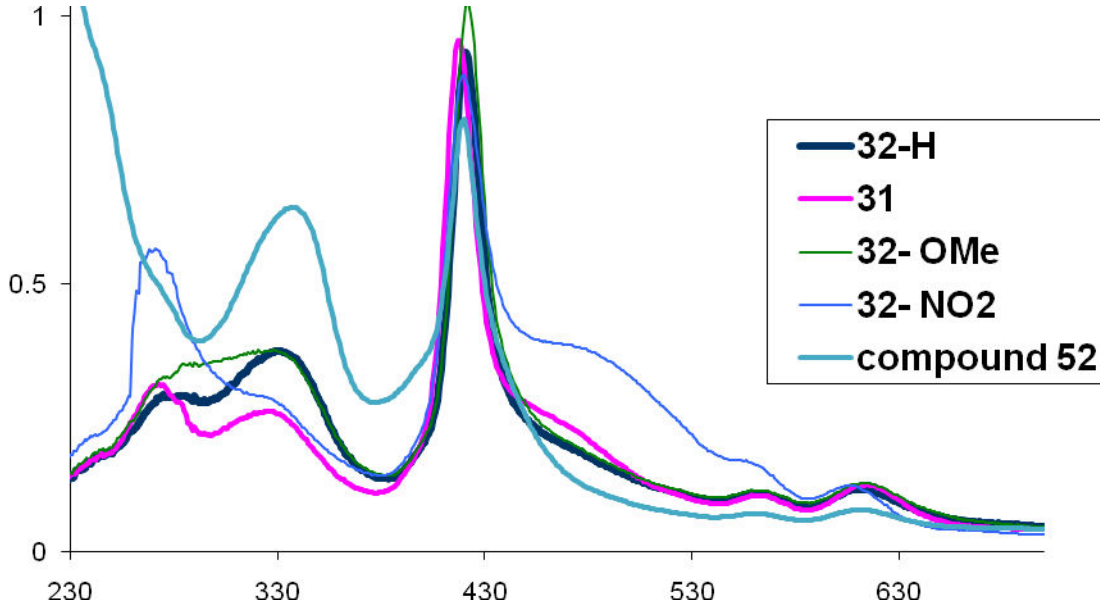

Figure 10 : UV-Visible absorption at 25°C at a concentration 10^{-6} M of (a) zinc complex **31,** (b) ruthenium complex **32-X** and **52** in CH_2Cl_2

In comparison, the UV-Visible absorption spectra of acetylides of ruthenium complexes **31** and **32-X**, are again presented (**Figure 10**). All bands are red shifted for **32-X** (**Table 2**); this was dicussed in the previous part.

More specific, the UV-vis spectrum for the dendrimer **52** shows the Soret band at 420 nm which is slightly red shifted from the precursor **31** (418 nm). The two Q bands are observed at 565 and 613 nm, again red shifted compared to the precursor **31** (563, 615).

In addition, the UV band at 338 nm is red shifted as well with respect to **31** (327 nm). This band could be attributed to a charge transfer from the metal d orbitals to the π* orbital of the ligand $d_{Ru} \rightarrow \pi^*_{C\equiv CTPP}$ (MLCT). As a conclusion, no final net result could be obtained concerning the effect of substituents on the UV spectrum.

4. Iron Organometallic porphyrin assemblies

This project was done as collaboration with Dr. F. PAUL (OMC, University of Rennes 1) specialized in iron acetylide chemistry.[69] So, we could take the benefit of this experience and knowledge of **Iron Chemistry** to develop more our organometallic series, synthesize iron porphyrin complexes and study the third order of NLO. It will be interesting to compare the iron and the ruthenium series and deduce the effect of metal as well.

Recent collaboration results was the synthesis of iron porphyrin complex **54** and mixed iron ruthenium complex **55** as seen in **Figure 11**. These iron and iron-ruthenium complexes showed very interesting Z-scan studies.[37] In addition, it was clear that the results appear to be strongly influenced by the nature of the organometallic endgroups.

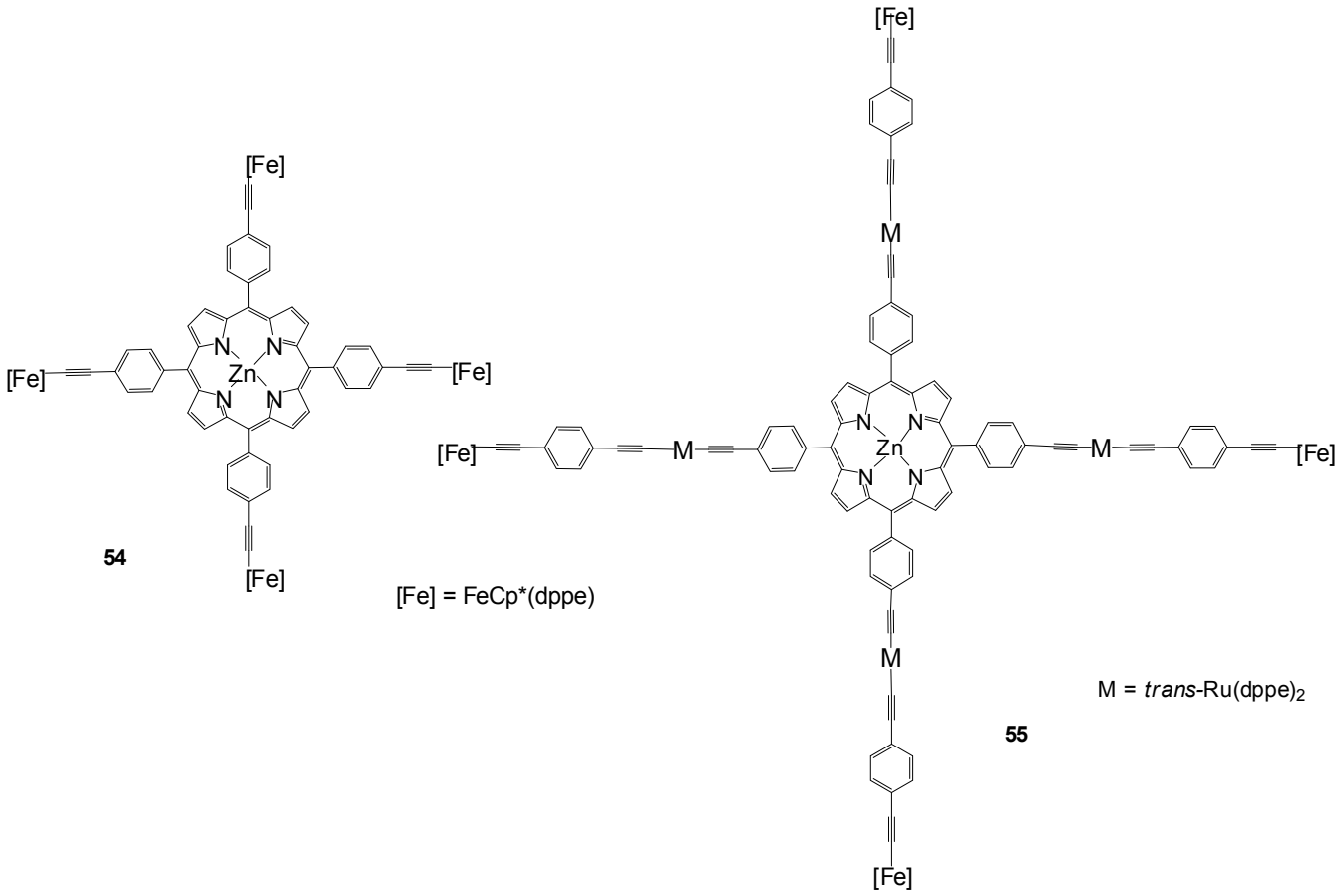

Figure 11 : Organoiron complexes

So, to understand more the effect of the substituents, another target was to functionalize the endgroups of the precursor **31** with ethynyl ferrocene units (**Figure 12**) so that it will be complementary to the previous series (**54** and **55**) where it will be interesting to compare these results willing to be able to draw out a certain conclusion concerning optimizing NLO response.

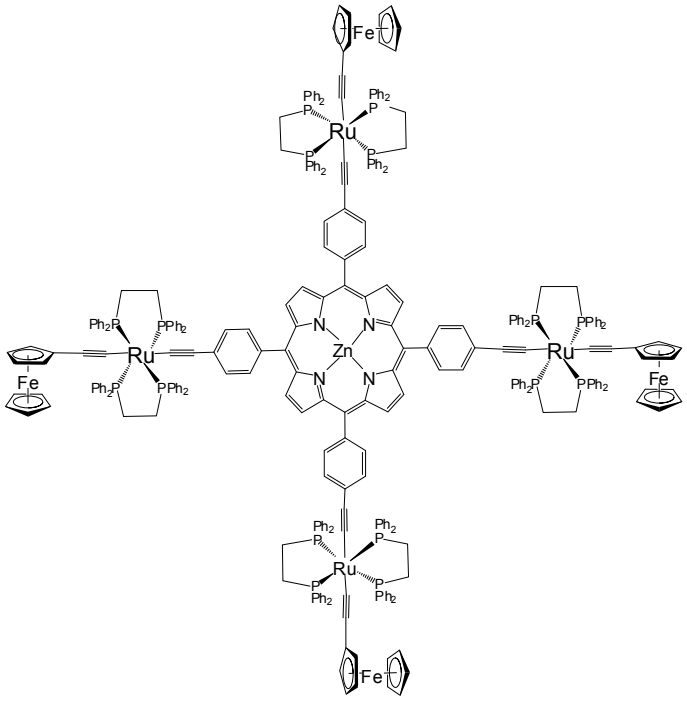

Figure 12 : The new organoiron target molecule **53**

4.1. Synthesis and characterization of 53

The organoiron target was obtained as a result of the reaction between ethynyl ferrocene (commercially available) and the porphyrin precursor in its vinylidene state **31'**. The reaction was carried in dichloromethane using triethylamine as a base at room temperature. The progress of the reaction was monitored by ^{31}**P NMR**, it was complete after 48 hours (**Scheme 14**). Then, the reaction mixture was filtered, concentrated under reduced pressure, and the desired product **53** was precipitated in hexane to yield a green solid as 71% yield.

This new organoiron complex was fully characterized by means of NMR spectroscopy, microanalysis, IR, UV and CV. Mass analysis could not be done since the molar mass of this complex exceeds the limit of the machine.

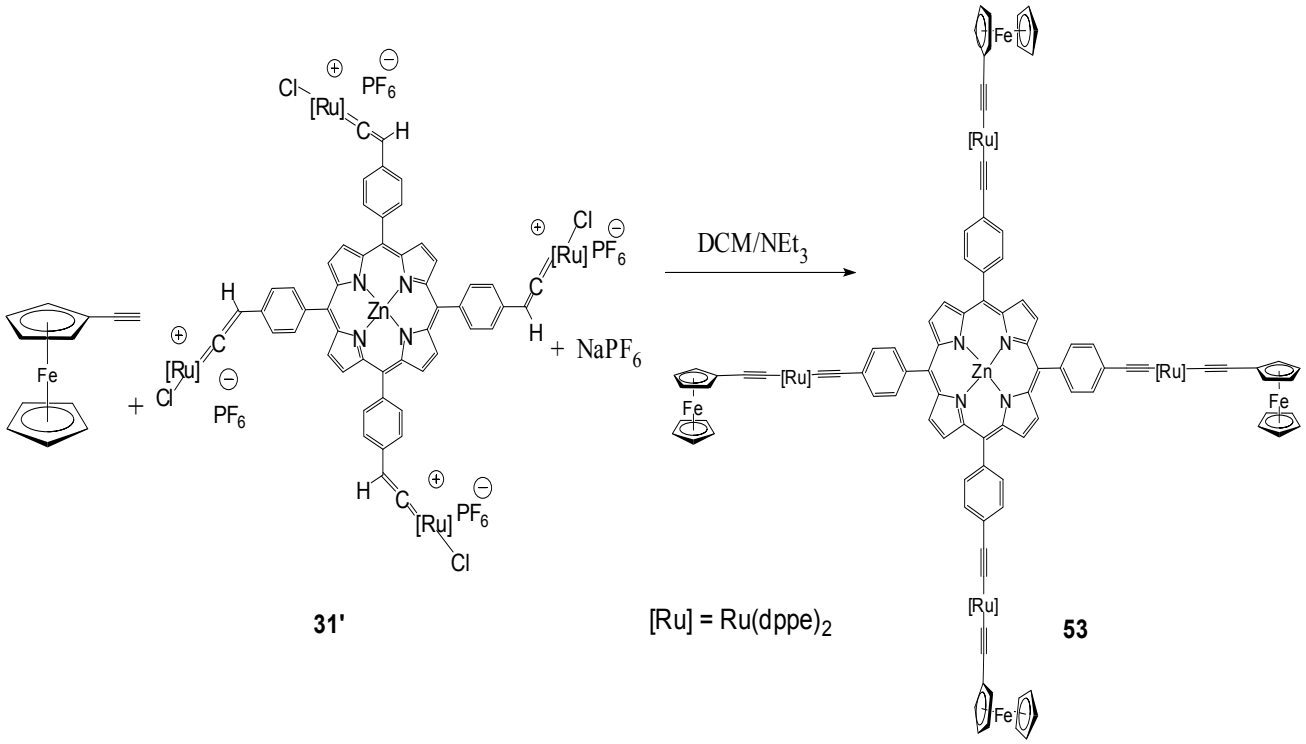

Scheme 14 : Synthesis of the organoiron complex **53**

The **^{1}H NMR** spectrum of the organometallic dendrimer **53** exhibits both the characteristic signals of porphyrin and ζ-acetylide complex of ruthenium. For example, a broad singlet corresponding to the CH_2 protons of the ruthenium dppe is observed at around 2.7 ppm. The protons of the ferrocene are identified at around 4.5 ppm. The signals of aromatic protons of the benzene groups and of the dppe are identified between 6.5 and 8.5 ppm. Another singlet around 9 ppm is associated to the eight equivalent β-pyrrole protons of the porphyrin macrocycle.

The **^{31}P NMR** spectrum, of **53** shows a singlet at 54.5 ppm that corresponds to the equivalent phosphorus from the ligand dppe of the ruthenium. The chemical shifts of this signal at 54 ppm is characteristic of disubstituted ζ-acetylide ruthenium complexes.[40]

The **UV-visible** spectrum for the compound **53** shows the Soret band at 421 nm which is slightly red shifted from the precursor **31** (418 nm), but not to the extent of complex **55** (424 nm).[37] This Soret band is considered as the source of the green color of this compound. The two Q bands are observed at 565 and 613 nm, again red shifted compared to the precursor **31** (563, 615) and that of **55** (560, 614).[37] In addition, the UV band at 332 nm is red shifted as well with respect to the precursor **31** (327 nm), but not with respect to **55** (351 nm).[37] This band could be attributed to a

charge transfer from the metal d orbitals to the π* orbital of the ligand $d_M \rightarrow \pi^*_{C\equiv CTPP}$ (MLCT), where M corresponds to Ru and Fe.

Bis-alkynyl Ru(II) complexes are known to have both $\nu_{C\equiv C}$ modes to appear as a single and broad absorption at around 2050 cm^{-1}. [68] The infrared studies of both complexes **31** and dendrimer **53** are mentioned to be able to compare both values. The organometallic precursor **31** has an intense vibration band at 2057 cm^{-1}. As for the porphyrin dendrimer **53** presents an intense band characteristic of complex ζ-acetylide ruthenium around 2055 cm^{-1}. As expected, for these characteristic vibration bands, for compound **53**, this band is slightly lowered to in comparison to the precursor compound **31**.

III. Conclusion and perspectives

In conclusion, a new series of porphyrin organometallic assemblies bearing **four ruthenium species 32-X** was synthesized, and fully characterized.[68] In addition, preliminary Z-scans were done and seemed very interesting for many reasons.

First, these measurements were able to derive non linear absorptive properties of these porphyrins from their imaginary part. It is true that for the moment, no final net conclusion can be drawn concerning the effect of substituents on these measurements. But, what is interesting in these results is that our porphyrins behave as two photon absorbers in the near infra red region.

Moreover, their effective cross sections are relatively important values when compared to other porphyrins in the literature. What we can conclude as well is the effect of inserting electron rich metals on the NLO behaviour. What could be done more, is to try to have a stable oxidation state of these assemblies to try if it is possible to apply the idea of **switch**.

Based on the data providing the influence of dendritic and organometallic effect on NLO response, a new organometallic porphyrin dendrimer bearing **12 ruthenium moieties** (**52**) was synthesized and fully characterized. Currently, Z-scan measurements are initiated in Canberra University (ANU). It will be interesting to compare the results with other organometallic dendrimers. It could be possible to come out with conclusions concerning structure of complexes that optimize NLO response.

As a final conclusion, a new organoiron complex **53** was synthesized, and characterized as well completing a series of iron and iron-ruthenium species. The Z- scan measurements will be done in Canberra. It will be a interesting to compare these results with the organoiron series so that we can tell if ferrocene will have a different effect from other iron moeities.[37]

Experimental Section

Synthesis of 5,10,15,20-tetrakis((4-(trimethylsilyl)ethynyl)phenyl)porphyrin : <u>28</u>

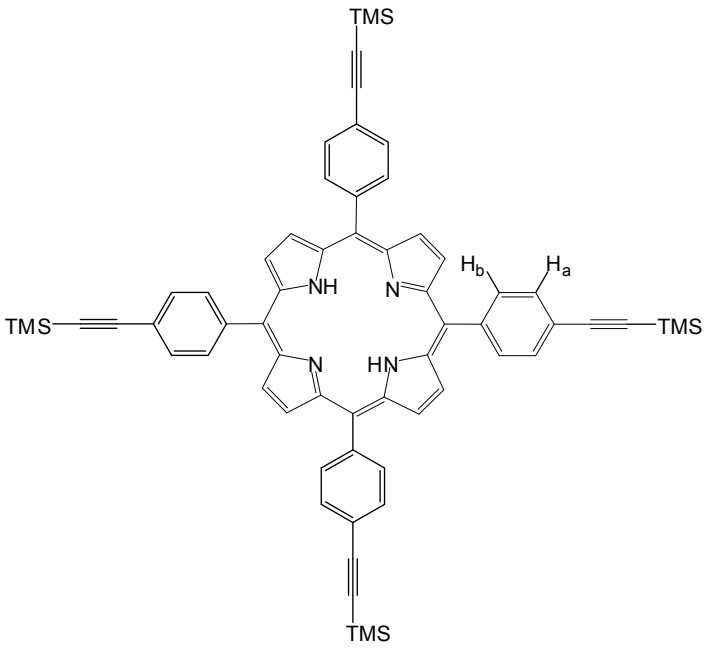

$BF_3.O(Et)_2$ (200 µL) was added to a solution of 4-((trimethylsilyl)ethynyl)benzaldehyde (1.00 g, 5.0 mmol) and pyrrole (0.34 mL, 5.0 mmol) in distilled CH_2Cl_2. The flask was covered with aluminium foil since the reaction is light sensitive at this stage. The reaction mixture was stirred at room temperature for 3 hours. Then, *p*-chloranil (1 g, 4.1 mmol) was added and the reaction was refluxed for 1 hour. The solution was cooled to room temperature. Two pipettes of triethylamine were added to neutralize the reaction mixture. Solvent was evaporated and the residue was filtered over silica with heptane/DCM (50 : 50) affording 625 mg (50%) of the desired porphyrin **28**.

^{1}H NMR (200 MHz, $CDCl_3$, δ in ppm) : 8.86 (s, 8H, $H_{\beta\text{-pyrrolic}}$), 8.18 (d, 8H, H_b), 7.91 (d, 8H, H_a), 0.37 (s, 36H, $Si(CH_3)_3$), - 2.80 (s, 2H, NH).

FT-IR (υ, KBr, cm^{-1}) : 2157 (C≡ C).

Synthesis of of 5,10,15,20- tetrakis ((4-ethynyl)phenyl)porphyrin : 29

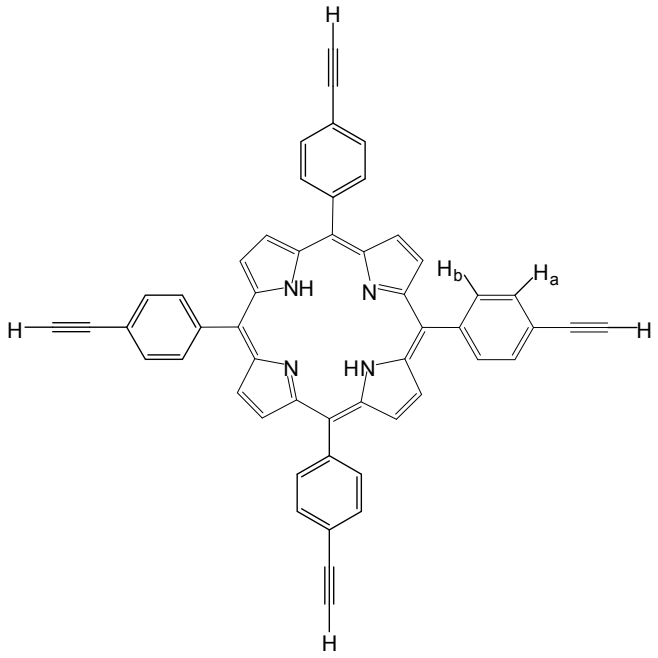

To a solution of porphyrin **28** (250 mg, 0.25 mmol) in CH_2Cl_2 and MeOH (3:1), K_2CO_3 (166 mg, 1.20 mmol) was added; the mixture was stirred overnight at room temperature. The solvents were removed under reduced pressure. The product was extracted with CH_2Cl_2 and washed with 10% $NaHCO_3$, dried ($MgSO_4$), filtered and concentrated to dryness. The residue was filtered over few centimetres of silica using DCM as eluent to afford 174 mg (98%) of the desired porphyrin **29**.

^{1}H NMR (200 MHz, $CDCl_3$, δ in ppm) : 8.88 (s, 8H, $H_{\beta\text{-pyrrolic}}$), 8.19 (d, 8H, H_b), 7.94 (d, 8H, H_a), 3.37 (s, 4H, C_{alkyne}-H), - 2.80 (s, 2H, NH).

FT-IR (υ, KBr, cm^{-1}): 2104 (C≡ C), 3300 (≡ C-H)

MALDI TOF-MS calcd for $C_{52}H_{30}N_4$: 711.250 $[MH]^+$, found : 711.077 $[MH]^+$.

Synthesis of zinc(II)-5,10,15,20- tetrakis ((4-ethynyl)phenyl)porphyrin : 30

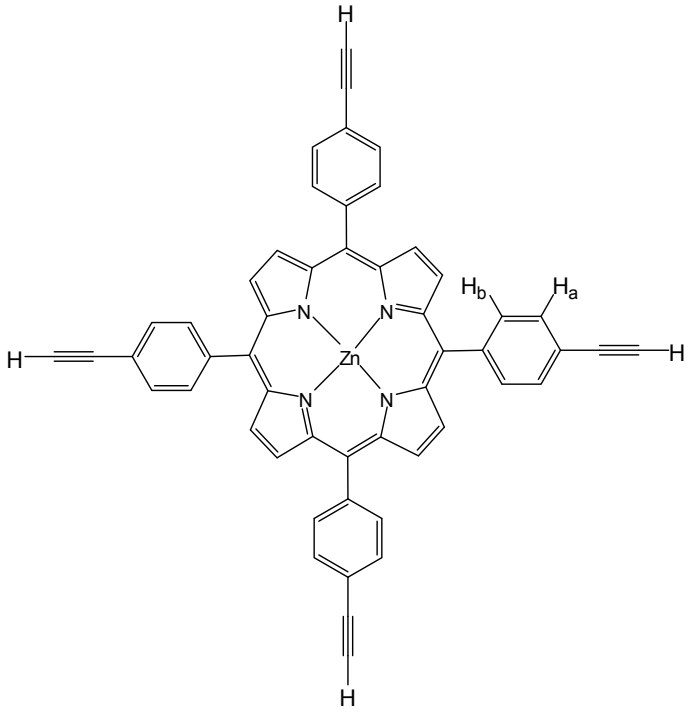

To a solution of free porphyrin **29** (109 mg, 0.15 mmol) in CH_2Cl_2 (37 mL) was added $Zn(OAc).2H_2O$ (164 mg, 0.75 mmol) in MeOH (12 mL). The reaction mixture was stirred overnight at room temperature. The reaction mixture was concentrated to dryness, extracted with CH_2Cl_2, washed with a solution of $NaHCO_3$, dried ($MgSO_4$), filtered and concentrated to dryness, affording 110 mg (95%) of the desired porphyrin **30**.

^{1}H NMR (200 MHz, $CDCl_3$, δ in ppm) : 8.98 (s, 8H, $H_{\beta\text{-pyrrolic}}$), 8.20 (d, 8H, H_b), 7.96 (d, 8H, H_a), 3.36 (s, 4H, C_{alkyne}-H).

FT-IR (υ, KBr, cm^{-1}) : 2105 (C≡C), 3260 (≡C-H)

UV-vis (λ max, CH_2Cl_2, nm) : 425, 552, 594.

C.V. (CH_2Cl_2, 0.1 M $[Bu_4N][PF_6]$, 20°C, 0.1 $V.s^{-1}$) E° in V vs. SCE : 0.87 (E^1_{Ox}), 1.14 (E^2_{Ox}).

Synthesis of zinc(II)-5,10,15,20-tetra{trans-(4-phenylethynyl)[ruthenium(II)bis(bis(1,2-(diphenylphosphino)ethane)](chloride)} : 31 and the corresponding salt 31'

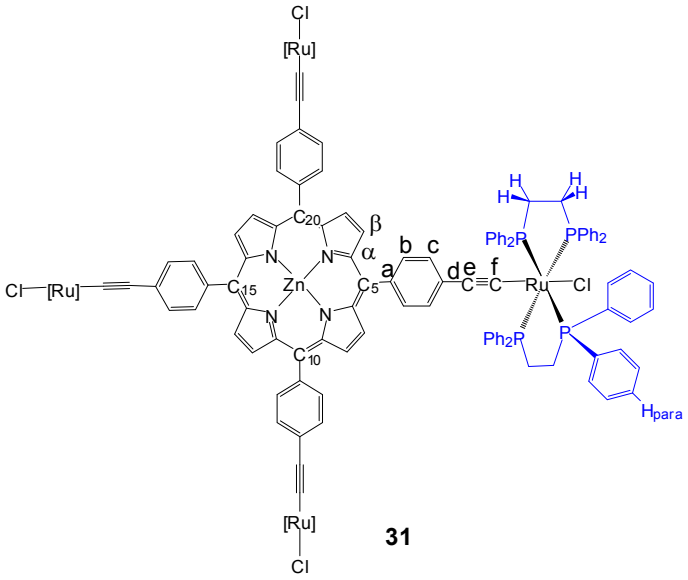

31

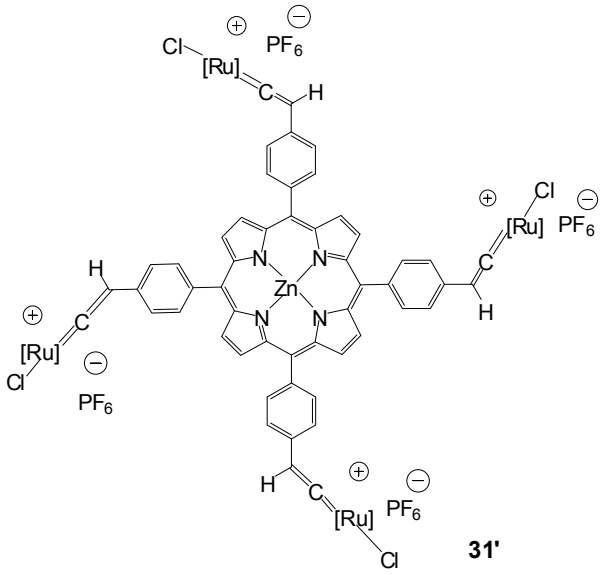

31'

$NaPF_6$ (95 mg, 0.57 mmol) was added to a solution of **30** (100 mg, 0.13 mmol) and *cis*-$[RuCl_2(dppe)_2]$ (551 mg, 0.57 mmol) in distilled CH_2Cl_2 (100 mL). This mixture was stirred at room temperature for 12 hours. The solution was filtered, and then precipitated in ether and the vinylidene form **31'** was isolated. The resulting precipitate was dissolved in CH_2Cl_2 and NEt_3 was added (1 mL). The solution was stirred for 10 minutes. The solution was concentrated and precipitated in hexane. The obtained residue was washed with MeOH (2×10 mL), to afford **31** as a green product (424 mg, 0.094 mmol). Yield : 73%.

^{1}H NMR (500 MHz, $CDCl_3$, δ in ppm) : 9.22 (s, 8H, $H_{\beta\text{-pyrrolic}}$), 8.05 (d, 8H, $^3J_{H,H}$ = 8.2 Hz, H_b), 7.79 (m, 32H, $H_{para/Ar/dppe}$), 7.40-7.03 (m, 128H, $H_{ortho\text{-}meta/Ar/dppe}$), 7.13 (d, 8H, $^3J_{H,H}$ = 8.2 Hz, H_c), 2.85 (m, 32H, $CH_{2/dppe}$).

^{13}C NMR (125 MHz, $CDCl_3$, δ in ppm) : 151.1 (s, $C_{\alpha\text{-pyrrolic}}$), 138.0 (s, $C_{Ar}[C_a]$), 137.6 and 136.3 (m, $C_{ipso/dppe}$), 135.3 and 135.2 (s, $CH_{Ar/dppe}$), 134.9 (s, $CH_{Ar}[C_b]$), 132.6 (s, $C_{\beta\text{-pyrrolic}}$), 130.2 (s, $C_{Ar}[C_d]$), 129.7 and 129.5 (s, $CH_{Ar/dppe}$), 128.9 (s, $CH_{Ar}[C_c]$), 128.1 and 127.7 (s, $CH_{Ar/dppe}$), 122.6 (s, C_{meso}), 114.8 (s, RuC≡C[C_f]), 31.7 (m, $CH_{2/dppe}$), 1RuC≡C[C_f] not observed, possibly overlapped.

^{31}P NMR (81 MHz, $CDCl_3$, δ in ppm) : 51.0 (s, 16P, $(dppe)_2Ru$).

Anal. calc. for $C_{260}H_{216}Cl_4N_4P_{16}Ru_4Zn.CHCl_3$: C, 67.81; H, 4.73; N, 1.21; found : C, 67.84; H, 4.77; N 1.32.

FT-IR (υ, KBr, cm^{-1}) : 2057 (vs, RuC≡C).

HRMS-ESI (m/z) : calcd for $[C_{260}H_{216}Cl_4N_4P_{16}Ru_4Zn]^{2+}$: 2251.8556, found : 2251.8359.

Synthesis of zinc(II)-5,10,15,20-tetra{trans-(4-phenylethynyl)[ruthenium(II)bis(bis(1,2-diphenylphosphino)ethane)](4-nitrophenylethynyl)} : 32-NO_2

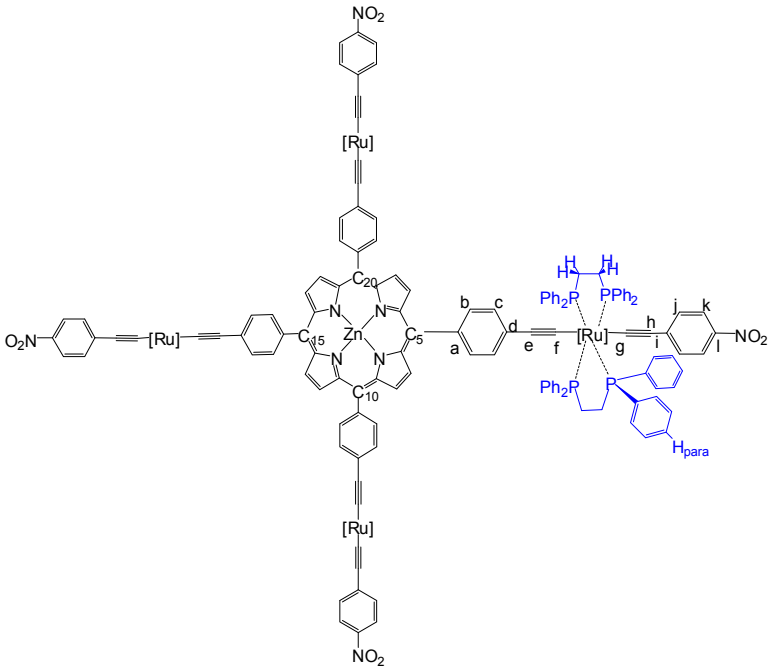

$NaPF_6$ (18 mg, 0.11 mmol) and NEt_3 (0.5 mL) were added to a solution of **31** (70 mg, 0.015 mmol) and 1-ethynyl-4-nitrobenzene (10 mg, 0.060mmol) in distilled CH_2Cl_2 (10 mL). The mixture was then refluxed for 72 h. Then, the reaction mixture was filtered, and precipitated in hexane. The residue was then washed with MeOH (2×10 mL) to afford **32-NO_2** as a green product (63 mg) as 85% yield.

^{1}H NMR (500 MHz, $CDCl_3$, δ in ppm) : 9.23 (s, 8H, $H_{β\text{-pyrrolic}}$), 8.13 (d, 8H, $^3J_{HH}$ = 7.6 Hz, H_b), 8.03 (d, 8H, $^3J_{H,H}$ = 8.5 Hz, H_k), 7.89 (m, 32H, $H_{para/Ar/dppe}$), 7.42 (m, 32H, $H_{Ar/dppe}$), 7.40-6.90 (m, 96H, $H_{Ar/dppe}$), 7.31 (d, 8H, $^3J_{H,H}$ = 8.1 Hz, H_c), 6.62 (d, 8H, $^3J_{H,H}$ = 8.4 Hz, H_j), 2.80 (m, 32H, $CH_{2/dppe}$).
^{13}C NMR (125 MHz, $CDCl_3$, δ in ppm): 150.9 (s, $C_{α\text{-pyrrolic}}$), 143.1 (s, $C_{Ar}[C_l]$), 138.4 (s, $C_{Ar}[C_a]$), 138.1 (s, $C_{Ar}[C_i]$), 137.5, 137.1 (m, $C_{ipso/dppe}$), 135.0 and 134.4 (s, $CH_{Ar/dppe}$), 134.8 (s, $C_{Ar}[C_i]$), 132.6 (s, $C_{β\text{-pyrrolic}}$), 130.4 (s, $CH_{Ar}[C_j]$), 129.9 (s, $C_{Ar}[C_d]$), 129.6 and 129.5 (s, $CH_{Ar/dppe}$), 128.5 (s, $CH_{Ar}[C_c]$), 127.9 and 127.7 (s, $CH_{Ar/dppe}$), 123.9 (s, $CH_{Ar}[C_k]$), 122.3 (s, C_{meso}), 119.4 and 119.0 (s, RuC≡C[$C_{e/h}$]), 32.0 (m, $CH_{2/dppe}$); 2RuC≡C[$C_{f/g}$] not observed, possibly overlapped.
^{31}P NMR (81 MHz, $CDCl_3$, δ in ppm) : 54.7 (s, 16P, $(dppe)_2Ru$).

Anal. calc. for $C_{292}H_{232}N_8O_8P_{16}Ru_4Zn.2CHCl_3$: C, 68.10; H, 4.55; N, 2.16; found : C, 68.47; H, 4.56; 2.25.
FT-IR (υ, KBr, cm^{-1}) : 2042 (RuC≡C).

Synthesis of zinc(II)-5,10,15,20-tetra{trans-(4-phenylethynyl)[ruthenium(II)bis(bis(1,2-diphenylphosphino)ethane)](phenylethynyl)} : <u>32-H</u>

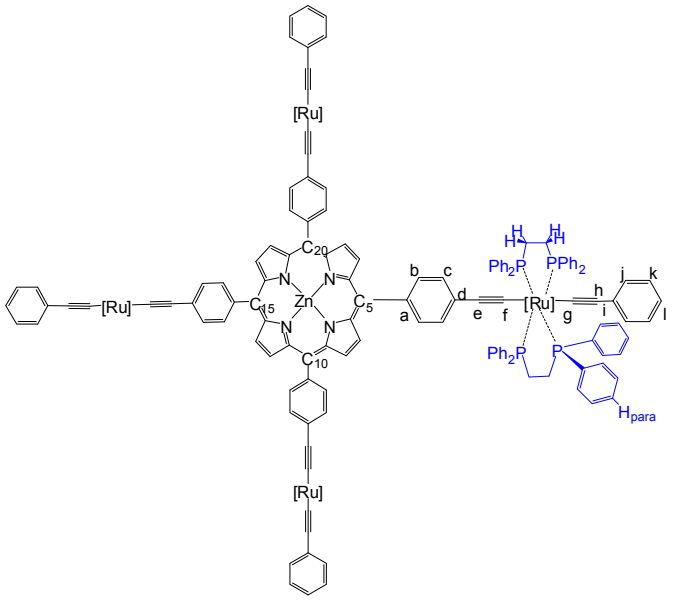

$NaPF_6$ (35 mg, 0.21 mmol) and NEt_3 (0.5 mL) were added to a solution of **31** (60 mg, 0.013 mmol) and phenylacetylene (9 µL, 0.08 mmol) in distilled CH_2Cl_2 (10 mL). The mixture was refluxed for 72 h. Then, the reaction mixture was filtered, and precipitated in hexane. The residue obtained was washed with MeOH (2×10 mL) to afford **32-H** as a green product (50 mg) as 79% yield.

^{1}H NMR (500 MHz, $CDCl_3$, δ in ppm) : 9.22 (s, 8H, $H_{\beta\text{-pyrrolic}}$), 8.12 (d, 8H, $^3J_{HH}$ = 8.1 Hz, H_b), 7.84 (m, 8H, $H_{Ar/dppe}$), 7.75 (m, 32H, $H_{para/Ar/dppe}$), 7.62 (m, 32H, $H_{Ar/dppe}$), 7.55-6.90 (m, 88H, $H_{Ar/dppe}$), 7.32 (t, 4H, $^3J_{H,H}$ = 7.3 Hz, H_l), 7.19 (d, 8H, $^3J_{H,H}$ = 7.3 Hz, H_c), 7.17 (d, 8H, $^3J_{H,H}$ = 7.2 Hz, H_k), 6.82 (d, 8H, $^3J_{H,H}$ = 7.1 Hz, H_j), 2.80 (m, 32H, $CH_{2/dppe}$).

^{13}C NMR (125 MHz, $CDCl_3$, δ in ppm) : 151.1 (s, $C_{\alpha\text{-pyrrolic}}$), 137.9 (m, $C_{ipso/dppe}$), 135.2 and 135.1 (s, $CH_{Ar/dppe}$+$CH_{Ar}[C_b]$), 132.6 (s, $C_{\beta\text{-pyrrolic}}$), 131.4 (s, $C_{Ar}[C_a]$), 130.7 (s, $CH_{Ar}[C_j]$), 130.4 ($C_{Ar}[C_d]$), 129.5 & 129.3 (s, $CH_{Ar/dppe}$ + $CH_{Ar}[C_c]$), 128.9 (s, $C_{Ar}[C_i]$), 128.1 (s, $CH_{Ar}[C_k]$), 127.9 and 127.8 (s, $CH_{Ar/dppe}$), 123.6 (C_l, $CH_{Ar}[C_l]$), 122.6 (s, C_{meso}), 117.6 and 117.5 (s, RuC≡C[$C_{e/h}$]), 32.3 (m, $CH_{2/dppe}$); 2RuC≡C[$C_{f/g}$] not observed, possibly overlapped.

^{31}P NMR (81 MHz, $CDCl_3$, δ in ppm) : 55.2 (s, 16P, $(dppe)_2Ru$).

Anal. calc. for $C_{292}H_{236}N_4P_{16}Ru_4Zn.2CHCl_3$: C, 70.55; H, 4.79; N, 1.12; found : C, 70.83; H, 5.04; N, 1.33.

FT-IR(υ, KBr, cm^{-1}) : 2056 (RuC≡C).

Synthesis of zinc(II)-5,10,15,20-tetra{trans-(4-phenylethynyl)[ruthenium(II)bis(bis(1,2-diphenylphosphino)ethane)](4-methoxyphenylethynyl)} : <u>32-OMe</u>

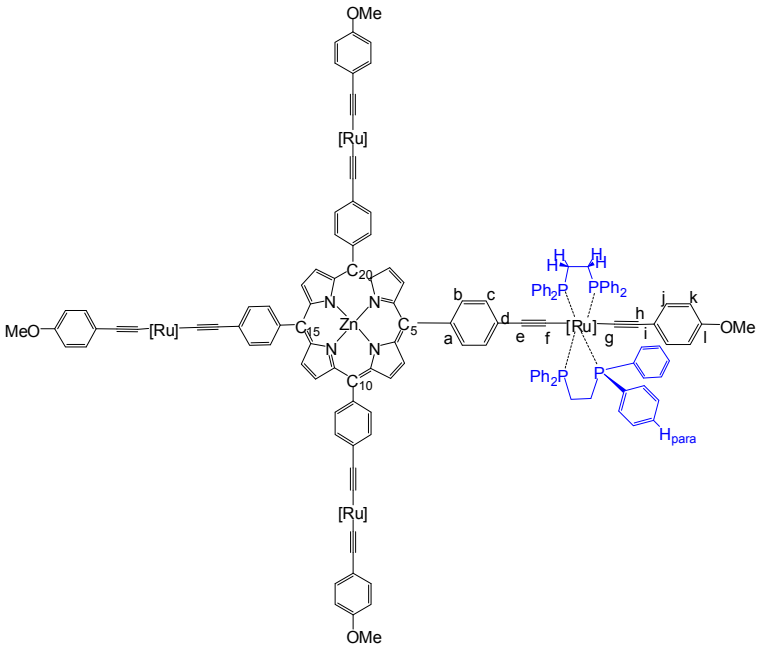

$NaPF_6$ (24 mg, 0.13 mmol) and NEt_3 (0.5 mL) were added to a solution of **31** (70 mg, 0.015 mmol) and 1-ethynyl-4-methoxybenzene (12 mg, 0.094 mmol) in CH_2Cl_2 (10 mL). The mixture was heated at reflux for 72 h and the reaction mixture was filtered. The compound was then precipitated in hexane and washed with MeOH (2×10 mL) to afford **32-OMe** as a green product (60 mg). Yield : 78%.

^{1}H NMR (500 MHz, $CDCl_3$, δ in ppm) : 9.23 (s, 8H, $H_{\beta\text{-pyrrolic}}$), 8.09 (d, 8H, $^3J_{H,H}$ = 8.1 Hz, H_b), 7.84 (m, 8H, $H_{Ar/dppe}$), 7.75 (m, 32H, $H_{Ar/dppe}$), 7.64 (m, 32H, $H_{Ar/dppe}$), 7.60-6.95 (m, 88H, $H_{Ar/dppe}$), 7.19 (d, 8H, $^3J_{H,H}$ = 7.6 Hz, H_c), 6.78 (m, 16H, H_{j+k}), 3.86 (s, 12H, OCH_3), 2.79 (m, 32H, $CH_{2/dppe}$).
^{13}C NMR(125 MHz, $CDCl_3$, δ in ppm) : 156.3(s, $C_{Ar}[C_l]$), 150.9 ($C_{\alpha\text{-pyrrolic}}$), 137.9 (m, $C_{ipso/dppe}$), 135.0 and 134.9 (s, $CH_{Ar/dppe}$), 134.7 (s, $CH_{Ar}[C_b]$), 132.4 (s, $C_{\beta\text{-pyrrolic}}$), 131.4 (s, $CH_{Ar}[C_j]$), 130.3 (s, $C_{Ar}[C_d]$), 129.2 and 129.1 (s, $CH_{Ar/dppe}$), 128.6 (s, $CH_{Ar}[C_c]$), 127.7 and 127.5 (s, $CH_{Ar/dppe}$), 124.3 (s, $C_{Ar}[C_i]$), 122.4 (s, C_{meso}), 117.3 and 116.2 (s, RuC≡C[$C_{e/h}$]), 113.6 (s, $CH_{Ar}[C_k]$), 55.7 (s, OCH_3), 32.1 (m, $CH_{2/dppe}$); 2 RuC≡C[$C_{f/g}$] and C_a not observed, possibly overlapped.
^{31}P NMR (81 MHz, $CDCl_3$, δ in ppm) : 55.1 (s, 16P, $(dppe)_2Ru$).

Anal. calc. for$C_{296}H_{244}N_4O_4P_{16}Ru_4Zn.7CHCl_3$: C, 63.60; H, 4.42; N, 0.98; found : C, 63.98; H, 4.64; N 1.31.
FT-IR (υ, KBr, cm^{-1}) : 2056 (RuC≡C).

Synthesis of 4-bromo(trimethylsilyl)ethynylbenzene : 39

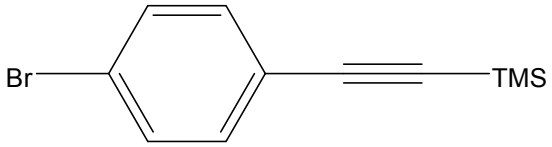

Trimethylsilylacetylene (1.086 mL, 7.64 mmol) was added to a solution of 4-bromoiodobenzene (2.23 g, 7.88 mmol), $PdCl_2(PPh_3)_2$ (10 mg, 0.014 mmol), and CuI (6 mg, 0.03 mmol) in degassed triethylamine (30 mL). The solution was stirred at 0˚C for three hours, and then filtered. The obtained filtrate was concentrated under reduced pressure, and then filtered over few cm of silica gel using hexane as an eluent to yield a colourless solid (1.87 g, 94%).

^{1}H NMR (δ, 300 MHz, $CDCl_3$) : 7.39 (d, 2H), 7.28 (d, 2H), 0.26 (s, 9H).

Synthesis of 4-iodo(trimethylsilyl)ethynylbenzene : 40

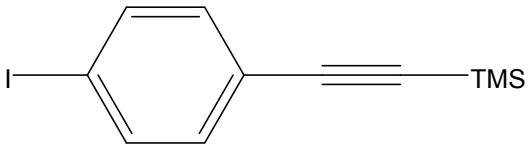

A solution of **39** (2.95 g, 11.6 mmol) in distilled ether (93 mL) under nitrogen, and cooled to – 78˚C by carbon ice and acetone. Then, n-BuLi (7.0 mL, 17.5 mmol) was added dropwise, and the reaction mixture was kept stirred at – 78˚C for 1 hour. A solution of I_2 (5.88 g, 23.2 mmol) in dry THF (20 mL) was slowly cannulated to the reaction mixture. The reaction mixture was allowed to warm at room temperature for one hour. A saturated solution of sodium thiosulfate (30 mL) was then added. The obtained mixture was extracted with DCM, dried over $MgSO_4$, filtered, and then taken to dryness. The obtained solid was purified by column chromatography on silica gel using hexane as an eluent to yield a colourless solid (2.00 g, 57%).

^{1}H NMR (δ, 300 MHz, $CDCl_3$) : 7.64 (d, 2H), 7.18 (d, 2H), 0.26 (s, 9H).

Synthesis of 4-((4-((trimethysilyl)ethynyl)phenyl)ethynyl)aniline : <u>41</u>

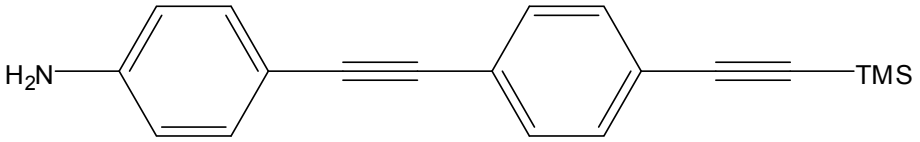

At O˚C, a solution of ((4-ethynyl phenyl)ethynyl)trimethylsilane (1.19 g, 6.03 mmol) in distilled THF (10 mL) was cannulated dropwise to a solution of 4- iodoaniline (1.10 g, 5.02 mmol), $PdCl_2(PPh_3)_2$ (0.09 g, 0.13 mmol), and CuI (0.05 g, 0.25 mmol) in distilled THF (25 mL) and diisopropylamine (25 mL) under nitrogen, and then heated at 60 ˚C overnight. The reaction mixture was evaporated under reduced pressure, extracted with ether, washed with water, dried over $MgSO_4$, and then taken into dryness. The obtained solid was purified by column chromatography of silica gel using hexane/DCM (3/2) as eluent to yield a white solid (1.20 g, 83%).

^{1}H NMR (δ, 300 MHz, $CDCl_3$) : 7.43 (s, 4H), 7.37 (d, 2H), 6.72 (d, 2H), 3.96 (s, 2H), 0.26 (s, 9H).

Synthesis of ((4-((4-iodophenyl)ethynyl)phenyl)trimethylsilane : <u>42</u>

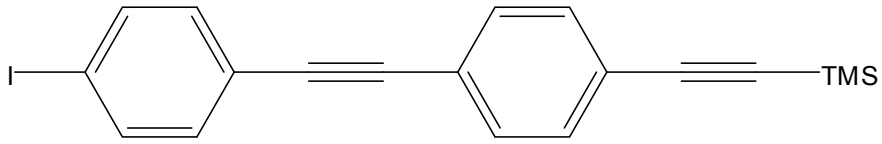

HCl (50 mL, 6M) was added to a round bottom flask that contains **41** (1.16 g, 4.01 mmol) at – 10 ˚C. A suspension was observed. A solution of $NaNO_2$ (0.29 g, 4.21 mmol) in H_2O (5 mL) was added dropwise, and the reaction mixture was stirred for 30 minutes at around -4 ˚C. A solution of KI (0.8 g, 4.81 mmol) in H_2O (10 mL) was added dropwise (color change to yellow then brown and production of nitrogen were noticed). Temperature must not exceed 0˚C. Then DCM (50 mL) was added, and the reaction heterogeneous mixture was kept to warm at room temperature overnight. The reaction mixture was transferred into a seperatory funnel, and the organic phase was washed with thiosulfate, dried over $MgSO_4$, and taken into dryness. The crude solid was purified by column chromatography on silica gel using hexane as an eluent. Three fractions that contain the desired product were crystallized in MeOH/$CHCl_3$ to yield a white pure solid (0.5 g, 31%).

^{1}H NMR (δ, 300 MHz, $CDCl_3$) : 7.64 (d, 2H), 7.44 (s, 4H), 7.18 (d, 2H), 0.26 (s, 9H).

Synthesis of 1,3,5-tris((trimethylsilyl)ethynyl)benzene : <u>43</u>

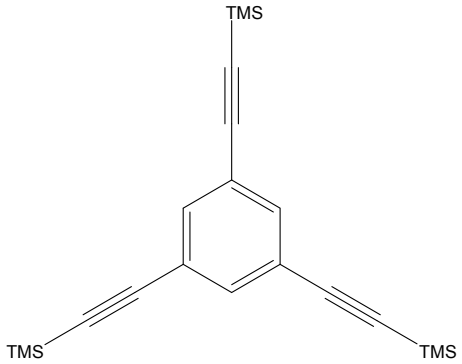

Trimethylsilylacetylene (6.7 mL, 47 mmol) was added to a solution of 1,3,5-tribromobenzene (1.50 g, 4.76 mmol), $PdCl_2(PPh_3)_2$ (0.16 g, 0.05 mmol), and CuI (0.09 g, 0.10 mmol) in dry THF (20 mL) and diisopropylamine (10 mL) under nitrogen, and the reaction mixture was heated at 60˚C for 48 hours. The reaction mixture was evaporated under reduced pressure. The residue was extracted in ether, washed with water, dried over $MgSO_4$, and then taken into dryness. The crude solid was then purified by column chromatography on silica gel using hexane as an eluent. The second afforded fraction was the desired product as a white solid (0.75 g, 44%).

^{1}H NMR (δ, 300 MHz, $CDCl_3$) : 7.56 (s, 3H), 0.26 (s, 27H).

Synthesis of 1,3,5-triethynylbenzene : <u>44</u>

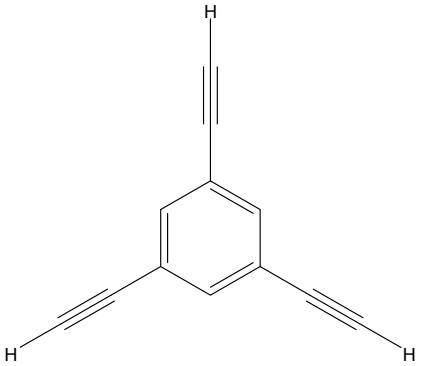

In a round bottom flask, a solution of 1,3,5-tris((trimethylsilyl)ethynyl)benzene (0.37 g, 1.02 mmol), and K_2CO_3 (0.63 g, 4.58 mmol) in DCM (25 mL) and MeOH (25 mL) was kept stirred at room temperature for six hours. The reaction mixture was evaporated under reduced pressure. The obtained solid was extracted with ether, washed with water, dried over $MgSO_4$, filtered, and taken into dryness. The crude solid was filtered over few cm column chromatograohy of silica gel using hexane as an eluent to yield a colourless solid (0.13 g, 84%).

^{1}H NMR (δ, 300 MHz, $CDCl_3$) : 7.57 (s, 3H), 3.11 (s, 3H).

Synthesis of the wedge precursor : 45

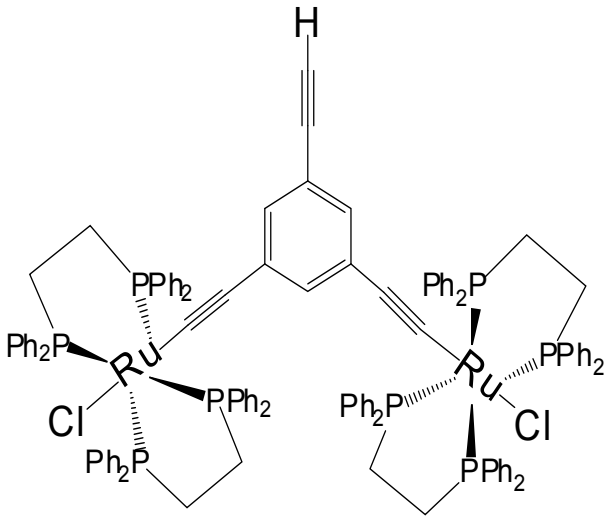

A solution of 1,3,5-triethynylbenzene (0.11 g, 0.72 mmol), and $[RuCl(dppe)_2]PF_6$ (1.88g, 1.75 mmol) in distilled DCM (95 mL) under nitrogen was kept at 40˚C overnight. The reaction mixture was cooled at room temperature, and filtered. The filtrate was concentrated under reduced pressure, and the vinylidene salt was precipitated in ether, and then filtered. The obtained silverish solid was dissolved in DCM with difficulty (low solubility in DCM) and triethylamine (4 mL) was added. The yellow solution was stirred for 10 minutes, concentrated under reduced pressure and filtered over a 10 cm basic alumina column using DCM and 2% NEt_3 as eluent. The yellow solution was concentrated under reduced pressure and then precipitated in hexane to yield a yellow solid (1.10 g, 78%).

^{1}H NMR (δ, 300 MHz, $CDCl_3$) : 6.80-7.70 (m, 80H), 6.55 (s, 1H), 6.41 (s, 2H), 3.01 (s, 1H), 2.68 (s, 16H).

^{31}P NMR (δ, 121 MHz, $CDCl_3$) : 50.5 (s).

Synthesis of the wedge 46

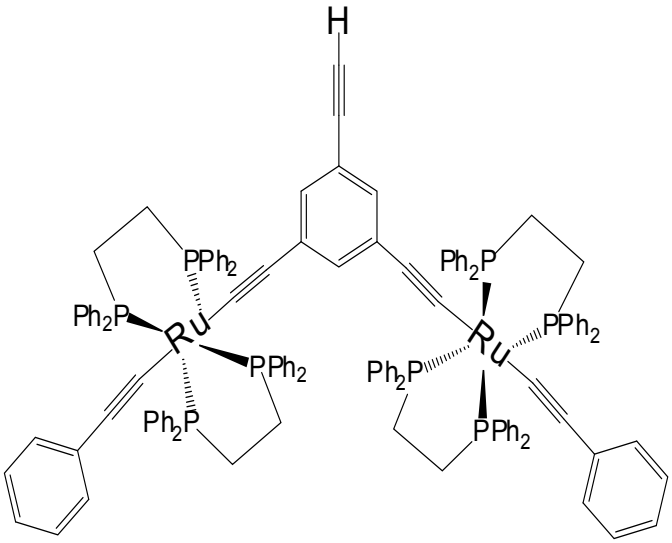

Ethynylbenzene (0.5 mL, 4.36 mmol), and triethylamine (5.5 mL) were added to a solution of **34** (1.10 g, 0.55 mmol) and $NaPF_6$ (0.73 g, 4.36 mmol) in distilled DCM (45 mL) under nitrogen. The reaction mixture was stirred at room temperature overnight.

The reaction was followed by **^{31}P NMR** and was stopped when only a peak at 54.5 ppm was observed. The reaction mixture was concentrated under reduced pressure and filtered over few cm of basic alumina using DCM and 2% NEt_3 as eluent. The yellow fraction was precipitated in hexane to yield a yellow solid (0.71 g, 71%).

^{1}H NMR (δ, 300 MHz, $CDCl_3$) : 6.80-7.70 (m, 90H), 6.55 (s, 1H), 6.41 (s, 2H), 3.02 (s, 1H), 2.64 (s, 16H).

^{31}P NMR (δ, 121 MHz, $CDCl_3$) : 54.5 (s).

Synthesis of the one phenyl extended wedge : 47

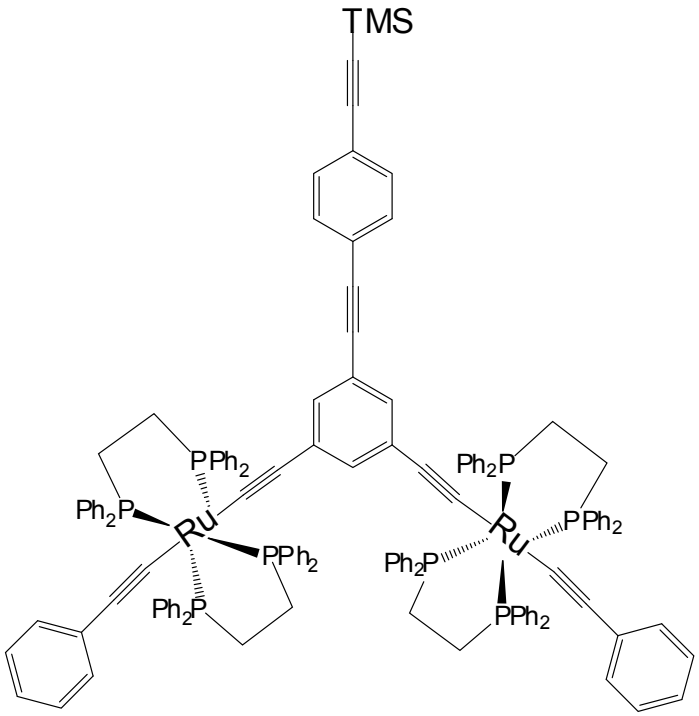

Small dendron **46** (0.10 g, 0.046 mmol) was added to a solution of **40** (0.021 g, 0.7 mmol), CuI (0.002 g, 0.011 mmol), and $Pd(PPh_3)_4$ (5 mg, 0.005 mmol) in a previously degassed mixture of DCM (10 mL) and NEt_3 (10 mL) under nitrogen. The reaction mixture was stirred at 40˚C overnight, concentrated under reduced pressure, and filtered over few centimeters of basic alumina using DCM and 2% NEt_3 as eluent. The yellow fraction was concentrated and precipitated in hexane to yield a yellow solid (0.067 g, 63%).

^{1}H NMR (δ, 300 MHz, $CDCl_3$) : 7.70-6.80 (m, 94H), 6.55 (s, 1H), 6.41 (s, 2H), 2.64 (s, 16H, $CH_{2/dppe}$), 0.26 (s, 9H, $Si(CH_3)_3$).

^{31}P NMR (δ, 121 MHz, $CDCl_3$) : 54.5 (s).

Synthesis of the one phenyl extended deprotected wedge : <u>48</u>

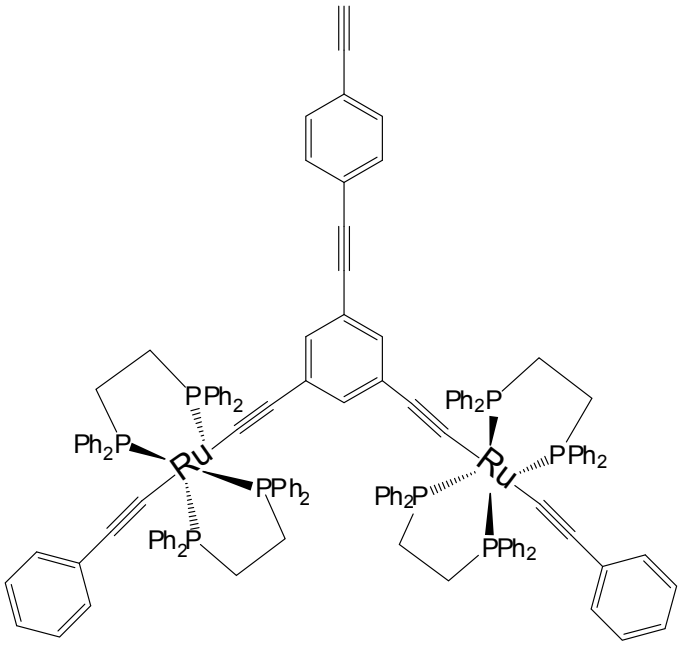

A solution of **47** (0.04 g, 0.017 mmol) and TBAF (0.4 mL) in distilled THF (5 mL) was prepared under nitrogen. The reaction mixture was stirred at room temperature for one hour, evaporated, and then filtered over basic alumina using DCM and 2% NEt_3 as eluent. The yellow fraction was concentrated and precipitated in hexane to yield a yellow solid (0.029 g, 75%)

^{1}H NMR (δ, 300 MHz, $CDCl_3$) : 7.70–6.80 (m, 98H), 6.55 (s, 1H), 6.41 (s, 2H), 3.19 (s, 1H, -C≡C-H), 2.64 (s, 16H, $CH_{2/dppe}$).

^{31}P NMR (δ, 121 MHz, $CDCl_3$) : 54.5 (s).

Synthesis of the two phenyl extended organometallic wedge : 49

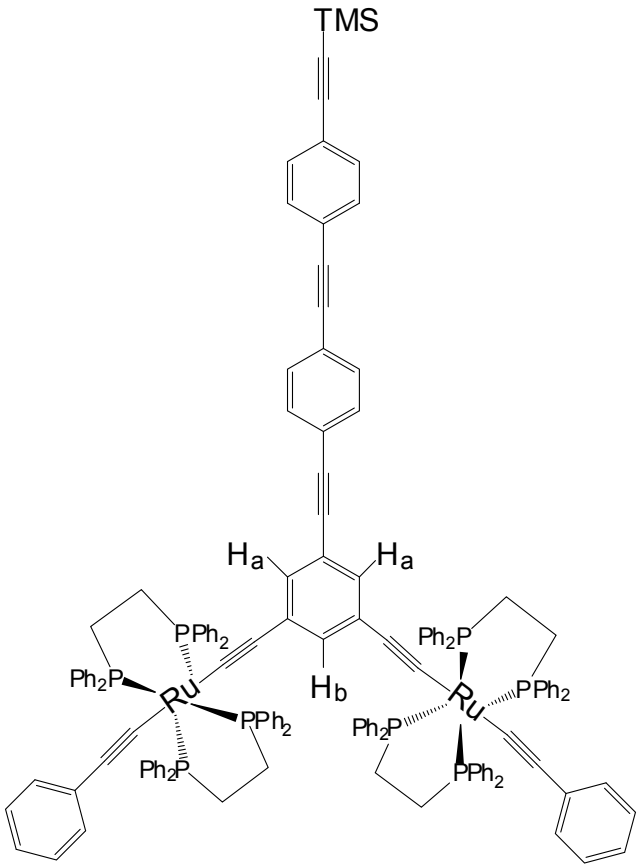

Dendron **46** (0.75 g, 0.35 mmol) was added to a solution of the two phenyl linker **42** (0.21 g, 0.52 mmol), CuI (0.01 g, 0.08 mmol), and $Pd(PPh_3)_4$ (0.04 g, 0.03 mmol) in a previously degassed mixture of DCM (60 mL), and NEt_3 (60 mL) under nitrogen. The reaction mixture was stirred at 40˚C overnight, concentrated under reduced pressure, and filtered over few centimeters of basic alumina using DCM and 2% NEt_3 as eluent. The yellow fraction was concentrated and precipitated in hexane to yield **49** as a yellow solid (0.69 g, 82%).

^{1}H NMR (δ, 300 MHz, $CDCl_3$) : 7.70-6.80 (m, 98H), 6.55 (s, 1H, H_b), 6.41 (s, 2H, H_a), 2.64 (s, 16H, $CH_{2/dppe}$), 0.26 (s, 9H, $Si(CH_3)_3$).

^{31}P NMR (δ, 121 MHz, $CDCl_3$) : 54.5 (s).

Synthesis of the deprotected two phenyl extended organometallic wedge : <u>50</u>

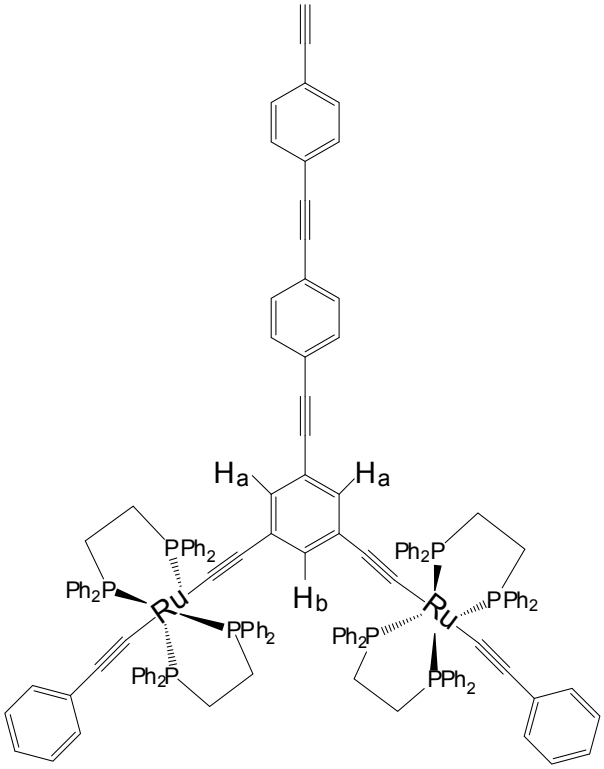

To a solution of **49** (0.25 g, 0.10 mmol) in distilled THF (30 mL) under nitrogen, TBAF (1.7 mL) was added, and the reaction mixture was stirred at room temperature for one hour. The reaction mixture was concentrated under reduced pressure, and filtered over a few centimeters of basic alumina using DCM and 2% NEt_3 as eluent. The yellow fraction was concentrated and precipitated in hexane to yield deprotected **50** as a yellow solid (0.19 g, 81%).

^{1}H NMR (δ, 300 MHz, $CDCl_3$) : 7.70-6.80 (m, 98H), 6.55 (s, 1H, H_b), 6.41 (s, 2H, H_a), 3.19 (s, 1H, -C≡C-H), 2.64 (s, 16H, $CH_{2/dppe}$).

^{31}P NMR (δ, 121 MHz, $CDCl_3$) : 54.5 (s).

Synthesis trial of small ruthenium alkynyl porphyrin dendrimer : <u>51</u>

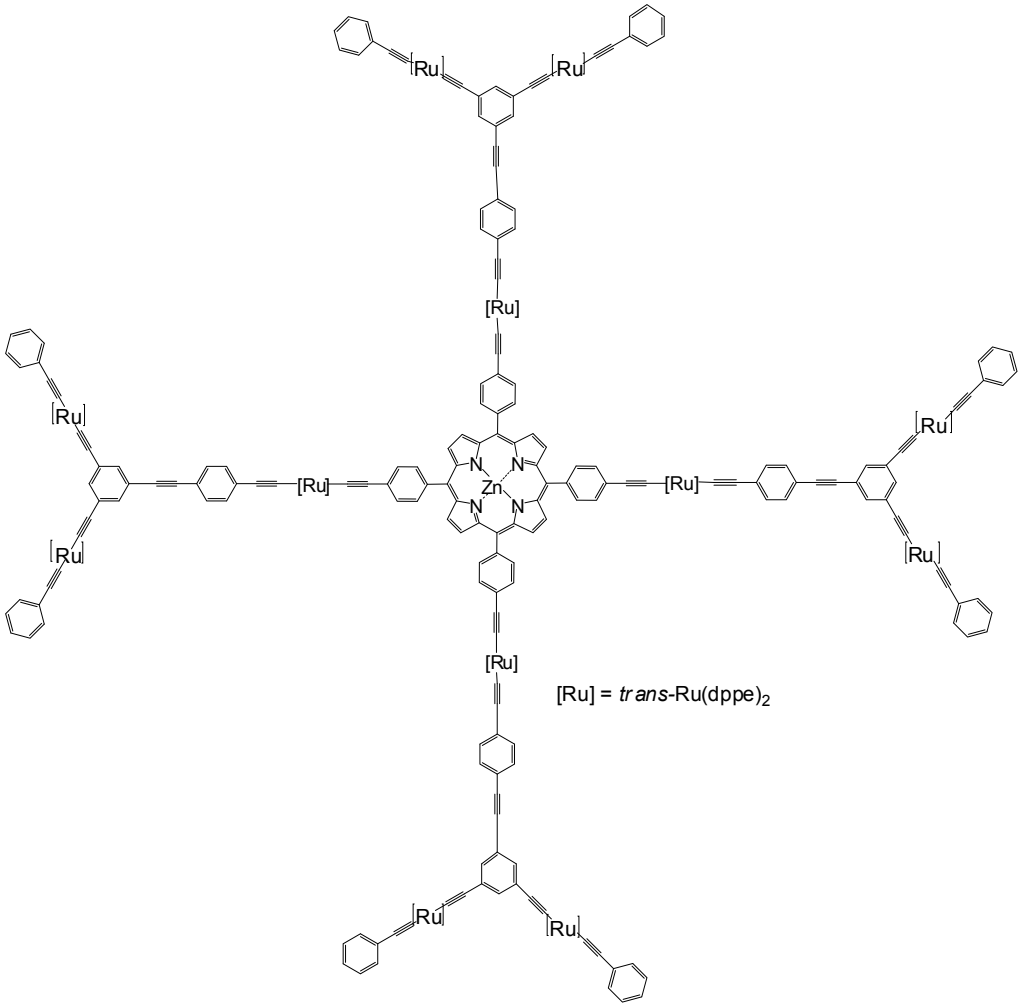

Triethylamine (0.02 mL) was added to a solution of zinc tetraruthenium vinylidene complex (**31'**) (21 mg, $4x10^{-3}$ mmol), four equivalents of wedge **48** (0.04 g, 0.017 mmol), and $NaPF_6$ (0.011 g, 0.066 mmol) in distilled DCM (10 mL) under nitrogen at room temperature. The reaction was monitored by **^{31}P NMR**, and after 48 hours the **^{31}P NMR** showed the peaks of the starting materials indicating that no reaction took place. Then, temperature was raised up to 40°C and after 48 hours same results were observed. Finally temperature was brought to 70°C and unfortunately after 48 hours, no evolution was noticed.

The reaction was repeated under the same scale, same conditions trying different solvents (THF….) varying temperatures but no reaction took place.

Synthesis trial of extended ruthenium alkynyl porphyrin dendrimer : <u>52</u>

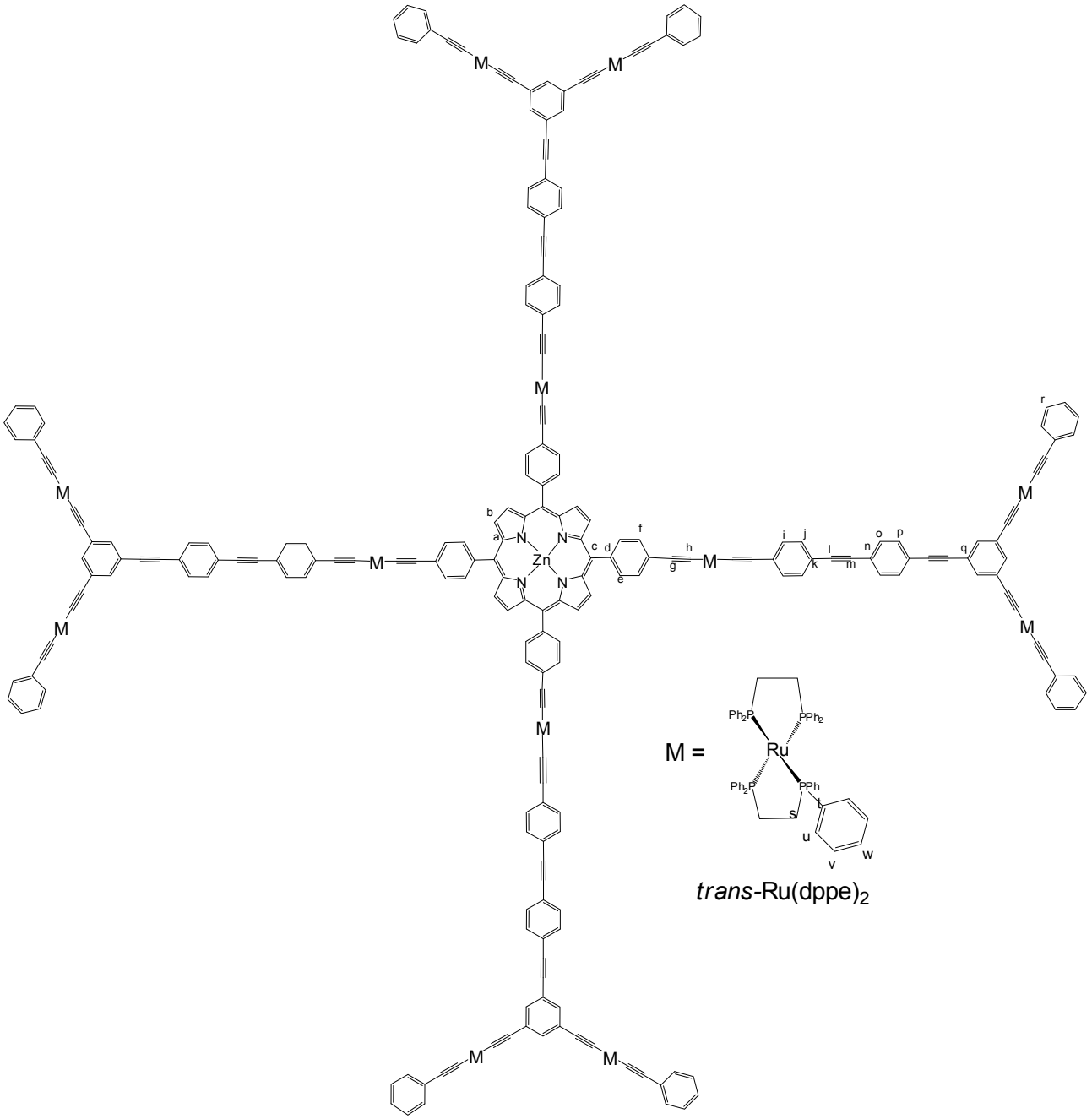

Triethylamine (0.05 mL) was added to a solution of zinc tetraruthenium vinylidene complex **31'** (0.06 g, 0.01 mmol), four equivalents of previously prepared dendron **42** (0.11 g, 0.047 mmol) and $NaPF_6$ (0.03 g, 0.18 mmol) in distilled DCM (12 mL) under nitrogen.

The reaction was followed by **^{31}P NMR**, and it was complete after 48 hours at room temperature. The reaction mixture was filtered, concentrated under reduced pressure, and the desired product was precipitated in hexane to yield a green solid (0.09 g) yield : 60%.

^{1}H NMR (300 MHz, $CDCl_3$, δ in ppm) : 9.20 (s, 8H, $H_{\beta\text{-pyrrolic}}$), 8.05 (d, 8H, H_e $^{3}J_{H,H}$ = 8.2 Hz, H_b), 7.70-6.50 (m, 572H, $H_{Ar/dppe}$), 2.70 (s, 96H, $CH_{2/dppe}$).

^{13}C NMR (125 MHz, $CDCl_3$, δ in ppm) : 150.3 (C_a), 137.1 (C_d), 137.0 (C_t), 136.9 (C_p), 134.2 (C_h), 134.1 ($C_{u,e}$), 133.0 (C_o), 132.0 (C_j), 131.3 (C_b), 131.0 (C_i), 130.0 (C_r), 128.6 ($C_{f,w}$), 127.1 (C_v), 123.0 (C_n), 122.8 (C_k), 122.4 (C_c), 122.0 (C_q), 116.0 (C_g), 89.7 (C_m), 89.5 (C_l), 31.7 (C_s).

^{31}P NMR (δ, 121MHz, $CDCl_3$) : 54.6 (s, 32P, $(dppe)_2Ru_{wedge}$), 54.3 (s, 16P, $(dppe)_2Ru_{porphyrin}$).

UV-vis (λ max, (ε, 10^{-3} $M^{-1}.cm^{-1}$), CH_2Cl_2, nm) : 336 (367), 420 (543), 564 (9.2), 613 (17.6).

Anal. : calc. for $C_{852}H_{684}N_4P_{48}Ru_{12}Zn$: C, 74.46; H, 5.02; N, 0.41; found : C, 74.35; H, 5.18; N, 0.42

FT-IR (n, KBr, cm^{-1}) : 2050 (RuC≡ C).

C.V. (CH_2Cl_2, 0.1 M $[Bu_4N][PF_6]$, 20°C, 0.1 $V.s^{-1}$) **E° in V vs. SCE** : 0.45 (wedge : 8Ru(III)/Ru(II)); 0.53 (porphyrin : 4Ru(III)/Ru(II)), 0.91 (E^1_{Ox}), 1.15 (E^2_{Ox}).

Synthesis of the iron organometallic porphyrin : 53

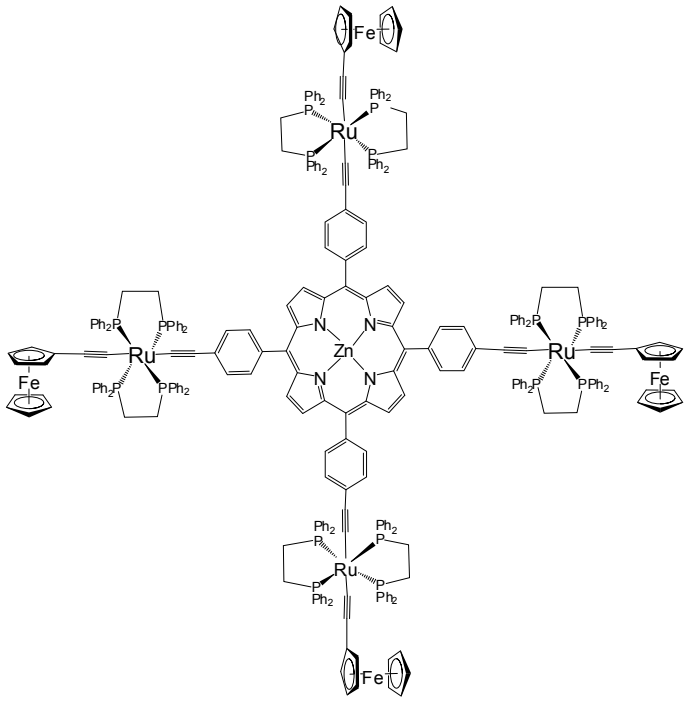

Triethylamine (0.15 mL) was added to a solution of porphyrin precursor **31** (0.12 g, 0.03 mmol), ethynyl ferrocene (0.03 g, 0.16 mmol), and $NaPF_6$ (0.07 g, 0.25 mmol) in distilled DCM (12 mL) under nitrogen. The reaction was followed by ^{31}P NMR, and it was judged that it was complete after 48 hours at room temperature. The reaction mixture was filtered, concentrated under reduced pressure, and the desired product was precipitated in hexane to yield a green solid (0.09 g, 70%).

^{1}H NMR (δ, 300 MHz, C_6D_6) : 2.70 (s, 32H), 4.25 (m, 36H), 7.06-7.80 (m, 168H), 8.39 (d, 8H), 9.41 (s, 8H).

^{31}P NMR (δ, 121MHz, C_6D_6) : 54.5 (s).

Analysis: calculated for $C_{308}H_{252}Fe_4N_4P_{16}Ru_4Zn$: C, 71.17; H, 4.89; N, 1.08; found : C, 70.89; H, 4.93; N: 1.31

UV-vis (λ max, (ε, 10^{-3} $M^{-1}.cm^{-1}$), CH_2Cl_2, nm) : 332 (135), 422 (371), 565 (33.6), 613 (40.6).

FT-IR (n, KBr, cm^{-1}) : 2055 (RuC≡ C)

References :

1. Kirtman, B.; Champagne, B. *Int. Rev. Phys. Chem* **1997**, *16*, 389.
2. Nalwa, H. S. *Appl. Organomet. Chem* **1991**, *5*, 349.
3. Ledoux-Rak, I. *L'onde électromagnétique* **1994**, *74*, 5.
4. Long, N. J. *Angew. Chem. Int. Ed.* **1995**, *34*, 21.
5. Whittall, I. R.; McDonagh, A. M.; Humphrey, M. G.; Samoc, M. *Adv. Organomet. Chem.* **1998**, *42*, 291.
6. Goeppert-Mayer, M. *Ann. Phys.* **1931**, *9*, 273.
7. Kaiser, W.; Garrett, C. G. B. **1961**, *7*, 229.
8. Abella, I. D. *Phys. Rev. Letters* **1962**, *9*, 453.
9. Sutherland, R. L. *"Handbook of Nonlinear Optics", Marcel Dekker: New York* **1996**.
10. Butcher, P. N.; Cotter, D. *in "The Elements of Nonlinear Optics", Cambridge Univ. Press: New York* **1990**.
11. Mongin, O.; Porrès, L.; Charlot, M.; Katan, C.; Blanchard-Desce, M. *Chem. Eur. J.* **2007**, *13*, 1481.
12. He, G. S.; Bhawalkar, J. D.; Zhao, C. F.; Park, C. K.; Prasad, P. N. *Opt. Lett.* **1995**, *20*, 2393.
13. Parthenopoulos, D. A.; Rentzepis, P. M. *Science* **1989**, *245*, 843.
14. Kawata, S.; Sun, H. B.; Tanaka, T.; Takada, K. *Nature* **2001**, *412*, 697.
15. Mendonca, C. R.; Correa, D. S.; Marlow, F.; Voss T.; Tayalia, P.; Mazur, E. *Appl. Phys. Lett.* **2009**, *95*, 113309.
16. Doughetry, T. J.; Marcus, S. L. *Eur. J. Cancer* **1992**, *28*, 1734.
17. Powell, C. E.; Hurst, S. K.; Morall, J. P.; Cifuentes, M. P.; Roberts, R. L.; Samoc, M.; Humphrey, M. G. *Organometallics* **2007**, *26*, 4456.
18. Morrall, J. P.; Dalton, G. T.; Humphrey, M. G.; Samoc, M. *Adv. Organomet. Chem.* **2008**, *55*, 61.
19. Green, K. A.; Cifuentes, M. P.; Samoc, M.; Humphrey, M. G. *Coord. Chem. Rev.* **2011**, *255*, 2530.
20. Humphrey, M. G.; Cifuentes, M. P.; Samoc, M. *Top. Organomet. Chem.* **2011**, *28*, 57.
21. Pawlicki, M.; Collins, H. A.; Denning, R. G.; Anderson, H. L. *Angew. Chem. Int. Ed. Engl.* **2009**, *48*, 3244.
22. De la Torre, G.; Vazquez, P.; Agullo-Lopez, F.; Torres, T. *Chem. Rev.* **2004**, *104*, 3723.
23. Rao, S. V.; Srinivas, N. K. M. N.; Rao, D. N.; Giribabu, L.; Maiya, B. G.; Philip, R.; Kumar, G. R. *Optics Commun.,* **2000**, *182*, 255.

24. Rao, D. V. G. L. N.; Aranda, F. J.; Roach, J. F.; Remy, D. E. *Appl. Phys. Lett.* **1991**, *58*, 1241.
25. Gauthier, N.; Argouarch, G.; Paul, F.; Toupet, L.; Ladjarafi, A.; Costuas, K.; Halet, J.-F.; Samoc, M.; Cifuentes, M. P.; Corkery, T. C.; Humphrey, M. G. *Chem. Eur. J.* **2011**, *17*, 5561.
26. Paul-Roth, C. O.; Rault-Berthelot, J.; Letessier, J.; Simonneaux, G.; Bergamini, J.-F. *J. Electroanal. Chem.* **2007**, *606*, 103.
27. Paul-Roth, C. O.; Simonneaux, G. *Tetrahedron Lett.* **2006**, *47*, 3275.
28. Bellows, D.; Ali, S. M.; Gros, C. P.; Ojaimi, M. E.; Barbe, J.-M.; Guillard, R.; Harvey, P. D. *Inorg. Chem.* **2009**, *48*, 7613.
29. Onitsuka, K.; Kitajima, H.; Fujimoto, M.; Iuchi, A.; Takei, F.; Takahashi, S. *Chem. Commun.* **2002**, 2576.
30. Gauthier, N.; Olivier, C.; Rigaut, S.; Touchard, D.; Roisnel, T.; Humphrey, M. G.; Paul, F. *Organometallics* **2008**, *27*, 1063.
31. Hurst, S. K.; Cifuentes, M. P.; Humphrey, M. G. *Organometallics* **2002**, *21*, 2353.
32. Fox, M. A.; Harris, J. E.; Heider, S.; Pérez-Gregorio, V.; Zakrzewska, M. E.; Farmer, J. D.; Yufit, D. S.; Howard, J. A. K.; Low, P. J. *J. Organomet. Chem.* **2009**, *694*, 2350.
33. Lindsey, J. S.; Hsu, H. C.; Schreiman, I. C. *Tetrahedron Lett.* **1986**, *27*, 4969.
34. Bonnet, J. J.; Eaton, S. S.; Eaton, G. R.; Holm, R. H.; Ibers, J. A. *J. Am. Chem. Soc.* **1973**, *95*, 2141.
35. Chaudret, B.; Commenges, G.; Poilblanc, R. *J. Chem. Soc. Dalton Trans.* **1984**, *1635*.
36. Touchard, D.; Haquette, P.; Guesmi, S.; Le Pichon, L.; Daridor, A.; Toupet, L.; Dixneuf, P. H. *Organometallics* **1997**, *16*, 3640.
37. Drouet, S.; Merhi, A.; Grelaud, G.; Cifuentes, M.; Humphrey, M.; Matczyszyn, K.; Samoc, M.; Toupet, L.; Paul-Roth, C. O.; Paul, F. *New J. Chem* **2012**, *36*, 2192.
38. Gauthier, N.; Tchouar, N.; Justaud, F.; Argouarch, G.; Cifuentes, M. P.; Toupet, L.; Touchard, D.; Halet, J.-F.; Rigaut, S.; Humphrey, M. G.; Costuas, K.; Paul, F. *Organometallics* **2009**, *28*, 2253.
39. Green, K. A.; Cifuentes, M. P.; Corkery, T. C.; Samoc, M.; Humphrey, M. G. *Angew. Chem. Int. Ed.* **2009**, *48*, 7867.
40. McDonagh, A. M.; Powell, C. E.; Morrall, J. P.; Cifuentes, M. P.; Humphrey, M. G. *Organometallics* **2003**, *22*, 1402.
41. Paul, F.; Mevellec, J.-Y.; Lapinte, C. *J. Chem. Soc., Dalton trans* **2002**, 1783.

42. Powell, C. E.; Cifuentes, M. P.; Morrall, J. P.; Stranger, R.; Humphrey, M. G.; Samoc, M.; Luther-Davies, B.; Heath, G. A. *J. Am. Chem. Soc.* **2003**, *125*, 602.
43. Rault-Berthelot, J.; Paul-Roth, C.; Poriel, C.; Juillard, S.; Ballut, S.; Drouet, S.; Simonneaux, G. *J. Electroanal. Chem.* **2008**, *623*, 204.
44. Paul-Roth, C.; Rault-Berthelot, J.; Simonneaux, G.; Poriel, C.; Abdalilah, M.; Letessier, J. *J. Electroanal. Chem.* **2006**, *597*, 19.
45. Paul, F.; Ellis, B. J.; Bruce, M. I.; Toupet, L.; Roisnel, T.; Costuas, K.; Halet, J.-F.; Lapinte, C. *Organometallics* **2006**, *25*, 649.
46. Bruce, M. I.; Burgun, A.; Gendron, F.; Grelaud, G.; Halet, J.-F.; Skelton, B. W. *Organometallics* **2011**, *30*, 2861.
47. Babgi, B.; Rigamonti, L.; Cifuentes, M. P.; Corkery, T. C.; Randles, M. D.; Schwich, T.; Petrie, S.; Stranger, R.; Teshome, A.; Asselberghs, I.; Clays, K.; Samoc, M.; Humphrey, M. G. *J. Am. Chem. Soc.* **2009**, *131*, 10293.
48. Dalton, G. T.; Cifuentes, M. P.; Watson, L. A.; Petrie, S.; Stranger, R.; Samoc, M.; Humphrey, M. G. *Inorg. Chem.* **2009**, *48*, 6534.
49. Rohde, G. T.; Sabin, J. R.; Barrett, C. D.; Nemykin, V. N. *New J. Chem* **2011**, *35*, 1440.
50. Schmidt, E. S.; Calderwood, T. S.; Bruice, T. C. *Inorg. Chem.* **1986**, *25*, 3718.
51. Cifuentes, M. P.; Powell, C. E.; Humphrey, M. G.; Heath, G. A.; Samoc, M.; Luther-Davies, B. *J. Phys. Chem* **2001**, *105*, 9625.
52. Cifuentes, M. P.; Powell, C. E.; Morall, J. P.; McDonagh, A. M.; Lucas, N. T.; Humphrey, M. G.; Samoc, M.; Houbrecht, S.; Asselberghs, I.; Clays, K.; Persoons, A.; Isoshima, T. *J. Am. Chem. Soc.* **2006**, *128*, 10819.
53. Odom, S. A.; Webster, S.; Padilha, L. A.; Peceli, D.; Hu, H.; Nootz, G.; Chung, S.-J.; Ohira, S.; Matichak, J. D.; Przhonska, O. V.; Kachkovski, A. D.; Barlow, S.; Brédas, J.-L.; Anderson, H. L.; Hagan, D. J.; Van Stryland, E. W.; Marder, S. R. *J. Am. Chem. Soc.* **2009**, *131*, 7510.
54. Drobizhev, M.; Stepanenko, Y.; Dzenis, Y.; Karotki, A.; Rebane, A.; Taylor, P. N.; Anderson, H. L. *J. Am. Chem. Soc.* **2004**, *126*, 15352.
55. Zhou, X.; Ren, A.-M.; Feng, J.-K.; Liu, X.-J.; Zhang, Y.-D. *Chem. Phys. Chem.* **2004**, *4*, 991.
56. Buhleier, E.; Wehner, W.; Vögtle, F. *Synthesis* **1978**.
57. Ohshiro, N.; Tkei, F.; Onitsuka, K.; Takahashi, S. *J. Organomet. Chem.* **1998**, *569*, 195.
58. Onitsuka, K.; Fujimoto, M.; Oshiro, N.; Takahashi, S. *Angew. Chem. Int. Ed.* **1999**, *38*, 689.
59. McDonagh, A. M.; Humphrey, M. G.; Samoc, M.; Luther-Davis, B.; Houbrechts, S.; Wada, T.; Sasabe, H.; Persoons, A. *J. Am. Chem. Soc.* **1999**, *121*, 1405.

60. Green, K. A.; Simpson, P. V.; Corkery, T. C.; Cifuentes, M. P.; Humphrey, M. G. *Macromol. Rapid Commun* **2012**, *33*, 573.
61. Varnavski, O.; Yan, X.; Mongin, O.; Blanchard-Desce, M.; Goodson, T. G. *J. Phys. Chem. C* **2007**, *111*, 149.
62. Roberts, R. L.; Schwich, T.; Corkery, T. C.; Cifuentes, M. P.; Green, K. A.; Farmer, J. D.; Low, P. J.; Marder, T. B.; Samoc, M.; Humphrey, M. G. *Adv. Mater.* **2009**, *21*, 2318.
63. Whittall, I. R.; Humphrey, M. G.; Houbrechts, S.; Maes, J.; Persoons, A.; Schmid, S.; Hockless, D. C. R. *Organomet. Chem* **1997**, *544*, 277.
64. Long, N. J.; Martin, A. J.; de Biani, F. F.; Zanello, P. *J. Chem. Soc., Dalton trans* **1998**, 2017.
65. McDonagh, A. M.; Whittall, I. R.; Humphrey, M. G.; Hockless, D. C. R.; Skelton, B. W.; White, A. H. *J. Organomet. Chem.* **1996**, *523*, 33.
66. McDonagh, A. M.; Cifuentes, M. P.; Whittall, I. R.; Humphrey, M. G.; Samoc, M.; Luther-Davis, B.; Hockless, D. C. R. *J. Organomet. Chem.* **1996**, *526*, 99.
67. Powell, C. E.; Cifuentes, M. P.; Humphrey, M. G.; Willis, A. C.; Morall, J. P.; Samoc, M. *Polyhedron* **2007**, *26*, 284.
68. Drouet, S.; Merhi, A.; Yao, D.; Cifuentes, M. P.; Humphrey, M. G.; Wielgus, M.; Olesiak-Banska, J.; Matczyszyn, K.; Samoc, M.; Paul, F.; Paul-Roth, C. O. *Tetrahedron* **2012**, *68*, 10351.
69. Paul, F.; Lapinte, C. *Coord. Chem. Rev.* **1998**, *178-180*, 431.

Chapter 5

Platinum porphyrin complexes

For OLEDs

I. Introduction

After presenting the synthesis and characterization of all these luminescent compounds in chapters 2 and 3, we will now consider their applications. We were particularly wondering how they could be used in Organic Light Emitting Diode (OLED).

The **OLED** device is a light-emitting diode (LED) with an organic emissive layer. Such devices can be used in small, portable screens such as mobile phones and watches and in television screens. In 2007, Sony announced the world's first **OLED TV** : only 11 inches, so a very small and expensive screen. Sony was very keen to be seen as an innovator, and is betting on OLEDs as the technology that will one day replace LCD or Plasma TVs. Since January 2012, a 55" OLED TV from Samsung is available, this TV screen is ultra-thin, and it can provide a broader range of colors. Also, the response time of the pixels is better so one can see faster-moving scenes with more fluidity and motion effects in 3D are better.

Currently, **OLEDs** are still actively exploited for the development of flat-panel display devices and for energy-efficient lighting.[1,2] In both cases, three primary colours, blue, green, and red, are necessary.

For commercial applications, the most success has been obtained for green emitters.[3] For the blue light-emitting materials, such as polyfluorenes, high efficiency has been achieved, but there are frequent problems with stabilities and lifetimes.[4] The development of red emitting systems is also challenging, partly due to the drop-off in emission quantum yield that is typically observed for lower energy excited states. This trend stems from the fact that non-radiative deactivation of excited states through intramolecular energy transfer into vibrations is favoured as the energy decreases.

Many porphyrins emit quite strongly in the red region of the spectrum, owing to their rigid, highly conjugated structures. Moreover, they have quite narrow bandwidths, potentially favouring high colour purity if used in an **OLED**.

Some studies have indeed used porphyrins as red **OLED** emitters; for example, a device comprising what is probably the most accessible of the porphyrin family, namely tetraphenylporphyrin (**TPP**), doped into a conjugated polymer, poly(9,9-dioctylfluorene), was described several years ago.[5] The importance of fluorene units in organic electronics and photonics makes the combination of porphyrins and fluorenes particularly intriguing. For example, a series of star-shaped porphyrins bearing pendent oligofluorene arms (**Figure 1**) were reported by Bo and co-

workers.[6,7] This group synthesized a series of porphyrins substituted by oligofluorenes. This series of compounds having a star-like structure, and fluorenes as substituents, gives access to form homogeneous films.

Figure 1 : Star porphyrin synthesized by **Bo**

Moreover, Agarwal reported the synthesis of porphyrins substituted by various fluorene derivatives at the *meso* position[8] as seen in **Figure 2**. The fluorescence studies of these porphyrins showed efficient energy transfer from the fuorenyl arms to the porphyrin core. In addition, they suggested based on their observations small aggregations composed of thin films.

Figure 2 : Presentation of **Agarwal** compounds

In the previous chapters, we presented **TFP**, incorporating fluorenyl substituents at the four *meso* positions of the porphyrin macrocycle. In terms of the photophysical properties, the fluorenyl substituents were found to lead to an increase in the fluorescence quantum yield of the free-base porphyrin (Φ_F = 0.24) relative to that of **TPP** (Φ_F = 0.13 under the same conditions), apparently owing largely to an increase in the radiative rate constant associated with distortion of the porphyrin macrocycle.[9] A density functional theory study on such compounds has been carried out by others.[10] Encouraged by these results, we have also prepared dendrimeric supramolecular assemblies bearing 12 and 24 fluorenyl peripheral donor groups surrounding the porphyrin core, as presented in **chapter 2**.[11-13] Having all this interesting photophysical studies done, we were wondering how we could use these promising red luminescent molecules for devices.

Over the past decade, many studies have focused on the use of luminescent organometallic complexes as emitting species in **OLEDs**. The high spin-orbit coupling constants associated with third-row transition metal ions such as Ir(III) and Pt(II) promotes the emission of light from triplet states that are formed upon charge recombination in an **OLED** in ratios as high as 3:1 over the singlets. In a device comprising a purely organic emitting material, the emission from the triplet states is forbidden through the spin selection rule $\Delta S=0$, limiting the maximum attainable internal efficiency to 25%. Transition metal-based systems allow this limit to be raised to 100%. Platinum(II) complexes of porphyrins are therefore of interest as **OLED** emitters. Indeed, the first tests on the use of phosphorescent transition metal complexes as **OLED** phosphors were carried out with platinum octaethylporphyrin (**PtOEP**) by Thomson in 1998.[14] This molecule (**Figure 3**) showed great interest at the level of **OLED** application. Then, the same group, developed their work on platinum complexes and their luminescence studies.[15]

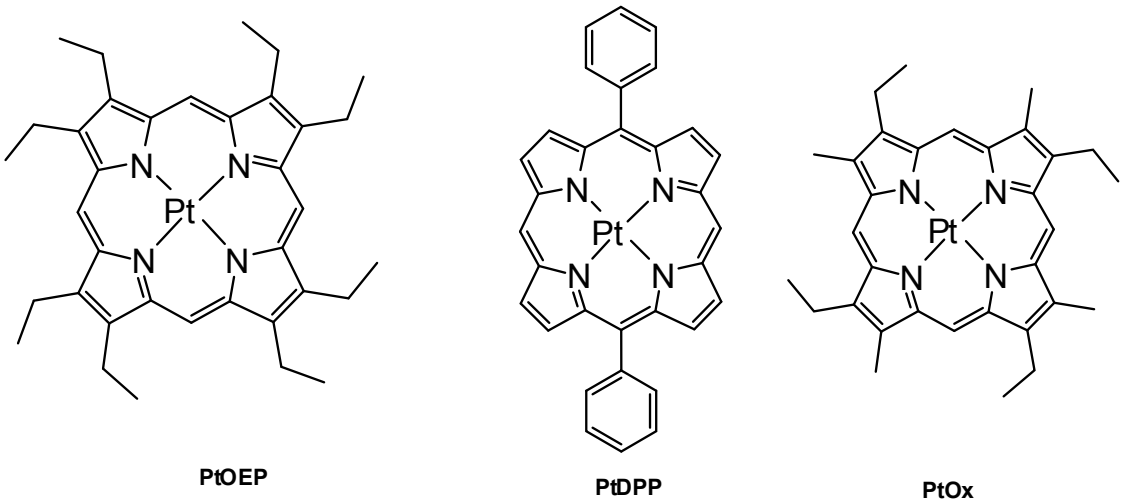

Figure 3 : Representation of **Thomson's** porphyrins

II. Previously platinum porphyrins used for OLED's elaboration

The synthesis of a free-base porphyrin **TFP** has been reported earlier by our group.[16] In addition, it was proved and discussed that the presence of the fluorenyl substituent serves to raise the quantum yield of fluorescence of the porphyrin.[9,17,18]

Given the increased radiative rate constant and increased quantum yield that we observed for **TFP** compared to **TPP** ($k_r = 3.0 \times 10^7$ and 1.5×10^7 s^{-1}; $\Phi_f = 0.24$ and 0.13 respectively),[9] it will be interesting to prepare the platinum porphyrin of **TFP** and to explore its performance in OLEDs.[19] For example, if the triplet radiative rate constant were to be similarly increased, this could help to counter the aforementioned drawback of the metalloporphyrins. So, combining the advantage of fluorenyl arm, porphyrins core, and transition metals, we propose the synthesis of metallated form of **TFP** by Pt.

1. Platinum complexes

The platinum complex, **PtTFP** was prepared in a similar way in our laboratory as **PtTPP**. That is, the metal **Pt** was inserted by reacting 4 equivalents of **$PtCl_2$** with one equivalent of **TFP** in benzonitrile under reflux as shown in **Figure 4**.

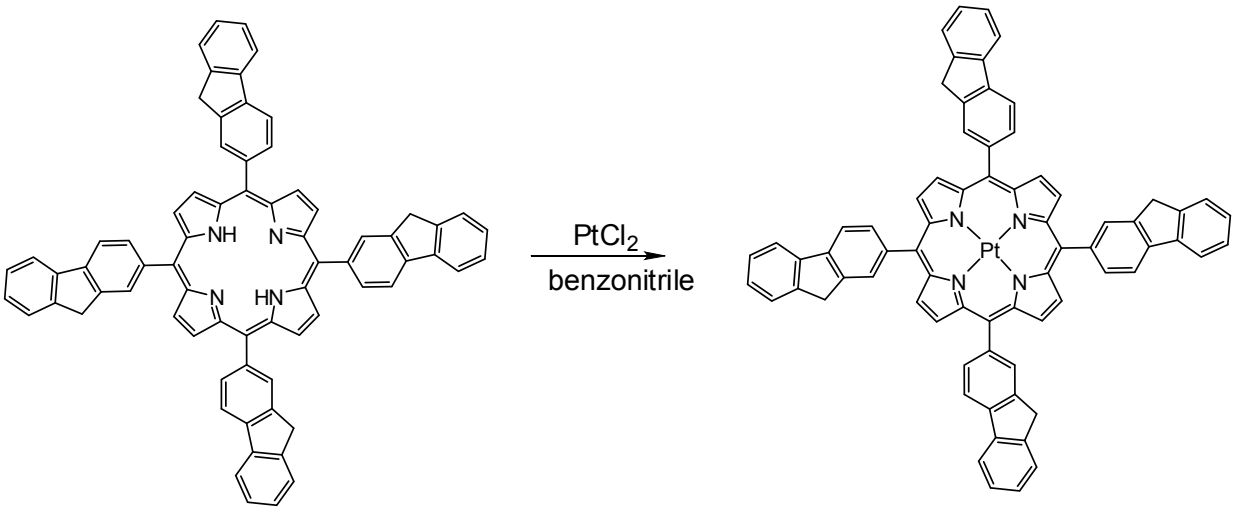

Figure 4 : Synthesis of the complex **PtTFP**

The photophysical studies of this complex, with comparison to its analogue **PtTPP** was done in solution and in dilute frozen glasses. Results are summarized below in **Table 1**.

1.1. Absorption studies of PtTFP

The absorption and emission data for the compound reported here, **PtTFP** with corresponding data recorded by G. Williams under the same conditions for the Pt porphyrin of **TPP** (**Table 1**). The absorption spectra of these complexes are similar to that of the model compounds.

1.2. Emission studies and lifetime of PtTFP

Excitation either in the UV or into the Soret bands leads to characteristic triplet emission from the metalloporphyrin in all cases. The emission spectra in CH_2Cl_2 at 298 K reveal two bands for each compound. Introduction of the fluorenyl units is seen to shift the emission of **PtTFP** to the red by around 10 nm compared to **PtTPP**. The lifetime of the phosphorescence is noticeably shorter for **PtTFP** (22 μs) than for **PtTPP** (59 μs). This reduction in lifetime is accompanied by a decrease in the quantum yield.

Assuming that the triplet emissive state is formed with approximately unitary efficiency upon light absorption (a reasonable assumption given the very fast S $\rightarrow$ T intersystem crossing expected to arise from the presence of the Pt ion), we can estimate the radiative (k_r) and non-radiative (Σk_{nr}) decay constants as follows :

$$k_r = \Phi/\tau \text{ and } k_{nr} = 1/\tau - k_r$$

The values presented in **Table 1**, indicate that k_r is indeed increased in the fluorenyl porphyrin **TFP** compared to **TPP**, in line with the effect we observed previously on the radiative decay of the singlet state for the corresponding free-base porphyrins.[9]

However, in the present instance, this beneficial effect is apparently partially offset by an increase in non-radiative decay in solution, which results in a net lowering of the phosphorescence quantum yield, at least under these conditions. In a frozen glass at 77 K the lifetime of **PtTFP** is 102 μs compared to 132 μs for **PtTPP**, which would be consistent with a modest increase in k_r, assuming that non-radiative pathways are comparable for the two systems under these rigid conditions.

	λ_{max}^{abs}/nm Soret ; Q	λ_{max}^{em}/nm 298K	τ/μs 298K	$\Phi_{lum} \times 10^2$ 298K	K_r/ $s^{-1(a)}$	$\Sigma k_{nr}/10^3$ $s^{-1(a)}$	$k_Q^{O2}/10^8$ $M^{-1}s^{-1(b)}$	λ_{max}^{em}/nm 77K	τ/ μs 77K
PtTPP	400; 508, 538	668, 734	59	4.6	780	16.2	6.8	655, 728	132
PtTFP	409; 512, 540 (sh)	679, 741	22	2.0	910	44.5	5.9	661,730	102

(a) K_r and Σk_{nr} are the radiative and the non raditive decay rate constants.

(b) k_Q^{O2} is the bimolecular rate constant for quenching by molecular oxygen in solution.

Table 1 : Absorption and emission data for the platinum(II) porphyrins in CH_2Cl_2 at 298 K and in diethyl ether / isopentane / ethanol (2:2:1 v/v) at 77 K

Based on these mentioned studies, **PtTFP** seems to be a promising candidate to be used in the elaboration of an emitting device. That is why solid state photoluminescence and electroluminescence studies are performed for **PtTFP**.

2. Solid state photoluminescence (PL) and electroluminescence (EL)

Before the elaboration of the **OLED**, we will consider the optical properties of our Pt(II) complexes in the solid state. For this, excitation and emission spectra (**Figure 5**) have been measured at room temperature for **PtTFP** at 5% wt in a bisphenol-A-polycarbonate (**PC**), *N,N'*-diphenyl-*N,N'*-bis(3-methylphenyl-(1,1'-biphenyl)-4,4'-diamine (**TPD**) solid film 70 nm thick. **TPD**, a good amorphous film-forming and good hole-transport material, has been chosen as the host for **PtTFP** because its emission, peaked in the range 400-420 nm, matches very well the strong Soret absorption band of the guest, which should favour efficient energy transfer to the porphyrin.

In fact, the **TPD** doped film shows only the red emission of the guest when excited in the host's absorption band, proving an efficient energy transfer from the host to the guest. The emission peak of 668 nm is blue-shifted by 10 nm compared to the room temperature solution value and much more similar to the 77 K one (see **Table 1**). This presumably reflects the greater rigidity of the environment, which may partially inhibit the conjugation of the fluorenyl and porphyrinic units in the excited state.

The PL yield measured in argon atmosphere was 0.20 ± 0.05, a value which is ten times greater than the solution one. Clearly, the molecule stiffening in the rigid solid matrix slows down the non-radiative decay.

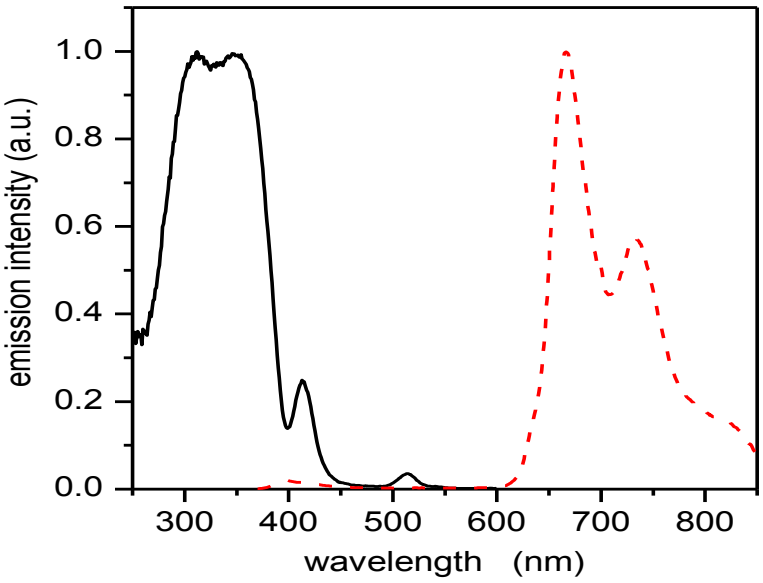

Figure 5 : Excitation (solid black) and emission (dashed red) spectra of a **PtTFP** : **TPD** [5:95 wt ratio] film 70 nm thick. The excitation is detected at 668 nm, and the emission is obtained exciting at 350 nm.

3. OLED device fabrication

Based on the motivating results obtained from solid state photoluminescence and electroluminescence, it is worth to try OLED fabrication. This was done as collaboration with V. Fattori at the University of Bologne.

The device for **EL** experiments was a simple double-layer **OLED** (**Figure 6**). The first layer, 70 nm thick and acting as holes transport and emitting layer, was spin-cast on **ITO** glass.

Then, a 3,5-bis-(4-tert-butyl-phenyl)-4-phenyl-4H-[1,2,4]triazole (**TAZ**) layer (thickness = 60 nm) to confine excitons and holes in the emitting layer, and a LiF film with an Al cap as the cathode were deposited.

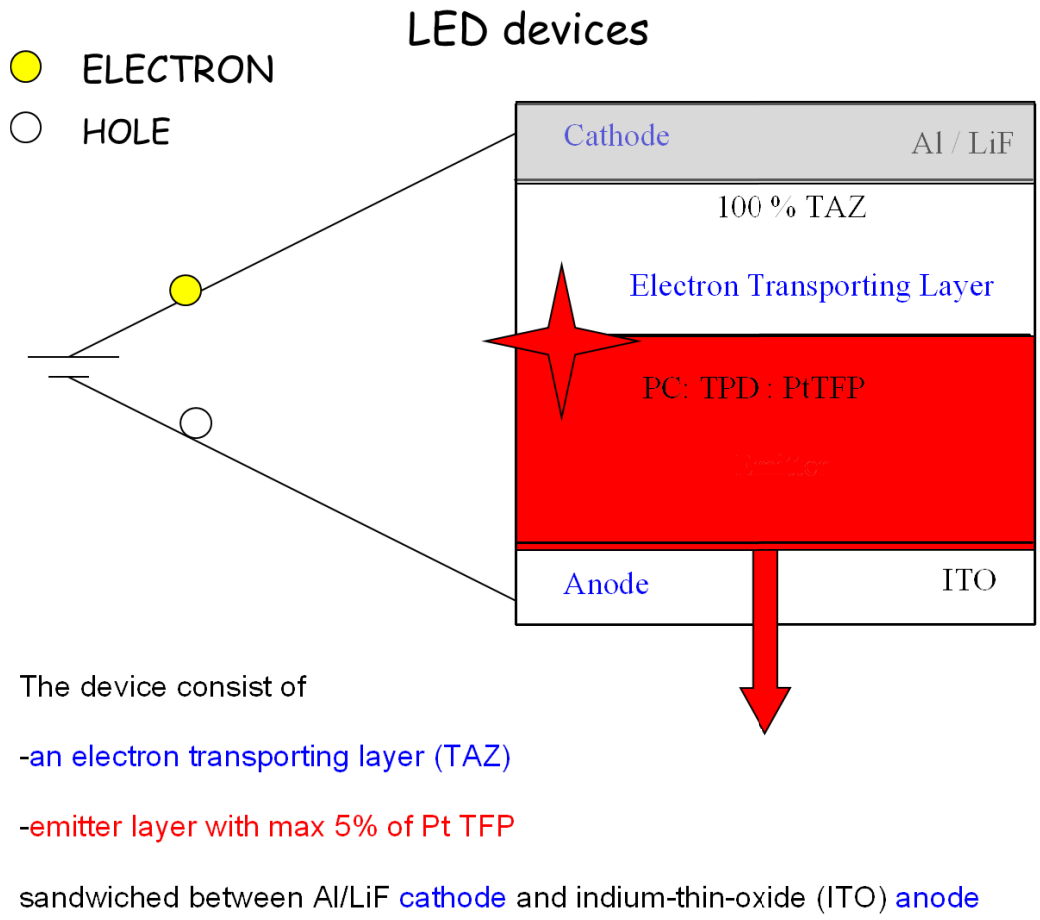

Figure 6 : Representation of a simple double-layer **OLED** elaborated in **Bologne**

3.1. Electroluminescent study of the OLED

The EL test was performed on a simple two-layer **OLED** structure similar to the previously reported paper on the well-studied **PtOEP**.[20] In this device, the first layer has to perform both hole transport and emission. Compound **TPD**; a good hole transport material, matches very well the absorption Soret-band of the guest and an efficient energy transfer from the host to the guest is proved by the PL data described above.

In addition, the energy of **PtTFP** triplet, which can be estimated to be 1.80 eV from the high energy maximum in the emission spectrum, is sufficiently low with respect to the host triplet energy (2.4 eV) to prevent back energy transfer.[21] The second layer of **TAZ** acts as an electron transporting/hole blocking layer, and has sufficiently high triplet energy (2.75 eV) to avoid **PtTFP** excitons from being quenched at the layer interface.

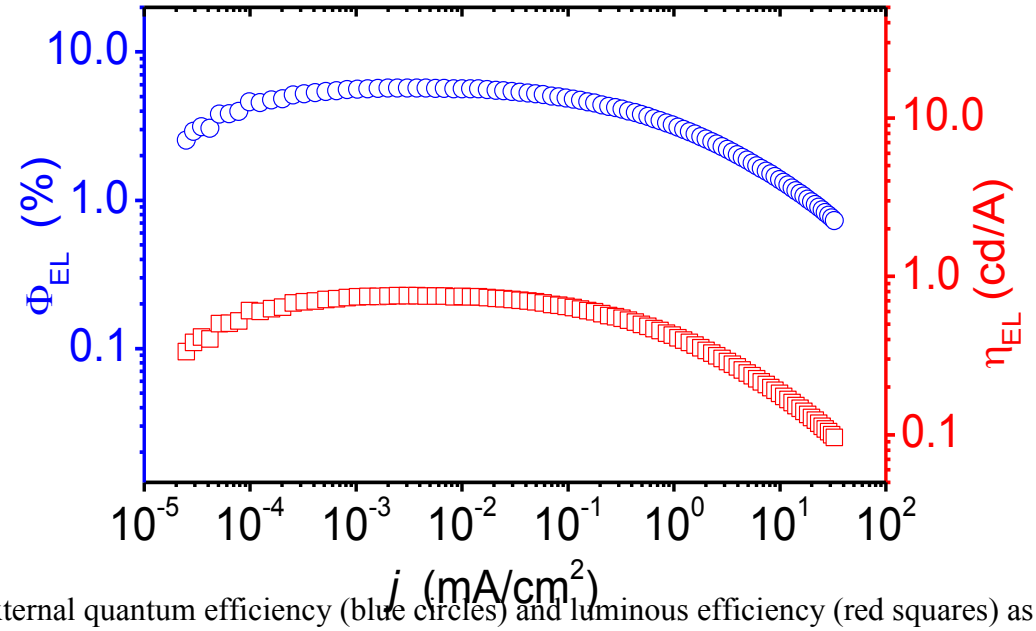

Figure 7 : External quantum efficiency (blue circles) and luminous efficiency (red squares) as a function of current density.

The EL behaviour of the OLED is reported in **Figure 7**. External quantum efficiency reaches a maximum value of 6% at 1x10^{-3} mA/cm^2 (10 V). The EL quantum efficiency shows the typical roll-off at high currents due to exciton-exciton and/or exciton/charge interaction and to high field induced exciton dissociation.[22] Nevertheless, the efficiency remains in excess of 5% for a wide range of current (voltage) values : from 1x10^{-4} mA/cm^2 (8 V) to 1x10^{-1} mA/cm^2 (14 V). In the same current range, quantum efficiency drops off an order of magnitude when other Pt-porphyrins have been employed as the emitting dopants.[23,24] Clearly, the shorter luminescence lifetime of the new **PtTFP** compared to other previously-studied Pt-porphyrins (*e.g.*, lifetimes in solid matrix are reported to be 73–110 μs for **PtOEP**[21,23] and 44 μs for **PtTPP**[25]) ensures that there is a lower probability of the excited state being quenched by the exciton-exciton and exciton-charge interactions.

Electroluminescence spectra show the red emission of **PtTFP** peaking at 668 nm. The pure red emission at voltages < 16 V comes together with the violet emission from the **TPD** host in the range 400–450 nm at voltages greater than this value

This **OLED** application is of great interest. In fact, all the previously mentioned studies show that porphyrins platinum complexes are good candidates to access to new emissive materials. That's why we were motivated to go forward in **OLED** application using other compounds synthesized by our group.[11]

III. Preparation of new platinum porphyrins dendrimers for OLED's elaboration

This time, the proposed candidates have a porphyrin **TPP** core with fluorenyl arms. The difference is that fluorenes are not directly connected to the porphyrin; instead, they are linked via an ether bond. The two free porphyrin dendrimers are : tetra-oxyfluorenylphenylporphyrin (**TOFP**), and octa-oxyfluorenylphenylporphyrin (**OOFP**); these dendrimers are presented in chapter 2, as shown in **Figure 8**.

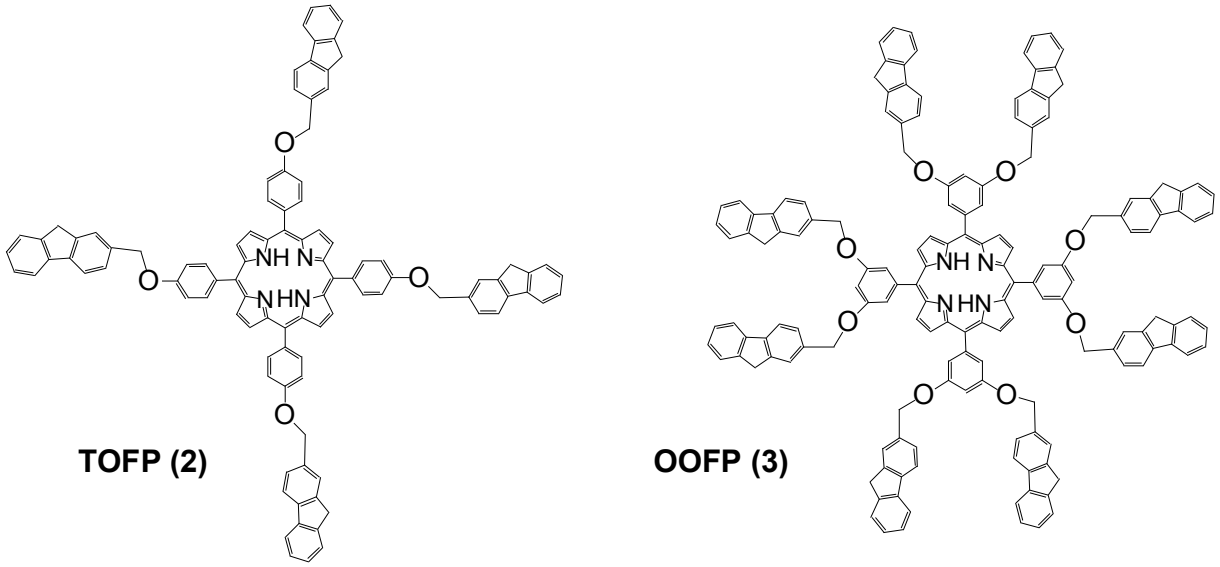

Figure 8 : The two porphyrins dendrimers **TOFP** and **OOFP**

So, the target is to metallate these two porphyrin dendrimers by platinum and then they could be used in the future **OLED** elaboration. The first proposal was to use the same technology used in case of **PtTFP** by **V. Fattoria**. But, unfortunately, these molecules don't sublime, instead decomposition takes place, so another technique is to be used.

In this case, collaboration with C. Pearson, in Prof Petty's group (in school of engineering, at Durham University) and G. Williams is carried to try **OLEDs** by spin coating deposition. It is important to mention that **PtTFP** is also tried using spin coating method, in Durham, so that comparison of the results is possible.

1. Synthesis and characterization of new platinum porphyrin dendrimers

The two free-base porphyrins **TOFP** and **OOFP** were synthesised as we reported previously[11] in chapter 2. Their platinum(II) complexes were prepared by using a method adapted from that used for the formation of **PtTPP**.[26] The platinum salt $PtCl_2$ was dissolved in benzonitrile and pre-heated at 100 °C for 1 h under an argon atmosphere, followed by addition of the free-base porphyrin and reflux for a further two hours.

The crude products were purified by chromatography on silica to give the desired compounds **PtTOFP** and **PtOOFP** as reddish-purple solids, which were characterised by **NMR** and **UV-visible** spectroscopy and mass spectrometry.

1.1. Absorption and emission spectra of TOFP and OOFP in solution

The UV-visible spectra of the free-base porphyrins exhibit a combination of bands as anticipated from the constituent units. The data for both compounds **TOFP** and for **OOFP** are presented in **Table 2**.

The intense Soret bands around 420 nm and Q bands around 590 and 650 nm, characteristic of *meso*-tetra-arylporphyrins, are accompanied by bands around 270 nm associated with the fluorene substituents. In both cases, the Soret and Q bands are a little red-shifted compared to **TPP**, more so for **TOFP**. That is probably due to the *para*-disposition of the electron-donating alkoxy substituent in this case.

The emission spectra of the free-base porphyrins in solution display the typical porphyrin-based fluorescence in the red region expected for a tetra-aryl porphyrin (**Table 2**). The emission spectra are essentially independent of the excitation wavelength: excitation at short wavelength into the fluorene bands gives the porphyrin emission, with no detectable fluorene emission at higher energy.

Likewise, the excitation spectra registered around 660 nm show bands attributable to excitation of the fluorenes at similar relative intensities to the fluorene bands in the absorption spectrum. Thus, we can conclude that energy transfer from the fluorene pendants to the porphyrin core occurs on a timescale that greatly exceeds that of fluorene fluorescence. The fluorescence lifetimes of the porphyrins are around 7 – 8 ns, similar to that of **TPP**.

	λ_{max}^{abs} / nm fluorenyl; Soret; Q	λ_{max}^{em} / nm 298 K	τ / ns 298 K	$\Phi_{lum} \times 10^2$ 298 K
TPP	---; 417; 513, 548; 589; 646	650, 714	8.6	13
TOFP	270; 422; 521, 560, 592, 653	659, 725	7.6	7.9
OOFP	270; 422; 516, 550, 590, 648	657, 718	7.5	11

Table 2 : Absorption and emission data for the free-base porphyrins in CH_2Cl_2 at 298 K

1.2. Absorption and emission spectra of PtTOFP and PtOOFP in solution

Metallation of the porphyrins is accompanied by a blue-shift in the Soret and Q bands, as typically observed for metalloporphyrins (**Table 3**). The platinum(II) complexes of the porphyrins display emission bands deeper into the red than the free-base analogues, with long lifetimes of around 50 μs, indicative of emission emanating from the triplet state (**Table 3**).

Again, no fluorene emission is detected upon excitation at high energy into the fluorene bands, confirming the fast energy transfer to the metalloporphyrin unit. The phosphorescence quantum yields are of the order of 0.04 – 0.10 (**Table 3**), and the emission is quenched efficiently by dissolved O_2. The bimolecular rate constants for diffusional-controlled oxygen quenching are in the order **PtTPP > PtTOFP > PtOOFP**, the values decreasing as the molecular weights increase (and hence as diffusion coefficients decrease).

	λ_{max}^{abs} / nm fluorenyl; Soret; Q	λ_{max}^{em} / nm 298 K	τ / μs 298 K	$\Phi_{lum} \times 10^2$ 298 K	k_Q^{O2} / 10^8 $M^{-1}s^{-1}$	λ_{max}^{em} / nm 77 K	τ / μs 77 K
PtTPP	---; 400; 508, 538	668, 734	59	4.6	6.8	655, 728	132
PtTOFP	267; 406; 511	683, 743	48	11	3.3	669, 741	105
PtOOFP	267; 406; 511, 541, 599	664, 729	54	4.2	0.63	652, 722	123

Table 3 : Absorption and emission data for the **Pt porphyrins** in CH_2Cl_2 at 298 K

1.3. Electronic and optoelectronic behaviour of OLEDs

These complexes were incorporated into **OLEDs** following a procedure previously described in the literature.[27] Initially, a layer of poly(3,4-ethylenedioxythiophene)/poly(styrenesulfonate) (PEDOT/PSS) was spin-coated onto the indium tin oxide (ITO) layer on a glass substrate, followed by a blended emissive layer. This consisted of the host, a polyvinylcarbazole (PVK), together with the platinum complex (3% by weight) and 1,3-bis(4-tert-butylphenyl-1,3,4-oxadiazolyl) phenylene (30% by weight), denoted OXD7 (structure in **Figure 9**), as an electron transport layer. This was also deposited by spin-coating, using chlorobenzene or chloroform as solvent.

Finally, a thin caesium fluoride layer and then the aluminium cathode were thermally evaporated under vacuum. In such a blended OLED structure, the emitting layer is formed from a single spin-coated layer, so devices should therefore be easy to fabricate.[28] The electronic and optoelectronic behaviour of OLEDs based upon the red platinum phosphorescent dyes reported here is presented, where the dye is doped into the PVK layer in each case.

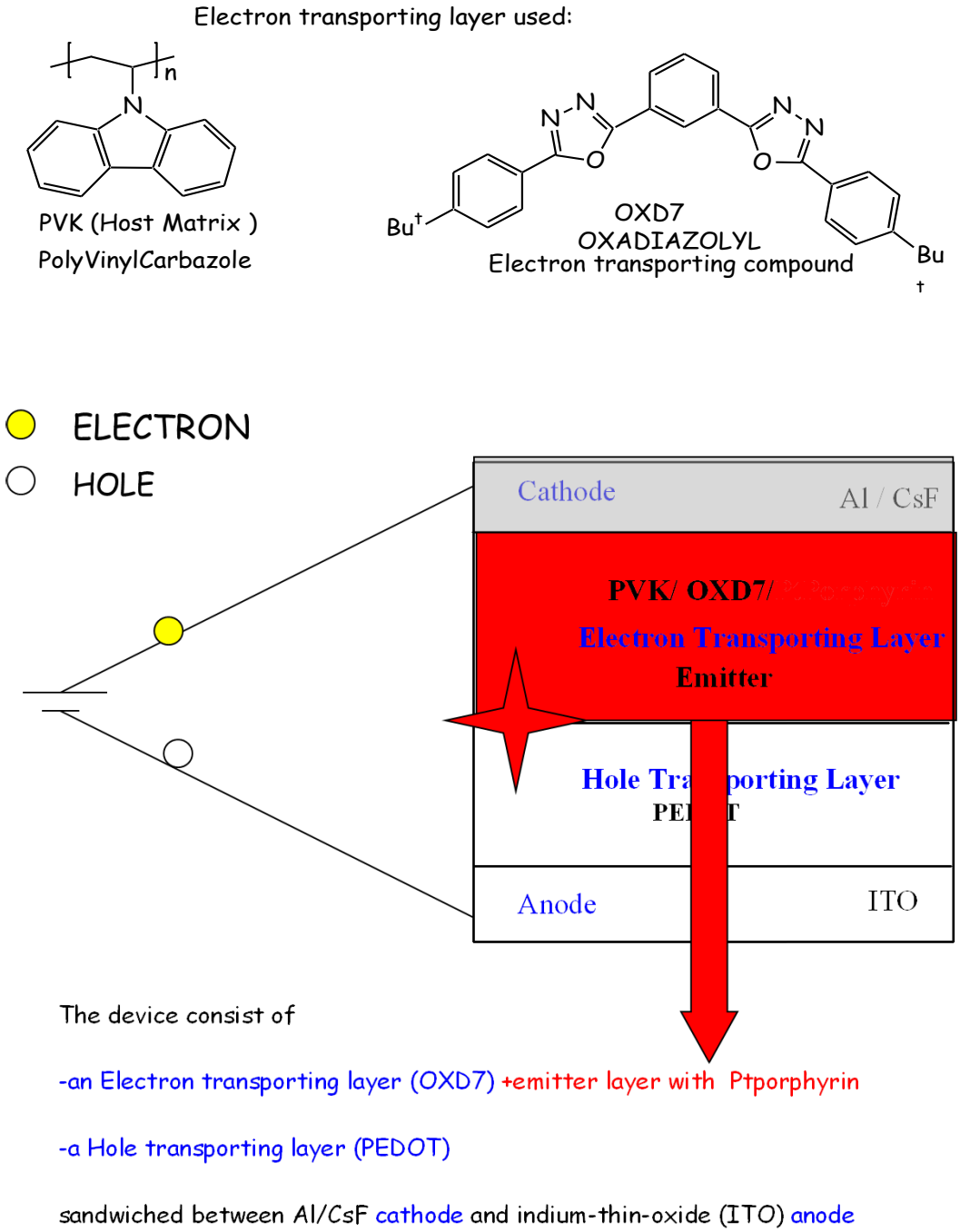

Figure 9 : Schematic diagram of the OLED configuration elaborated in **Durham**

The normalized EL spectra are shown in **Figure 10** for the set of devices having the configurations shown in the caption to the Figure. The spectra were measured at a current of 1 mA (current density 5.1 mA cm^{-2}). Emission from the PVK device was a maximum at 412 nm, with a second peak at 596 nm. The addition of OXD7 resulted in a broader EL spectrum with a maximum at

468 nm. This can be related to the formation of an exciplex between the two components (*i.e.,* the coupling of an excited singlet state of one molecule with the ground state of another). The addition of **PtOOFP** to the PVK-OXD7 device resulted in a broad emission from 400 to 600 nm, with peaks at 470 nm (from the PVK-OXD7 exciplex) and 540 nm and a shoulder at 516 nm for the device prepared from chlorobenzene. For the device where chloroform was used as the solvent, peaks at 544 and 576 nm and shoulders at 460 and 512 nm were observed. Both devices exhibited a maximum red EL at 668 nm with an additional peak at 730 nm.

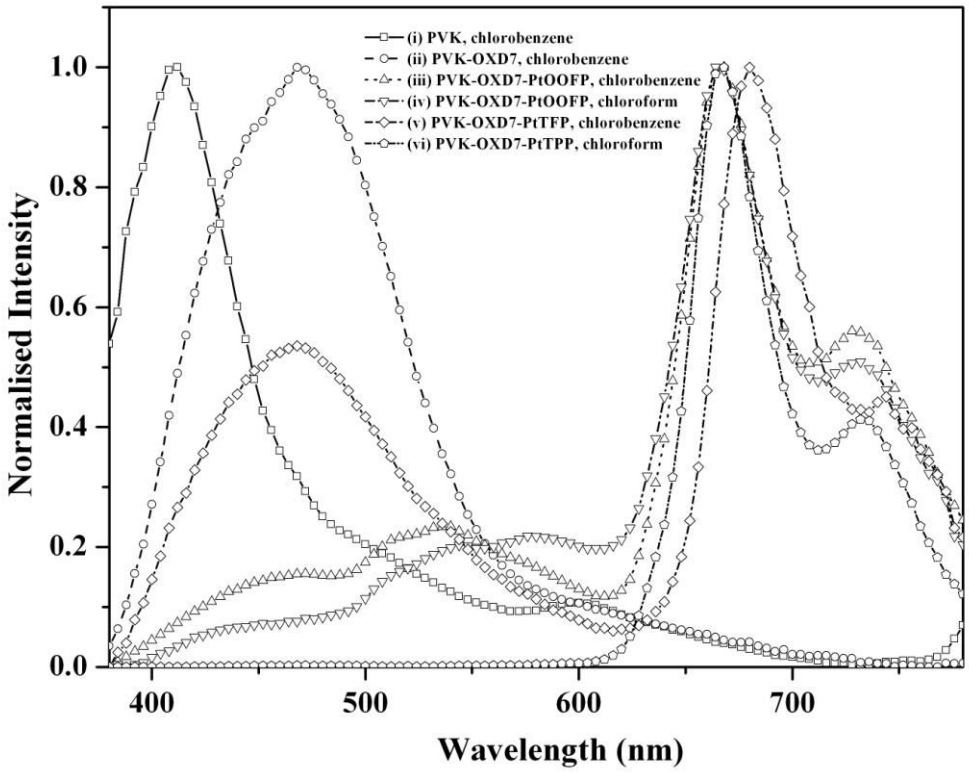

Figure 10 : Normalised EL spectra of OLEDs with the following configurations:
(i) ITO/PEDOT/PVK/CsF/Al, chlorobenzene solvent (full line);
(ii) ITO/PEDOT/PVK-OXD7/CsF/Al, chlorobenzene solvent (dashed line);
(iii) ITO/PEDOT/PVK-OXD7-PtOOFP/CsF/Al, chlorobenzene solvent (dotted line);
(iv) ITO/PEDOT/PVK-OXD7-PtOOFP/CsF/Al, chloroform solvent (dash-dotted line);
(v) ITO/PEDOT/PVK-OXD7-PtTFP/CsF/Al, chlorobenzene solvent (dash-dot-dotted line);
(vi) ITO/PEDOT/PVK-OXD7-PtTPP/CsF/Al, chloroform solvent (short dash-dotted line). >

The device containing **PtTFP** exhibited a broad emission at 468 nm (from the PVK-OXD7 exciplex) with maximum red EL at 680 nm and a second peak at 744 nm. The emission from the

PVK-OXD exciplex in this device suggests that there is only partial energy transfer between the host matrix and the guest dye. Finally, the device containing **PtTPP**, prepared from chloroform solvent, exhibited only red emission, with a maximum EL at 668 nm and a second peak at 732 nm. The red emission peaks from these devices agree well with those observed in our previous work.[19]

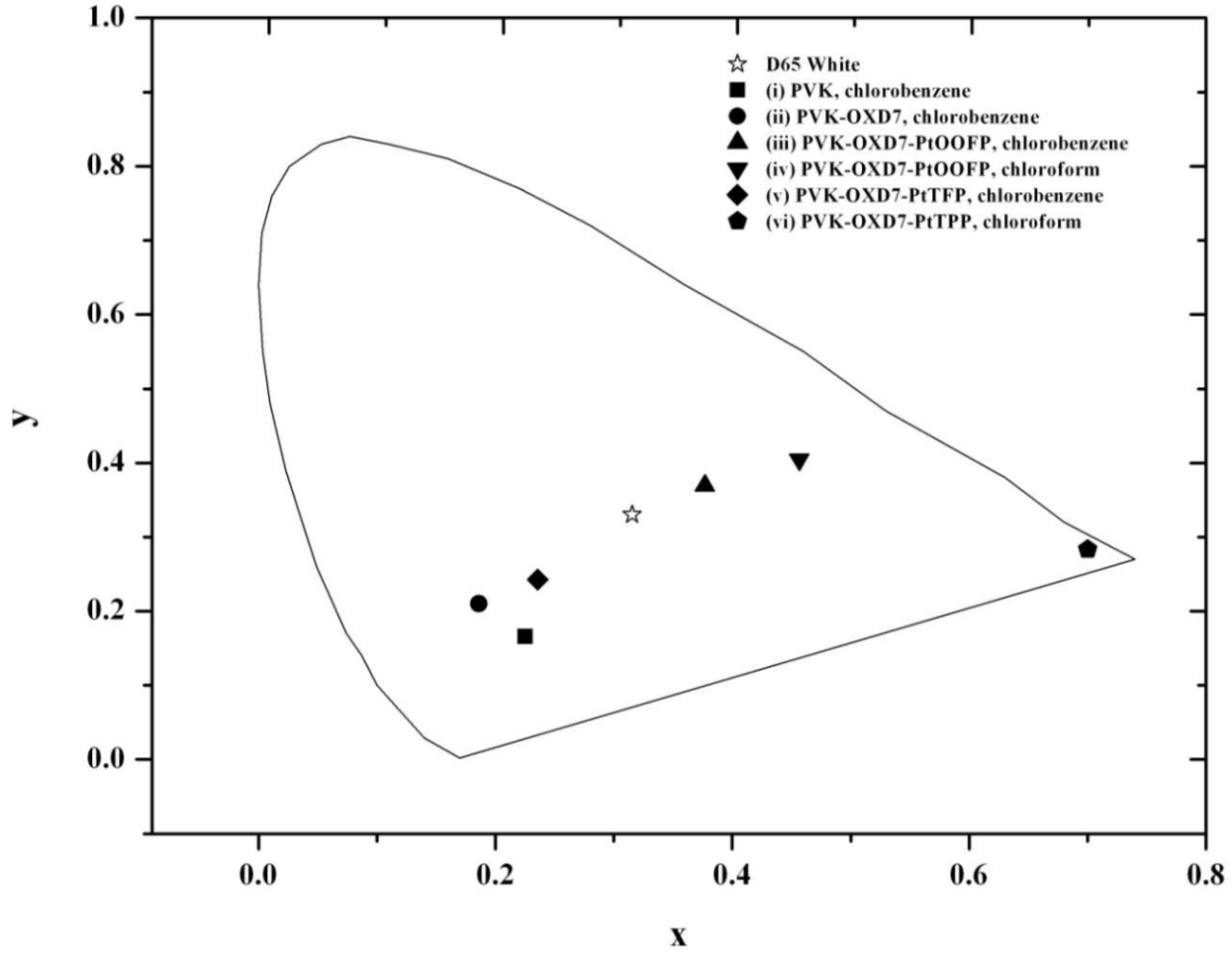

Figure 11 : CIE coordinates for the OLEDs prepared in **Durham**

The Commission Internationale de I'Eclairage (CIE) coordinates corresponding to the spectra shown in **Figure 10** are plotted in **Figure 11**. The D65 white point (star) is also included on the diagram as a reference. The EL from the PVK (i) and PVK-OXD7 (ii) devices was blue in colour, as was that from the device containing **PtTFP** (v) (due to the broad emission from the PVK-OXD7 exciplex). The broad blue/green emissions combined with the red peaks in the spectra of the devices containing **PtOOFP** (iii and iv) gave the EL from these devices a white appearance (particularly the device prepared from chlorobenzene solvent). The emission from the device containing **PtTPP** (vi)

was confined to the long wavelength part of the spectrum, giving the EL from this device a red colour.

The turn-on voltages, (bias required to produce a current of 1 nA from the photodiode detector) current and power efficiencies are presented in **Table 4**. Surprisingly, the turn-on voltage for the two devices containing **PtOOFP**, (iii) and (iv), varies dramatically, despite them being identical other than in the solvent used for preparation. The device where chlorobenzene was used displays a turn-on voltage of 6.9 V, compared to 21.9 V for the chloroform analogue, similar to device containing **PtTPP** (vi). For the device containing **PtTFP** (v), this value is quite low (8.2 V). The CIE_x and CIE_y coordinates of all of these six devices are reported in **Table 4**.

Device	(i)	(ii)	(iii)	(iv)	(v)	(vi)
Turn on voltage (V)	5.9	5.5	6.9	21.9	8.2	21.5
Current efficiency (cd A^{-1})	0.21	0.29	0.27	0.18	0.11	0.14
Power efficiency (lm W^{-1})	0.06	0.06	0.06	0.01	0.03	0.01
CIE_x	0.219	0.179	0.372	0.453	0.230	0.699
CIE_y	0.166	0.210	0.369	0.405	0.242	0.283

Table 4 : Electroluminescence data for OLEDs (i) to (vi).
Turn-on voltages given at 1 nA of photocurrent, as measured by the photodiode detector.
All other data were measured at a current of 1 mA (current density 5.1 mA cm^{-2}).

IV. Conclusion

In this last chapter, first, the photophysical properties of the platinum(II) complex of **TFP** are recalled and compared to that of **PtTPP** in solution.

Previously, an **OLED** has been fabricated using **PtTFP** as a red phosphor, giving a maximum brightness of 40 cd/m^2 and a maximum external quantum efficiency of 6% with slow roll-off. The electroluminescence emission is located in the red-purple region of the visible spectrum. These values – obtained in a very simple two layer device – seem to locate **PtTFP** in an encouraging position compared to other red emitters of the same type.

In other words, the choice of *meso*-aryl substituents can allow the properties of porphyrins to be optimised for OLEDs. In the present instance, the shorter lifetime of the fluorenyl-substituted complex **PtTFP** delays the onset of the high-current roll-off that normally plagues porphyrin-based systems. Moreover, these fluorenyl-appended compounds constitute interesting building blocks to access new emissive materials.

Based on the cited encouraging results, our project was extended to synthesize and characterize new platinum(II) porphyrin complexes **PtTOFP** and **PtOOFP** bearing four and eight fluorenyl pendant arms at the *meso*-positions, respectively.

These new platinum(II) complexes **PtTOFP** and **PtOOFP** were shown to emit essentially red light after selective UV irradiation and visible irradiation. We have also investigated the electronic and optoelectronic behaviour of OLEDs based on these red phosphorescent dyes, as well as earlier reported **PtTFP** and reference **PtTPP**, doped into a layer of PVK host.

The EL from the device containing **PtTFP** was blue in colour, due to the residual emission from the PVK-OXD7 exciplex. The two devices containing **PtOOFP** gave the EL a white appearance. In contrast, the emission from the device containing reference **PtTPP** was a red colour.

These OLEDs have been obtained using a relatively simple device configuration, which should be comparatively easy to manufacture. However, it is clear that the choice of solvent used in the preparation of the device can influence the device characteristics, including a subtle effect on the colour and a much more significant effect on the turn-on voltage.[29]

Experimental part

Synthesis of *meso*-(5,10,15,20-tetra(4-(2 methyloxyfluorenyl)phenyl)porphyrinato platinum(II) : PtTOFP

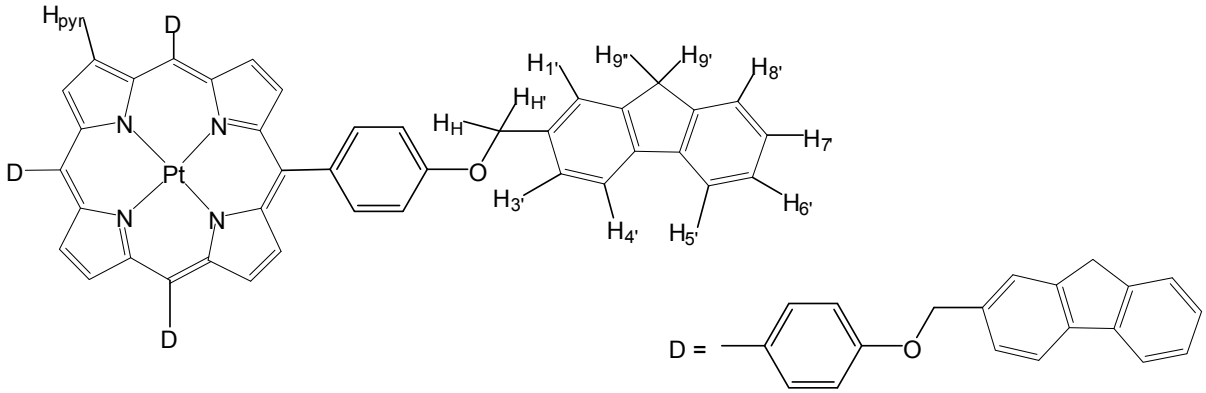

The platinum complex **PtTOFP** was prepared by platinum insertion in **TOFP** following an adapted procedure of the platinum insertion in **TPP**. The $PtCl_2$ (0.04 g, 0.15 mmol) was dissolved in 12 mL of purified benzonitrile and preheated at 100°C for 1 h under argon atmosphere. Free-base porphyrin **TOFP** (0.05 g, 0.04 mmol) was added to the previous solution and the mixture was refluxed for another 4 h. Reaction progress is monitored by TLC, spotting directly from the organic layer. This mixture was cooled to room temperature and the precipitate collected by filtration. The precipitate was washed thoroughly with MeOH and CH_2Cl_2 to give the desired product (yield 90%) as a reddish-purple solid.

This relatively insoluble porphyrin complex **PtTOFP** was characterised by NMR, mass spectrometry and UV-Vis.

^{1}H NMR ($CDCl_3$, 200 MHz, ppm) : 8.80 (large s, 8H, $H_{\beta\text{-pyrrolic}}$), 8.40-7.40 (m, 44H, $H_{\text{fluorenyl-phenyl}}$), 5.30 (s, 8H, $H_{H\text{-}H'}$), 3.90 (large s, 8H, $H_{9'\text{-}9''}$).

UV-visible (in CH_2Cl_2) : 267 nm (fluorene), 406 nm (Soret band), 511 nm (Q band).

MS (Maldi –TOF) : calcd for $C_{100}H_{68}N_4O_4Pt$: 1583.4900 $[MH]^+$, found : 1583.4170 $[MH]^+$.

Synthesis of *meso*-(5,10,15,20-tetra(4-(3,5dimethyloxyfluorenyl)phenyl)porphyrinato platinum(II) : <u>PtOOFP</u>

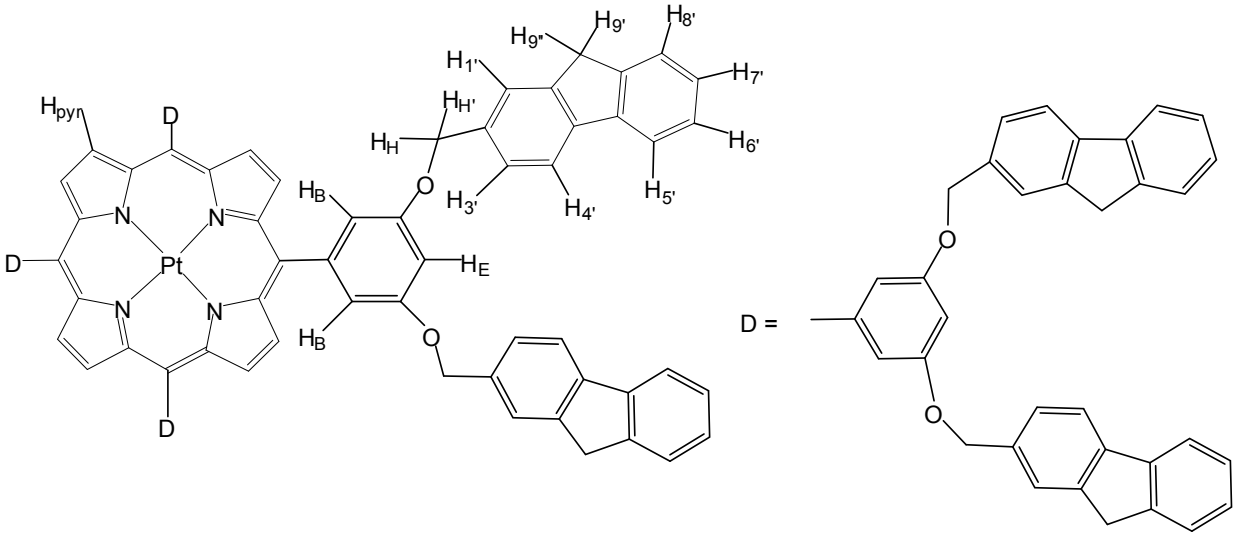

The porphyrin complex **PtOOFP** was prepared by platinum insertion in **OOFP**, following the same procedure.[26] $PtCl_2$ (0.104 g, 0.39 mmol) was dissolved in 20 mL of purified benzonitrile and preheated at 100 °C for 1 h under argon atmosphere. Free-base porphyrin **OOFP** (0.20 g, 0.09 mmol) was added to the previous solution and the mixture was refluxed for another 2 h. Reaction progress is monitored by TLC, spotting directly from the organic layer. This mixture was condensed by vacuum distillation and cooled to room temperature. The crude product was chromatographed on silica gel and eluted with (10:1 dichloromethane/methanol) to give the desired product (yield 95%) as a reddish-purple solid.

This soluble porphyrin complex **PtOOFP** was characterised by NMR, mass spectrometry, micro-analysis and UV-Vis.

^{1}H NMR ($CDCl_3$, 200MHz, ppm) : 8.77 (s, 8H, $H_{\beta\text{-pyrrolic}}$), 7.99-7.32, (m, 68H, $H_{\text{fluorenyl-phenyl}}$), 5.30 (s, 16H, $H_{H\text{-}H'}$), 3.91 (s, 16H, $H_{9'\text{-}9''}$).

UV-visible (in CH_2Cl_2) : 267 nm (fluorene), 406 nm (Soret band), 511, 541, 599 nm (Q bands).

MS (Maldi –TOF) : calcd for $C_{156}H_{106}N_4O_8Pt$: 2358.7700 $[MH]^+$, found : 2358.2260 $[MH]^+$.

Analysis: calcd for $C_{156}H_{106}N_4O_8Pt.2CH_2Cl_2$: C, 75.02; H, 4.38; N, 2.21 found : C, 75.47; H, 4.94; N, 2.22.

References :

1. Sheat, J. R.; Antoniadis, H.; Hueschen, M.; Leonard, W.; Miller, J.; Moon, R.; Roitman, D.; Stocking, A. *Science* **1996**, *273*, 884.
2. Burroughes, J. H.; Bradley, D. D. C.; Brown, A. R.; Marks, R. N.; Mackay, K.; Friend, R. H.; Burn, P. L.; Holmes, A. B. *Nature* **1990**, *347*, 539.
3. Kraft, A.; Grimsdale, A. C.; Holmes, A. B. *Angew. Chem., Int. Ed.* **1998**, *37*, 402.
4. Rault-Berthelot, J. *Electrochemistry* **2003**, *10*, 265.
5. Virgili, T.; Lidzey, D. G.; Bradley, D. C. *Synth. Metals* **2000**, *111-112*, 203.
6. Li, B.; Xu, X.; Sun, M.; Fu, Y.; Yu, G.; Liu, Y.; Bo, Z. *Macromolecules* **2006**, *39*, 456.
7. Li, B.; Li, J.; Fu, Y.; Bo, Z. *J. Am. Chem. Soc.* **2004**, *126*, 3430.
8. Agarwal, N. *Dyes and Pigments* **2009**, *83*, 328.
9. Paul-Roth, C.; Williams, G.; Letessier, J.; Simonneaux, G. *Tetrahedron Lett.* **2007**, *48*, 4317.
10. Ren, X.; Ren, A.; Feng, J.; Sun, C. *Journal of Photochemistry and Photobiology A: Chemistry* **2009**, *203*, 92.
11. Drouet, S.; Paul-Roth, C.; Simonneaux, G. *Tetrahedron* **2009**, *65*, 2975.
12. Drouet, S.; Paul-Roth, C. O. *Tetrahedron* **2009**, *65*, 10693.
13. Drouet, S.; Merhi, A.; Argouarch, G.; Paul, F.; Mongin, O.; Blanchard-Desce, M.; Paul-Roth, C. O. *Tetrahedron* **2012**, *68*, 98.
14. Thomson, M. E.; Shoustikov, A.; You, Y.; Sibley, S.; Baldo, M.; Koslov, V.; Burrows, E.; Forrest, S. R. *MRS Abstract, G2.4, Spring Meeting* **1998**.
15. Kwong, R. C.; Sibley, S.; Dubovoy, T.; Baldo, M.; Forrest, S. R.; Thomson, M. E. *Chem. Mater.* **1999**, *11*, 3709.
16. Paul-Roth, C.; Rault-Berthelot, J.; Simonneaux, G. *Tetrahedron* **2004**, *60*, 12169.
17. Paul-Roth, C. O.; Simonneaux , G. *C.R. Acad. Sci., Ser. IIb: Chim.* **2006**, *9*, 1277.
18. Paul-Roth, C. O.; Simonneaux, G. *Tetrahedron Lett.* **2006**, *47*, 3275.
19. Drouet, S.; Paul-Roth, C. O.; Fattori, V.; Cocchi, M.; Williams, J. A. G. *New J. Chem.* **2011**, *35*, 438.
20. Cocchi, M.; Fattori, V.; Sabatini, C.; Di Marco, P.; Maestri, M.; Kalinowski, J. *Applied Physics Letters* **2004**, *84*, 1052.
21. Kalinowski, J.; Stampor, W.; Cocchi, M.; Virgili, D.; Fattori, V.; Di Marco, P. *Chemical Physics Letters* **2004**, *297*, 39.
22. Kalinowski, J.; Stampor, W.; Szmytkowski, J.; Virgili, D.; Cocchi, M.; Fattori, V.; Sabatini, C. *Physical Review B* **2006**, *74*, 85316.

23. Kalinowski, J.; Stampor, W.; Szmytkowski, J.; Cocchi, M.; Virgili, D.; Fattori, V.; Di Marco, P. *The Journal of Chemical Physics* **2005**, *122*, 154710.
24. O'Brien, D. F.; Baldo, M. A.; Thompson, M. E.; Forrest, S. R. *Applied Physics Letters* **1999**, *74*, 442.
25. Montes, V. A.; Pérez-Bolivar, C.; Agarwal, N.; Shinar, J.; Anzenbacher, P. *J. Am. Chem. Soc.* **2006**, *128*, 12436.
26. Mink, L. M.; Neitzel, M. L.; Bellomy, L. M.; Falvo, R. E.; Boggess, R. K.; Trainum, B. T.; Yeaman, P. *Polyhedron* **1997**, *16*, 2809.
27. Pearson, C.; Cadd, D. H.; Petty, M. C.; Hua, Y. L. *J. of App. Phys.* **2009**, *106*, 064516.
28. Ahn, J. H.; Wang, C.; Perepichka, I. F.; Bryce, M. R.; Petty, M. C. *J.Mater. Chem.* **2007**, *17*, 2996.
29. Paul-Roth, C. O.; Drouet, S.; Merhi, A.; Williams, J. A. G.; Gildea, L. F.; Pearson, C.; Petty, M. C. *New J. Chem* **2013**, *submitted*.

List of compounds :

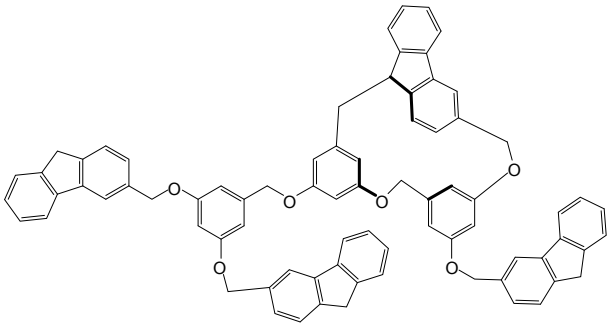

Macrocycle (1)

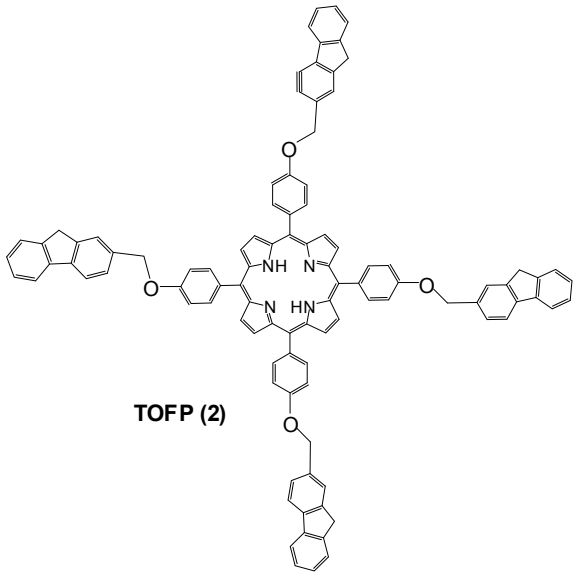

TOFP (2)

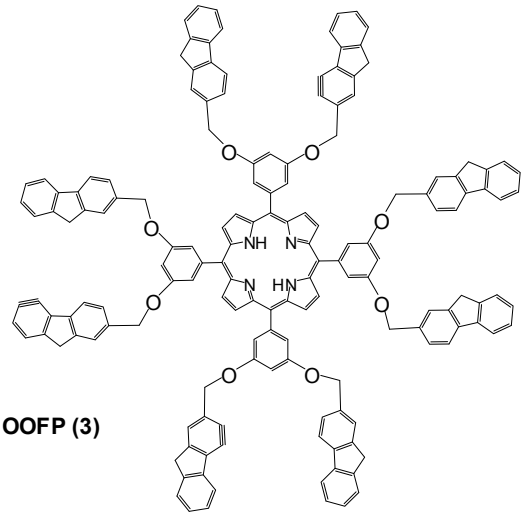

OOFP (3)

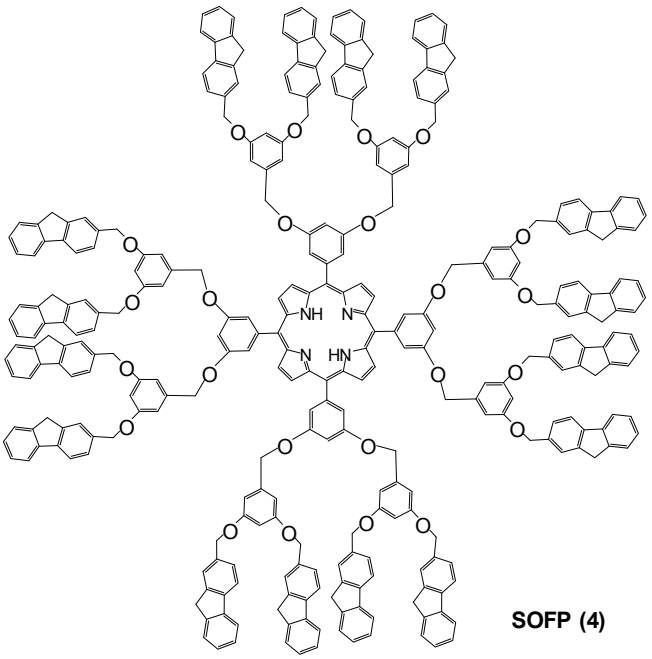

SOFP (4)

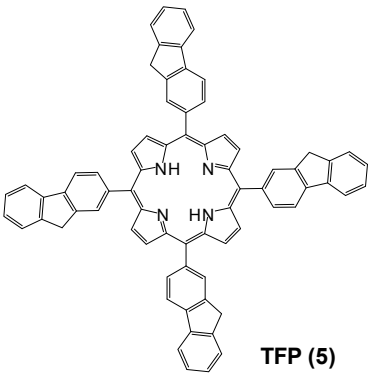

TFP (5)

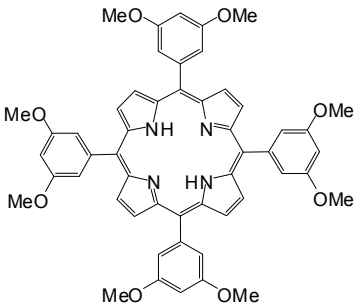

(6)

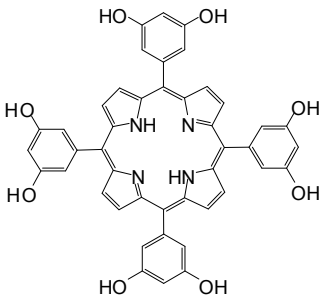

(7)

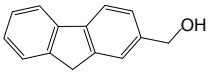

(8)

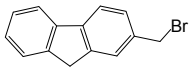

(9)

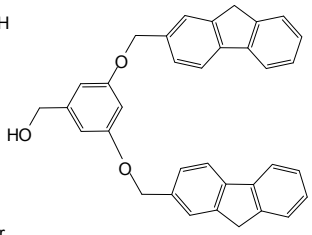

(10)

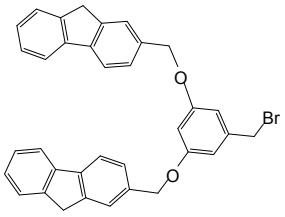

(11)

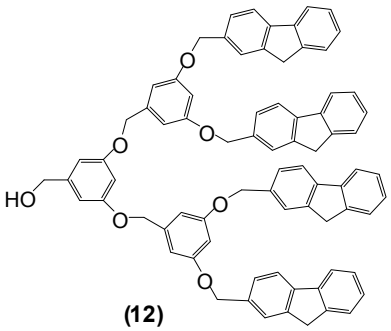

(12)

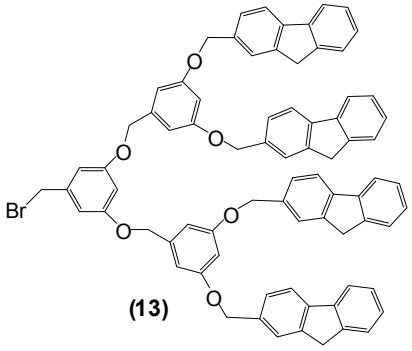

(13)

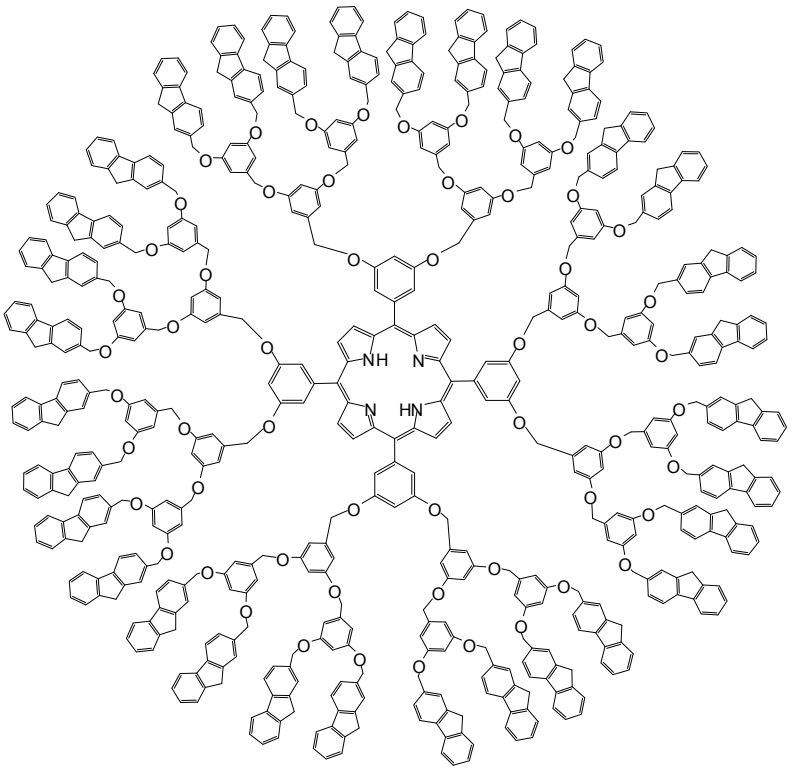

(32F)

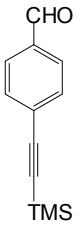

(14)

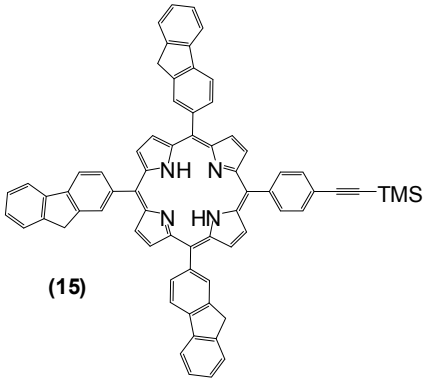

(15)

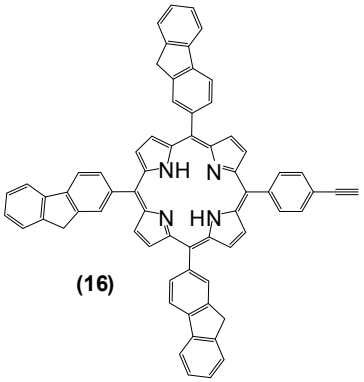

(16)

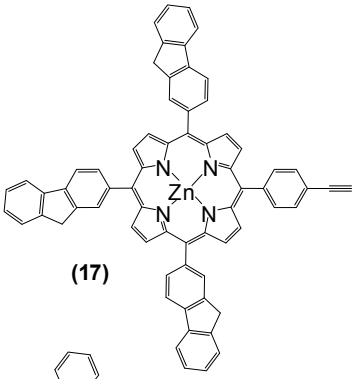

(17)

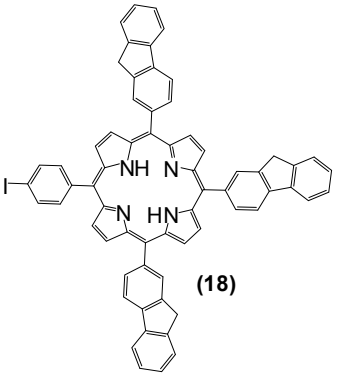

(18)

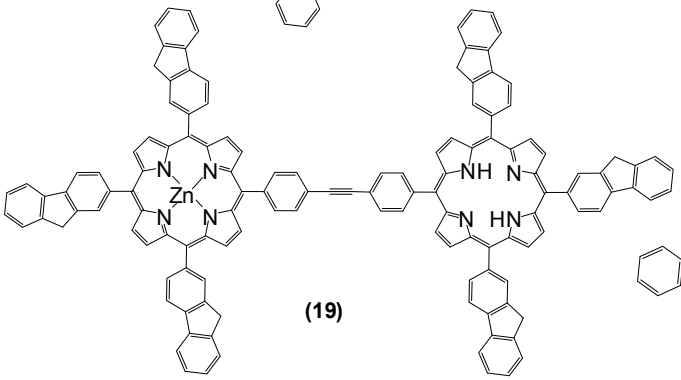

(19)

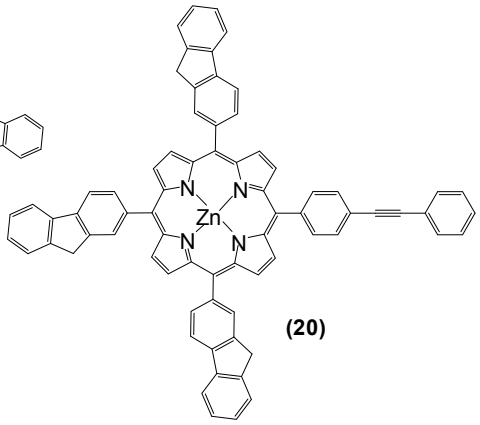

(20)

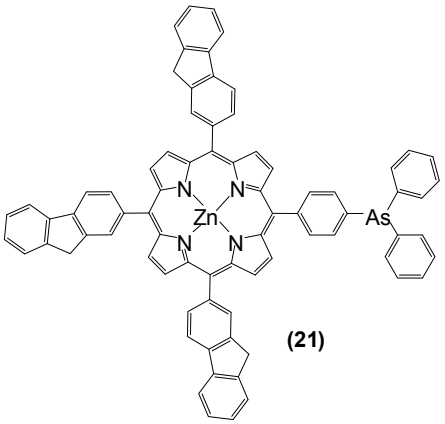

(21)

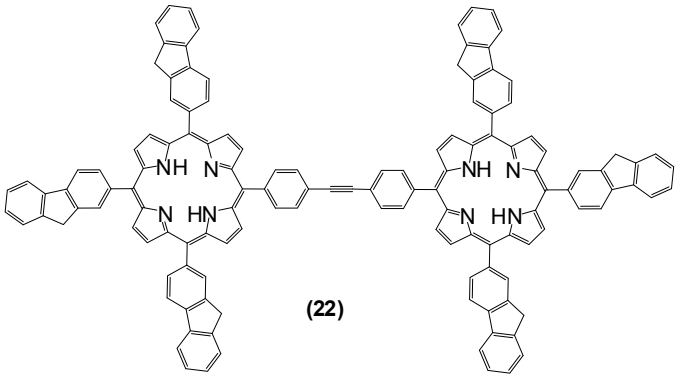

(22)

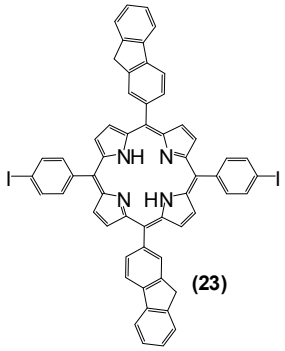

(23)

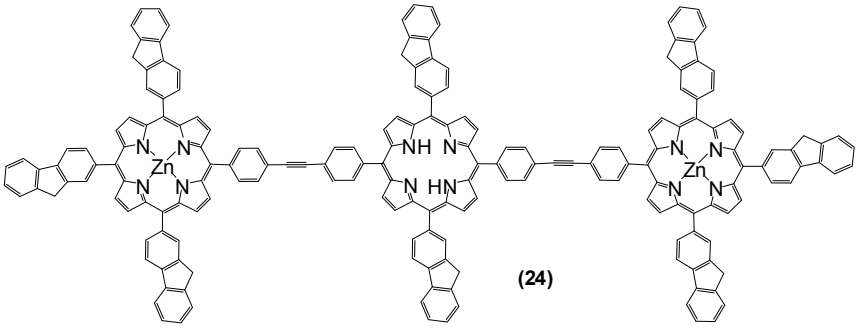

(24)

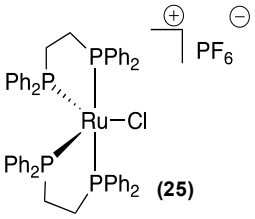

(25)

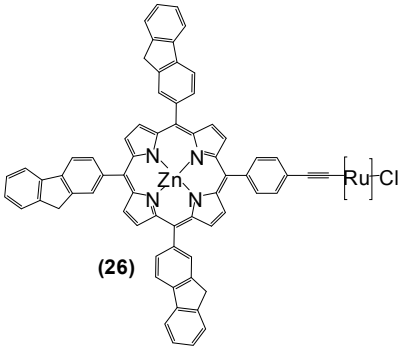

(26)

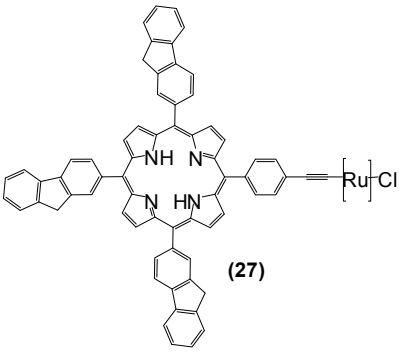

(27)

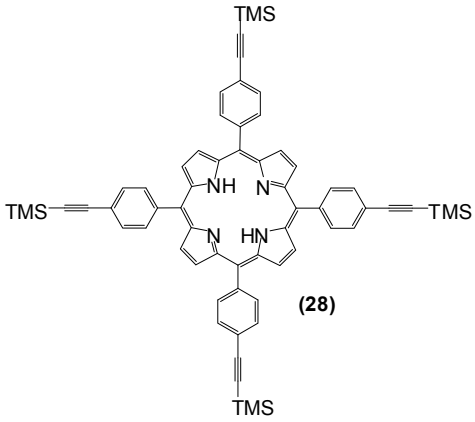

(28)

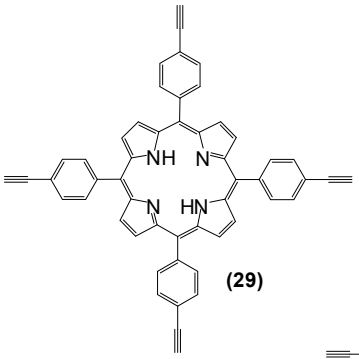

(29)

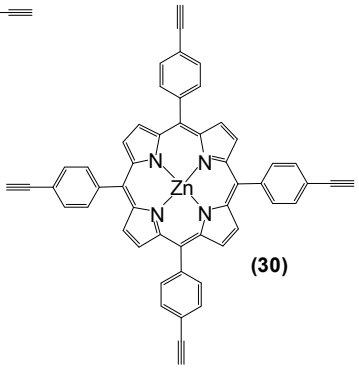

(30)

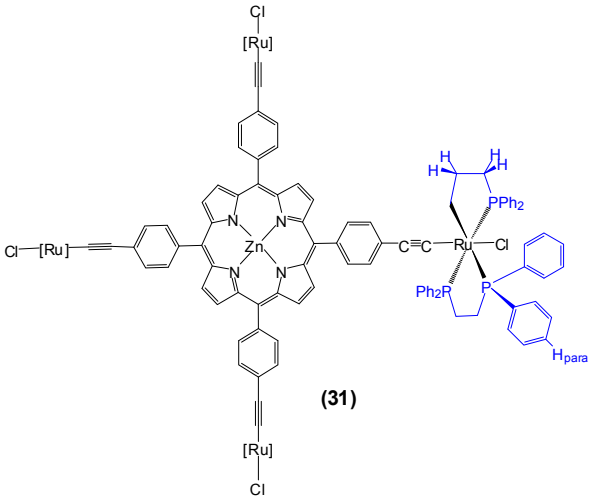

(31)

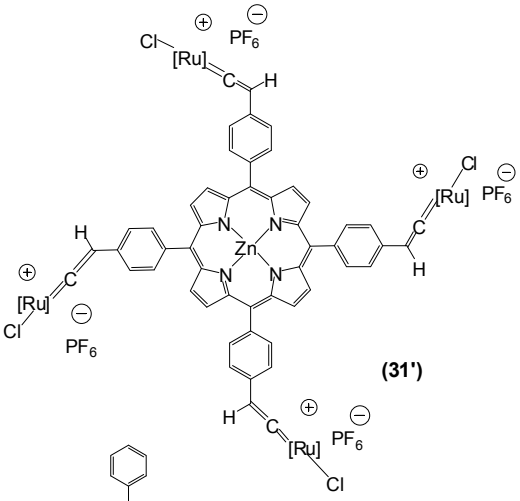

(31')

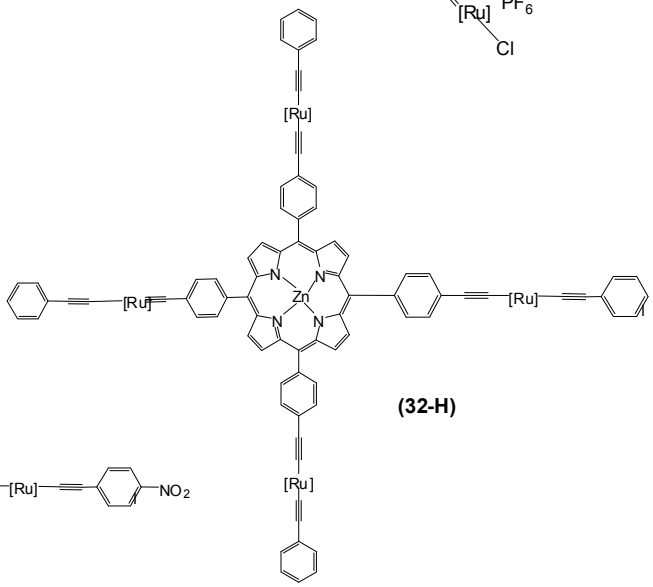

(32-H)

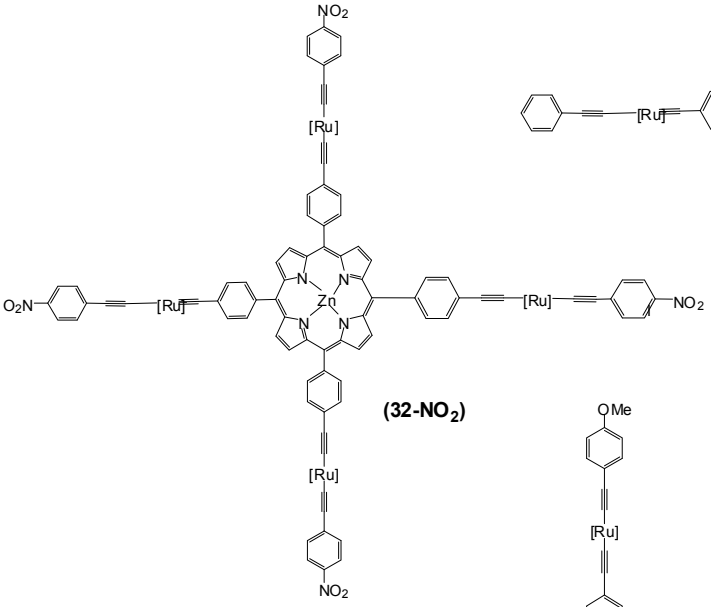

(32-NO_2)

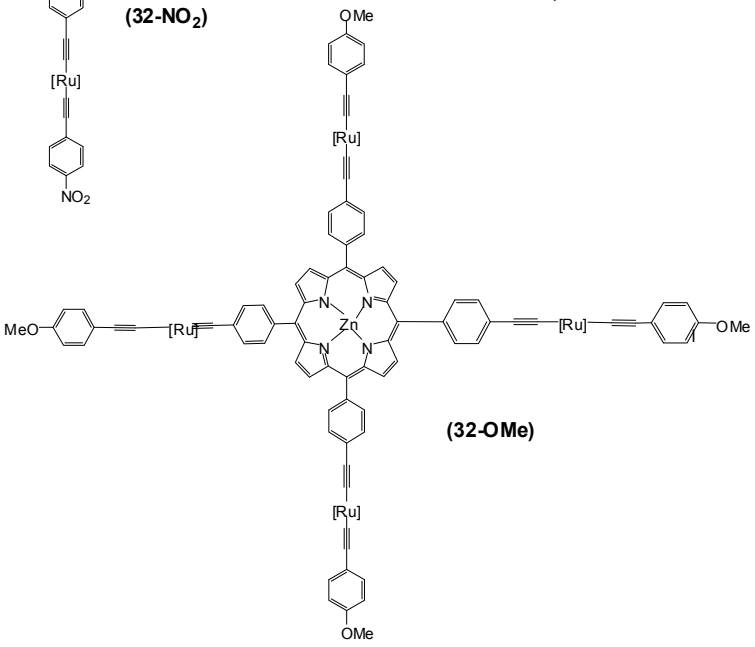

(32-OMe)

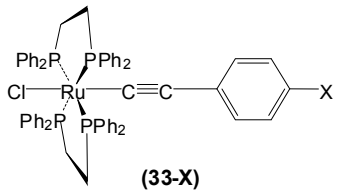

(33-X)

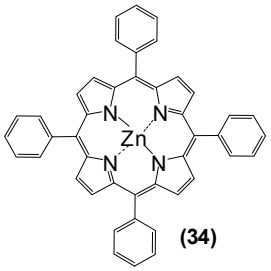

(34)

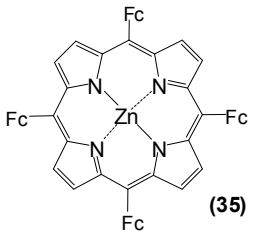

(35)

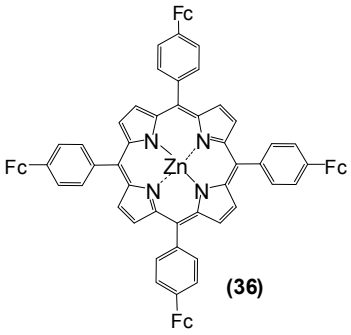

(36)

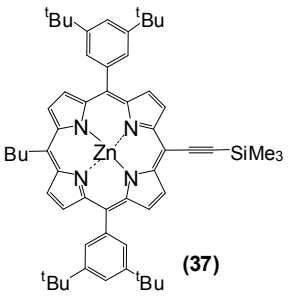

(37)

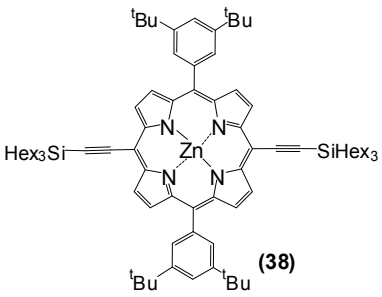

(38)

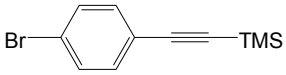

(39)

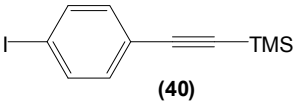

(40)

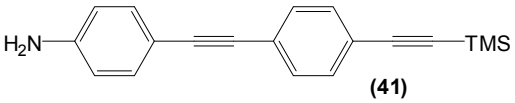

(41)

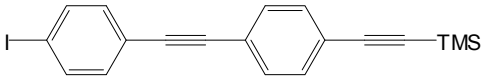

(42)

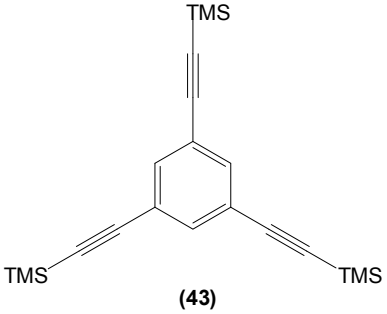

(43)

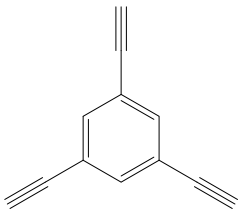

(44)

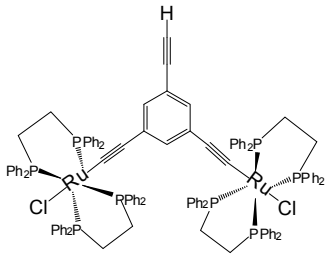

(45)

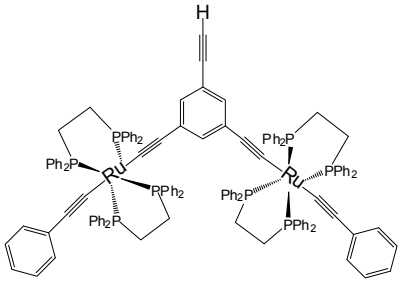

(46)

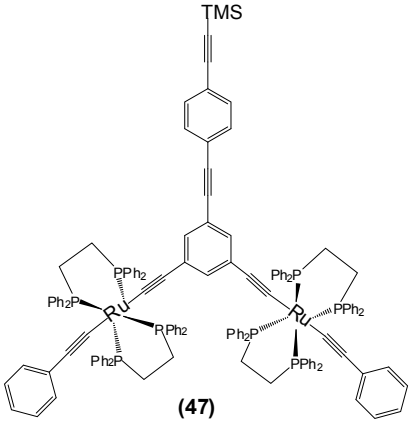

(47)

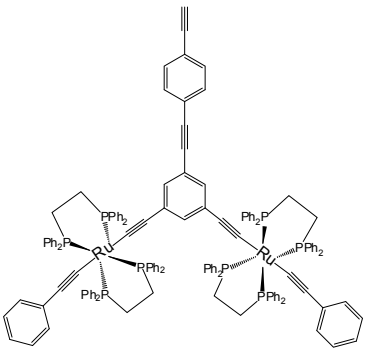

(48)

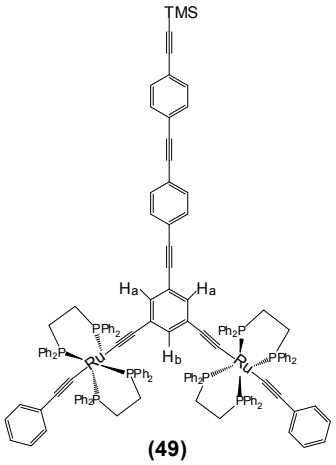

(49)

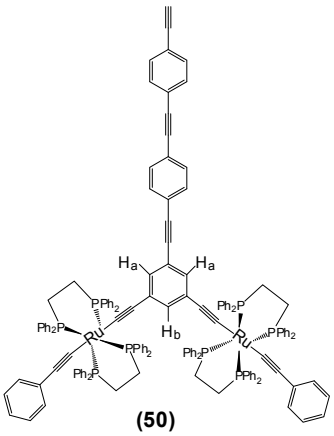

(50)

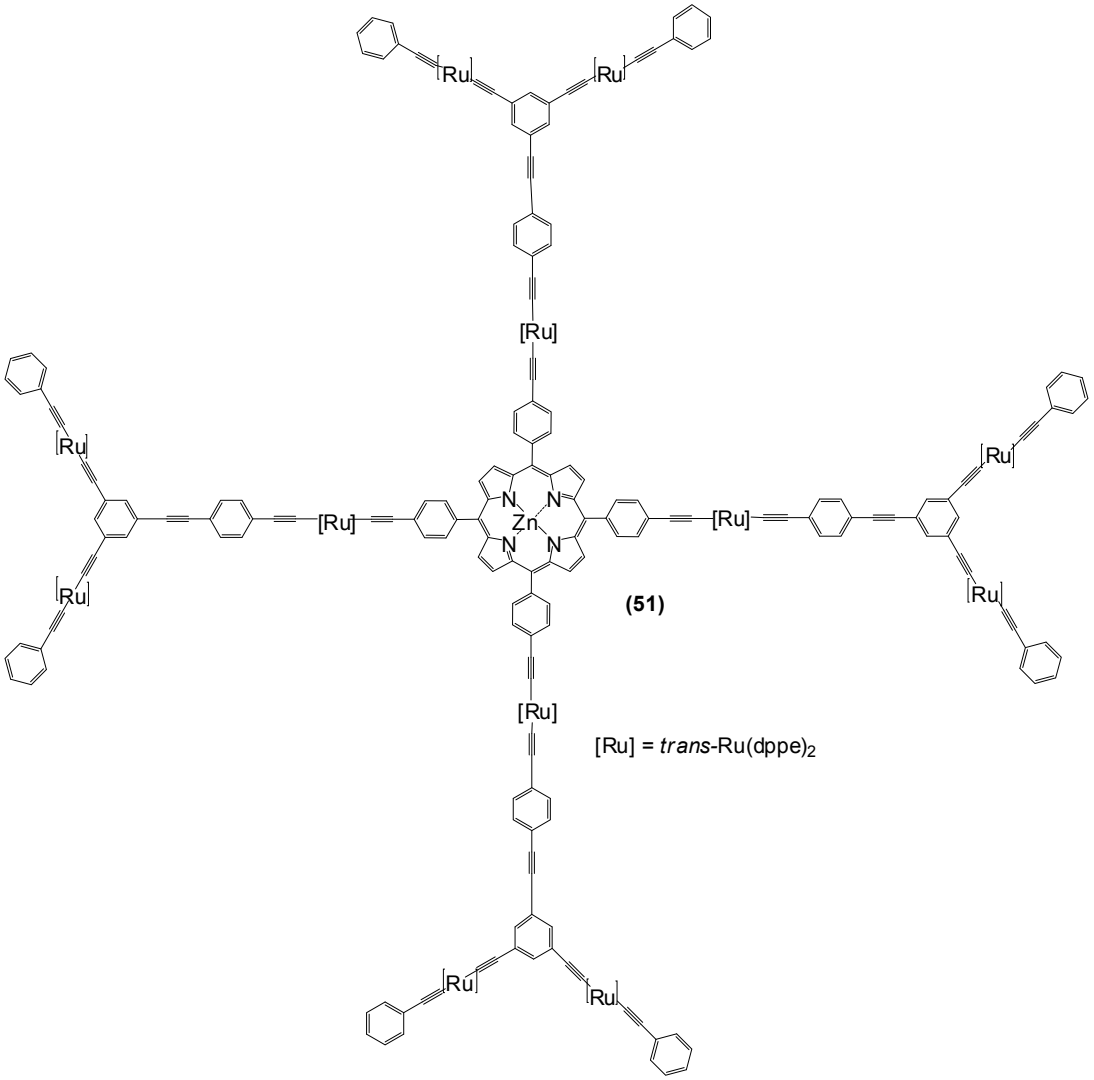

(51)

[Ru] = *trans*-Ru(dppe)$_2$

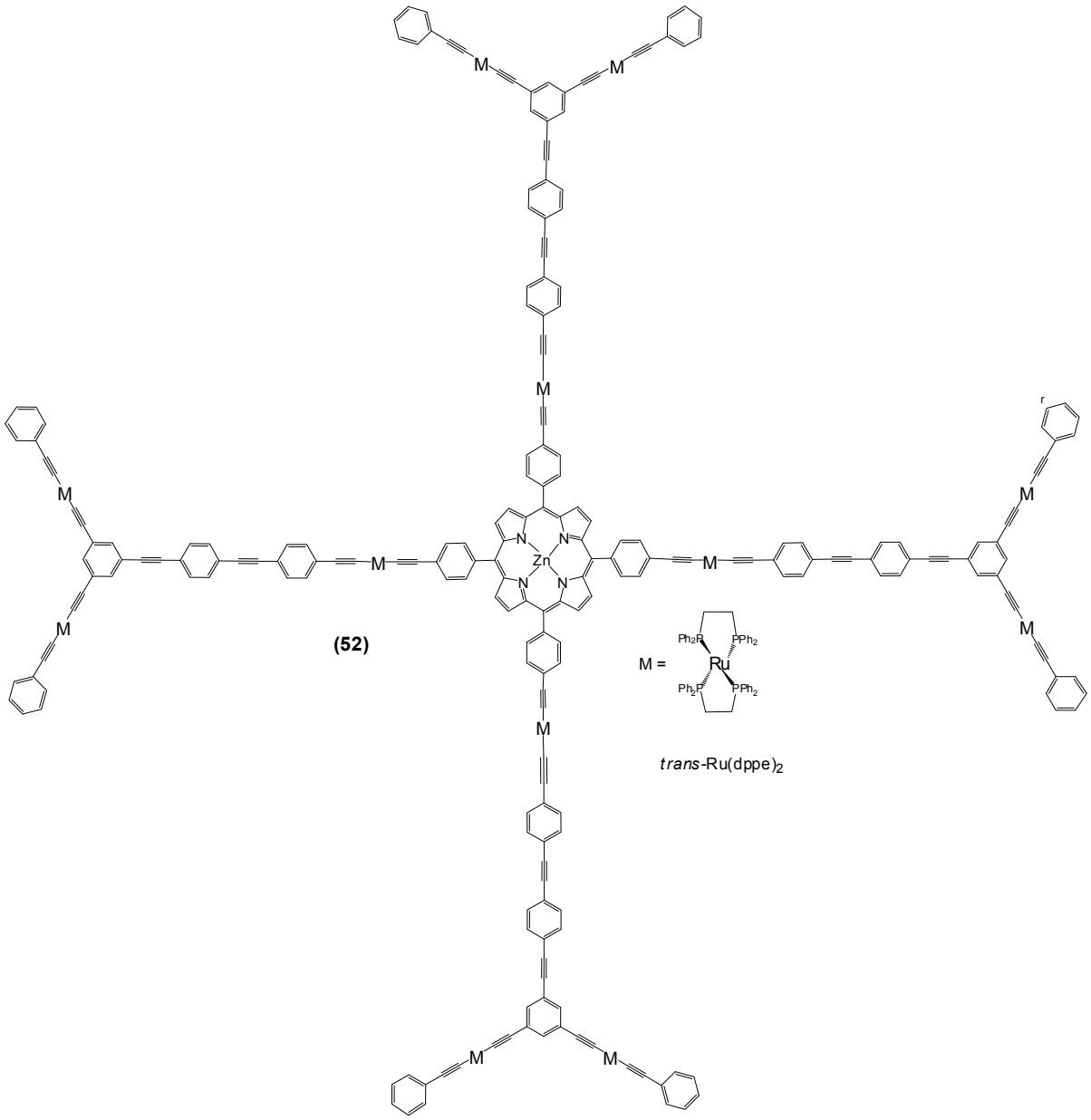

(52)

trans-Ru(dppe)$_2$

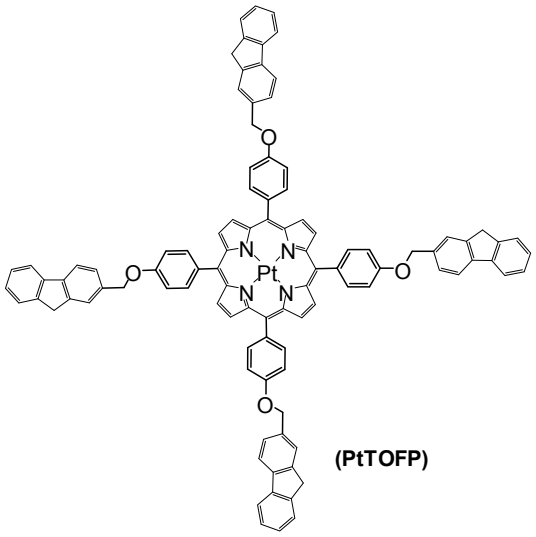

(PtTOFP)

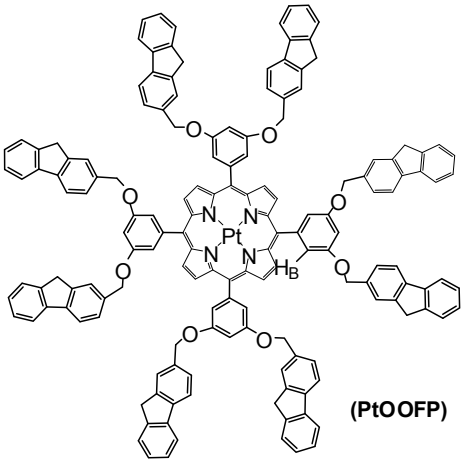

(PtOOFP)

Résumé

Les porphyrines sont des **macrocycles aromatiques à 18 électrons π** conjugués (**Figure 1**), constituées de quatre unités pyrroliques liées entre elles par des ponts méthines. Cette forte conjugaison implique une bonne stabilité et une forte absorption dans le domaine du visible de ces composés.

Figure 1: Structure de la **porphine** proposée par Kuster et numérotation IUPAC

Les porphyrines peuvent aussi se comporter comme des diacides ou des dibases et elles peuvent par conséquent, être métallées par presque tous les métaux de la classification périodique. Dans le premier cas, la porphyrine est dite “base libre”, dans le second cas, elle est dite “métallée”.

Le but de ce travail est d’utiliser la porphyrine comme brique moléculaire pour l’élaboration de composés ayant des activités optiques linéaires et non linéaires intéressantes. De plus, la porphyrine métallée peut être utilisée dans la fabrication d’OLEDs, dont les propriétés luminescentes seront étudiées.

La préparation de porphyrines a fait l’objet de nombreuses études depuis la première synthèse de l’hémine en 1929. L’intérêt principal de ces études est dû au rôle que joue ce macrocycle dans le milieu naturel, ce qui nous laisse la possibilité de préparer des composés qui peuvent modéliser les processus biologiques essentiels tels que la photosynthèse (chlorophylle), le transport et le stockage de l’oxygène (hémoglobine et myoglobine), la catalyse enzymatique (cytochrome P450) et la reconnaissance moléculaire (**Figure 2**).

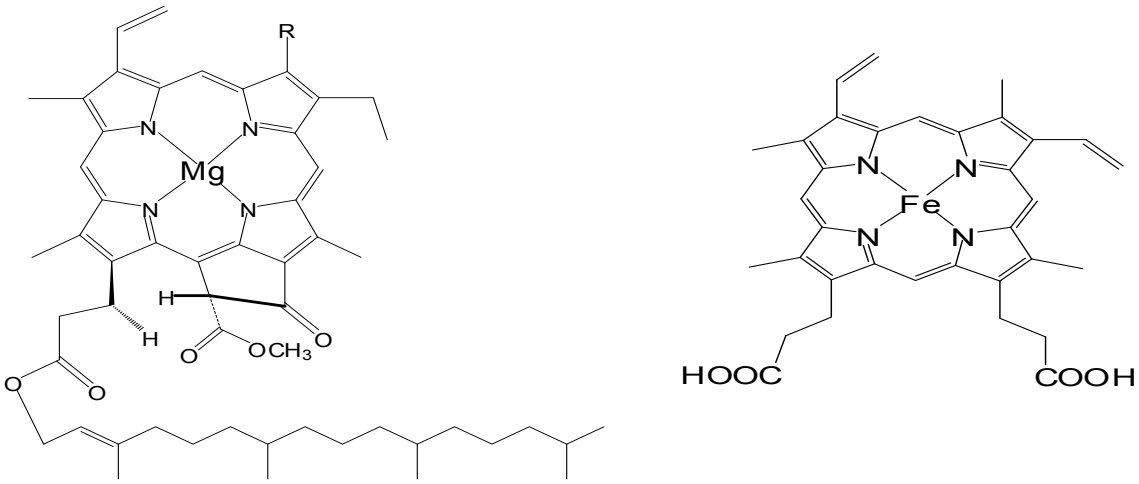

Chlorophyll a (R = CH_3)
Chlorophyll b (R = CHO)

Heme

Figure 2 : Exemples des porphyrines naturelles

Le premier chapitre porte dans un premier temps à détailler les méthodes de synthèse et de caractérisation de **porphyrines** décrites dans la littérature. Nous allons également introduire l'unité **fluorène** qui possède des propriétés photophysiques très intéressantes comme antenne collectrice de lumière. Cette unité fluorène (**Figure 3**) permet l'élaboration de modèles artificiels du système photosynthétique. Ensuite, nous présenterons les caractérisations classiques de la porphyrine comme l'étude RMN de proton, du carbone, spectroscopies UV-visible, et études électrochimiques.

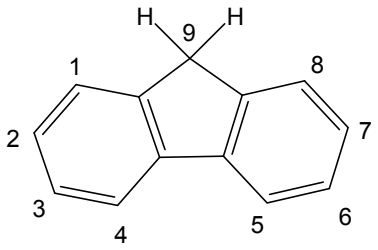

Figure 3 : Structure de fluorène

Dans un deuxième temps, le **transfert d'énergie** est détaillé. Pour présenter ce concept, nous introduirons d'abord le transfert d'électron.

Il existe deux types de transfert d'énergie : le transfert d'énergie de **type Dexter** privilégié dans le cas d'interactions à courte distance et le transfert d'énergie de **type Förster** dans les autres cas. Le transfert d'énergie singulet-singulet, entre deux

chromophores maintenus à une certaine distance, peut se représenter de la manière suivante (**Figure 4**) :

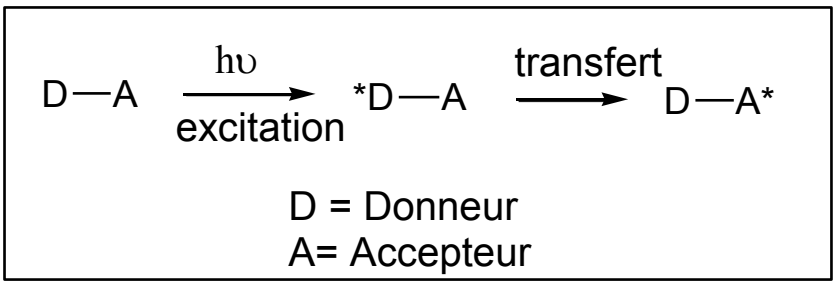

Figure 4 : Transfert d'énergie entre deux chromophores **D** et **A**

Dans **le second chapitre**, sur le modèle de ces systèmes biologiques décrits dans le chapitre précédant, nous présenterons la synthèse et les études photophysiques de porphyrines dendrimères.

Les **dendrimères** forment une famille de molécules possédant une structure arborescente. Ils présentent des propriétés variables qui peuvent être adaptées et contrôlées telles que la taille, la forme de la molécule et la position des groupements fonctionnels. Ces macromolécules sont constituées d'unité de base, les monomères, qui s'associent selon un processus arborescent autour d'un cœur polyfonctionnel. Leur architecture rappelle celle des complexes collecteurs de lumière dans les photosystèmes. Leur construction arborescente s'effectue par la répétition d'une même séquence de réactions qui permet l'obtention à la fin du cycle réactionnel, d'une nouvelle génération appelée **G** et d'un nombre croissant de branches identiques (**Figure 5**) Ce sont des molécules tridimensionnelles, de taille et de structure bien définies, hautement symétriques, généralement de hauts poids moléculaire, possédant un grand nombre de chaînes terminales afin d'assurer leur solubilité.

Figure 5 : Représentation schématique d'un dendrimère.

Il existe deux voix de synthèse principales pour la préparation des dendrimères. La première utilisée fut la synthèse dite **divergente** utilisée par les groupes de Vögtle, Newkome et Tomalia. Ce n'est que plus tard que la synthèse **convergente** fut introduite par Fréchet et Miller, au début des années 90. Elle permet un meilleur contrôle de l'architecture et du placement des groupes fonctionnels, c'est la voie de synthèse que nous utiliserons pour notre travail exploratoire

Pour cette méthode **convergente** le processus de croissance débute par la partie qui deviendra finalement la surface du dendrimère. Tout d'abord, cette méthode consiste en l'élaboration de branches dendritiques appelés « dendrons », puis une fois le dendron de génération désiré obtenu, il est ensuite lié au cœur polyfonctionnel ; la porphyrine dans notre cas, pour donner un dendrimère complet. Dans l'exemple choisi, le dendron possédant deux points de jonction est relié au noyau multifonctionnel et on obtient alors directement la porphyrine dendrimère de génération $\mathbf{G_2}$ (**Figure 7**).

Figure 7 : Préparation de porphyrine dendrimère par voie **convergente**.

Nous avons tout d'abord réalisé la synthèse de deux porphyrines précurseurs : l'une possédant quatre groupements hydroxyles et l'autre, huit groupements hydroxyles. Ces groupements hydroxyles permettent ultérieurement le greffage des dendrons (**Figure 8**).

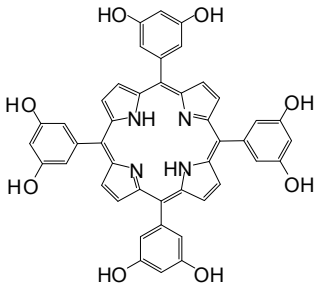

Figure 8 : La porphyrine qui possède huit groupements hydroxyles

Après la synthèse des dendrons, la synthèse de la série dendrimère présentée (**Figure 9**) est effectuée. De plus, les propriétés photophysiques sont étudiées et les rendements quantiques sont calculés.

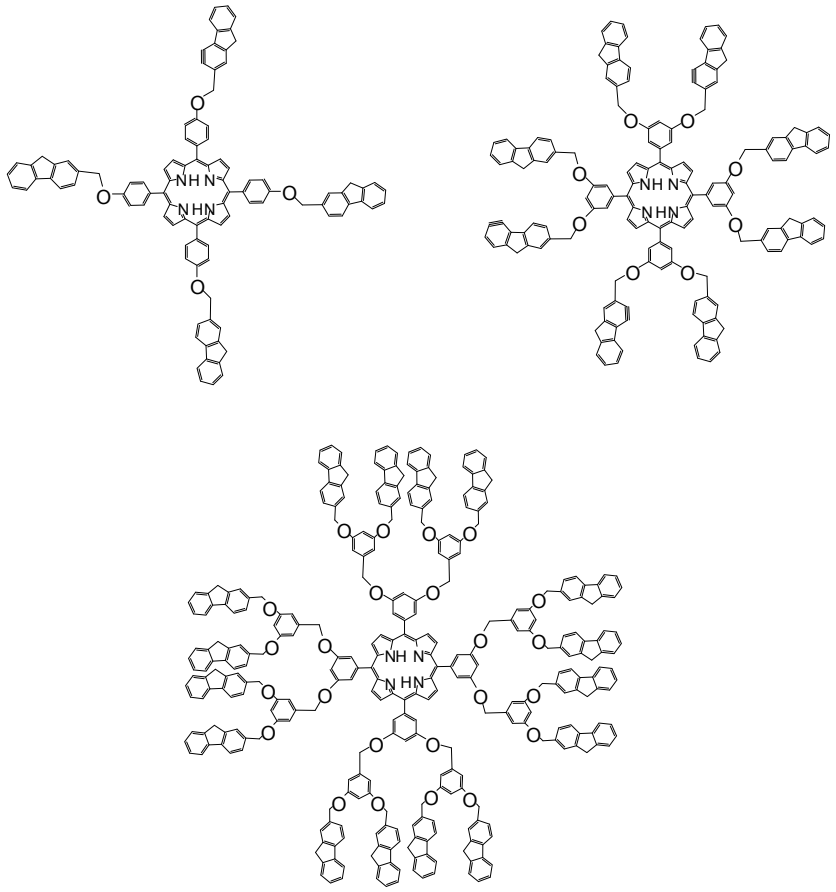

Figure 9 : La série des dendrimères synthétisés

Suite à ces études, il s'avère que ces porphyrines dendrimères sont des briques moléculaires intéressantes pour le transfert d'énergie et donc pour la collecte de lumière. On peut espérer, en rapprochant ces briques moléculaires dans l'espace, observer un effet encore plus efficace pour la collecte de lumière par effet synergique.

Concernant le troisième Chapitre : récemment au laboratoire, une nouvelle famille de composés porphyriniques a été synthétisée. Une porphyrine tétrasubstituée en position *meso* par des groupements fluorényles, le tétrafluorénylporphyrine (**TFP**), a été obtenue. Des études ont montré qu'après une excitation sélective des antennes fluorényles par lumière UV ou de la bande de Soret, le cœur de la porphyrine émettait une forte lumière rouge. De plus, le rendement quantique de luminescence était considérablement amélioré pour ce composé **TFP** comparé à la tétraphénylporphyrine (**TPP**). En effet, le rendement quantique passe de 13% à 22%.

Le but de **troisième chapitre** et de présenter la synthèse de nouveaux **dimère** de porphyrine (6 bras de fluorène), et trimère (8 bras de fluorène), puis d'étudier les propriétés photophysiques pour tester l'effet d'augmentation du nombre des bras fluorènyles et comparer leurs rendement quantique avec la référence du laboratoire : **TFP** (**Figure 10**).

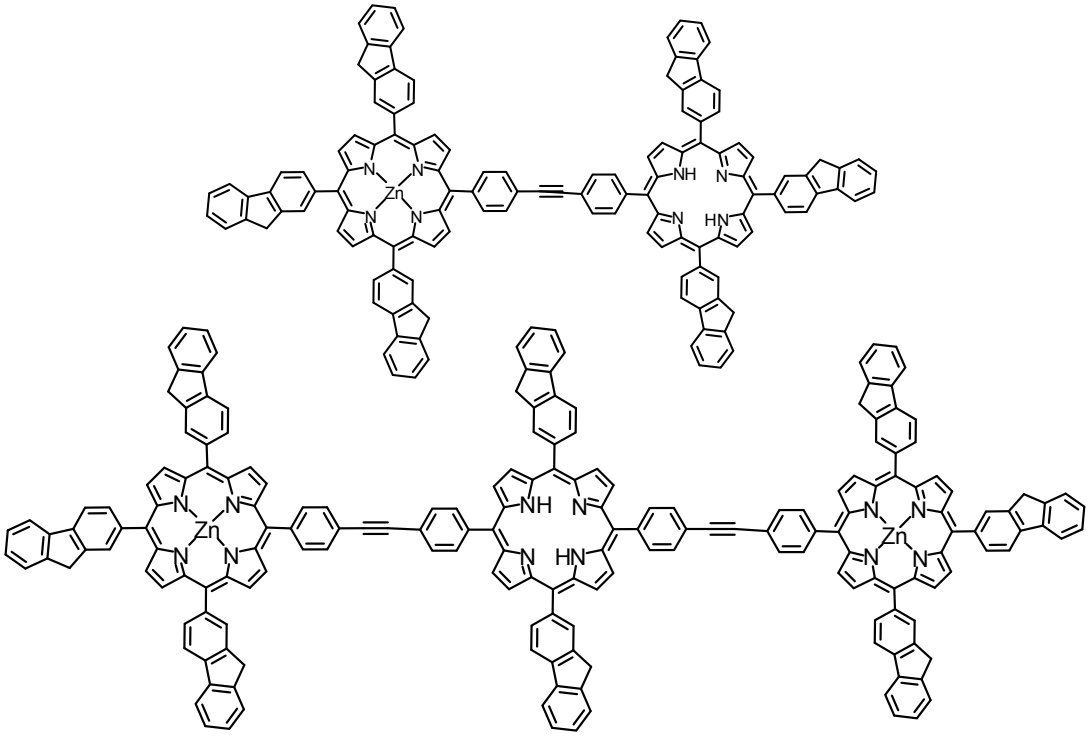

Figure 10 : Dimère et **Trimère** de porphyrine

Concernant le **Chapitre 4** de ce travail de thèse, le « design » des molécules étant fait dans le but d'obtenir des espèces très actives en Optique Non Linéaire, nous allons préalablement rappeler les conditions nécessaires à de telles applications.

L'Optique Non Linéaire (ONL) depuis sa découverte, au début des années 60, a fait l'objet de nombreuses études par plusieurs groupes de recherche. Ces travaux ont conduit à des critères permettant l'élaboration de nouvelles molécules très actives en ONL.

Ces recherches en ONL s'orientent maintenant vers le développement de composés stables, facilement accessibles et comportant des non linéarités importantes. L'intérêt se porte également sur la réalisation de matériaux multistables pouvant permettre une modulation de cette activité non linéaire par action d'un stimulus externe (électrique, optique, magnétique…).

La chimie de coordination et la **chimie organométallique** ont permis de développer des systèmes avec des activités en **ONL de troisième ordre (TO)** très importantes. Malgré la complexité de ces phénomènes non linéaires du troisième ordre, l'introduction de complexes organométalliques présente certaines particularités et l'apparition de nouvelles transitions électroniques influence grandement la réponse ONL de TO.

De part leurs nombreux sites de coordination, les métaux permettent d'accéder facilement à des géométries diverses par complexation et peuvent être utilisés en tant que connecteurs dans des systèmes polymétalliques en donnant ainsi des composés multidimensionnels comportant de fortes activités en **ONL TO**.

En vue d'atteindre des édifices moléculaires en trois dimensions avec de fortes absorptions à deux photons, les dendrimères organométalliques se sont avérés être de très bons candidats. Humphrey *et coll*. ont ainsi développé de nombreux systèmes **dendritiques organométalliques** à base de complexe de ruthénium. Les propriétés **ONL** de **TO** ont été mesurées par la technique de **Z-scan** à 800 nm. De plus, les systèmes dendritiques permettent d'accroitre très fortement le nombre de chromophores actifs en **ONL TO** et ainsi d'atteindre des activités particulièrement importantes.

Dans **ce quatrième chapitre**, en collaboration avec l'équipe du **Pr. M. Humphrey**, nous avons synthétisé une famille de complexes organométalliques de type **acétylure de ruthénium** à partir de la porphyrine zinc(II)-5,10,15,20-((4-éthynyl)phényl)porphyrine

(**Figure 11**). En effet, lors d'un séjour de trois mois à **l'Université de Canberra** (ANU), dans ce laboratoire, j'ai pu bénéficier de leur longue expertise en synthèse organométallique.

Nous avons commencé par la synthèse et l'étude du complexe organométalliques de ruthénium possédant quatre ligands chloro **–Cl**. Comme nous avons vu précédemment, l'augmentation de chromophores actifs permet d'accroître les propriétés optiques non linéaires ; nous avons donc ensuite substitué les ligands chloro du complexe par des ligands plus riches en électrons et comportant des électrons π pour accéder aux analogues **–Ph**, **–$C_6H_4NO_2$** et **–C_6H_4OMe** (**Figure** 11).

Figure 11 : Complexes organométalliques de ruthénium.

Ensuite, un nouveau dendrimère organométallique qui possède 12 espèces de ruthénium est synthétisé et étudié (**Figure 12**).

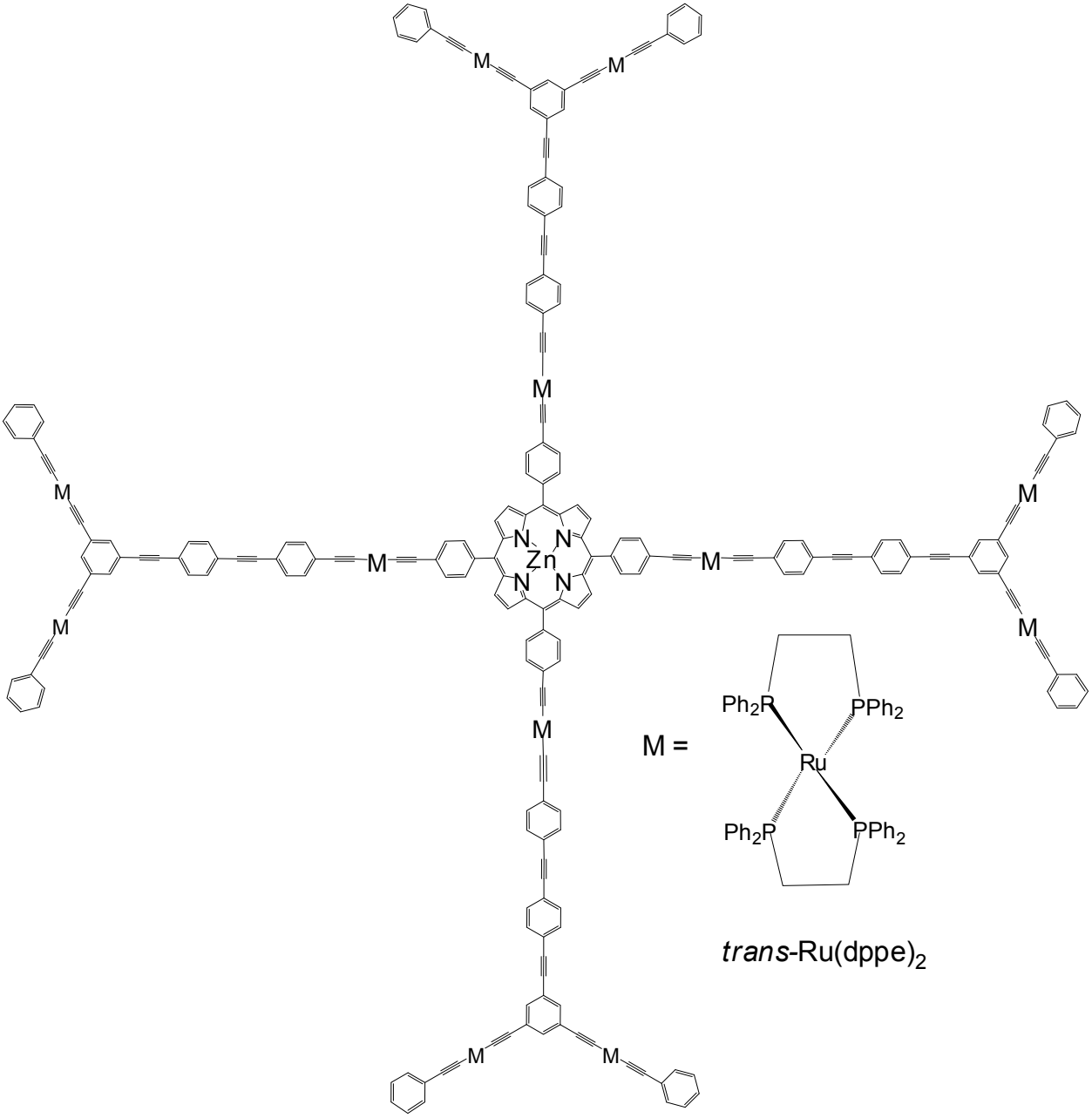

Figure 12 : Nouveau Dendrimère organométallique étendu

Dans un deuxième temps, en collaboration avec l'équipe du **Dr. F. Paul** (**Université de Rennes1**), nous avons synthétisé un nouveau complexe organométallique d'acétylure de fer (**Figure 13**) afin de comparer son activité ONL avec ceux de ruthénium. A nouveau, j'ai pu bénéficier de l'expertise de ce laboratoire, localisé à Rennes, en synthèse organométallique, spécialisé en acétylure de fer. Il faut noter que pour ces nouveaux

complexes de Fe(II), il n'y a pas d'extension possible comme c'est le cas du ruthénium vu précédemment.

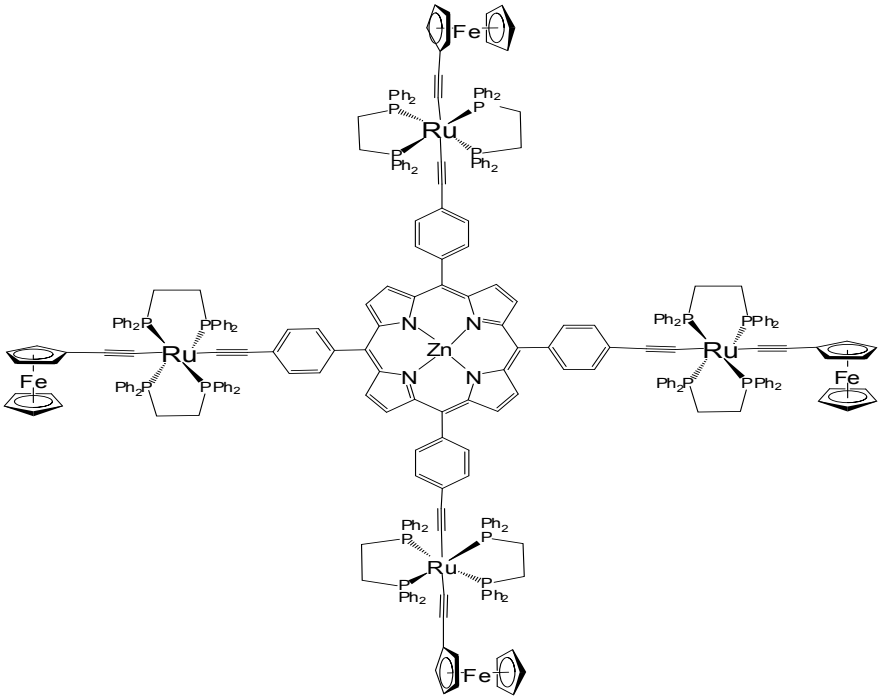

Figure 13 : Nouveau complexe d'organofer

Dans le **dernier chapitre**, c'est-à-dire **<u>le Chapitre 5</u>**, nous présenterons un exemple d'application de ces molécules hautement luminescentes dans le rouge. Ces dernières années, la recherche dans le domaine des dispositifs électroluminescents à base de matériaux organiques (OLED) s'est largement intensifiée, ces dispositifs ont permis l'élaboration d'un nouveau type d'affichage. Des tels dispositifs très performants, comme vu sur les photos ci-dessous, ont pu être obtenus grâce à l'utilisation de complexes de porphyrines synthétisées au laboratoire (**Figure 14**).

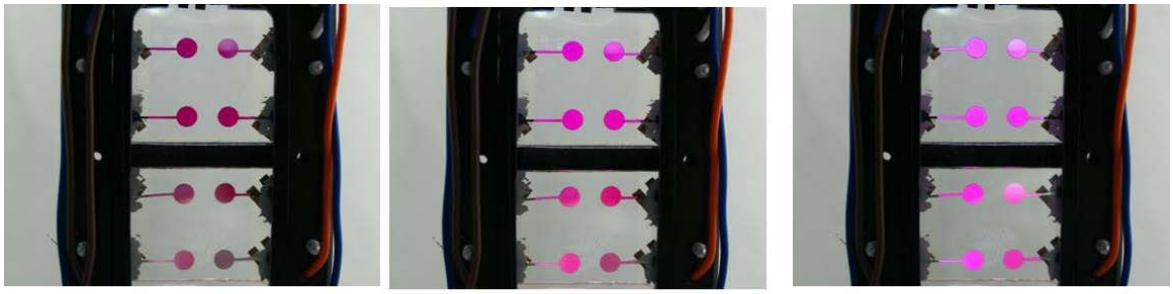

Figure 14 : Photographies de dispositif élaboré à différentes tensions supérieures à 16 Volts

Comme les nouvelles porphyrines synthétisées, telles les porphyrines dendrimères, présentent une forte émission dans le rouge, elles ont donc été testées sous la forme de complexes phosphorescents à base de platine(II), comme matériaux organiques émissifs pour de tels dispositifs. Nous présenterons l'élaboration, puis les études de photoluminescence et d'électroluminescence ainsi que les caractéristiques de ces nouveaux dispositifs OLEDs (**Figure 15**).

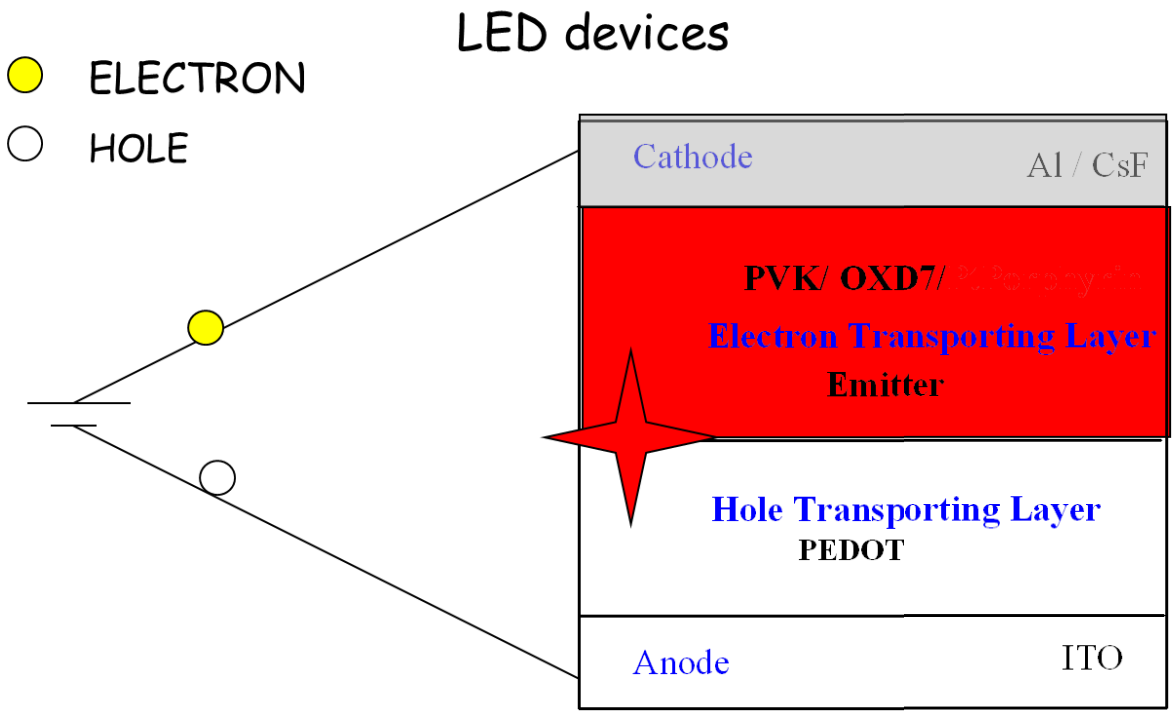

Figure 15 : Présentation d'un nouveau dispositif OLED à base de notre porphyrine dendrimère

INSA de RENNES
Service des Formations

AVIS DU JURY SUR LA REPRODUCTION DE LA THESE SOUTENUE

Titre de la thèse:
Synthèse de nouveaux assemblages à base de Porphyrines Organiques et Organométalliques pour l'Optique

Nom Prénom de l'auteur : MERHI AREEJ

Membres du jury :
- Monsieur DUBREUIL Didier
- Madame LEDOUX Isabelle
- Monsieur MONGIN Olivier
- Madame PAUL-ROTH Christine
- Monsieur PAUL Frédéric
- Monsieur TRIPIER Raphaël
- Monsieur SAMOC Marek

Président du jury : Mme LEDOUX Isabelle

Date de la soutenance : 20 Septembre 2013

Reproduction de la these soutenue

☒ Thèse pouvant être reproduite en l'état
☐ Thèse pouvant être reproduite après corrections suggérées

Fait à Rennes, le 20 Septembre 2013

Signature du président de jury

Le Directeur,

M'hamed DRISSI

Résumé

Au cours de cette thèse, nous avons synthétisé et caractérisé de nouveaux composés en utilisant le macrocycle porphyrinique comme brique moléculaire de départ.

Le but de ce travail étant l'étude des propriétés optiques de ces nouveaux composés obtenus.

Après avoir effectué l'étude bibliographique sur les porphyrines, nous avons fait une présentation générale des porphyrines symétriques et non symétriques, de leurs propriétés et de leurs synthèses. D'autre part, nous avons aussi considéré l'unité fluorène qui possède des propriétés photophysiques très intéressantes comme antenne collectrice de lumière.

Puis, nous avons abordé des méthodes de synthèse permettant d'associer le macrocycle porphyrinique avec de nombreuses unités fluorènes. Cette association a pu être réalisée de différentes manières : soit de façon dendritique ou par connexion directe sur la porphyrine (dimère et trimère).

Nous avons également décrit l'obtention d'une nouvelle famille de porphyrines substituées par des groupements organométalliques de type acétylure de ruthénium et de fer pour l'optique non linéaire de troisième ordre (ONL TO).

Lors de la dernière partie de mes travaux de thèse, comme application de ces composés luminescents dans le rouge, nous avons reporté l'élaboration de différents dispositifs de diodes électroluminescentes (OLED) émettant dans le rouge.

.

Abstract

During this thesis, we have worked on the synthesis and characterization of new compounds using the porphyrin macrocycle as a starting material.

The aim, after synthesis, is to study the photophysical properties of these new molecules.

A general bibliographic study was presented followed by introducing the synthetic methods of porphyrins and characterization means. Then, fluorene was considered to be an attracting unit due to its interesting photophysical properties: acting as efficient antennae for collecting light.

First, we have presented the synthesis of porphyrin dendrimers having fluorenyl arms of different generations. That is to test the effect of number of fluorenes on the photophysical properties. Another way is to connect the fluorenes directly to the porphyrin core by synthesizing porphyrin dimer and trimer.

We have also detailed the synthesis and characterization of a new family of porphyrin organometallic assemblies possessing ruthenium and iron moieties. In addition, a new organometallic porphyrin dendrimer bearing twelve ruthenium species was reported as well. These organometallic porphyrins are of interest in the third order of Nonlinear Optics (NLO).

In the last chapter of this thesis we showed an example of application of porphyrin chemistry. We reported the elaboration of a new organic light emitting Diode (OLED) using these new porphyrins that emits in the red region.

Utiliser la police Arial Taille 9 en bleu dans les champs texte « résumé » et « abstract » - Texte justifié -
Ne pas dépasser le nombre de caractères des cadres de texte ci-dessus.
Ne pas modifier la taille des cadres de texte

N° d'ordre : 13ISAR 22 / D13 - 22

Institut National des Sciences Appliquées de Rennes
20, Avenue des Buttes de Coëmes • CS 70839 • F-35708 Rennes Cedex
Tel : 02 23 23 82 00 - Fax : 02 23 23 83 96